University of Alberta

Multivariate Analysis of Diverse Data for Improved Geostatistical Reservoir Modeling

by

Sahyun Hong

A thesis submitted to the Faculty of Graduate Studies and Research
in partial fulfillment of the requirements for the degree of

Doctor of Philosophy

in

Mining Engineering
Department of Civil and Environmental Engineering

Fall 2010

Edmonton, Alberta

Examining Committee

Dr. Clayton Deutsch (Supervisor) , Civil and Environmental Engineering

Dr. Jozef Szymanski (Chair and Examiner), Civil and Environmental Engineering

Dr. Jerry Jensen (External Examiner), Chemical and Petroleum Engineering, Univ. of Calgary

Dr. Peter Hooper (Examiner), Mathematical and Statistical sciences

Dr. Hooman Askari-Nasab (Examiner), Civil and Environmental Engineering

Abstract

Improved numerical reservoir models are constructed when all available diverse data sources are accounted for to the maximum extent possible. Integrating various diverse data is not a simple problem because data show different precision and relevance to the primary variables being modeled, nonlinear relations and different qualities. Previous approaches rely on a strong Gaussian assumption or the combination of the source-specific probabilities that are individually calibrated from each data source.

This dissertation develops different approaches to integrate diverse earth science data. First approach is based on combining probability. Each of diverse data is calibrated to generate individual conditional probabilities, and they are combined by a combination model. Some existing models are reviewed and a combination model is proposed with a new weighting scheme. Weakness of the probability combination schemes (PCS) is addressed. Alternative to the PCS, this dissertation develops a multivariate analysis technique. The method models the multivariate distributions without a parametric distribution assumption and without ad-hoc probability combination procedures. The method accounts for nonlinear features and different types of the data. Once the multivariate distribution is modeled, the marginal distribution constraints are evaluated. A sequential iteration algorithm is proposed for the evaluation. The algorithm compares the extracted marginal distributions from the modeled multivariate distribution with the known marginal distributions and corrects the multivariate distribution. Ultimately, the corrected distribution satisfies all axioms of probability distribution functions as well as the complex features among the given data.

The methodology is applied to several applications including: (1) integration of continuous data for a categorical attribute modeling, (2) integration of continuous and a discrete geologic map for categorical attribute modeling, (3) integration of continuous data for a continuous attribute modeling. Results are evaluated based on the defined criteria such as the fairness of the estimated probability or probability distribution and reasonable reproduction of input statistics.

Acknowledgement

First of all, I would like to thank Dr. Clayton V. Deutsch for his guidance, patience and unexhausted ideas. Both his mentorship and friendship made my times during my PhD exciting and enjoyable.

My special thanks go to the industrial sponsors of Centre for Computational Geostatistics (CCG) company members for their financial supports. Also, the financial supports for this research provided by Provost Doctoral Entrance Award and J Gordon Kaplan Graduate Student Award in the University of Alberta are greatly appreciated.

I would like to thank my parents for their endless love, support and for always having confidence in me. My children Lindsay and Lynnwoo give me a lot of joy and happiness in my life. Most importantly, I want to thank my wife, Jina. I would not be here without your love and support.

Contents

List of Tables

List of Figures

Chapter 1

Introduction

Building numerical reservoir models is an intermediate but essential step for reservoir management. Numerical models are used to plan new wells, calculate overall hydrocarbon reserves, predict the reservoir performance in a flow simulator, and to analyze the uncertainty in reservoir performance forecasts. Accurate reservoir models may lead to accurate predictions of reservoir performance and improve reservoir management decisions with less uncertainty. Thus, constructing numerical geologic models is an important step in reservoir management. Accurate reservoir modeling, however, is difficult to achieve given the few directly measured data; the reservoir properties such as facies, porosities, permeabilities, hydrocarbon saturations, occurrence of fault are typically sampled at very few well locations. These reservoir properties are heterogeneous and the distribution is never known exactly. Moreover, these properties are highly coupled with complex geological structures. Due to these reasons it is not desirable to consider only one quantitative description of a reservoir in a deterministic way (Haldorsen and Damsleth, 1990; Ballin et al., 1992). Equally probable descriptions or realizations of the reservoir are useful to account for a lack of knowledge or uncertainty. Stochastically generated realizations allow quantifying the uncertainty in the spatial distribution of reservoir properties and the distribution of reservoir responses. Risk-qualified decision making techniques can be applied with multiple realizations to reach a final decision (Srivastava, 1987).

Improved numerical reservoir models can be constructed when all available diverse data are integrated to the maximum extent possible. The uncertainty in the model will generally decrease with additional data sources. The reservoir attribute of modeling is supplemented by additional information from various data sources. Diverse data are commonly available in petroleum applications. These data include seismic related attributes from the seismic exploration,

conceptual geologic map from geologist or analogue data and historical production data from well test. Other reservoir related information such as reservoir top surface, bottom surface and thickness are useful data though they do not arise from different sources.

The main purpose of reconciling these diverse data is to provide accurate models and reduce the uncertainty in the reservoir performance predictions in a consistent manner. However, there are some issues that should be addressed when accounting for the secondary data. Each data source carries information on the reservoir properties at different scales and with varying levels of precision (Deutsch and Hewett, 1996). For example, 3D seismic attributes data contain information on reservoir properties such as the spatial distribution of major faults, lithofacies, porosity and fluids carried by their respective porous rock and they are imprecisely related to the reservoir properties of consideration (Lumley et al., 1997). Geologic map data reflect a geologic realism of reservoir created by complex physical process. A certain geologic feature such as connectivity of high and low permeable rock that is a first-order impact on fluid flow can be better understood from incorporating geologic map. Production data consists of time series of pressure and flow rate that are direct measurements of reservoir performance. Incorporating production data could provide a coarse scale map of permeability. Despite increasing availability of secondary data, integrating those data is not straightforward because of the various scale of each data. For instance, seismic data are typically at a coarser vertical resolution than geological models, usually 10 – 100 times the resolution of a geologic modeling cell although the horizontal resolution of seismic data is often comparable with the modeling cells. A geologic map may be established from a geologist's hand-drawing or analog database from similar depositional settings at a relatively large scale. Production data are measured in a single point but represent a large volume and they are interpreted as effective properties representing that volume. All these issues related with scale, precision and coverage should be overcome when constructing numerical models. Figure 1.1 illustrates the varying degree of vertical resolution and reservoir coverage of available data.

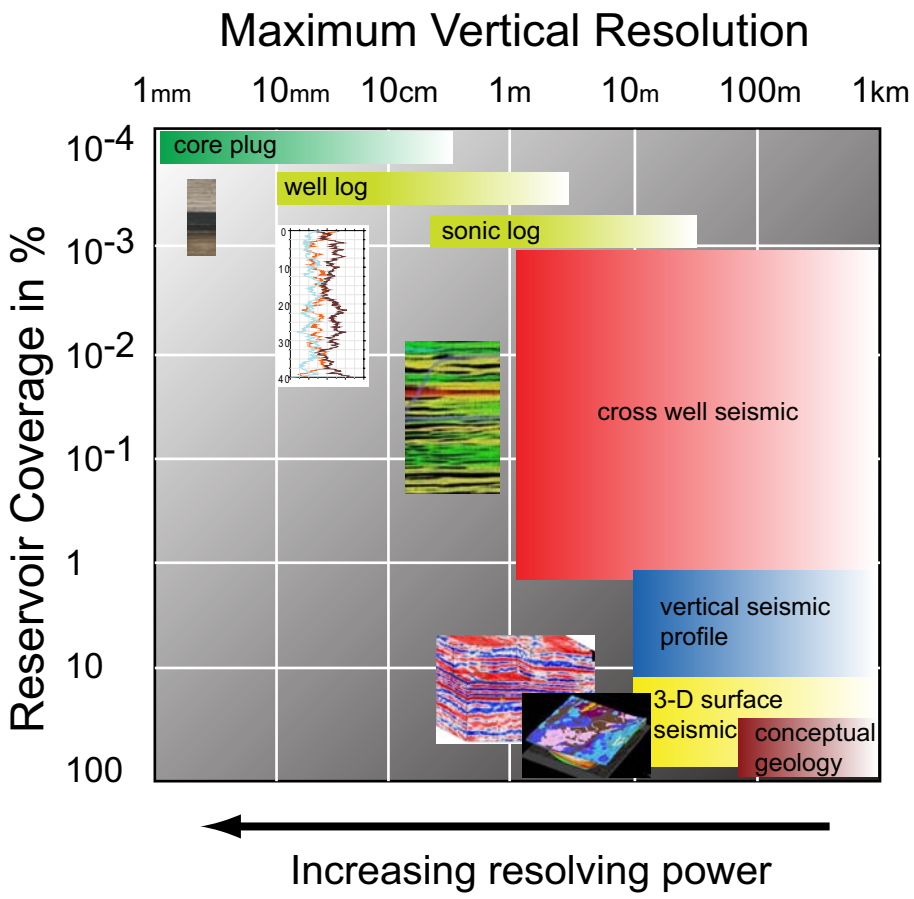

Figure 1.1: Various scales and reservoir coverage of data (modified from Harris and Langan, 1997)

1.1 Primary and Secondary Data

In geostatistical terminology, the data used for modeling can be divided into two types: *primary* and *secondary* data. Direct measurements of target reservoir property are denoted as *primary* data, while data that provide indirect measurements are denoted as *secondary* data. Primary data are assumed to be direct measurements of the reservoir properties being predicted, but they are sparsely available at the limited locations. Well log data are typical examples of the primary data in geostatistical applications even if the raw well data are not direct measure of the reservoir properties. Well logs are calibrated with core data and then well log inferred data are finally ready for use as the primary data. Compared to the well data, seismic data are typical examples of the secondary data. Seismic data are available exhaustively over the reservoir and they are related to the reservoir properties being modeled. Previously simulated variables related to the reservoir properties can be secondary data. Secondary data are often referred to as *soft* data

because their spatial coverage is extensive rather than primary data whose spatial extent is fairly limited. Production data measure and vertical seismic profiles are important sources of information, however, gridded data covering the entire spatial extent of study domain are considered as the secondary data of interest throughout the work. For example, seismic amplitude or inverted high resolution seismic attributes and geologic map data are taken into consideration. Integrating dynamic data with static data is another active research area (Datta-Gupta et al., 1995; Wen et al., 2005; Castro, 2006).

1.2 Data Integration

Reconciling various data types is not easy because of several problems. The procedure of geostatistical reservoir modeling with secondary data can be divided into two parts: secondary data are first integrated together generating probability distributions related to the primary variable, and then these distributions are integrated with the primary data. In the first part, secondary data with comparable scales and sample density are integrated. The correlation between primary and secondary data is modeled based on the collocated samples. The spatial variability of the primary variable is not modeled. Conditional probability distributions given the secondary values are derived in this step. In the second part, results from secondary data integration are combined with available primary data. The cross correlation between the primary and the integrated results from the first step are modeled. A spatial interpolator such as cokriging is then applied to predict the primary attribute.

The sketch shown in Figure 1.2 demonstrates the overall workflow for reservoir modeling in the presence of multiple secondary data. Exhaustiveness of the secondary data is an inherent assumption. Qualitative maps from geologic interpretation should be converted into digitized images. Data aggregation step is aimed at reducing the number of original secondary data by removing irrelevant data, merging the relevant secondary data and both removing and merging. The data aggregating step should be performed when too many secondary data, e.g., more than 6, are initially prepared. Merged data will be treated as new secondary data for subsequent integration. In the first integration step, the primary data are used only for calibrating the relation between the primary and a set of secondary data. The spatial correlation of the primary data is not considered in this step. No scale difference is assumed among the gridded secondary data. As a result of the first step, several secondary data are converted into a single probability or probability distribution term summarizing all secondary information. The relevance of the secondary data to the primary data is fully accounted for in this step. For instance, higher

acoustic impedance may represent lower porosity or lower proportion of porous rock, and this relation is quantified through probability distribution modeling. The second part in the overall workflow (Figure 1.2) is to combine the primary data and the secondary data-derived probabilities or probability distribution. Spatial cross correlation is modeled in this step. Although the multiple secondary data are initially considered, a single calibrated secondary variable is used hereafter because the first step integrates the multiple secondary data into a single secondary derived variable. The effort of cross variogram modeling is considerably reduced; one cross variogram is necessary regardless of the number of secondary data. The secondary data themselves could be used as secondary variables for estimation and simulation without first integration step. The secondary data calibration enters through the modeling of cross correlation between the primary and secondary data. The relevance and redundancy of the secondary data are implicitly modeled in cokriging (Journel and Huijbregts, 1978). Despite the flexibility of cokriging, the two step modeling process is preferred because: (1) the inference of the cross variogram becomes tedious in a direct use of secondary data, (2) any non-linear relations among secondary data can be modeled in the secondary data integration, and (3) the integrated results themselves may give useful information about the spatial variability of the primary variable which could be used for reservoir management.

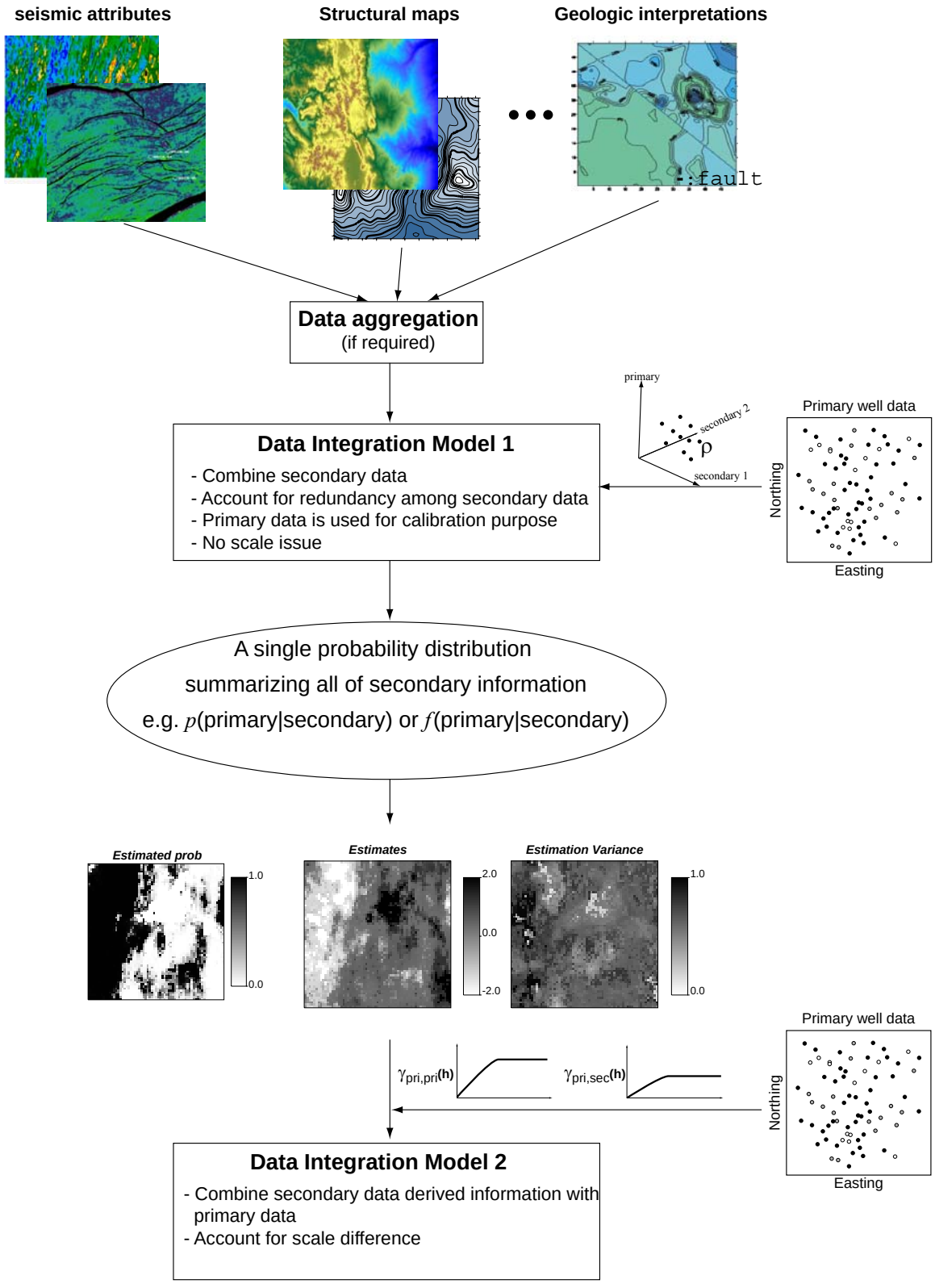

Figure 1.2: A workflow of geostatistical reservoir modeling in the presence of multiple secondary data.

Cokriging is a spatial interpolator based on the spatial cross correlation; it is a well established method for the second integration step of the workflow demonstrated in Figure 1.2. The scale differences are accounted for by volume averaging covariances, and the redundancy of the conditioning data are considered in the cokriging system of equations.

1.3 Problem Setting

This dissertation primarily focuses on the development of statistical approaches to integrate secondary data. The necessity of an integrated probability that honors all of the given data is universal in many scientific disciplines. Some previous works reached this goal by combining probabilities that are individually calibrated with each data: see Winkler (1981), Bordley (1982) and Clemen and Winkler (1999) in decision analysis, Lee et al. (1987) and Benediktsson and Swain (1992) in image data fusion, and Journel (2002), Krishnan (2004), Krishnan et al. (2005) and Polyakova and Journel (2007) in petroleum reservoir modeling. Individual conditional probabilities, for example, p(sand|secondary data), can be the result of a physical equation or statistical calibration. The univariate conditional probabilities are then combined leading to a unified probability that is assumed to be jointly conditioned to all secondary data. The joint relation modeling of the given data is not performed. In this approach, the important issue is to reliably account for the *redundancy* or dependency among the secondary data. Data redundancy is used as a term describing how much information originating from the diverse data are redundant or overlapped. Redundancy could be alternatively interpreted as correlation between data; high correlation means high redundancy and low correlation means less redundancy. As pointed out by previous works, properly accounting for redundancy is crucial in the final probability estimate (Benediktsson and Swain, 1992; Krishnan et al., 2004). Results could be highly biased if the redundancy is not properly considered.

Another approach to integrate multiple secondary data is to model the joint relations directly rather than calibrating and unifying the source-specific probabilities. In this approach, the multivariate distribution is directly modeled and redundancy is implicitly accounted for through the joint modeling. An external redundancy calibration, thus, is not required. Figure 1.3 demonstrates a brief sketch of two different methods to obtain the final probability conditioned to all secondary data.

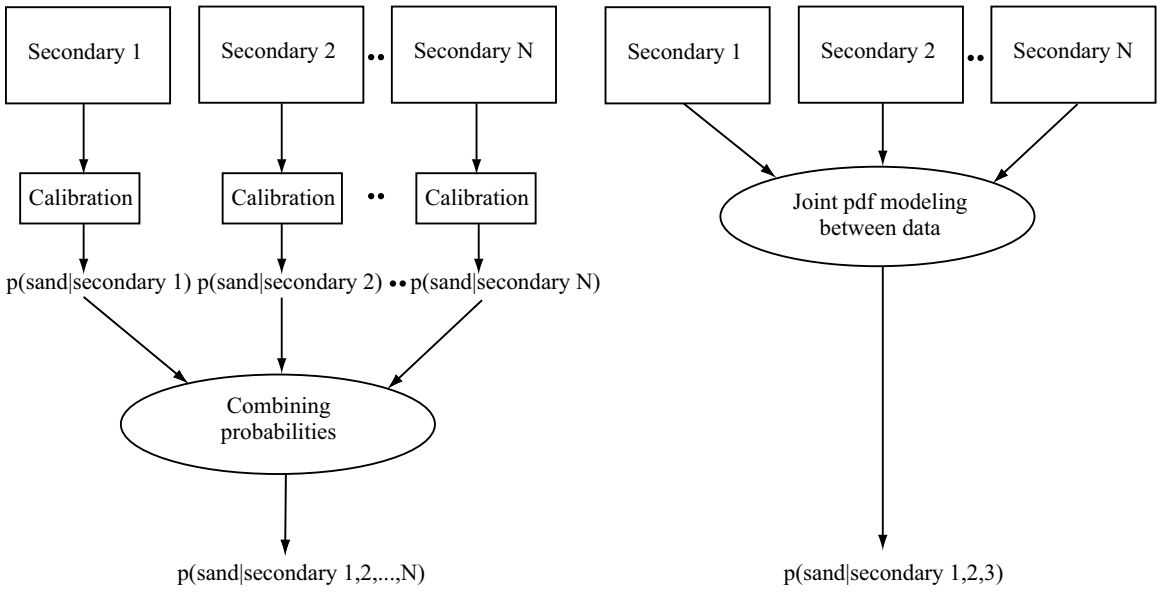

Figure 1.3: An illustration for showing two different methods to estimate final conditional probability given multiple secondary data.

Some of previous works used machine learning algorithms (Saggaf et al., 2003; Saggaf and Robinson, 2003; de Matos et al., 2007) and others used a statistical nonparametric technique for the multivariate modeling (Dumay and Fournier, 1988; Fournier and Derain, 1995; Mukerji et al., 2001; John et al., 2008). In the joint modeling approach, the complex multivariate features of the data are reproduced and redundancy between the secondary data is implicitly accounted for.

Figure 1.4 illustrates the effect of incremental redundant information with and without considering redundancy. Probability of sand is estimated at an unsampled location with varying levels of secondary data. Each secondary data has a linear correlation of about 0.46 to the primary variable, and the secondary data themselves have linear correlations between 0.46 – 0.82. The conditional probability of sand is derived by the developed multivariate modeling method (properly accounting for redundancy), and by probability combination method with independence assumption (no accounting for redundancy). These probabilities are represented as dashed and solid lines, respectively in Figure 1.4. The global proportion of sand is taken when no secondary data are considered. As the secondary data are used, the conditional probability of sand increases or decreases because more secondary data gives us more confidence of being sand or not being sand at the estimation location. Uncertainty of being sand and not being sand, thus, is decreased. This behavior is observed in the estimated probability shown as red and blue in Figure 1.4. The estimated conditional probability of sand; however, become close to 0 or 1 too quickly when the data redundancy is ignored. For example, the conditional probability of sand becomes 0.99 when

four secondary data are integrated without considering redundancy. This very high or very low probability seems to be good in that the uncertainty is reduced in the resulting probability, however, it has a risk of overestimation. The result with accounting for redundancy shows that the probability is not as close to the extremes as the result without accounting for redundancy. The increase in the estimated probability is not steep. The additional data becomes less helpful if the added data are redundant. No or incorrectly accounting for redundancy leads to bias in the estimated probability and it affects the final stochastic models.

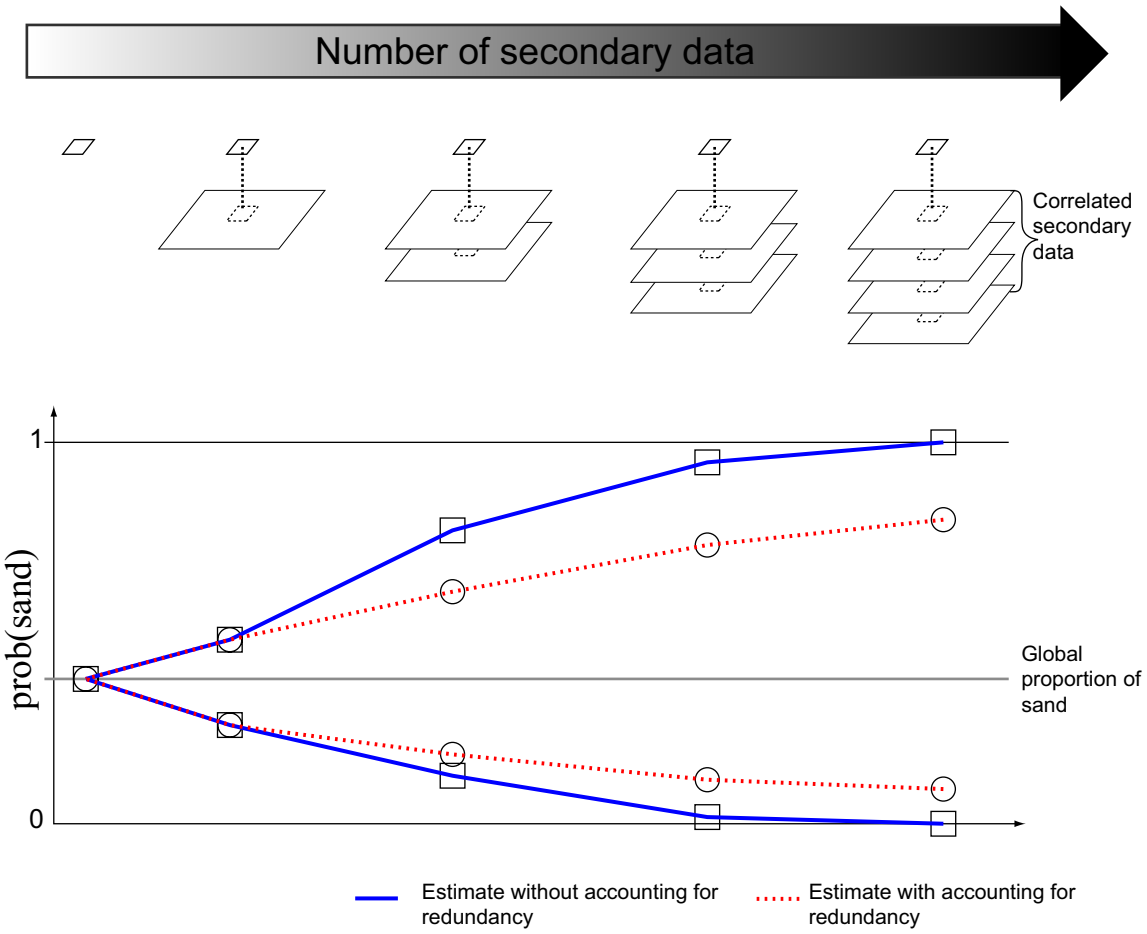

Figure 1.4: An example illustrating incremental information impact on the probability estimate. Probabilities are estimated with and without accounting for data redundancy.

In the reservoir modeling studies, the use of multivariate density modeling is not new. This dissertation advances a nonparametric multivariate analysis framework further; the joint relation of the data is modeled in which different types of the data is not an issue and it is corrected by the distribution constraints. The developed methodology leads to the joint distribution that ultimately

satisfies all axioms of probability distribution functions as well as the complex features among the given data.

1.4 Dissertation Outline

Chapter 2 presents an overview of probabilistic modeling and fundamental geostatistical concepts. Random function concepts and spatial variability are briefly introduced. Collocated cokriging method is explained as a method to integrate primary well data and secondary derived results. Debiasing with soft secondary data is addressed as a way to obtain representative global statistics. Because the advanced debiasing technique with multiple soft secondary data is proposed in Chapter 5, a key idea of debiasing is introduced in Chapter 2.

Chapter 3 introduces probability combination approaches for the secondary data integration. The existing combination models are reviewed and some interesting points among them are addressed. New weighted combination method, the Lamda-model, is developed and a key contribution of the method is discussed. Some interesting features of the different combination models are noted through a small 1-D example. The accuracy assessment criteria are introduced in Chapter 3 that are used to evaluate the result through this dissertation.

Chapter 4 and 5 are involved in developing the multivariate density estimation technique to the secondary data integration. In Chapter 4, the kernel density estimation method is introduced as a nonparametric distribution modeling technique. Issues related to the choice of kernel bandwidth and computational costs are explained. In the latter part of Chapter 4, marginality constraints are introduced and how to impose them is discussed. An iterative marginal fitting algorithm is proposed. The idea of the algorithm is to evaluate the extracted marginals from the obtained joint distribution with the given reference marginals, and to correct the obtained distribution by the amount of marginal differences. The convergence of the iteration is proved at the end of the chapter. Chapter 5 presents application of the proposed multivariate analysis framework to the facies modeling. Integrating multiple soft secondary data with varying scales and integrating soft secondary and a geologic map are studied. Chapter 6 presents a derivation of Bayesian updating in great details and proposes a new form of the updating equation. The application of the multivariate modeling method to the Bayesian updating is presented with real example.

Chapter 7 concludes the dissertation. The main contribution of this work, advantages and disadvantages of the discussed methods are reviewed including possible future work.

Appendix A discusses the factorial kriging that is used to identify the spatial features or factors based on scales. The technique can be used for filtering the unwanted noise or enhancing the spatial features in the exhaustive secondary data before the secondary data integration. The improved factorial kriging method is introduced in the appendix.

Chapter 2

Probabilistic Reservoir Modeling

A probabilistic approach is preferentially adopted for numerical reservoir modeling because the probabilistic model helps to describe the uncertainty in the constructed geologic model. At an early stage of reservoir modeling, it is especially important to model the uncertainty associated with the reservoir properties since this uncertainty could have a great impact on subsequent reservoir modeling and the accuracy of reservoir forecasting. This chapter introduces geostatistical theory, concepts and techniques that are used to quantify the uncertainty. Geostatistical estimation and simulation methods are described briefly. One could also refer to books on geostatistics for extensive discussions (Journel and Huigjbregts, 1978, Goovaerts, 1997, Isaaks and Srivastava, 1989, Wackernagel, 2003).

2.1 Probabilistic Approach

Modeling the reservoir properties involves the uncertainty from the fact that the available data is not exhaustive over the study domain. Let $\{z(\mathbf{u}_\alpha), \alpha=1,\ldots,n\}$ be the set of n measurements of attribute z at n different locations. Samples are assumed to characterize the unknown population over the domain $\boldsymbol{A}$. A model is required to characterize the attribute z over the entire domain. A model is a representation of the unknown reality. The reality may be deemed as spatial distribution of facies, porosities, permeabilities, and fluid saturations in petroleum reservoir modeling. A sequential modeling of reservoir properties is often followed. The facies rock types

are modeled first because they have first order impact on the distribution of other reservoir properties. Porosities and permeabilities are then modeled on a by-facies basis.

A deterministic model associates a single estimated value $z^*(\mathbf{u})$ to each unknown value $z(\mathbf{u})$. A single estimate may rely on the physics that governs the phenomenon and thus the single value is estimated without significant errors. The possibility of other potential states of reservoir properties is neglected in a deterministic model. Instead of a single estimated value for each unknown $z(\mathbf{u})$, the probabilistic approach generates a set of possible with corresponding probabilities. A probabilistic model quantitatively describes our uncertainty about the value by probabilities.

Probabilistic models rely on data-driven statistics. For example, the spatial dependence of a single attribute or the cross dependence of multiple attributes are inferred from the available samples.

2.2 Geostatistical Techniques for Reservoir Modeling

Geostatistics is a branch of applied statistics dealing with spatial data. The goal of geostatistical interpolation is to estimate the attribute of interest at unsampled locations and constructing the probability distribution of the attribute. The constructed probability distribution characterizes the local uncertainty. Stochastic heterogeneity modeling is based on these local uncertainty distributions. Geostatistics has played an important role in building probabilistic models of petroleum reservoirs. In particular, geostatistics is gaining applicability due to usefulness in incorporating secondary data. Geostatistical techniques can build a probability distribution conditioned to all primary and secondary information.

2.2.1 Random Function Concept

Geostatistics is largely based on the concept of a random function, whereby the set of unknown values is regarded as a set of spatially dependent random variables. The local uncertainty about the attribute value at any particular location $\mathbf{u}$ is modeled through the set of possible realizations of the random variable at that location. The random function concept allows us to account for structures in the spatial variation of the attribute. The set of realizations of the random function models the uncertainty about the spatial distribution of the attribute over the entire area. The location dependent random variable Z is denoted by $Z(\mathbf{u})$. The random variable $Z(\mathbf{u})$ is fully

characterized by its cumulative distribution function (cdf), which gives the probability that the variable Z at location $\mathbf{u}$ is no greater than any given threshold z:

$$F(\mathbf{u};z) = \text{Prob}(Z(\mathbf{u}) \le z)$$

This cdf describes our uncertainty about the true value at the unsampled location $\mathbf{u}$. Discrete variables representing facies or rock type are denoted by $S(\mathbf{u})$ and they take an integer code s=1,…,K representing different types of facies. The probability of each category s=1,…,K to prevail at location $\mathbf{u}$ is denoted as:

$$p(\mathbf{u};s) = \text{Prob}(\text{S}(\mathbf{u}) = s), s = 1,...,K$$

Of course, the K probabilities $p(\mathbf{u};s)$ must be non-negative and sum to one:

$$\sum_{s=1}^{K} p(\mathbf{u};s) = 1$$

A random function is defined as a set of usually dependent random variables Z($\mathbf{u}$), one for each location $\mathbf{u}$ in the study area $\boldsymbol{A}$, $\{Z(\mathbf{u}), \forall \mathbf{u} \in \boldsymbol{A}\}$. Any set of N locations $\mathbf{u}_\alpha$, α=1,…,N corresponds a vector of N random variables $\{Z(\mathbf{u}_1),\ldots,Z(\mathbf{u}_\alpha)\}$ that is characterized by the N-variate of N-point cdf:

$$F(\mathbf{u}_1,...,\mathbf{u}_N;z_1,...,z_N) = \text{Prob}(Z(\mathbf{u}_1) \le z_1,...,Z(\mathbf{u}_N) \le z_N)$$

This joint cdf characterizes the joint uncertainty about the N values at N locations $\{z(\mathbf{u}_1),\ldots,z(\mathbf{u}_N)\}$. This spatial dependence defined by the multivariate cdf (equivalently pdf) is referred to as spatial law of the random function $Z(\mathbf{u})$. The joint uncertainty about the N categorical values at N different locations can be similarly defined:

$$p(\mathbf{u}_1,...,\mathbf{u}_N;s_1,...,s_N) = \text{Prob}(S(\mathbf{u}_1) = s_1,...,S(\mathbf{u}_N) = s_N)$$

2.2.2 Measure of Spatial Dependence

One of the characteristics of earth science data is their spatial continuity. Whether the aim is the estimation of unknown values at unsampled locations or simply the exploratory analysis of the

data set, the spatial continuity of the variable is an important factor. The foundation of geostatistical algorithms, thus, is the description and inference of spatial continuity.

Covariance

The covariance is a measurement of similarity between data values separated by vector **h**. The conventional covariance function defined between two random variables is extended to a single attribute at different locations:

$$\begin{aligned} Cov(Z(\mathbf{u}), Z(\mathbf{u}+\mathbf{h})) &= E\{Z(\mathbf{u})Z(\mathbf{u}+\mathbf{h})\} - E\{Z(\mathbf{u})\}E\{Z(\mathbf{u}+\mathbf{h})\} \\ &= E\{Z(\mathbf{u})Z(\mathbf{u}+\mathbf{h})\} - m^2 \\ &= C(\mathbf{h}) \end{aligned}$$

where m is the stationary mean under the assumption of stationary. The covariance between non-collocated data values is then a function of the separation vector **h**. Since the covariance is dependent on the separation vector **h**, it is computed at many different distance and direction vectors. At **h**=0, the stationary covariance C(0) equals the variance of the random variable $Z(\mathbf{u})$.

Variogram

Traditionally, the geostatisticians use the variogram to characterize the spatial variability. Unlike the covariance, the semivariogram measures the average dissimilarity between data separated by a vector **h** and it is defined by:

$$2\gamma(\mathbf{h}) = E\left\{\left(Z(\mathbf{u}) - Z(\mathbf{u}+\mathbf{h})\right)^2\right\}$$

Squared differences between data separated by **h** are calculated and divided by the number of pairs within a separation vector **h**. The variogram does not call for the stationary mean, m, and variance, σ^2, however, variogram and covariance are equivalent each other in terms of characterizing the two point variability. The variogram is expanded as:

$$\begin{aligned} 2\gamma(\mathbf{h}) = E\left\{\left(Z(\mathbf{u}) - Z(\mathbf{u}+\mathbf{h})\right)^2\right\} &= E\left\{Z(\mathbf{u})^2 + Z(\mathbf{u}+\mathbf{h})^2 - 2Z(\mathbf{u})Z(\mathbf{u}+\mathbf{h})\right\} \\ &= E\left\{Z(\mathbf{u})^2\right\} + E\left\{Z(\mathbf{u}+\mathbf{h})^2\right\} - 2E\left\{Z(\mathbf{u})Z(\mathbf{u}+\mathbf{h})\right\} \\ &= 2C(0) - 2C(\mathbf{h}) \end{aligned}$$

This relation provides a key interpretation of variogram; (1) variogram and covariance have an inverse relation, (2) at **h**=0, the variogram $\gamma(0)$ is zero, (3) when **h** become large enough to have no spatial correlation, then C(**h**) becomes zero leaving $\gamma(\mathbf{h})=C(0)=\sigma^2$.

Indicator Variogram

Like the variogram of continuous random variable, spatial dependence of indicator variable can be measured. Note that indicator variables are exclusive such as:

$$I(\mathbf{u};s)=\begin{cases}1, & \text{if facies } s \text{ occurs at } \mathbf{u}\\ 0, & \text{otherwise}\end{cases}$$

Indicator covariance and variogram are calculated for the corresponding s=1,…,K as follows:

$$C(\mathbf{h};s)=E\left\{\mathrm{I}(\mathbf{u};s)\mathrm{I}(\mathbf{u}+\mathbf{h};s)\right\}-p^2(s)$$

and

$$\gamma(\mathbf{h};s)=E\left\{\left(\mathrm{I}(\mathbf{u};s)-\mathrm{I}(\mathbf{u}+\mathbf{h};s)\right)^2\right\}$$

$p(s)$ is the stationary proportion of category s=1,…,K. Different categories surely show different pattern of the spatial continuity so that the variogram, equivalently covariance of different facies may be different. The indicator variogram and covariance have the following relation:

$$\gamma(\mathbf{h};s)=C(0;s)-C(\mathbf{h};s),\ s=1,...,K$$

2.2.3 Representative Statistics

Data are rarely collected with the goal of statistical representivity. Wells are often drilled in areas with a greater probability of good reservoir quality. Core measurements are taken preferentially from good quality reservoir rock. Physical inaccessibility also leads to data clustering. In almost all cases, regular sampling is not practical. Naïve statistics from well samples could be biased. The (unbiased) statistics, mean and variance, are needed as an input to the geostatistical estimation and simulation. The importance of representative input parameters for geostatistical simulation is well discussed in Pyrcz et al. (2006). Moreover, they provide a quick understanding about the attribute being modeled over the domain: overall amount of porosities and oil saturation.

The mean computed from the unbiased distribution is a global estimate over the domain. The mean is a naïve estimate at unsampled location without introducing any complicated local estimation method.

Declustering

The original mean and standard deviation are calculated with the equal weights as:

$$\hat{m} = \frac{1}{n}\sum_{i=1}^{n} x_i \text{ and } \hat{\sigma} = \sqrt{\frac{1}{n}\sum_{i=1}^{n}(x_i - \hat{m})^2}$$

where each datum x_i, i=1,…,n has an equal impact for calculating the mean and standard deviation. Declustering techniques assign each datum different weights, w_i, i=1,…,n, based on its closeness to surrounding data (Isaaks and Srivastava 1989; Deutsch and Journel, 1998). Declustered mean and standard deviation are computed by:

$$m_{declustered} = \sum_{i=1}^{n} w_i x_i \text{ and } \sigma_{declustered} = \sqrt{\sum_{i=1}^{n} w_i (x_i - m_{declustered})^2}$$

where weights w_i are greater than 0 and add to 1. Cell declustering methods computes the weights based on the number of samples falling within the given cells (Deutsch, 2002). Polygonal method calculates the weights based on the construction of polygons of influence about each of the sample data (Isaaks and Srivastava, 1987).

Declustering with Soft Secondary Data

Declustering with the soft secondary data is another method to correct a biased distribution of a primary variable being predicted. It assumes that the soft secondary data is representative of the entire area of interest, and an understanding of the relationship between the primary and soft secondary data. The underlying relation could be either linear or non-linear. The debiased distribution of the primary variable could be obtained by numerical integral of the conditional distribution over the range of all secondary data:

$$f^{Debiased}(z) = \int_{\mathbf{y}} f(z \mid \mathbf{y}) f(\mathbf{y}) d\mathbf{y}$$

where z and $\mathbf{y}$ are random variables of the primary and secondary data. $f(z|\mathbf{y})$ is a conditional distribution of the primary given the secondary data. In Chapter 5, debiasing technique using the multivariate modeling framework is explained.

2.2.4 Geostatistical Estimation Algorithms

Kriging is a well-established methodology that provides the best linear unbiased estimate and its variance at the unsampled locations. In theory, kriging is a statistically optimal interpolator in the sense that it minimizes estimation variance when the covariance or variogram is known and under the assumption of the stationarity.

Accounting for a Single Variable

Consider the problem of estimating the value of a continuous attribute z at an unsampled location $\mathbf{u}$ using z-data available within the chosen area $\boldsymbol{A}$. Most kriging estimators are linear combination of the nearby conditioning data $\{z(\mathbf{u}_\alpha), \alpha=1,\ldots n\}$. The kriged estimate is written:

$$Z^*(\mathbf{u}) - m = \sum_{\alpha=1}^{n} \lambda(\mathbf{u}_\alpha)[Z(\mathbf{u}_\alpha) - m]$$

where n is the number of nearby data $Z(\mathbf{u}_\alpha)$ and $\lambda(\mathbf{u}_\alpha)$ are kriging weights assigned to datum $Z(\mathbf{u}_\alpha)$ at the corresponding location $\mathbf{u}_\alpha$. m is the expectation of random variable $Z(\mathbf{u})$ being assumed stationary. n is the number of associated nearby data to estimate $Z(\mathbf{u})$ at unsampled location. Solving the kriging equation is a process to achieve the kriging weights. Least square estimation allows one to define the error variance between the estimate $Z^*(\mathbf{u})$ and the unknown true value $Z(\mathbf{u})$:

$$\sigma^2_{error}(\mathbf{u}) = E\{(Z^*(\mathbf{u}) - Z(\mathbf{u}))^2\}$$

The system of simple kriging equations is derived by minimizing the error variance as follows (Goovaerts, 1997):

$$\sum_{\beta=1}^{n} \lambda(\mathbf{u}_\beta) C(\mathbf{u}_\alpha - \mathbf{u}_\beta) = C(\mathbf{u}_\alpha - \mathbf{u}) \quad \alpha = 1,\ldots,n$$

or equivalently the simple kriging equations can be written in matrix form:

$$\begin{pmatrix} C(\mathbf{u}_1-\mathbf{u}_1) & \cdots & C(\mathbf{u}_1-\mathbf{u}_n) \\ \vdots & \vdots & \vdots \\ C(\mathbf{u}_n-\mathbf{u}_1) & \cdots & C(\mathbf{u}_n-\mathbf{u}_n) \end{pmatrix} \begin{pmatrix} \lambda(\mathbf{u}_1) \\ \vdots \\ \lambda(\mathbf{u}_n) \end{pmatrix} = \begin{pmatrix} C(\mathbf{u}_1-\mathbf{u}) \\ \vdots \\ C(\mathbf{u}_n-\mathbf{u}) \end{pmatrix}$$

The full derivation of the simple kriging equations is not introduced here, but readers can refer to many introductory geostatistics materials (Journel and Huijbregrs, 1978; Goovaerts, 1997, Isaaks and Srivastava, 1989, Wackernagel, 2003). The kriging system of equation accounts for both data-to-data redundancy and data-to-unknown closeness. The left-hand side covariance matrix calls for redundancy between the (n) data.

Simple indicator kriging can be similarly derived. Indicator estimate at an unsampled location **u** is:

$$i^*(\mathbf{u};s) - p(s) = \sum_{\alpha=1}^{n} \lambda^s(\mathbf{u}_\alpha)\left[I(\mathbf{u}_\alpha;s) - p(s)\right]$$

and simple kriging weights are obtained by solving the kriging equation

$$\begin{pmatrix} C(\mathbf{u}_1-\mathbf{u}_1;s) & \cdots & C(\mathbf{u}_1-\mathbf{u}_n;s) \\ \vdots & \vdots & \vdots \\ C(\mathbf{u}_n-\mathbf{u}_1;s) & \cdots & C(\mathbf{u}_n-\mathbf{u}_n;s) \end{pmatrix} \begin{pmatrix} \lambda^s(\mathbf{u}_1) \\ \vdots \\ \lambda^s(\mathbf{u}_n) \end{pmatrix} = \begin{pmatrix} C(\mathbf{u}_1-\mathbf{u};s) \\ \vdots \\ C(\mathbf{u}_n-\mathbf{u};s) \end{pmatrix}$$

The covariance $C(\mathbf{h};s)$ and kriging weights $\lambda^s(\mathbf{u})$ will be different for the different category $s=1,\ldots,K$.

Accounting for Secondary Variables

Direct measurements of the primary attribute of interest are often supported by secondary information originated from other related attributes. The estimation generally improves when this additional and usually denser information is taken into consideration, particularly when the primary data are sparse or poorly correlated in space. Secondary information is reasonably assumed to be exhaustively sampled over the domain. Exhaustive sampling calls for the secondary information that is available at every location **u**. If the secondary data are not available at each **u** where the primary variable is to be estimated, simulating the secondary data is a

reasonable approximation to complete the exhaustiveness of the secondary information (Almeida and Journel, 1994).

Locally varying means Approach

The secondary data are integrated as a local mean when estimating the primary variable. Stationary mean m is replaced by $m(\mathbf{u})$ calibrated from the secondary data:

$$Z^*(\mathbf{u}) - m(\mathbf{u}) = \sum_{\alpha=1}^{n} \lambda^{LVM}(\mathbf{u}_\alpha)[Z(\mathbf{u}_\alpha) - m(\mathbf{u}_\alpha)]$$

This approach is simple way to incorporate secondary data. A shortcoming of the use of secondary data as a locally varying means is that the information extracted from the soft secondary data may not all relate to trends of the primary variable (Kupfersberger et al., 1998). Besides, the ways of use as local means does not take into account the spatial correlation of primary and secondary data.

The Collocated Cokriging Approach

Kriging accounts for the spatial dependence of a single variable. Cokriging is a multivariate extension of kriging; it accounts for spatial correlation of the primary variable, spatial correlation of the secondary variable, and cross spatial correlation of the primary and secondary variable (Goovaerts, 1997; Wackernagel, 2003). Collocated cokriging is a simplified form of cokriging where the neighborhood of the secondary variable is reduced to the estimation location only. The value of the secondary variable Y($\mathbf{u}$) are said to be collocated with the variable of interest $Z(\mathbf{u})$ at the estimation location $\mathbf{u}$.

Consider the situation where the primary variable Z($\mathbf{u}$) is estimated using the nearby primary data Z($\mathbf{u}_\alpha$) and the secondary data Y($\mathbf{u}$). Then, the estimate of the primary variable Z($\mathbf{u}$) is written as:

$$Z^*(\mathbf{u}) - m = \sum_{\alpha=1}^{n} \lambda(\mathbf{u}_\alpha)\left[z(\mathbf{u}_\alpha) - m\right] + \mu\left[Y(\mathbf{u}) - m_Y\right]$$

where λs are the weights assigned to the primary data z($\mathbf{u}_\alpha$), α=1,…,n and μ is the weight assigned to the collocated secondary data Y($\mathbf{u}$). The means of the primary and secondary variable

are denoted by m and m_Y, respectively. The cokriging equation is derived by minimizing the error variance:

$$\sigma^2_{error}(\mathbf{u}) = E\left\{(Z^*(\mathbf{u}) - Z(\mathbf{u}))^2\right\}$$

The full system of collocated cokriging equation is followed by in a matrix form:

$$\begin{bmatrix} C_{ZZ}(\mathbf{u}_1-\mathbf{u}_1) & \cdots & C_{ZZ}(\mathbf{u}_1-\mathbf{u}_a) & C_{ZY}(\mathbf{u}_1-\mathbf{u}) \\ \vdots & \ddots & \vdots & \vdots \\ C_{ZZ}(\mathbf{u}_\alpha-\mathbf{u}_1) & \cdots & C_{ZZ}(\mathbf{u}_\alpha-\mathbf{u}_a) & C_{ZY}(\mathbf{u}_\alpha-\mathbf{u}) \\ C_{YZ}(\mathbf{u}-\mathbf{u}_1) & \cdots & C_{YZ}(\mathbf{u}-\mathbf{u}_\alpha) & C_{YY}(0) \end{bmatrix} \begin{bmatrix} \lambda(\mathbf{u}_1) \\ \vdots \\ \lambda(\mathbf{u}_\alpha) \\ \mu(\mathbf{u}) \end{bmatrix} = \begin{bmatrix} c_{ZZ}(\mathbf{u}_1-\mathbf{u}) \\ \vdots \\ c_{ZZ}(\mathbf{u}_1-\mathbf{u}) \\ c_{YZ}(0) \end{bmatrix}$$

where the covariance C_{zz} is the left hand matrix of the simple kriging system of $Z(\mathbf{u})$ and c_{ZZ} is the corresponding right hand side covariance vector. The vector c_{YZ} contains the cross covariances between the n samples of Z and the estimation location $\mathbf{u}$ with its collocated secondary value $Y(\mathbf{u})$. $C_{YY}(0)$ is the variance of Y and $c_{YZ}(0)$ is the cross-covariance between the collocated $Z(\mathbf{u})$ and $Y(\mathbf{u})$.

The cross covariance c_{YZ} is usually approximated using the Markov model (Journel, 1999). The collocated cokriging system of equations can be written using the Markov model for the cross covariance:

$$\begin{bmatrix} C_{ZZ}(\mathbf{u}_1-\mathbf{u}_1) & \cdots & C_{ZZ}(\mathbf{u}_1-\mathbf{u}_a) & bC_{ZZ}(\mathbf{u}_1-\mathbf{u}) \\ \vdots & \ddots & \vdots & \vdots \\ C_{ZZ}(\mathbf{u}_\alpha-\mathbf{u}_1) & \cdots & C_{ZZ}(\mathbf{u}_\alpha-\mathbf{u}_a) & bC_{ZZ}(\mathbf{u}_\alpha-\mathbf{u}) \\ bC_{ZZ}(\mathbf{u}-\mathbf{u}_1) & \cdots & bC_{ZZ}(\mathbf{u}-\mathbf{u}_\alpha) & C_{YY}(0) \end{bmatrix} \begin{bmatrix} \lambda(\mathbf{u}_1) \\ \vdots \\ \lambda(\mathbf{u}_\alpha) \\ \mu(\mathbf{u}) \end{bmatrix} = \begin{bmatrix} c_{ZZ}(\mathbf{u}_1-\mathbf{u}) \\ \vdots \\ c_{ZZ}(\mathbf{u}_1-\mathbf{u}) \\ c_{YZ}(0) \end{bmatrix}$$

where $b = \left(\sqrt{C_Z(0)} \Big/ \sqrt{C_Y(0)}\right) \cdot \rho_{YZ}(0)$, $\rho_{YZ}(0)$ is the correlation coefficient of the collocated Z and Y. The collocated cokriging approach with the Markov model only requires the primary variable covariance function, the variance of the secondary data and the correlation coefficient between the primary and the secondary data. Retaining the collocated secondary data may not affect the estimates, however, the cokriging variances are often overestimated which can cause a serious problem in a sequential simulation (Deutsch, 2002).

The Bayesian Updating Approach

The collocated cokriging with the Markov model is equivalent to the Bayesian expression of the cokriging estimate (Doyen, 1996; Chiles and Delfiner, 1999). For example, the cokriging estimate and variance are the mean and variance of the probability distribution conditioned to the nearby primary and the collocated secondary data:

$$f(z(\mathbf{u}) \mid z(\mathbf{u}_1),...,z(\mathbf{u}_\alpha), y(\mathbf{u})) = \frac{f(z(\mathbf{u}) \mid z(\mathbf{u}_1),...,z(\mathbf{u}_\alpha))}{f(z(\mathbf{u}))} f(z(\mathbf{u})) f(y(\mathbf{u}) \mid z(\mathbf{u})) \cdot C, \ \mathbf{u} \in A$$

where the C is the normalizing term and it does not affect the mean and variance of the probability distribution. The conditional independence assumption is made to separate the $f(z(\mathbf{u})|z(\mathbf{u}_1),\ldots, z(\mathbf{u}_\alpha),y(\mathbf{u})$ into the product of $f(z(\mathbf{u})|z(\mathbf{u}_1),\ldots,z(\mathbf{u}_\alpha))$ and $f(y(\mathbf{u})|z(\mathbf{u}))$. The conditional probability function $f(y(\mathbf{u})|z(\mathbf{u}))$ is a likelihood because the $z(\mathbf{u})$ is the unknown and the $y(\mathbf{u})$ is the given known value. It is re-expressed as:

$$f(y(\mathbf{u}) \mid z(\mathbf{u})) = \frac{f(z(\mathbf{u}) \mid y(\mathbf{u}))}{f(z(\mathbf{u}))} f(y(\mathbf{u}))$$

and then the following Bayesian updating equation can be derived,

$$f(z(\mathbf{u}) \mid z(\mathbf{u}_1),...,z(\mathbf{u}_\alpha), y(\mathbf{u})) = \frac{f(z(\mathbf{u}) \mid z(\mathbf{u}_1),...,z(\mathbf{u}_\alpha))}{f(z(\mathbf{u}))} \frac{f(z(\mathbf{u}) \mid y(\mathbf{u}))}{f(z(\mathbf{u}))} f(z(\mathbf{u})) \cdot C, \ \mathbf{u} \in A$$

where the probability distribution functions that are not related to the $z(\mathbf{u})$ are absorbed in the normalizing term C. Finally, the conditional probability function of interest is shown as the production of two probability functions conditioned to the set of the primary data $z(\mathbf{u}_1),\ldots,z(\mathbf{u}_\alpha)$ and the collocated secondary data $y(\mathbf{u})$, and the univariate probability function of $z(\mathbf{u})$, $f(z(\mathbf{u}))$. Under the stationarity of the $z(\mathbf{u})$, the $f(z(\mathbf{u}))$ is replaced as the global pdf $f(z)$. The simple kriging estimate and estimation variance are the mean and variance of $f(z(\mathbf{u})|z(\mathbf{u}_1),\ldots,z(\mathbf{u}_\alpha))$ under the multiGaussian assumption among $z(\mathbf{u}),z(\mathbf{u}_1),\ldots,z(\mathbf{u}_\alpha)$ (Verly, 1983). The mean and variance of $f(z(\mathbf{u})|y(\mathbf{u}))$ can be simplified using the correlation coefficient between Z and Y. Thus, the final estimate and estimation variance of $z(\mathbf{u})$ that are the mean and variance of the conditional probability function above can be obtained by the simple kriging estimate and estimation variance, linear correlation coefficient, and the global mean and variance. Similarly, the Bayesian expression for the categorical variable can be shown as,

$$p(i(\mathbf{u}) \mid i(\mathbf{u}_1),...,i(\mathbf{u}_\alpha), y(\mathbf{u})) = \frac{p(i(\mathbf{u}) \mid i(\mathbf{u}_1),...,i(\mathbf{u}_\alpha))}{p(s)} \frac{p(i(\mathbf{u}) \mid y(\mathbf{u}))}{p(s)} p(s) \cdot C, \ \mathbf{u} \in A$$

where the conditioning data $i(\mathbf{u}_\alpha)$, α=1,…,n are indicators. These Bayesian expressions are often useful to understand clearly: they decompose the final conditional probability of interest into the primary variable-related and the secondary variable-related terms.

2.2.5 Geostatistical Simulation

Geostatistical simulation adds a random component to the kriging estimate to reproduce the realistic heterogeneity of the reservoir. Multiple realizations of heterogeneity are obtained from randomly drawing different random components. These realizations can provide an assessment of the uncertainty about the reservoir properties being modeled. Motivations for the simulation are in two aspects. First of all, geostatistical simulation corrects the smoothness in the kriging estimates. Kriging estimates are theoretically right, however, it smears out the high frequency features (Wackernagel, 2003). Secondly, geostatistical simulation allows the calculation of the joint uncertainty when several locations are considered together. Quantifying the joint uncertainty is very important to reflect the geologic heterogeneity and critical to the reservoir performance.

There are many approaches that can be used for the geostatistical simulation. The most popular and simplest technique is the sequential Gaussian simulation for the continuous variable, and sequential indicator simulation for the categorical variable. Sequential simulation is based on the application of the Bayes law to decompose the multivariate distribution at different locations into a series of conditional distributions for each location. The random component that corrects kriging smoothness is drawn from the local probability distributions that are obtained from kriging or cokriging. Procedures for sequential simulation are well described in Goovaerts (1997), Deutsch (2002) and other standard geostatistics references.

2.3 Discussions

Fundamental concepts of geostatistics are briefly reviewed. The goal of the geostatistical estimation algorithm is to build the local conditional probability distribution. Geostatistical simulation describes the uncertainty of the underlying geologic variability based on the local conditional distribution.

Cokriging is a well-established technique to build local distribution using the primary and the secondary data. Tedious efforts for cross variogram modeling required for the cokriging can be eliminated using the Markov assumption, and thus, the collocated cokriging with the Markov model is widely used in practice.

The collocated cokriging estimate and Bayesian expressions are exactly equivalent. However, Bayesian form is easier to understand how different distributions conditioned to different data are combined leading to a final conditional distribution.

Chapter 3

Probability Combination Schemes

This chapter presents probability combination methods for calculating the probability of a primary attribute conditioned to multiple secondary data. These approaches combine conditional probabilities derived from calibrating each secondary data, possibly with different calibration techniques. Probability combination schemes (PCS in short) have been developed independently in many research areas in order to find a unified probability from using several single source derived probabilities (Winkler, 1981; Bordley, 1982; Lee et al., 1987; Benediktsson and Swain 1992; Clemen and Winkler, 1999). Probability combination schemes were recently applied in reservoir modeling for an improved reservoir characterization using various secondary data (Krishnan, 2004; Liu et al., 2004; Polyakova and Journel, 2007; Castro et al., 2005).

The main goal of PCS is to approximate the target conditional probability through linking the individual probabilities that are computed using individual data sources. The use of PCS is very attractive when the conditional probability $p(s|D_1,\ldots,D_m)$ where s is facies or rock type and $(D_1,\ldots,D_m)$ are m secondary data, is hard to obtain or even impossible to model in a coherent manner. Alternatively, there may be no access to the data themselves directly but only access to the calibrated probabilities $p(s|D_i)$. For example, the data D_i for i=1,…,m can be seismic attributes, trends from geology, analogue data and expert knowledge. PCS approaches approximate the joint probability by linking probabilities individually calibrated with data D_i, i=1,…,m subject to the primary variable s. Inference of individual probabilities $p(s|D_i)$ is not an interest. Each data could have a different calibration method based on statistical modeling,

physical process equations or expert judgment. This chapter focuses on how to combine conditional probabilities that have been already calculated.

Section 3.1 investigates how the probability distribution of secondary data can be decomposed into the combination of univariate conditional probabilities. Sections 3.2 and 3.3 introduce several combination models that have been developed in the geostatistical literature and a new weighted combination model developed in this dissertation. Sections 3.4 and 3.5 show the application of the PCS to 1-D synthetic and 2-D field data. An assessment tool for the estimated local probabilities is discussed in Section 3.6. Different PCS are evaluated using the discussed accuracy criteria. Section 3.7 considers building a high resolution facies model from secondary data. The results obtained from different PCS are integrated into the stochastic modeling and the influence of them is investigated.

3.1 Combining Probabilities

Secondary data are denoted as D_i, i=1,…,m where m is the number of secondary data and they can be seismic attributes, trends, analogue data, expert knowledge. Discrete rock type or facies are considered as the primary attribute of interest denoted as s=1,…,K, where K is the number of discrete facies or rock types. The probability of interest is then expressed as $p(\mathbf{u};s|D_1(\mathbf{u})\ldots,D_m(\mathbf{u}))$, $\mathbf{u}\in\boldsymbol{A}$ where $\boldsymbol{A}$ is the entire domain of study. The location vector $\mathbf{u}$ is shown since the final conditional probability is locally estimated depending on the local conditioning data $(D_1(\mathbf{u}),\ldots,D_m(\mathbf{u}))$. For the simple notation, the location vector $\mathbf{u}$ is dropped hereafter. This conditional probability is exactly expanded by the definition of a conditional probability (Bayes law):

$$p(s \mid D_1,...,D_m) = \frac{f(D_1,...,D_m \mid s)p(s)}{f(D_1,...,D_m)} \tag{3-1}$$

$p(s)$ is the global proportion that is constant over the area, $f(D_1,\ldots,D_m)$ is the joint distribution of the secondary data, and $f(D_1,\ldots,D_m|s)$ is the likelihood. The global proportion of s=1,…,K, $p(s)$, is a prior information derived from the direct measurements at well locations. Sand and shale, for example, cannot exist simultaneously at a single location. Thus, the global proportion can be obtained by simply counting the number of samples out of total samples for each facies. Knowledge of the joint relation between $(D_1,\ldots,D_m)$ conditioned to s is required to derive the conditional probability $p(s|D_1,\ldots,D_m)$. The main motivation of probability combination schemes

is based on the unavailability of the joint distribution. Some assumptions are required to approximate the conditional probability without modeling the joint probability distribution.

3.2 Simple Combination Models

A simple combination model assumes the data ($D_1,\ldots,D_m$) are conditionally independent. These assumptions greatly simplify the process of calculating the final conditional probability at the possible expense of a loss in accuracy of the probability estimate.

3.2.1 Conditional Independence Model

A less strict assumption is that the secondary data ($D_1,\ldots,D_m$) are independent conditioned to the possible outcomes of the primary variable s=1,…,K. The conditional independence assumption decomposes the joint probability $f(D_1,\ldots,D_m|s)$ into the linear product of $f(D_1|s)\times\cdots\times f(D_m|s)$. Equation (3-1) is expanded as:

$$\begin{aligned} & p(s \mid D_1,...,D_m) \\ & = \frac{f(D_1,...,D_m \mid s)p(s)}{f(D_1,...,D_m)} \\ & = \frac{f(D_1 \mid s)\cdots f(D_m \mid s)p(s)}{f(D_1,...,D_m)} \\ & = \frac{p(s \mid D_1)}{p(s)}\cdots\frac{p(s \mid D_m)}{p(s)}p(s)\frac{f(D_1)\cdots f(D_m)}{f(D_1,...,D_m)} \end{aligned} \tag{3-2}$$

Because $f(D_1)\times\cdots\times f(D_m)/f(D_1,\ldots,D_m)$ does not affect the final conditional probability $p(s|D_1,\ldots,D_m)$, it is collapsed into a normalizing term C:

$$p(s \mid D_1,...,D_m) = \frac{p(s \mid D_1)}{p(s)}\cdots\frac{p(s \mid D_m)}{p(s)}p(s)C \tag{3-3}$$

Thus, the conditional probability $p(s|D_1,\ldots,D_m)$ can be now approximated by the product of probability ratios $p(s|D_i)/p(s)$, i=1,…,m and the global proportion $p(s)$. For example, consider three data seen as three different secondary data D_1, D_2 and D_3 informing about the probability of facies s=1,2 and 3 occurring. The global proportion and individual probability of facies are illustrated in the table below,

	$p(s)$	$p(s\|D_1)$	$p(s\|D_2)$	$p(s\|D_1,D_2)$
s=1	0.2	0.3	0.45	0.535
s=2	0.3	0.4	0.35	0.37
s=3	0.5	0.3	0.2	0.095
marginal	1	1	1	1

Note that each data assess the possibility of facies s=1, 2 at higher probability than the global proportion, and that of facies s=3 at lower probability than the global proportion. The combined probability is shown in the last column. The marginal sum of $p(s|D_1,D_2)$ amounts to 1 because of standardization. An interesting aspect of the combined probabilities is that they become larger or smaller if the individual conditional probabilities are all larger or smaller than the global proportion. This phenomenon of pushing the resulting probability toward to the extremes is called non-convexity and this property is discussed more in sections 3.4 and 3.5 through examples. Note that the probabilities shown in the table above are arbitrarily injected merely to see the non-convexity of the combined probability.

3.2.2 Permanence of Ratios Model (PR model)

Journel (2002) developed a permanence of ratios (PR) model that approximates the probability assuming that ratios of probability increments from different data sources are constant. Although the PR model was independently developed in the geostatistics literature, it is also used in other fields (Pearl, 1988; Friedman et al., 1997). The principle of PR is that ratios are more stable than the increments themselves (Journel, 2002). Consider the ratios of probability of s:

$$a = \frac{p(\tilde{s})}{p(s)} \in [0, \infty]$$

what can be interpreted as the probability distance to s occurring, e.g. if $p(s)$=1 (s certainly occurs) $\Rightarrow$ a=0 (distance) and if $p(s)$=0 (s certainly does not occur)$\Rightarrow$ a=∞ (infinite distance). Note that $p(\tilde{s})$ is the probability of not s that is, $1-p(s)$. Similarly, the probability distances to s given the data D_1 and D_2 are, respectively:

$$d_1 = \frac{p(\tilde{s} \mid D_1)}{p(s \mid D_1)} \in [0,\infty] \text{ and } d_2 = \frac{p(\tilde{s} \mid D_2)}{p(s \mid D_2)} \in [0,\infty]$$

The probability distance to be estimated is then:

$$x = \frac{p(\tilde{s} \mid D_1, D_2)}{p(s \mid D_1, D_2)} \in [0,\infty]$$

Permanence of ratios assumes that the incremental contribution of D_2 to an event s with knowledge of D_1 is the same as that of D_2 to an event s without knowing D_1. This assumption is expressed as the following equality:

$$\frac{x}{d_1} = \frac{d_2}{a}$$

The ratio x/d_1 represents the contribution of data D_2 knowing D_1; if data D_2 has no contribution to s then the ratio becomes unity. The ratio d_2/a represents the contribution of data D_2 to s. The conditional probability of interest $p(s|D_1,D_2)$ is now derived from the PR model (denoted as p_{PR}):

$$p_{PR}(s \mid D_1, D_2) = \frac{1}{1+x} = \frac{a}{a + d_1 d_2} = \frac{\dfrac{1-p(s)}{p(s)}}{\dfrac{1-p(s)}{p(s)} + \left(\dfrac{1-p(s \mid D_1)}{p(s \mid D_1)}\right)\left(\dfrac{1-p(s \mid D_2)}{p(s \mid D_2)}\right)} \in [0,1]$$

This equation can be generalized with many conditioning data ($D_1,\ldots,D_m$) by:

$$p_{PR}(s \mid D_1, ..., D_m) = \frac{\left(\dfrac{1-p(s)}{p(s)}\right)^{m-1}}{\left(\dfrac{1-p(s)}{p(s)}\right)^{m-1} + \prod_{i=1}^{m}\left(\dfrac{1-p(s \mid D_i)}{p(s \mid D_i)}\right)} \in [0,1] \qquad (3\text{-}4)$$

The estimated probability p_{PR} meets the closure condition and non negativity regardless of number of conditioning data D_i, i=1,…,m. The PR model, however, is limited to binary variable modeling. For instance, consider that s can take three outcomes such as sand (coded as s=1), intermediate sand (coded as s=2) and shale (coded as s=3). Arbitrary $p(s)$, $p(s|D_1)$ and $p(s|D_2)$,

s=1,2,3 are shown in the table below. The combined probability using the PR model is indicated in the right column.

	$p(s)$	$p(s\|D_1)$	$p(s\|D_2)$	$p_{PR}(s\|D_1,D_2)$
s=1	0.2	0.3	0.45	0.584
s=2	0.3	0.4	0.35	0.456
s=3	0.5	0.3	0.2	0.097
marginal	1	1	1	1.136

The marginal sum of $p_{PR}(s|D_1,D_2)$ does not equal to 1 as shown in the lower right corner. This violation of the closure condition is not limited to this particular numeric example.

The assumption made in the PR model is the same as the independence assumption of (D_1,…,D_m) conditioned to primary variable s. Equivalence of the PR model and conditional independence is proved for the binary case. As shown in Equation (3-3), the conditional independence obtains the probability of interest as (denoted as p_{CI}):

$$p_{CI}(s \mid D_1,...,D_m) = p(s)\frac{p(s \mid D_1)}{p(s)} \times \cdots \times \frac{p(s \mid D_m)}{p(s)} C \qquad (3\text{-}5)$$
$$= p(s)\prod_{i=1}^{m}\left(\frac{p(s \mid D_i)}{p(s)}\right) C \in [0,1]$$

C is the unknown normalizing term. By enforcing the closure condition, the C term will be removed by standardization:

$$p_{CI}(s \mid D_1,...,D_m) = \frac{p(s)\prod_{i=1}^{m}\left(\frac{p(s \mid D_i)}{p(s)}\right)C}{p(s)\prod_{i=1}^{m}\left(\frac{p(s \mid D_i)}{p(s)}\right)C + (1-p(s))\prod_{i=1}^{m}\left(\frac{1-p(s \mid D_i)}{1-p(s)}\right)C}$$

$$= \frac{1}{1+\left(\frac{1-p(s)}{p(s)}\right)\left(\frac{p(s)}{1-p(s)}\right)^{m}\prod_{i=1}^{m}\left(\frac{1-p(s \mid D_i)}{p(s \mid D_i)}\right)}$$

$$= \frac{\left(\frac{1-p(s)}{p(s)}\right)^{m-1}}{\left(\frac{1-p(s)}{p(s)}\right)^{m-1} + \prod_{i=1}^{m}\left(\frac{1-p(s \mid D_i)}{p(s \mid D_i)}\right)} = p_{PR}(s \mid D_1,...,D_m) \in [0,1]$$

This equivalence holds for the binary case. The PR model is not strictly valid when more than two categories are considered. Instead, conditional independence can be used for any case because it enforces the closure condition, for example when three categories are considered with s=1,2, and 3:

$$p_{CI}(s \mid D_1,...,D_m) = \frac{p(s)\prod_{i=1}^{m}\left(\frac{p(s \mid D_i)}{p(s)}\right)}{p(s)\prod_{i=1}^{m}\left(\frac{p(s \mid D_i)}{p(s)}\right) + p(s')\prod_{i=1}^{m}\left(\frac{p(s' \mid D_i)}{p(s')}\right) + p(s'')\prod_{i=1}^{m}\left(\frac{p(s'' \mid D_i)}{p(s'')}\right)} \in [0,1] \quad (3\text{-}6)$$

where $s' \neq s'' \neq s$=1,2,3. The conditional independence model should be used in the case of multiple categories.

The permanence of ratios and conditional independence models assume independence among the secondary data conditioned to the primary attribute of interest. By adopting this independence assumption, the task of combining probabilities is simplified into the product of individual probabilities, $p(s|D_i)$ for i=1,…,m. Correlation or redundancy among the data is simply ignored for the convenience of calculation. In some cases, however, those simple models could introduce a serious bias in the resulting probability. Advanced probability combination methods to account for data redundancy are discussed next.

3.3 Weighted Combination Model

Ignoring the data redundancy assumes all secondary data are uncorrelated with little information overlap. This could make the resulting combined probability close to an extreme probability of 0 or 1 as shown in the introductory example in Figure 1.4. The property of falling outside the input probability $p(s)$ and $p(s|D_i)$, is called non-convex property. This non-convexity is desirable if the data are not highly correlated with each other, but may not be desirable if the data are highly correlated. In reality, the secondary data are correlated to some degree through the primary variable being modeled.

Weighted combination models were developed to mitigate the effect of the independence assumption by adjusting the relative influence of the secondary data. If the data ($D_1,\ldots,D_m$) are redundant with moderate to high degree then their influence should be reduced because some of the data largely explain the rest of data. The tau model is one example proposed by Journel (2002). In the tau model, probability ratios are weighted by exponents denoted as τ. Varying the τ values adjusts the impact of individual probabilities on the combined probability. Krishanan (2008) derived analytical solutions of these weight parameters that exactly quantify the redundancy of the given conditioning data. Although the solution is analytically derived, they are case dependent without general form. Another model, the Lamda model, is developed in this thesis. Power weights are imposed on the individual probability ratios, but the calibration is different from the Tau model. Weighted combination models can be expressed with data specific power weights ($w_1,\ldots,w_m$):

$$\frac{p(s\,|\,D_1,\ldots,D_m)}{p(s)} = \left(\frac{p(s\,|\,D_1)}{p(s)}\right)^{w_1} \times \ldots \times \left(\frac{p(s\,|\,D_m)}{p(s)}\right)^{w_m} C \tag{3-7}$$

Equation (3-7) reverts to the conditional independence model when the data specific weights w_i are all 1. If the weights are not unity, the contribution of $p(s|D_i)$ is adjusted. The degree of adjustment depends on the data redundancy.

3.3.1 Tau model

The Tau model is one example of weighted combination methods. If the weights w_i in Equation (3-7) are replaced by τ_i and the binary category is considered then the weighted combination

shown in Equation (3-7) is referred to as the Tau model. Equivalence between Equation (3-7) with the replaced τ_i and the original form of the Tau model is proved in the end of this section. The Tau model is expressed as by Journel (2002):

$$\frac{x}{d_1} = \left(\frac{d_2}{a}\right)^{\tau} \tag{3-8}$$

where τ is dependent on the relation between D_1 and D_2. The range of the parameter τ is within $[0,\infty]$ to make the resulting probability $p(s|D_1,D_2)$ in [0,1]. By introducing this power weight, the ratio (d_2/a) will be increased or decreased. Equation (3-8) can be generalized with many data ($D_1,\ldots,D_m$) by introducing successive m weights:

$$\frac{x}{a} = \prod_{i=1}^{m}\left(\frac{d_i}{a}\right)^{\tau_i} \Leftrightarrow x = a\prod_{i=1}^{m}\left(\frac{d_i}{a}\right)^{\tau_i} \tag{3-9}$$

The important factor in the Tau model is τ_i for i=1,…,m that can be in $[-\infty,\infty]$ (Krishnan, 2008). The probability of interest is derived from Equation (3-9) as:

$$x = a\prod_{i=1}^{m}\left(\frac{d_i}{a}\right)^{\tau_i} \Leftrightarrow$$

$$\frac{1-p(s\mid D_1,\ldots,D_m)}{p(s\mid D_1,\ldots,D_m)} = \frac{1-p(s)}{p(s)}\left(\frac{\frac{1-p(s\mid D_1)}{p(s\mid D_1)}}{\frac{1-p(s)}{p(s)}}\right)^{\tau_1}\times\cdots\times\left(\frac{\frac{1-p(s\mid D_m)}{p(s\mid D_m)}}{\frac{1-p(s)}{p(s)}}\right)^{\tau_m}$$

And,

$$p(s\mid D_1,\ldots,D_m) = \frac{1}{1+\frac{1-p(s)}{p(s)}\left(\frac{\frac{1-p(s\mid D_1)}{p(s\mid D_1)}}{\frac{1-p(s)}{p(s)}}\right)^{\tau_1}\times\cdots\times\left(\frac{\frac{1-p(s\mid D_m)}{p(s\mid D_m)}}{\frac{1-p(s)}{p(s)}}\right)^{\tau_m}}$$

$$= \frac{1}{1+\frac{1-p(s)}{p(s)}\left(\frac{1-p(s\mid D_1)}{p(s\mid D_1)}\times\frac{p(s)}{1-p(s)}\right)^{\tau_1}\times\cdots\times\left(\frac{1-p(s\mid D_m)}{p(s\mid D_m)}\times\frac{p(s)}{1-p(s)}\right)^{\tau_m}}$$

$$= \frac{1}{1+\frac{1-p(s)}{p(s)}\left(\frac{p(s)}{1-p(s)}\right)^{\sum_{i=1}^{m}\tau_i}\left(\frac{1-p(s\mid D_1)}{p(s\mid D_1)}\right)^{\tau_1}\times\cdots\times\left(\frac{1-p(s\mid D_m)}{p(s\mid D_m)}\right)^{\tau_m}}$$

$$= \frac{\frac{1}{\frac{1-p(s)}{p(s)}\left(\frac{p(s)}{1-p(s)}\right)^{\sum_{i=1}^{m}\tau_i}}}{\frac{1}{\frac{1-p(s)}{p(s)}\left(\frac{p(s)}{1-p(s)}\right)^{\sum_{i=1}^{m}\tau_i}}+\prod_{i=1}^{m}\left(\frac{1-p(s\mid D_i)}{p(s\mid D_i)}\right)^{\tau_i}}$$

The above equation is rearranged:

$$p_{Tau}(s\mid D_1,...,D_m)=\frac{\frac{p(s)}{1-p(s)}\left(\frac{1-p(s)}{p(s)}\right)^{\sum_{i=1}^{m}\tau_i}}{\frac{p(s)}{1-p(s)}\left(\frac{1-p(s)}{p(s)}\right)^{\sum_{i=1}^{m}\tau_i}+\prod_{i=1}^{m}\left(\frac{1-p(s\mid D_i)}{p(s\mid D_i)}\right)^{\tau_i}}\in[0,1] \tag{3-10}$$

which is the Tau model that approximates the conditional probability of interest from the weighted combination of individual probabilities. Similar to the PR model, the Tau model ensures the closure condition only for the binary case of primary variable s. The closure condition of $p_{\text{Tau}}(s|D_1,\ldots,D_m)$ over $s=1,\ldots,K$ is not guaranteed. Equation (3-10) is a standardized expression of Equation (3-7) using the complementary probability $1-p(s|D_i)$ and $1-p(s)$, which removes the constant term C as:

$$p(s\mid D_1,...,D_m)=\left(\frac{p(s\mid D_1)}{p(s)}\right)^{w_1}\times\ldots\times\left(\frac{p(s\mid D_m)}{p(s)}\right)^{w_m}p(s)C$$

$$=\frac{p(s)\prod_{i=1}^{m}\left(\frac{p(s\mid D_i)}{p(s)}\right)^{w_i}}{p(s)\prod_{i=1}^{m}\left(\frac{p(s\mid D_i)}{p(s)}\right)^{w_i}+(1-p(s))\prod_{i=1}^{m}\left(\frac{1-p(s\mid D_i)}{1-p(s)}\right)^{w_i}}$$

Note here that because the Tau and PR model holds for the binary category only the equivalence between the weighted combination with w_i shown in Equation (3-7) and the Tau model is proved for the binary case only.

$$
\begin{aligned}
p(s \mid D_1,\ldots,D_m) &= \frac{p(s)\prod_{i=1}^{m}\left(\frac{p(s \mid D_i)}{p(s)}\right)^{w_i}}{p(s)\prod_{i=1}^{m}\left(\frac{p(s \mid D_i)}{p(s)}\right)^{w_i} + (1-p(s))\prod_{i=1}^{m}\left(\frac{1-p(s \mid D_i)}{1-p(s)}\right)^{w_i}} \\
&= \frac{1}{1+\frac{1-p(s)}{p(s)}\prod_{i=1}^{m}\left(\frac{(1-p(s \mid D_i))\,p(s)}{p(s \mid D_i)(1-p(s))}\right)^{w_i}} \\
&= \frac{1}{1+\frac{1-p(s)}{p(s)}\left(\frac{p(s)}{1-p(s)}\right)^{\sum_{i=1}^{m} w_i}\prod_{i=1}^{m}\left(\frac{1-p(s \mid D_i)}{p(s \mid D_i)}\right)^{w_i}} \\
&= \frac{\frac{p(s)}{1-p(s)}\left(\frac{1-p(s)}{p(s)}\right)^{\sum_{i=1}^{m} w_i}}{\frac{p(s)}{1-p(s)}\left(\frac{1-p(s)}{p(s)}\right)^{\sum_{i=1}^{m} w_i} + \prod_{i=1}^{m}\left(\frac{1-p(s \mid D_i)}{p(s \mid D_i)}\right)^{w_i}}
\end{aligned}
$$

If the weights w_i are replaced by τ_i then the last equation in the above expansion is identical to the Tau model shown in Equation (3-10).

Finding the τ parameters is as important as the individual data calibration (Krishnan, 2008). Incorrectly selected τ values will generate wrong results. Analytical solutions of the τ parameters are shown in Krishanan (2008), however, those are obtained from specific examples with no general equation. One simple way for choosing the τ weight would be to use the linear correlation coefficient such as $\tau = 1-|\rho|$. For example, if two secondary data D_1 and D_2 are highly correlated then the full use of information in (D_1,D_2) is not necessary because information from D_1 (or D_2) is not much different from that from D_2 (or D_1). Therefore, the influence of either D_1 or D_2 should be reduced by the degree of correlation. The simple use of the linear correlation to get the τ parameters would be straightforward when only two data are considered; weight of one datum (τ_1) is fixed as 1 and weight of other data (τ_2) is extracted by $1-|\rho_{D_1D_2}|$. It is not

straightforward when more than two secondary data are considered because multivariate correlation coefficient may be required such as $\tau_1=1$, $\tau_2=1-|\rho_{D_1D_2}|$, and $\tau_3=1-|\rho_{D_1D_2D_3}|$.

3.3.2 Lamda Model

The Lamda model, an original contribution of this thesis, can be interpreted as an expanded version of conditional independence with introducing data specific weights that are denoted as λ_i, $i=1,\ldots,m$. The main principle of the Lamda model is to mitigate the independence assumption applied when decomposing the $f(D_1,\ldots,D_m|s)$ into $f(D_1|s)\times\cdots\times f(D_m|s)$. Weights are imposed on each data-specific likelihood $f(D_i|s)$ and then $p(s|D_1,\ldots,D_m)$ becomes:

$$\begin{aligned}
&p(s \mid D_1,...,D_m) \\
&= \frac{f(D_1,...,D_m \mid s)p(s)}{f(D_1,...,D_m)} \\
&= f(D_1 \mid s)^{\lambda_1} \times \cdots \times f(D_m \mid s)^{\lambda_m} p(s) \frac{1}{f(D_1,...,D_m)} \\
&= p(s)\left(\frac{p(s \mid D_1)f(D_1)}{p(s)}\right)^{\lambda_1} \times \cdots \times \left(\frac{p(s \mid D_m)f(D_m)}{p(s)}\right)^{\lambda_m} C \\
&= p(s)\prod_{i=1}^{m}\left(\frac{p(s \mid D_i)}{p(s)}\right)^{\lambda_i} C \in [0,1]
\end{aligned}$$

By enforcing the closure condition:

$$p_{Lamda}(s \mid D_1,...,D_m) = \frac{p(s)\prod_{i=1}^{m}\left(\frac{p(s \mid D_i)}{p(s)}\right)^{\lambda_i}}{\sum_{s=1,...,K}\left(p(s)\prod_{i=1}^{m}\left(\frac{p(s \mid D_i)}{p(s)}\right)^{\lambda_i}\right)} \in [0,1]$$

and (3-11)

$$\sum_{s=1,...,K} p_{Lamda}(s \mid D_1,...,D_m) = 1$$

If λ_i are replaced by τ_i for i=1,…,m and the primary variable s only takes binary category then p_{Tau} and p_{Lamda} are exactly same. The key difference of the Lamda and Tau model is in the calculation of the λs.

Calibration Method 1

The combined probabilities with the weights λ_i:

$$p_{Lamda1}(s \mid D_1,...,D_m) = p(s)\prod_{i=1}^{m}\left(\frac{p(s \mid D_i)}{p(s)}\right)^{\lambda_i} C \tag{3-12}$$

The estimated probabilities may be close to 0 or 1 when the truth is known. For instance, p(sand|all secondary data) at sample location **u** is close to 1 if the true facies is sand at that location **u**, otherwise the estimated probability of sand is close to 0. The differences between the combined probability and true values can be evaluated for all of sample locations $\mathbf{u}_\alpha$, α=1,…,n, where n is the number of samples. In the first calibration method, parameters λ_i, i=1,…,m are determined to minimize these differences. Taking the probability ratio of $p_{\text{Lamda 1}}(s|D_1,\ldots,D_m)$ to $p_{\text{Lamda 1}}(\tilde{s}\,|D_1,\ldots,D_m)$ removes the unknown term C:

$$\frac{p_{Lamda1}(s \mid D_1,...,D_m)}{p_{Lamda1}(\tilde{s} \mid D_1,...,D_m)} = \frac{p(s)\prod_{i=1}^{m}\left(\frac{p(s \mid D_i)}{p(s)}\right)^{\lambda_i}}{p(\tilde{s})\prod_{i=1}^{m}\left(\frac{p(\tilde{s} \mid D_i)}{p(\tilde{s})}\right)^{\lambda_i}} = \frac{p(s)}{p(\tilde{s})}\prod_{i=1}^{m}\left(\frac{p(\tilde{s})p(s \mid D_i)}{p(s)p(\tilde{s} \mid D_i)}\right)^{\lambda_i}$$

Taking the logarithm makes this equation linear,

$$\ln\left(\frac{p_{Lamda1}(s \mid D_1,...,D_m)}{p_{Lamda1}(\tilde{s} \mid D_1,...,D_m)}\frac{p(\tilde{s})}{p(s)}\right) = \sum_{i=1}^{m}\lambda_i \ln\left(\frac{p(\tilde{s})p(s \mid D_i)}{p(s)p(\tilde{s} \mid D_i)}\right) \tag{3-13}$$

The right hand side of Equation (3-13) is the weighted linear sum of log probability ratios that consist of the known $p(s|D_i)$, i=1,…,m and $p(s)$. The left hand side is the log probability ratio with the unknown $p_{\text{Lamda1}}(s|D_1,\ldots,D_m)$ that is to be estimated. Though the $p_{\text{Lamda 1}}(s|D_1,\ldots,D_m)$ is not known for the every estimation locations the probability should be close to either 0 or 1 at the sample locations when true values are known. For example, the $p_{\text{Lamda 1}}(s|D_1,\ldots,D_m)$ is close to 1 when the true facies is s, and the $p_{\text{Lamda1}}(\tilde{s}\,|D_1,\ldots,D_m)$ is close to 0 at the same locations. The left hand side of Equation (3-13) is the unknown log probability ratios that should be reached by the

weighted linear combination of log ratios of conditional probabilities and global proportions in the right hand side. Since we have many pairs of input probabilities corresponding to the number of samples (n), Equation (3-13) can be expressed as a matrix equation:

$$\begin{bmatrix} b(\mathbf{u}_1;s) \\ b(\mathbf{u}_2;s) \\ \vdots \\ b(\mathbf{u}_n;s) \end{bmatrix} = \begin{bmatrix} a(\mathbf{u}_1;s\,|\,D_1) & a(\mathbf{u}_1;s\,|\,D_2) & \cdots & a(\mathbf{u}_1;s\,|\,D_m) \\ a(\mathbf{u}_2;s\,|\,D_1) & a(\mathbf{u}_2;s\,|\,D_2) & \cdots & a(\mathbf{u}_2;s\,|\,D_m) \\ \vdots & \vdots & \cdots & \vdots \\ a(\mathbf{u}_n;s\,|\,D_1) & a(\mathbf{u}_n;s\,|\,D_2) & \cdots & a(\mathbf{u}_n;s\,|\,D_m) \end{bmatrix} \begin{bmatrix} \lambda_1 \\ \lambda_2 \\ \vdots \\ \lambda_m \end{bmatrix}$$

or

$$\mathbf{B} = \mathbf{A} \bullet \boldsymbol{\lambda} \tag{3-14}$$

$a(\mathbf{u}_1;s|D_1)$, for example, represents $\ln\left(p(s\,|\,D_1)p(\tilde{s}) \Big/ p(\tilde{s}\,|\,D_1)p(s) \right)$ at the location $\mathbf{u}_1$ where the truth is s, $b(\mathbf{u}_1;s)$ represents a target value at the location $\mathbf{u}_1$ $\ln\left(p_{Lamda1}(s\,|\,D_1,...,D_m)p(\tilde{s}) \Big/ p_{Lamda1}(\tilde{s}\,|\,D_1,...,D_m)p(s) \right)$. Note that the complementary probability in the denominator of $a(\mathbf{u}_\alpha;s|D_i)$ and $b(\mathbf{u}_\alpha;s)$ cannot be zero. In practice, a very small value would be substituted for the exact zero probability in the denominator of $b(\mathbf{u}_\alpha;s)$, $\alpha=1,\ldots,n$. The unknown weights are derived by minimizing the squared differences between $\mathbf{B}$ and $\mathbf{A}\boldsymbol{\lambda}$ such as $||\mathrm{B} - \mathrm{A}\lambda||^2$. The least square n solution of $\boldsymbol{\lambda}$ can be followed as:

$$\boldsymbol{\lambda} = (\mathbf{A}'\mathbf{A})^{-1}\mathbf{A}'\mathbf{B} \tag{3-15}$$

where $\mathbf{A}'$ is the transpose of $\mathbf{A}$. Figure 3.1 illustrates graphically how to build elements of the matrix Equation (3-14). Two secondary data D_1 and D_2 are assumed to be processed to make $p(s|D_1)$ and $p(s|D_2)$ where s takes ternary codes represented as black, dark and light gray colors. Based on 7 well samples where the true facies are known, matrices for calculating weights are built. The weights λ_i are obtained by accounting for the closeness of the combined probabilities to the true probabilities at sample locations.

The motivation for putting weight parameters is to mitigate the independence assumption made in the simple combination model. The levels of redundancy between the secondary data may be different depending on different s. When taking the probability ratios in Equation (3-13), however, λs are assumed to be independent of s.

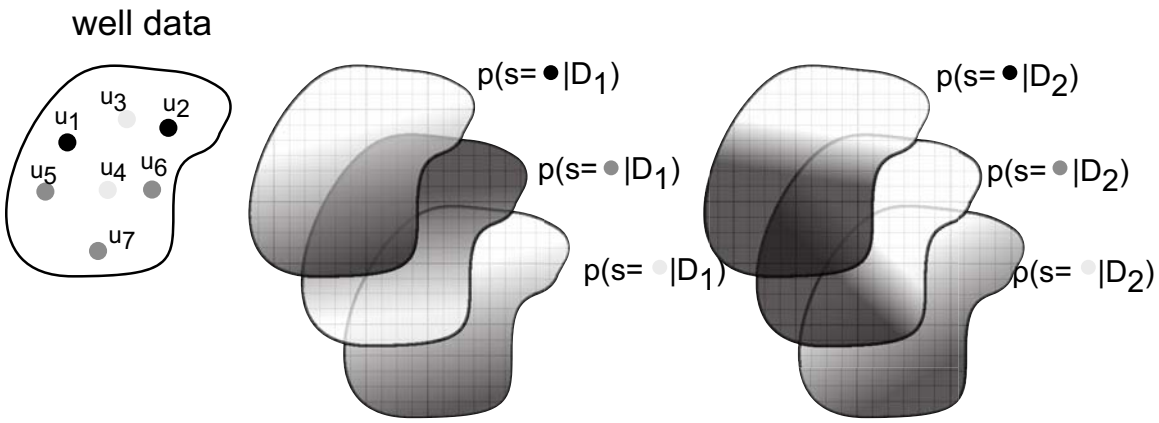

Matrix for weights calculation

$$\begin{bmatrix} b(\mathbf{u}_1;\ s=\bullet) \\ b(\mathbf{u}_2;\ s=\bullet) \\ b(\mathbf{u}_3;\ s=\circ) \\ b(\mathbf{u}_4;\ s=\circ) \\ b(\mathbf{u}_5;\ s=\bullet) \\ b(\mathbf{u}_6;\ s=\bullet) \\ b(\mathbf{u}_7;\ s=\bullet) \end{bmatrix} = \begin{bmatrix} a(\mathbf{u}_1;\ s=\bullet, D_1) & a(\mathbf{u}_1;\ s=\bullet, D_2) \\ a(\mathbf{u}_2;\ s=\bullet, D_1) & a(\mathbf{u}_2;\ s=\bullet, D_2) \\ a(\mathbf{u}_3;\ s=\circ, D_1) & a(\mathbf{u}_3;\ s=\circ, D_2) \\ a(\mathbf{u}_4;\ s=\circ, D_1) & a(\mathbf{u}_4;\ s=\circ, D_2) \\ a(\mathbf{u}_5;\ s=\bullet, D_1) & a(\mathbf{u}_5;\ s=\bullet, D_2) \\ a(\mathbf{u}_6;\ s=\bullet, D_1) & a(\mathbf{u}_6;\ s=\bullet, D_2) \\ a(\mathbf{u}_7;\ s=\bullet, D_1) & a(\mathbf{u}_7;\ s=\bullet, D_2) \end{bmatrix} \begin{bmatrix} \lambda_1 \\ \lambda_2 \end{bmatrix}$$

$$p_{Lamda}(s=\bullet \mid D_1, D_2) = p(s=\bullet)\left(\frac{p(s=\bullet \mid D_1)}{p(s=\bullet)}\right)^{\lambda_1}\left(\frac{p(s=\bullet \mid D_2)}{p(s=\bullet)}\right)^{\lambda_2} C$$

$$p_{Lamda}(s=\circ \mid D_1, D_2) = p(s=\circ)\left(\frac{p(s=\circ \mid D_1)}{p(s=\circ)}\right)^{\lambda_1}\left(\frac{p(s=\circ \mid D_2)}{p(s=\circ)}\right)^{\lambda_2} C$$

$$p_{Lamda}(s=\bullet \mid D_1, D_2) = p(s=\bullet)\left(\frac{p(s=\bullet \mid D_1)}{p(s=\bullet)}\right)^{\lambda_1}\left(\frac{p(s=\bullet \mid D_2)}{p(s=\bullet)}\right)^{\lambda_2} C$$

Figure 3.1: A graphical illustration for calculating weights using weight calibration method 1. Weights are calculated based on the differences between true and combined probabilities.

Calibration Method 2

The second calibration method borrows from the kriging-type solution to estimate the weights. Recall Equation (3-13) where the unknown probability $p(s|D_1,\ldots,D_m)$ is obtained by a linear weighted sum of log probability ratios. This form is similar to a cokriging estimate by linear weighting of several collocated secondary data where redundancy between secondary data and closeness between primary and secondary data are quantified by linear correlation. In the context of this problem, Equation (3-13) is re-expressed as a cokriging equation:

$$b = \sum_{i=1}^{m} \lambda_i a_i$$
$$\text{where } a_i = \ln\left(\frac{p(s \mid D_i)p(\tilde{s})}{p(\tilde{s} \mid D_i)p(s)}\right) \text{ and } b = \ln\left(\frac{p(s \mid D_1,\ldots,D_m)p(\tilde{s})}{p(\tilde{s} \mid D_1,\ldots,D_m)p(s)}\right) \tag{3-16}$$

a_i and b are treated as random variables with the range of $[-\infty,\infty]$. The weights could be obtained by solving the matrix equation:

$$\begin{bmatrix} \rho_{a_1,a_1} & \cdots & \rho_{a_1,a_m} \\ \vdots & \ddots & \vdots \\ \rho_{a_m,a_1} & \cdots & \rho_{a_m,a_m} \end{bmatrix} \begin{bmatrix} \lambda_1 \\ \vdots \\ \lambda_m \end{bmatrix} = \begin{bmatrix} 1 \\ \vdots \\ 1 \end{bmatrix} \tag{3-17}$$

This equation can be seen such that the left hand side matrix describes the redundancy between a_i and a_j and the right hand side matrix describes the closeness between a_i and b for the facies s under consideration. Because the log function is monotonic, redundancy between a_i and a_j is directly related to the redundancy between $p(s|D_i)$ and $p(s|D_j)$ and equivalently the redundancy between the data D_i and D_j. The closeness of a_i to b is assumed to be 1 in the right hand side of Equation (3-17) (full closeness) and this permits considering only redundancy among the conditioned data $(D_1,\ldots,D_m)$ for the weight calculation regardless of the closeness of b and a_i, $i=1,\ldots,m$. For example, if the data D_i and D_j are not redundant then the correlation between the corresponding log probability ratios is nearly zero then the redundancy matrix becomes an identity matrix and the calibrated weights are very close to 1.

3.4 **1-D Example**

A small 1-D example is presented with the different probability combination methods for graphical convenience. Figure 3.2 illustrates the sampled facies (rectangles), global proportion (horizontal line) and calibrated conditional probabilities of facies code 1 (three dashed lines) at every 1m along the horizontal transect. The generated conditional probabilities are positively correlated each other with moderate-to-high probabilities of the correct facies in which the given conditioning data D_1, D_2 and D_3 are deemed to be redundant.

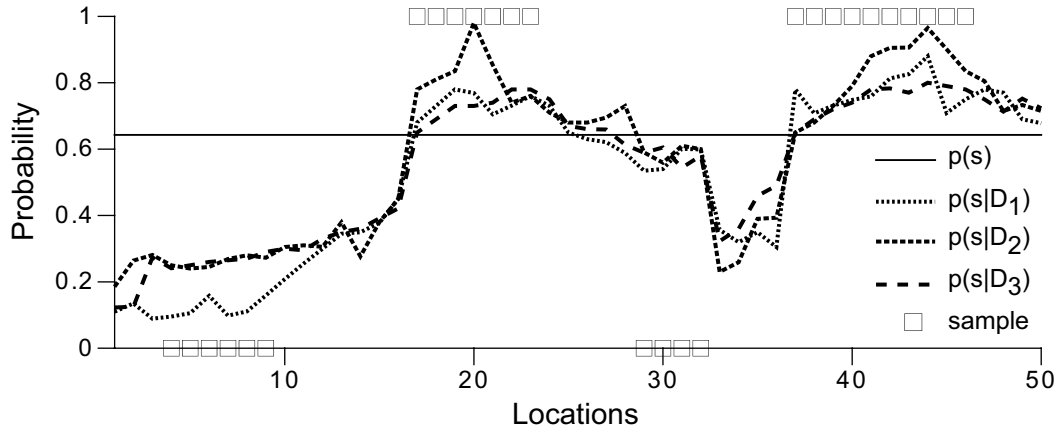

Figure 3.2: 1-D example along the horizontal transect. Modeling for the binary category is considered. Three conditioning secondary data D_1,D_2 and D_3 are assumed to redundant since the probabilities $p(s|D_i)$ are positively correlated. The global proportion $p(s)$ and the primary hard data (□) are shown.

$p(s|D_i)$ for i=1,2,3 reasonably honors the primary hard data; they correctly inform the presence or absence of the true facies overall. Inaccuracy of $p(s|D_i)$ is intentionally injected into around the location index of 30 to underline the impact of different combination schemes. As shown in later in Figure 3.6, the combined probability by the calibration method 1 corrects this artificially injected inaccuracy. The conditional probability lines are combined using the conditional independence model first and it is shown in Figure 3.3. Though the conditional independence is equivalent to the PR model for this particular example (binary category modeling), the conditional independence approach is only considered as a simple combination method because the validity of the PR method is not general in multiple facies. The combined probability changes drastically and it is not within the global and three conditional probability lines except in transition zones where the conditional probabilities pass by the global proportion. The combination method that makes the combined probability close to 0 or 1 seems to reduce the

uncertainty in the final combined probability, and shows a high closeness to the true values at sample locations. In particular, when the elementary conditional probabilities are highly redundant, the combined probability should not be far away from the input conditional probability. The danger of the conditional independence model is overfitting that would harm the fairness of the final probability.

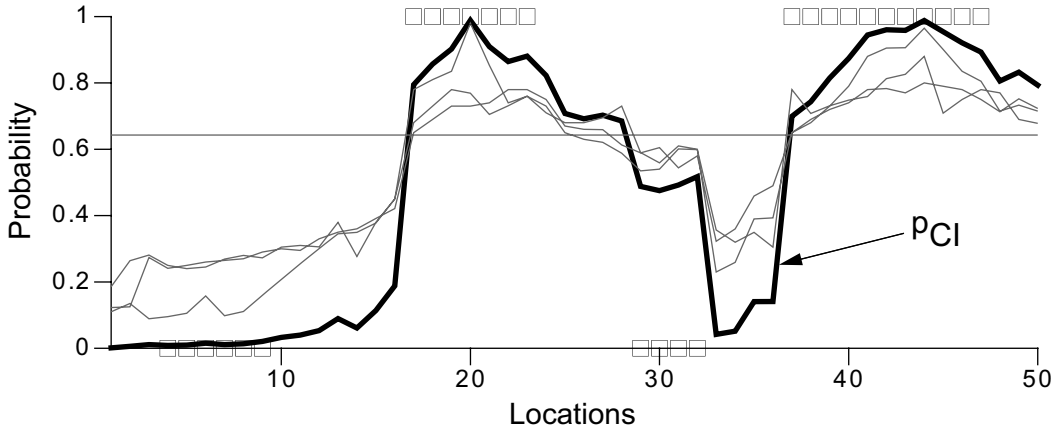

Figure 3.3: The combined probability using the conditional independence model (p_{CI}).

The result of the Lamda model with the first calibration method is shown in Figure 3.4. The calibration method computes the weights by minimizing the differences between the combined probability and the true probability at sample locations. For the present 1-D example, 28 samples are used to build the matrix equation 3-15: the individual conditional probabilities at 28 sample locations constitute the matrix **A**, the true probability at sample locations constitute the vector **B**. Care must be taken in building the vector **B** because the log ratio in the vector **B** becomes infinity when the complementary probability $p(\tilde{s}\,|D_1,\ldots,D_m)$ in the denominator has zero probability when the true facies is s. To overcome this numerical instability, a minimum bound of probability (denoted as ε) is used instead of exactly zero in the elements of the vector **B**. The combined probability shown at the top of Figure 3.4 is obtained by substituting ε=0.001 for zero and it overfits more than the conditional independence model. This is due to the fact that the considered weight calibration method calculates the weight not by accounting for the redundancy but by minimizing the least square errors. Thus, the w_i parameters are chosen to make the resulting probability as close as possible to the true probability (either 0 or 1) at sample locations. Note, however, that the overfitting can be controlled by adjusting the artificial small value of probability that is used when building the vector **B** in Equation (3-15). As smaller value is used, the differences between the true and combined probability are elevated more, and thus the

magnitude of the weights becomes larger to minimize these differences. The bottom of Figure 3.4 shows several combined probability lines using the different ε. The use of small ε (such as 0.001) leads to overfit combined probabilities. The use of a relatively large value such as ε=0.1, on the contrary, mitigates the accuracy of the elementary probabilities $p(s|D_i)$. The combined probability should be reasonably close to the true probability where we know the correct facies and it should be fair as well. Cross validation such as accuracy assessment discussed in Section 3.6 could be used for selecting the appropriate small value of ε.

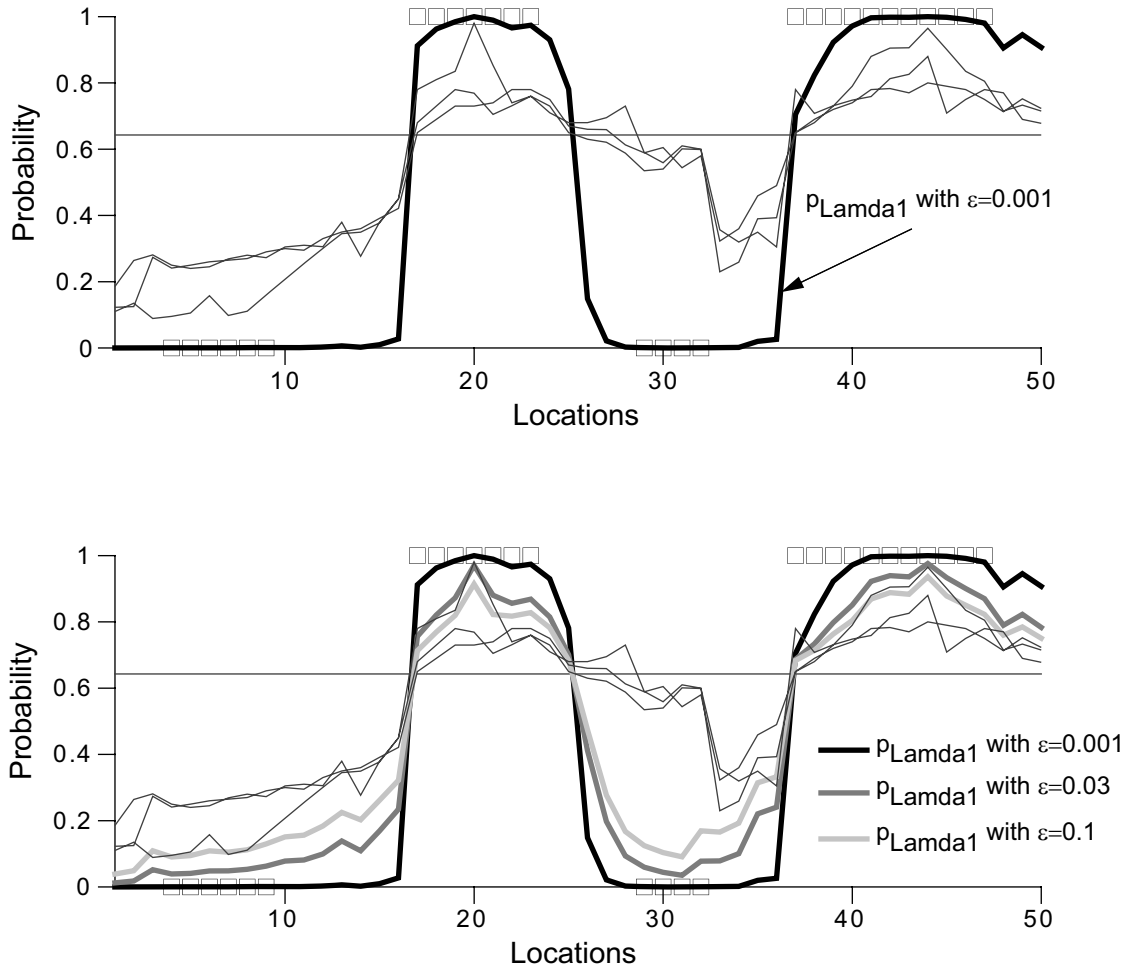

Figure 3.4: The combined probability using the Lamda model with the first calibration method. To avoid the numerical instability, an artificial small value (ε) is injected to the calibration equation and the results become different based on the used small values.

Unlike the first calibration method, the second calibration method accounts for the redundancy among the individual conditional probability obtained from each data. Equation (3-17) for obtaining the weight is established as below,

$$\begin{bmatrix} 1 & 0.903 & 0.94 \\ 0.903 & 1 & 0.89 \\ 0.94 & 0.89 & 1 \end{bmatrix} \begin{bmatrix} \lambda_1 \\ \lambda_2 \\ \lambda_3 \end{bmatrix} = \begin{bmatrix} 1 \\ 1 \\ 1 \end{bmatrix}$$

The weights are derived by solving the matrix equation:

	Weights from calibration method 2
λ_1	0.253
λ_2	0.448
λ_3	0.364

The calibrated weights are smaller than 1 because of the high correlation between the input conditional probabilities. If the data had little redundancy (small correlation in the left hand side matrix) then the weights would be close to 1. The data D_1 receives the smallest weight and the weight λ_1=0.253 reduces the influence of $p(s|D_1)/p(s)$. The data D_2 receives the largest weight and the weight λ_2=0.448 least reduces the influence of $p(s|D_2)/p(s)$. The combined probability with the obtained weights above is shown in Figure 3.5. Weights less than 1 weaken the effect of the non-convexity such as reducing the contribution of the probability ratio $p(s|D_i)/p(s)$ to the final probability. For example, if the probability ratio is less than 1 then the weighted probability ratio is increased by the applied weight less than 1, and thus the combined probability becomes not far below the input $p(s|D_i)$ and $p(s)$. Likewise, if the probability ratio is greater than 1 then the weighted probability ratio is decreased by applying the weight less than 1, and the combined probability becomes not far above the input $p(s|D_i)$ and $p(s)$. In particular, if the given data are highly redundant such as in this example, the calibration method 2 generates small weights that make the probabilities more reasonable and less overfit.

One interesting aspect about the calculated weights from the second calibration method is that their sum could represent the overall data redundancy quantitatively. For example, the sum of the calculated weights for the illustrated 1-D example is about 1.06 and intuitively, this could be interpreted that three conditioning data D_1, D_2 and D_3 are regarded virtually as a single data. The sum of weights would be interpreted as following:

	Interpretations
$\sum_{i=1}^{m} \lambda_i \approx m$	m secondary data are nearly independent
$\sum_{i=1}^{m} \lambda_i < m$	m secondary data are somewhat redundant

The overall redundancy among the given secondary data could be quantified as $\left[1-\left(\sum_{i=1}^{m}\lambda_i\right)/m\right]\times 100$ in %.

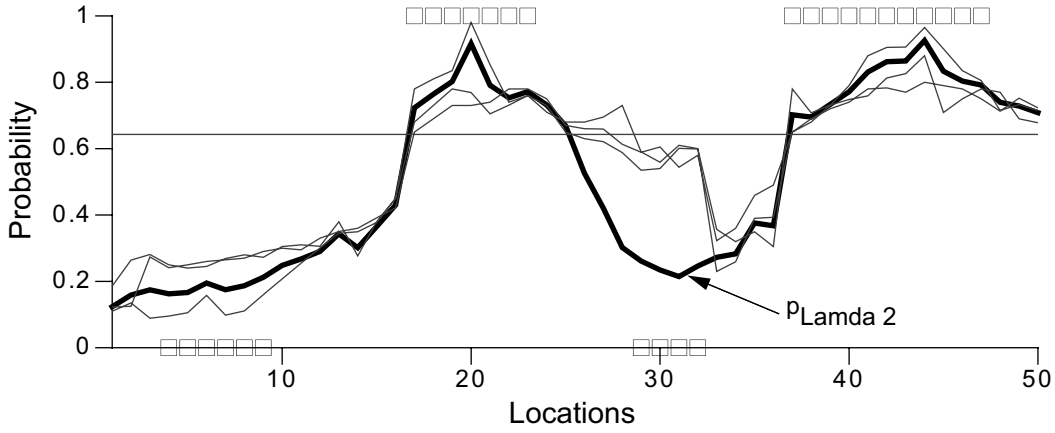

Figure 3.5: The combined probability using the Lamda model with the second calibration method.

The combined probabilities with the different combination schemes are demonstrated together in one plot in Figure 3.6. The uncertainty in the final probability is decreased after integrating different probabilities conditioned to the diverse data; however, the degree of reduction in the uncertainty is different for each combination scheme. The simple combination method assumes that the given conditioning data are independent and the method makes the probability quite extreme. As mentioned previously, this overfitting becomes more risky when the given secondary data redundant. The weighted combination methods do not pull the resulting probability toward extremes as much as the simple combination method does. Among the two calibration methods for the Lamda model, the result with the least square calibration method honors the true values at sample locations very well and especially the result is in a good accordance with the samples around 30m where other methods cannot account for. This is due to the fact that the conditional independence and the Lamda model with the second calibration

method do not consider the accuracy of the resulting probability when calibrating the weight parameters.

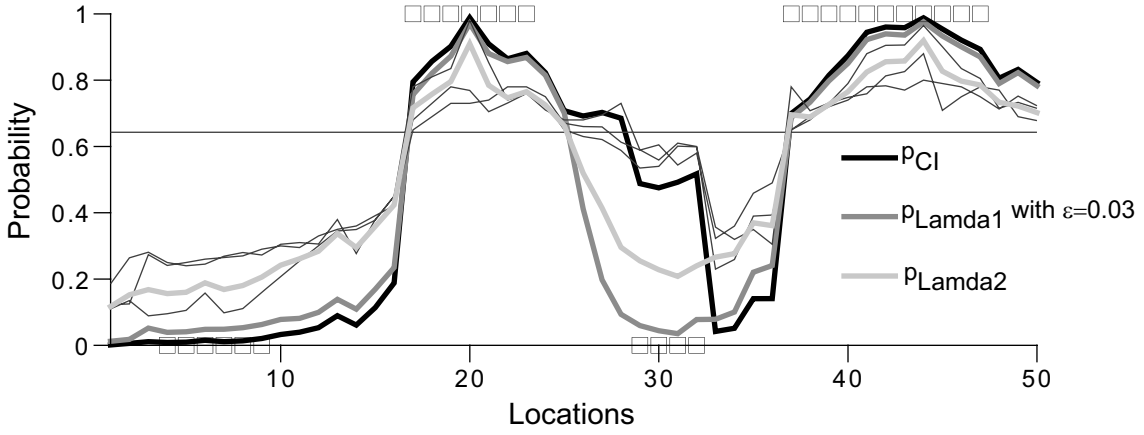

Figure 3.6: The resulting combined probability from the different models: conditional independence and the Lamda model with different calibration approaches.

3.5 Applications of Combining Approaches

The Amoco data set extracted from a West Texas Permian Basin reservoir has been used for testing geostatistical algorithms (Deutsch, 2003; Pyrcz et al., 2006). The reservoir extends 10,400ft × 10,400ft in area and facies types are measured from 62 wells. Two facies types are identified over the reservoir: high porous (coded as 1) and low porous (coded as 2) facies. Binary codes are represented as black and white circles in the 62 well location map shown in Figure 3.7.

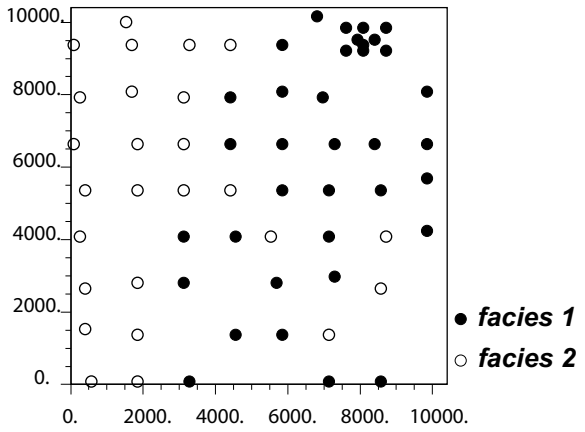

Figure 3.7: 62 well location map of Amoco data. Scales are in ft.

A seismic amplitude data is available over the area. The seismic measurements at the 62 well locations are calibrated with the facies type at those locations. Nonparametric statistical distribution modeling was used to build the probability distributions. Figure 3.8 illustrates the seismic data map (left) and the calibrated facies probability distributions (middle). Well data shown in the seismic amplitude map are used for the probability distribution calibration. Based on the modeled probability distributions, the conditional probability of facies given the seismic value is extracted. A 2-D map shown in the right of Figure 3.8 represents the probability of facies 1 given the seismic data.

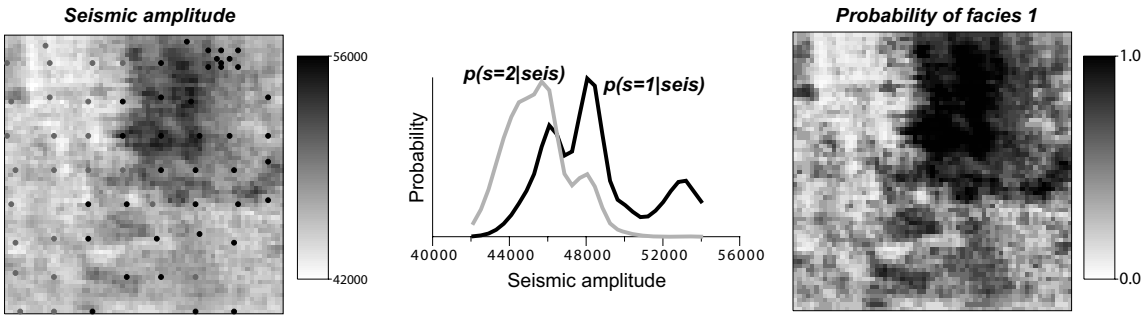

Figure 3.8: A seismic amplitude map (left), probability distributions calibrated from the 62 wells (centre), and the derived facies probability map (right).

There is one secondary data available. Two more secondary data are generated to illustrate the effect of integrating several secondary data. A trend is considered as secondary information and it is generated using the 62 well data. Trends are important features that should be adequately accounted for in the final geostatistical model. Simple indicator kriging with an isotropic variogram using a large range (half of the domain) is used to make a smooth map of facies trend. Explicit modeling of the trend and incorporating the trend into the final geostatistical model is a widely used approach. Figure 3.9 shows the modeled trend of facies 1.

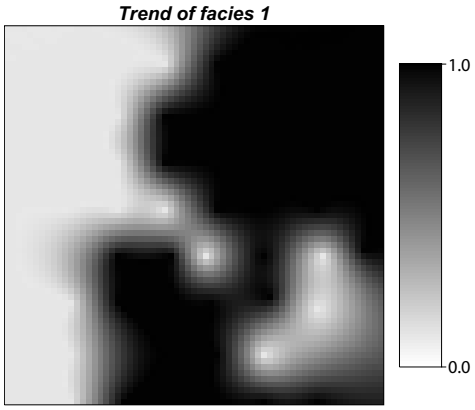

Figure 3.9: The trend of facies 1 generated by simple indicator kriging with isotropic variogram.

A deterministic facies model is considered as another secondary data. In practice, the deterministic facies model may be built from geological interpretation over the area. Integrating this external expertise is also important to model the reservoir more realistically. An example of a deterministic facies model is illustrated in the left of Figure 3.10. The sharp boundary between two facies is drawn subjectively. Uncertainty exists in the deterministic model and the uncertainty may be enlarged around the hard boundary between facies. A moving window is applied to make the soft boundary and it can better consider the uncertainty rather than does the hard boundary. The right image in Figure 3.10 shows the facies proportion by applying the moving window to the deterministic facies model. An anisotropic moving window could be applied to account for the anisotropy in the facies.

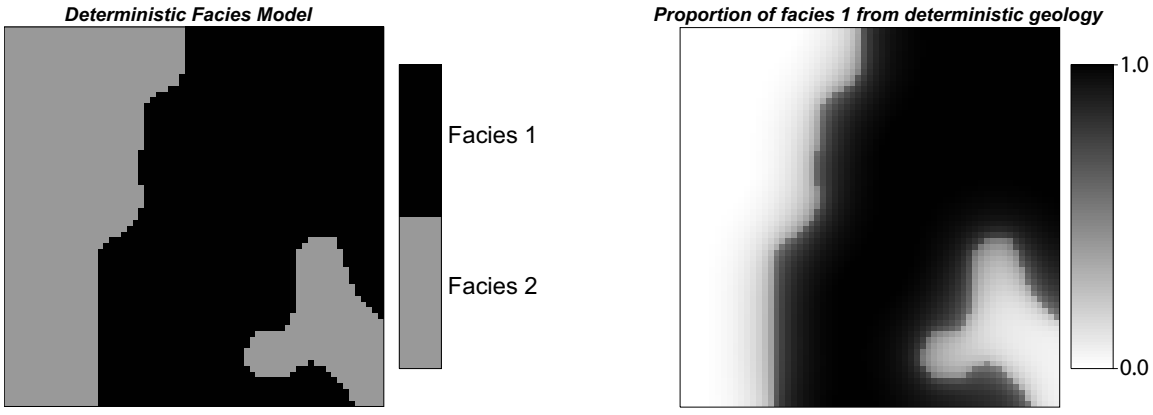

Figure 3.10: A deterministic facies model is generated by subject drawing the facies boundary. Facies proportions are derived from the deterministic model by applying a moving window.

The three facies probability maps appear to be very similar. The considered secondary data (seismic, trend and deterministic geology) are deemed highly redundant. The discussed probability combination methods are applied to the derived facies probability maps from each data. Figure 3.11 represents the resulting combined probability of facies 1. The subscripts denoted as CI, Lamda 1 and Lamda 2 indicate the combination methods of conditional independence, Lamda model with calibration method 1 and 2, respectively. ε=0.005 is used as the small value of probability for the Lamda 1 and the weights are obtained as:

	Calibration method 1
λ_1	0.049
λ_2	0.740
λ_3	0.251

The weights are obtained by minimizing the differences between the combined probability and the true probability at sample locations. The trend data receives the highest weight and the seismic data receives the lowest weight because the facies trend map (shown in Figure 3.9) shows higher agreement with the true facies at sample locations than do the seismic and deterministic facies map. The weights from the second calibration method are shown in the table below:

	Calibration method 2
λ_1	0.644
λ_2	0.473
λ_3	0.224

The weights are calculated by accounting for the redundancy among the data specific individual probability. The agreement of the combined probability with the true facies is not considered in this calibration. The conditional probability p(s|D1) receives the highest weight and p(s|D2) and p(s|D2) receive lower weights. This is due to that the data D2 (trend) and D3 (geologic map) are highly redundant each other and the data D1 (seismic) is less redundant among other D2 and D3. The sum of weights from this calibration method would be useful to give an insight into the

overall redundancy; 55% ($1-\sum_{i=1}^{3}\lambda_i / 3 = 1-0.45$) information from the each data is redundant on the average.

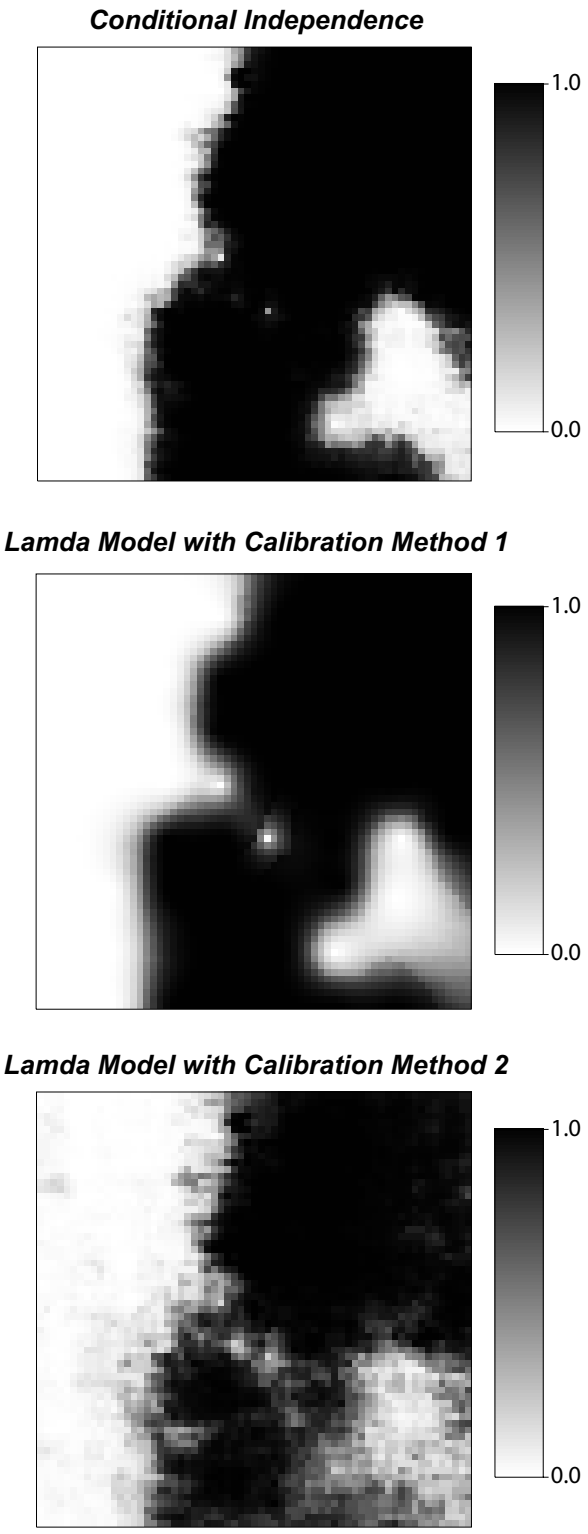

Figure 3.11: The estimated facies probabilities from three different combination schemes: the conditional independence (top), Lamda model with calibration method 1 (middle) and 2 (bottom).

Non-convex Property of the Combined Probability

The non-convex property refers to the situation when the integrated probability is not within the range of the input probabilities $p(s|D_i)$ and the global proportion $p(s)$. Non-convexity is natural in data integration. Integrating diverse data amplifies the impact of data sources if they represent the same direction of probability. The degree of non-convexity is affected by how redundant the data D_i are among themselves. Although all of the elementary probabilities $p(s|D_i)$ are in the same direction (they are all higher or lower than the global $p(s)$), non-convexity may not be significant when data are highly redundant, and thus the combined probability should not be very high or very low for this case. Plotting the input individual probabilities and the integrated probability is useful to check the degree of non-convexity of the result and checking the non-convexity would be a justification for the calculated goodness measure that will be mentioned in the next section. Figure 3.12 shows the scatter plots between the input individual probabilities and the combined probability from the considered different combination methods. Plotting is performed only when the input probabilities are greater than the global proportion for the facies 1 ($p(s=1)=0.514$). The individual probabilities greater than the global proportion are along the abscissa and the combined probability with these individual probabilities are along the ordinate. Points falling above the diagonal line represents non-convexity. The conditional independence model shows stronger non-convexity than the weighted combination schemes. The independence approach always leads to a combined probability that is higher than any of the input individual probabilities. In other words, the compounding effect of corroborating information is the most significant in the conditional independence model. In the plots from the weighted combination, the majority of points are plotted above the diagonal line. The departure from the line and the non-convexity are not so dramatic as the independence approach. Some points are plotted below the diagonal line, which indicates the integrated probability becomes even smaller than the input individual probabilities; 7% and 22% of total plotted dots are below the diagonal line for the Lamda model with the weight calibration method 1 and 2, respectively. This is because the weights are not calculated locally but globally.

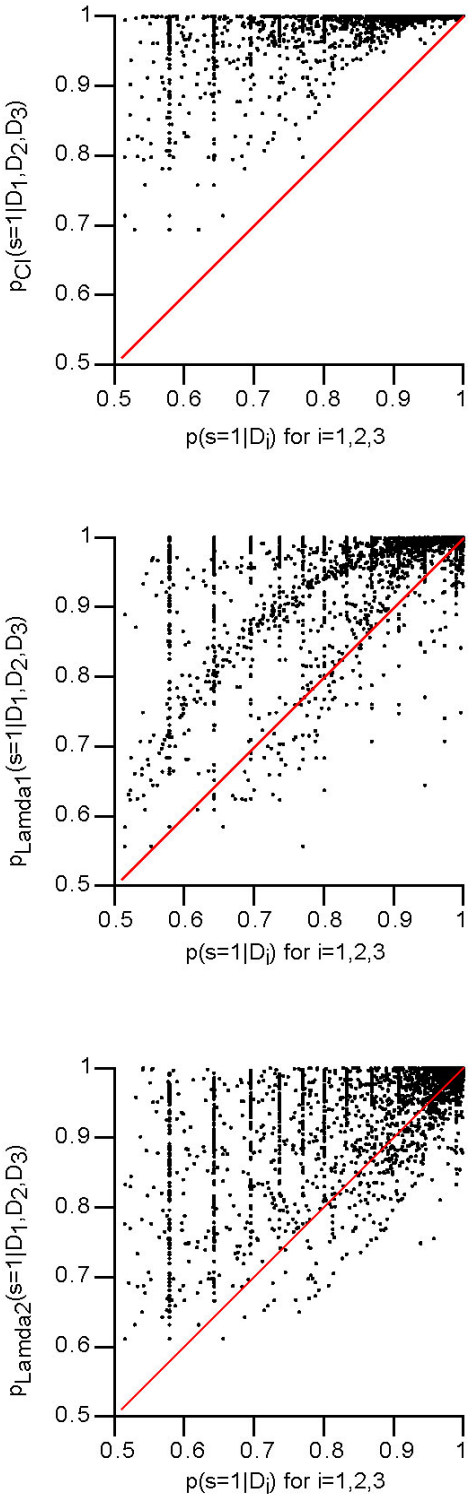

Figure 3.12: Cross plots for showing the non-convex behavior of the combined probability; the input individual probabilities $p(s=1|D_i)$ for $i=1,2,3$ and the combined probabilities $p(s=1|D_1,D_2,D_3)$ from the different combination methods are plotted. Plotting is made when the $p(s|D_i)$ for $i=1,2,3$ are all greater than the global proportion $p(s=1)=0.514$.

The non-convexity is observed in Figure 3.12 when the input probabilities are larger than the global proportion, however, the same result can be made for the case of plotting probabilities smaller than the global proportion.

Although the non-convexity is a desirable property in data integration in terms of making the final integrated probability be a certainty (push toward 0 or 1), the magnitude of non-convexity relies on how redundant the data are, and thus the reasonableness must be judged by understanding and quantifying the data redundancy. Alternatively, the resulting integrated probability is directly assessed by cross validation techniques so as to check the reasonableness of the applied weights and the non-convex behavior.

3.6 Accuracy Assessment

If the additional information is properly combined, integrating the secondary data helps build a reservoir model with less uncertainty and high accuracy. The relevance between the secondary and the primary data must be fully utilized and redundancy between secondary data is reasonably accounted for. Secondary derived facies probabilities are evaluated before being incorporated in sequential simulation for building the final facies model. There is a classical measure of performance that assigns the most likely facies with a maximum probability and then count the actual and predicted pixel number. A confusion matrix summarizes these results (Johnson and Wichern, 2002):

	Predicted pixel number		
Actual pixel number		Facies 1	Facies 2
	Facies 1	n_{11}	n_{12}
	Facies 2	n_{21}	n_{22}

For example, n_{11} is the number of pixels correctly classified as facies 1 and n_{21} is the number of pixels actually facies 1 that are misclassified. The classification accuracy of facies 1 is then calculated by $n_{11}/(n_{11}+n_{12})$. This simple evaluation method does not consider the uncertainty or probabilities. Figure 3.13 illustrates a drawback of accuracy calculation using the classical confusion matrix. A small 4 grid example is shown for illustration.

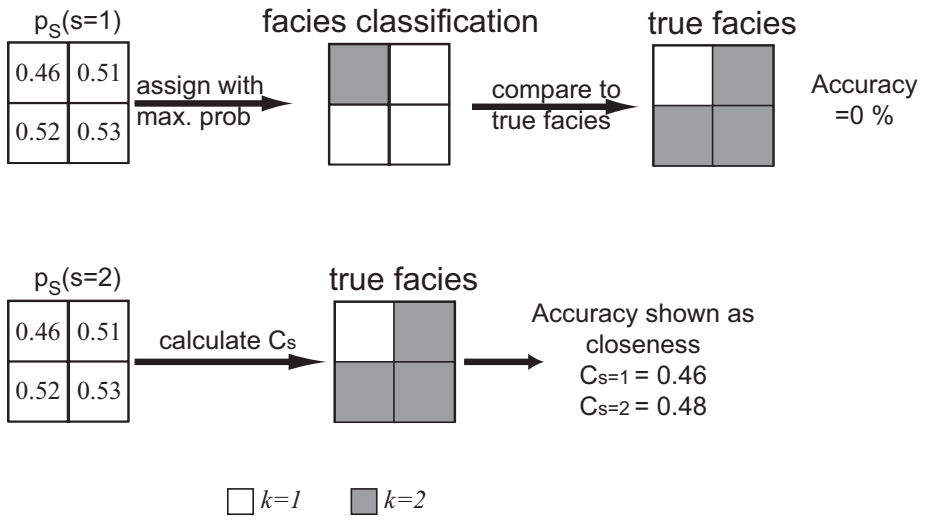

Figure 3.13: Small example showing the risk of the classical accuracy measure.

Probabilities around 0.5 are assigned at each location which introduces high uncertainty when assigning facies 1 or 2 with the largest probability. Classification accuracy is calculated as 0% for both facies. Based on 0% classification accuracy, it might be concluded that the secondary data is useless when one wants to use them for identifying facies or the considered probabilistic model is completely invalid. The classical accuracy measure does not account for the high degree of uncertainty indicated by the estimated probability just below and above 0.5.

Reproduction of Global Proportions

Close reproduction of the global proportions is a quick check. The average of $p(s|D_1,D_2,D_3)$ over the domain should be close to the representative global proportions of s. The reproduced proportions from the different combination methods for the previous example are summarized.

	Facies 1 (s=1)	Facies 2 (s=2)
$\overline{p_{CI}}(s \mid D_1, D_2, D_3)$	0.597(16.1%)	0.403(17.1%)
$\overline{p_{Lamda1}}(s \mid D_1, D_2, D_3)$	0.57(10.8%)	0.43(11.3%)
$\overline{p_{Lamda2}}(s \mid D_1, D_2, D_3)$	0.575(11.9%)	0.425(12.6%)

Differences in % with the input global proportions are shown in the parentheses. The combination models reasonably reproduce the input proportions.

Accuracy of Local Estimated Probabilities

The next criterion is to assess the accuracy or fairness of the locally estimated probabilities. When a model predicts the occurrence of sand with 10% probability, there should be actually be sand at about 10% of those locations (Isaaks and Srivastava, 1989; Deutsch, 1997). The locally estimated probabilities can be said to be accurate or fair if they reflect the true fraction of times the predicted facies occurs (Deutsch, 2002). For example, consider all locations where we predict 0.3 probability of sand, then it is fair that 30% of those locations are sand. A fairness check is conducted over 0 – 100% prediction intervals with user-input incremental levels. The fairness measure is:

$$\text{Actual Fraction} = E\left\{ I(\mathbf{u}_\alpha; s) \mid p(\mathbf{u}_\alpha; s) = p \right\}, \ \forall p, \ s = 1, ..., K \tag{3-18}$$

where $p(\mathbf{u}_\alpha;s)$ are probabilities at sample location $\mathbf{u}_\alpha$, $\alpha=1,\ldots,n$. p is a predicted probability. Indicator function $I(\cdot)$ takes either 0 or 1 depending on facies type s. The actual fraction at p is an average of indicator values under the predicted p. This actual fraction is calculated at all p values and then plotted against p. The predicted probability and the actual fractions could be summarized in a table:

Table 3.1: An example of the fairness measure for categorical variable

Predicted probability p	Total number (n_0) of samples predicted as p	Actual number (n_1) of samples identified as facies s among n_0	Actual fractions (n_1/n_0)	Ideal fractions
0.05 – 0.15	3	20	0.15	0.1
•	•	•	•	•
•	•	•	•	•
•	•	•	•	•
0.95 – 1.15	9	10	0.9	1.0
Sum	Total sample number (n)	Total sample number of facies s (n_s)	-	-

The most fair or accurate case is when the actual fractions are identical to the predicted probabilities for all intervals of predicted p. The calculated actual fractions, however, are affected by the number of samples. For instance, if the total number of samples is 30 and predicted probabilities have intervals of 0.1 then each interval of predicted probabilities might

have very few number of samples at the given predicted p, that is, 3 on the average. The calculated fractions may be close to 0 in a low predicted p and close to 1 in a high predicted p. Figure 3.14 shows the fairness measure in one plot. The plots shown in Figure 3.14 are overall fairness measure (all facies), but one can plot by-facies fairness plot. Distant plotting from the diagonal line will be a problem; falling in the lower area would suggest an overfitting of the estimated probability to the sample data and falling in the above area would indicate the probability of the facies but not to the extent of a high enough probability. Probability intervals of 0.1 are applied to the predicted probability. The corresponding actual fractions are plotted as dots. Plotting is not made when the actual fractions with zero number of n_0 in which the actual fractions cannot be computed. This qualitative checking method is aimed at identifying the case where the actual fractions are significantly departed from the given predicted probability (Deutsch, 1999). Figure 3.14 shows that the results from different combination schemes accurately reflect the true fraction of times predicted facies present only when very high or very low predicted probabilities are given. For this particular example, this may be caused by that the elementary probabilities $p(s|D_i)$ are very extreme so that the combined probabilities are toward extreme as well. The result from the independence model is relatively inaccurate given the intermediate predicted probabilities of 0.45-0.55.

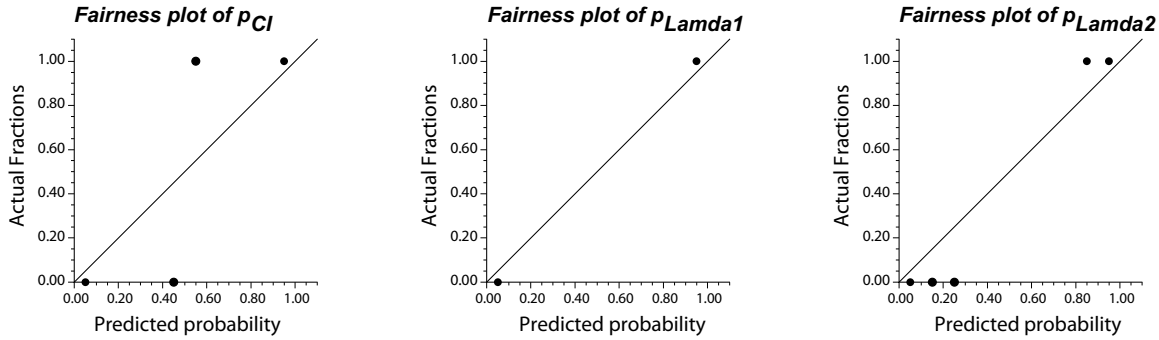

Figure 3.14: Fairness plots of the combined probabilities from different combination models. The plotted fairness measure is averaged over facies s=1,2.

3.7 Building High Resolution Stochastic Model

If the secondary data have been integrated to the units of the primary attribute, indicator kriging can be used to integrate that information into an improved conditional probability for sequential simulation. The uncertainty from different methods for integrating diverse secondary data will be used in simulated realizations. Poor results caused by invalid secondary data integration methods

could lead to worse results and could be amplified during the simulation. This section describes how the simulated facies realizations are affected by the different probability combination methods. No direct comparison with the reference reservoir responses will be performed. Instead, statistical consistency checks are done in terms of reasonable reproduction of the input statistics.

The Bayesian updating technique is adopted inside the sequential simulation to build the local probability conditioned to the collocated secondary derived estimate and nearby primary indicators,

$$i^{**}(\mathbf{u};s) = \frac{i^{*}(\mathbf{u};s)}{p(s)} \frac{p^{\text{sec}}(s(\mathbf{u}) \mid D_1(\mathbf{u}), D_2(\mathbf{u}), D_3(\mathbf{u}))}{p(s)} p(s)C \tag{3-19}$$

where $i^{**}(\mathbf{u};s)$ are the updated local probabilities for simulation, $p^{\text{sec}}(s|D_1,D_2,D_3)$ is the secondary-derived probability of facies s. The full derivation of Equation (3-19) is described in section 2.2.4. The superscript sec indicates different probability combination methods such as the CI, Lamda model with weight calibration method 1 and 2. C is a normalizing constant to ensure a licit probability of $i^{**}(\mathbf{u};s)$. Experimental and the fitted variogram are shown in Figure 3.15. As a large scale feature, the facies has anisotropic spatial variation with N-S as the principal continuity and E-W as the minor continuity. The small scale features are better modeled with an isotropic variogram model.

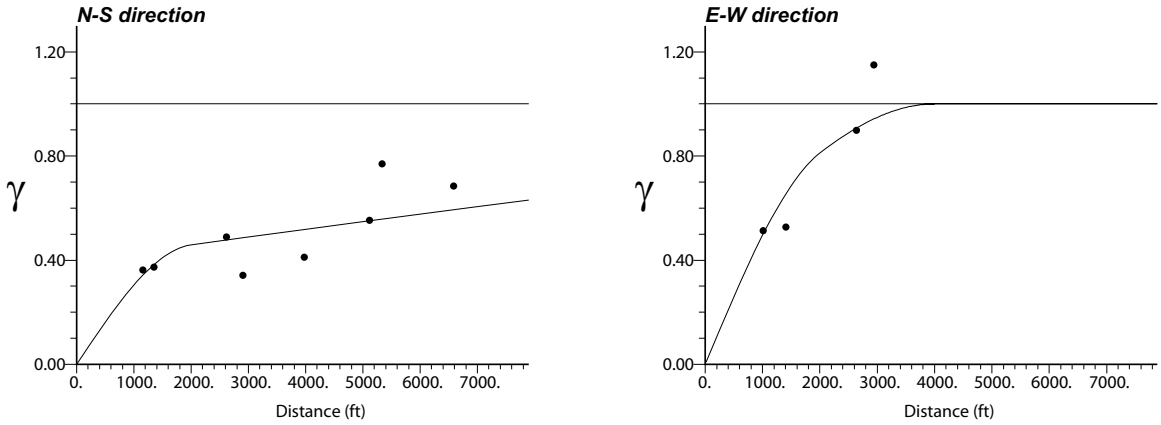

$$\gamma(\mathbf{h}) = 0.4Sph(\mathbf{h})_{\substack{a_{\text{hmax}}=2000 \\ a_{\text{hmin}}=2000}} + 0.6Sph(\mathbf{h})_{\substack{a_{\text{hmax}}=30000 \\ a_{\text{hmin}}=4000}}$$

Figure 3.15: Variogram of indicator variable representing facies: experimental variograms (dots) and their fitted variograms (lines).

Sequential indicator simulation is performed with the updating Equation (3-20). Multiple realizations are generated using each secondary-derived probability. For a consistent comparison, the same kriging parameters such as the number of original (12) and previously simulated data (6) and search radius (10000) are applied.

Reproduction of Input Proportions

The reproduction of the global proportions is a basic check for the simulated realizations. Accepting the reasonable tolerance between the reproduced and input ones, multiple realizations should honor the input representative proportions. Table 3.2 compares the reproduced proportions from 21 facies realizations with the various simulation scenarios. They have reasonably good reproduction of the global proportions.

Table 3.2: Comparison of the reproduced global proportions from the generated realizations with the input proportion $p(s=1)=0.514$ and $p(s=2)=0.486$.

	Facies 1	Facies 2
SISIM	0.566	0.434
SISIM with p_{CI}	0.565	0.435
SISIM with p_{Lamda1}	0.567	0.433
SISIM with p_{Lamda2}	0.561	0.439

Reproduction of Variograms

Once the input global proportions are reasonably reproduced, the next criterion involves checking the spatial variations. Figure 3.16 shows the reproduced variograms that are calculated from 21 realizations in the NS major continuity direction for each simulation scenario: simulation without secondary data integration and with secondary derived probabilities from three combination models. The reproduced variograms (dashed lines) are compared with the modeled variogram (solid lines). Realizations without secondary data have a satisfactory matching with the input variogram with a relatively large fluctuation. Reproduced variograms from using the p_{CI} have narrow fluctuations, but they depart from the input variogram. Despite reducing the uncertainty in the spatial variation, over-confidence of the secondary derived probability, p_{CI} affects the spatial variability. Realizations using p_{Lamda1} and p_{Lamda2} have satisfactory reproduction of the input variogram with small fluctuations.

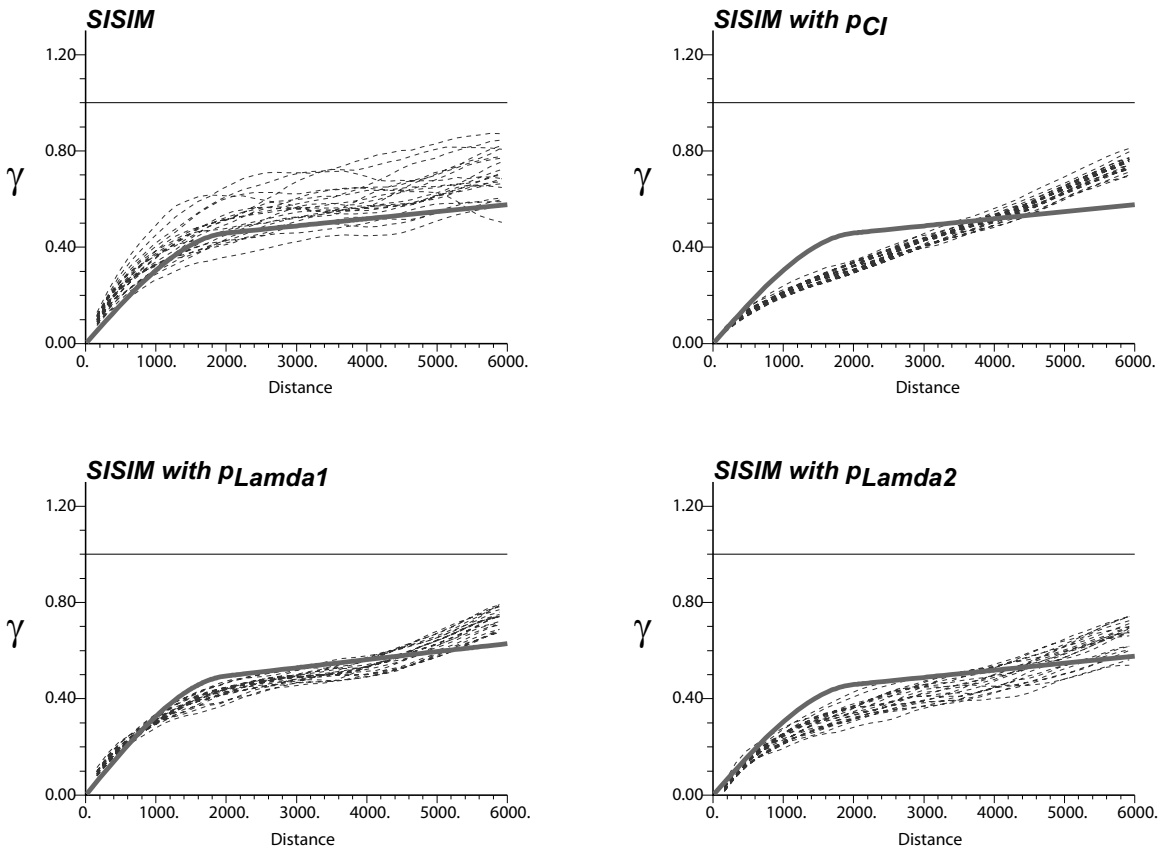

Figure 3.16: Reproduced variograms (dashed lines) from the 21 realizations that are made by different simulation scenarios: simulation with well data only (SISIM) and with integrating secondary derived probabilities obtained from the different methods (SISIM with p_{CI}, p_{Lamda1}, p_{Lamda2}). The input variogram is shown as heavy sold line.

3.8 Remarks on the PCS

The probability combination schemes are discussed as methods to integrate multiple secondary data. The approaches indirectly approximate the conditional probability that should be jointly conditioned to several data through linking the individual probability that are separately conditioned to each data. A very naïve model assumes the conditional independence between the given secondary data conditioned to the facies type *s*. The independence model, however, simply ignores the redundancy which causes inaccurate resulting combined probability. Weighted combination models seem to generate reasonable results; however, the calibrated weights are highly dependent on the calibration procedures. A calibration method 1 with the Lamda model performs well in particular examples. The combined probability with that calibration method seems to reasonably account for the redundancy. However, the relation between the calculated weights and data redundancy is not clearly understood. One way to check the reasonableness of

the calculated weights is to use the pre-defined criteria such as the fairness of the local estimated probability or reasonable reproduction of the input information from stochastic modeling.

An alternative approach to the PCS is discussed in the next chapter. The new method directly models the joint distribution among variables and the conditional probability is immediately derived from the modeled joint distribution. It does not require an external weight calibration. Instead, the method inherently accounts for the data redundancy during the joint pdf modeling.

Chapter 4

Direct Modeling of Multivariate Distribution

Chapter 3 investigated probability combination schemes that are calibrated to individual secondary data. Some theoretical drawbacks and difficulties in quantifying redundancy were presented.

This chapter investigates directly estimating the joint probability distribution between all secondary and primary variables instead of approximating the joint probability through linking the individual probabilities. The proposed idea is motivated by some key points: (1) there are suitable techniques for modeling the joint relations among variables including nonparametric approaches and (2) one characteristic of secondary data is exhaustiveness and so the joint distribution of secondary data can be modeled very reliably. By directly modeling the joint distribution, data redundancy among variables is accounted for directly. Complicated weight calibration is no longer required. Moreover, non-Gaussian features between variables can be captured by applying non-parametric technique. The second motivation related to exhaustiveness of the secondary data, plays a key role in the proposed approach. The secondary data distribution is also modeled non-parametrically, but the modeling has very little uncertainty due to the vast number of samples. One marginality condition of the joint distribution of interest is a reasonable reproduction of the distribution of secondary variables where the secondary data distribution is used as a reference marginal distribution. The other marginality condition is the reproduction of the distribution of the primary variables. The modeled joint distribution between primary and all

of secondary variables is evaluated by these conditions and the joint distribution is modified if differences are observed. An iterative algorithm is developed for the modification.

Section 4.1 discusses the details of kernel density estimation as a nonparametric density modeling technique. Theoretical analysis on the accuracy of kernel density estimates, choices of parameters and computational costs are discussed in this section. Section 4.2 investigates the suggested marginal fitting algorithm that updates the joint distribution in a sequential manner, termed sequential marginal fitting method. Detailed steps are described for refining the initially modeled joint distribution under the known reference marginals. The convergence of the proposed iterative procedure is discussed in Section 4.3.

4.1 Modeling the Multivariate Probability Densities

The joint pdf $f(s,D_1,\ldots,D_m)$ is constructed based on the collocated samples of $(s,D_1,\ldots,D_m)$ extracted from wells. One simple way for modeling $f(s,D_1,\ldots,D_m)$ is to assume a multivariate Gaussian distribution between all variables. For example, if porosity is the primary variable of interest and seismic attributes are the secondary data, then the $(m+1)$ dimensional joint pdf can be parametrically modeled:

$$f_{\mathbf{X}}(\mathbf{x}) = (2\pi)^{(m+1)/2} |\sum|^{-1/2} \exp\left\{-\frac{1}{2}(\mathbf{x}-\boldsymbol{\mu})^t \sum^{-1}(\mathbf{x}-\boldsymbol{\mu})\right\} \tag{4-1}$$

where the random vector $\mathbf{x}$ consists of porosity and seismic attribute variables. The mean vector $\boldsymbol{\mu}$ and covariance matrix $\sum$ are calculated at well locations. When the primary variable is not continuous but categorical variable, the joint distribution would be parametrically modeled based on categories by (Krzanowski, 1993; Li and Racine, 2003):

$$f(s,\mathbf{y}) = p(s)(2\pi)^{-m/2} |\sum_s|^{-1/2} \exp\left\{-\frac{1}{2}(\mathbf{y}-\boldsymbol{\mu}_s)^t \sum_s^{-1}(\mathbf{y}-\boldsymbol{\mu}_s)\right\},\ s=1,\ldots,K \tag{4-2}$$

where the joint modeling can be viewed as portioning the $f(\mathbf{y})$ with different outcomes of categories $s=1,\ldots,K$. The mean vector $\boldsymbol{\mu}_s$ and covariance matrix Σ_s are calculated for each category. The multivariate Gaussian assumption cannot account for non-Gaussian features between the variables.

Nonparametric density modeling techniques are distribution free methods that do not rely on the assumption that the data are drawn from a given probability distribution. Various

nonparametric density estimation techniques such as the kernel method and its several variants such as adaptive kernel estimator, maximum likelihood, nearest neighborhood, orthogonal series estimators have evolved and they have demonstrated satisfactory results in various statistical discriminant and inference applications (Izenman, 1991; Scott, 1992; Roberts, 1996; Bressan and Vitria, 2003).

Kernel Density Estimator (Parzen Window Method)

Kernel density estimation (KDE) or the Parzen window method is used for nonparametric modeling of data distribution since it is widely used and studied (Parzen, 1962; Silverman, 1986). The KDE method models the data distribution smoothly through applying the kernel function or weighting function centered on observation data and summing the calculated function values. The kernel estimate for 1-D is defined by (Parzen, 1962; Silverman, 1986):

$$f_{KDE}(x) = \frac{1}{nh}\sum_{i=1}^{n} W\left(\frac{x - X_i}{h}\right) \text{ for } 1-\text{D} \tag{4-3}$$

where h is a bandwidth of the applied kernel function, also referred to the smoothing parameter because h controls the smoothness of the resulting density estimates. $W(\cdot)$ is a 1-D kernel function satisfying $W(x)\geq 0$ and $\int W(x)\mathrm{d}x = 1$ and these conditions make the resulting density estimates be positive and grand total of densities be 1. Quite often kernel function is taken to be a standard Gaussian function with mean of 0 and variance of 1. X_i, i=1,…,n is a set of observation data. Figure 4.1 shows 1-D kernel density estimation example with different bandwidths.

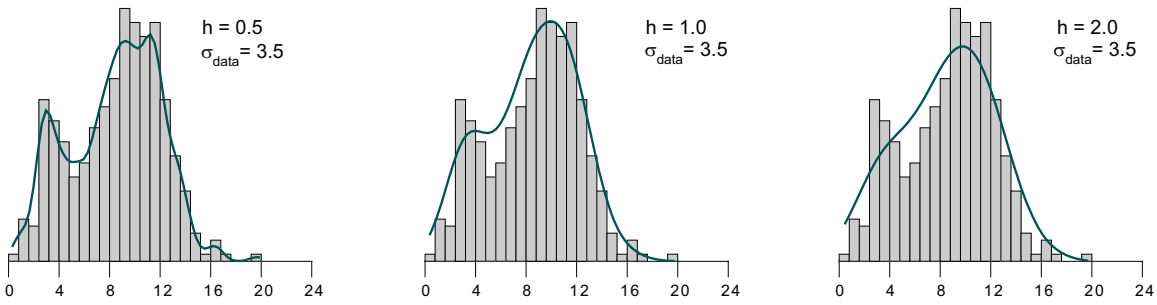

Figure 4.1: Examples of 1-D kernel density estimates with varying bandwidths h. Standard deviation of experimental data σ_{data} is 3.5 and h is arbitrarily chosen with approximately 14%, 28% and 57% of σ_{data}, respectively.

The shape of the estimated density function changes depending on the choice of kernel bandwidth *h*: small *h* makes less smooth and larger *h* makes more smooth density estimates. The choice of bandwidth will be discussed below.

Accuracy of the Estimated Density Functions

Figure 4.1 illustrates the effect of varying the smoothing widths. Improper selection of *h* could result in unreliable density estimates: too small *h* overestimates and too large *h* underestimates the sample histogram. Theoretical accuracy analysis of kernel density estimate was investigated by Rosenblatt (1956) and reviewed by others (Silverman, 1986; Izenman, 1991; Scott, 1992). This section follows the work of Silverman (1986) to assess the accuracy of kernel density estimate. The mean integrated square errors (MISE) between $f_{\mathrm{KDE}}(x)$ and $f(x)$ are defined as (Silverman, 1986):

$$MISE(f_{KDE}(x)) = E\int \left\{ f_{KDE}(x) - f(x) \right\}^2 dx \tag{4-4}$$

Since the integral and expectation operator are commutative, Equation (4-4) gives:

$$\begin{aligned} MISE(f_{KDE}(x)) &= \int E\left\{ f_{KDE}(x) - f(x) \right\}^2 dx \\ &= \int MSE\left\{ f_{KDE}(x) \right\} dx \\ &= \int \left\{ Ef_{KDE}(x) - f(x) \right\}^2 dx + \int \mathrm{var}\, f_{KDE}(x) dx \\ &= \int bias(x)^2 dx - \int \mathrm{var}\, f_{KDE}(x) dx \end{aligned} \tag{4-5}$$

The mean integrated square error is sum of integrated squared bias and integrated variance. These terms both depend on *h*. The bias term is expanded by Taylor expansions (see pages 39–41 in Silverman, 1986) then the integrated squared bias is approximated as:

$$\int bias(x)^2 dx \approx \frac{1}{4} h^4 \mathrm{w}_2 \int f''(x)^2 dx \tag{4-6}$$

where w_2 is a second derivative term of the kernel function *W*:

$$\int t^2 W(t) dt = \mathrm{w}_2 \neq 0 \tag{4-7}$$

Equation (4-6) shows that bias in the estimation of $f(x)$ is proportional to h: smaller h leads to an unbiased estimate, and vice versa. Also, the variance term is expanded and shown as:

$$\int \text{var}\, f_{KDE}(x)dx \approx \frac{1}{nh}\int W(t)^2 dt \tag{4-8}$$

Equation (4-8) shows the variance of $f_{\text{KDE}}(x)$ is inversely proportional to h: smaller h makes larger estimation variance. Comparing Equations (4-6) with (4-8), there is a conflict when choosing an appropriate h. Attempts to reduce bias increase variance.

Selection of Kernel Bandwidths

The choice of a smoothing parameter is a trade-off in terms of minimizing the mean integrated square error. Scott (1992) suggested plotting the density estimates and finding the appropriate h in accordance with the user's knowledge about the distribution. It should be noted that the integrated estimation variance, as shown in Equation (4-8), depends not only on h but also on the number of data n used for density modeling. Increasing the number of samples can relax the necessity of a large h.

A large volume of literature exists on the selection of optimal bandwidth for kernel density estimation (Marron 1987; Park and Marron, 1990; Hall et al., 1991; Jones et al., 1996). Analytical optimal bandwidths were derived to minimize the estimation errors, however, they are not available in practice since they rely on the true unknown density f. Alternatively, the amount of smoothness is chosen based on the data. The following equation is an option for selecting the data driven optimal h (Scott, 1992):

$$h = 1.06\hat{\sigma}n^{-1/5} \quad \text{for} \quad 1-\text{D} \tag{4-9}$$

where $\hat{\sigma}$ is a standard deviation of experimental data. The above relation is derived assuming that the unknown true density function is a normal distribution with variance $\hat{\sigma}^2$. Scott (1992) recommend several attempts with ±20% changes based on the h to finally choose the best smoothing parameter for the data at hand.

Kernel Density Estimation for Multivariate Data

The kernel density estimator in 1-D can be extended in a multivariate case. In its most general form, the multivariate kernel density estimator is defined by (Silverman, 1986; Wand and Jones, 1996):

$$f(\mathbf{x}) = \frac{1}{n}\sum_{i=1}^{n} \mathbf{W}_{\mathbf{H}}\left((\mathbf{x} - \mathbf{X}_i)\right) \tag{4-10}$$

for d-dimension. $\mathbf{W}_{\mathbf{H}}(\mathbf{x})=|\mathbf{H}|^{-1/2}\mathbf{W}(\mathbf{H}^{-1/2}\mathbf{x})$, $\mathbf{W}(\cdot)$ is a multivariate kernel function, and $\mathbf{H}$ is a symmetric positive definite $d\times d$ matrix known as the bandwidth matrix. The multivariate normal distribution is usually used as a kernel function $\mathbf{W}$. Similar to the 1-D kernel estimate, the choice of bandwidth matrix $\mathbf{H}$ is crucial to the multivariate density estimates. Sain et al. (1992) discussed the performance of bootstrap and cross-validation methods for selecting the smoothing parameters in multivariate density estimation, and found that the complexity of finding an optimal bandwidth grows prohibitively as the dimension of data increases.

Product Kernel Implementation

Multivariate kernel density estimation requires the multidimensional kernel function $\mathbf{W}_{\mathbf{H}}$, which comes at a cost: inversion of the $d\times d$ covariance matrix and matrix multiplications are necessary for n observation data at each density estimation step. A more practical implementation is to use product kernel approach which estimates the multivariate densities by multiplying the 1-D kernel estimates (Cacoullos, 1966; Sain et. al., 1992; Scott, 1992):

$$f(\mathbf{x}) = \frac{1}{nh_1 \times \cdots \times h_d}\sum_{i=1}^{n} \mathrm{W}\left(\frac{(x_1 - X_{1,i})}{h_1}\right) \times \cdots \times \mathrm{W}\left(\frac{(x_d - X_{d,i})}{h_d}\right) \tag{4-11}$$

for d-dimension. $\mathrm{W}(\cdot)$ is a 1-D kernel function applied to each variable X_j, j=1,…,d. Kernel bandwidths h_j, j=1,…,d could be different for different variables. Scott (1992) recommended a data-based optimal bandwidth:

$$h_i = \hat{\sigma}_i n^{-1/(d+4)} \tag{4-12}$$

The use of the multivariate kernel function described in Equation (4-10) is theoretically correct; however, the product kernel estimate has little differences in terms of accuracy (Scott, 1992).

Computational Considerations

The flexibility of nonparametric density estimation techniques is placed at the expense of computational cost. Kernel density estimator used through this work evaluates densities at every bin where we want to estimate density. For example, if we have 3 variables (1 primary and 2 secondary variables), 30 sample data and we want density estimates at every 50 bins of variables, then total of $50^3 \times 30 = 3{,}750{,}000$ calculations are required for constructing a 3-dimensional probability density functions. The complexity is expressed in general:

$$(\#\ of\ \ bins)^{(\#\text{ of variables})} \times (\#\text{ of samples}) \tag{4-13}$$

Practical implementation would limit the number of variables by merging secondary variables. More than 5 secondary variables should be merged into less than 6 by aggregating closely related variables

4.2 Marginal Conditions of the Multivariate Distribution

This section is aimed at checking axioms of the joint probability distributions: non negative density functions, closure condition and reproduction of lower order marginal distributions. The kernel density estimator meets the first two axioms if the kernel function $W(\cdot)$ follows $W(x) \geq 0$ and $\int W(x)dx = 1$. The third condition, reproduction of lower order marginal distribution, is a marginality condition that the p-variate joint distribution should reproduce p'-variate distribution where $p' < p$. The followings are possible marginal conditions that the modeled joint distribution $f(s, D_1, \ldots, D_m)$ must meet:

$$\int \cdots \int f(s, D_1, ..., D_m) dD_1 \cdots dD_m = p(s) \tag{4-14}$$

$$\sum_{s=1,...,K} f(s, D_1, ..., D_m) = f(D_1, ..., D_m) \tag{4-15}$$

The marginal relation described in (4-14) states that integration of the multivariate probability distribution over possible outcomes of the secondary data should amount to the 1-D global

probability of the primary variable, p(s). The second marginal relation (4-15) states that integration of the joint probability distribution over possible outcomes of primary variable should reproduce the m-dimensional joint distribution, $f(D_1,\ldots,D_m)$.

The global distribution of the primary variable $p(s)$ is built from well data. Declustering technique such as cell or polygonal declustering is used to obtain representative $p(s)$ if there is a bias in data distribution caused by spatial clustering of wells. The secondary data distribution $f(D_1,\ldots,D_m)$ is modeled with the densely sampled values over the area. The modeling of $f(D_1,\ldots,D_m)$ is very reliable.

There is no guarantee, however, that the modeled joint distributions meet these marginal conditions. $f(s,D_1,\ldots,D_m)$ is modeled based on the limited samples (n) that is much less than the number of secondary values that constitute the marginal distribution $f(D_1,...,D_m)$. The collocated secondary data at the sample locations $\mathbf{u}_i$, i=1,…,n normally does not cover the full range of the secondary data; therefore, the marginal distribution may not match the secondary marginal distribution. Figure 4.2 illustrates this case. The bivariate distribution f_{KDE} (thin solid line) is modeled using four data points (filled circles). Integration of the bivariate distribution over the primary variable (shown as dashed line on horizontal axis) has less variability and nearly zero densities outside the collocated secondary values even if there are some non zero frequencies over that range. The thick solid line on the abscissa represents a secondary data pdf denoted as $f_{\mathrm{reference}}$ and it is built from large number of samples. $f_{\mathrm{reference}}$ have variations in densities through the entire range of secondary values. Moreover, if the global distribution $p(s)$ is a declustered distribution being different from the naïve one then the joint distribution (f_{KDE}) may not lead to the marginal $p(s)$ as well.

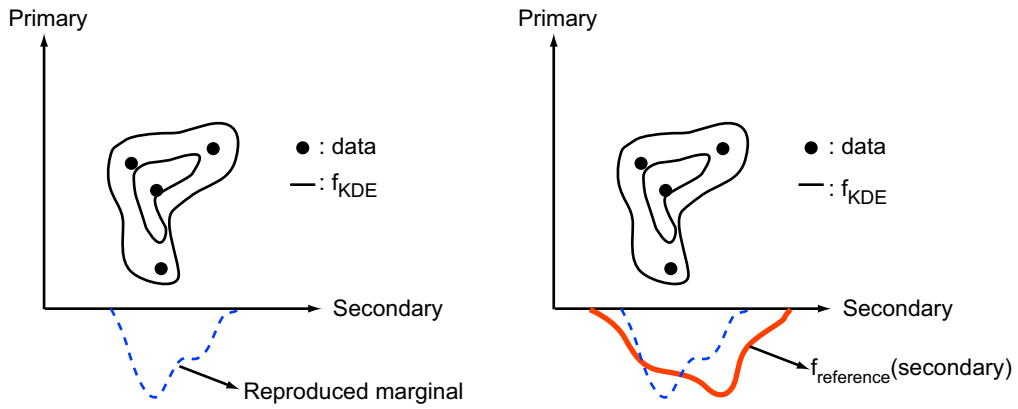

Figure 4.2: Schematic illustration for comparing the reproduced with the known marginal distribution. Since the joint distribution is modeled with the limited well samples its reproduced marginal is not consistent with the (very well-known) marginal pdf which is a distribution of secondary data.

4.2.1 Imposing Marginal Conditions

The defined marginal conditions are requirements of the modeled joint distribution. One option for constraining the marginals is to account for the given marginal constraints while modeling the joint distribution. Copulas function has been devised for this purpose in statistics (Nelson, 2006). This mathematical approach formulates a joint distribution through specifying the relation of transformed marginal variables following uniform distribution (Nelson, 2006).

Exhaustive search algorithms have been applied to make a constrained distribution (Deutsch, 1996; Caers and Ma, 2002, John et al., 2008). They generate a smoothed joint distribution under the user-defined constraints such as mean, variance, correlation coefficient and quantiles that are each combined as objective functions. Despite the flexibility of those techniques to various nonlinear problems, parameter tuning and long search time are concerns.

Given the marginal relations described in Equations (4-14) and (4-15), an algorithm is proposed to impose them on the joint probability distribution. The marginals are derived from initial joint distribution and compared with the reference marginals. The differences are directly accounted for which leads to the updated joint distributions. A similar method was proposed by Deming and Stephan (1940), Ireland and Kullback (1968) and Bishop et al. (1977). The method named as iterative proportional fitting procedure (or IPFP in short) estimates cell probabilities in a 2-D contingency table under the marginal totals. Although the principle of the proposed method in this section is similar to that of the previous study, the method is expanded into the

multidimensional problem with continuous variables. This correcting process is performed by the following steps:

Step1. Model the joint distribution of secondary data, $f(D_1,\ldots,D_m)$ and global distribution of primary variable, $p(s)$. Declustering is considered for obtaining an unbiased $p(s)$ if required.

Step2. Model the joint distribution $f(s,D_1,\ldots,D_m)$ and define it as $f^{(0)}$ to differentiate it from the resulting joint distribution.

Step3. Scale the $f^{(0)}$ to ensure the marginal distribution shown in Equation (4-15). The scaling equation below is proposed for ensuring the imposed marginal condition:

$$f^{(0)}(s,D_1,...,D_m)\times\frac{f(D_1,...,D_m)}{\sum_{s=1,...,K} f^{(0)}(s,D_1,...,D_m)}\rightarrow f^{(1)}(s,D_1,...,D_m) \tag{4-16}$$

The ratio $f(D_1,\ldots,D_m)/\Sigma_{s=1,\ldots,K}f(s,D_1,\ldots,D_m)$ is a modifying factor. If the marginal relation (4-15) is satisfied then this factor becomes 1 leading to no changes in $f^{(0)}$. Otherwise, $f^{(0)}$ is adjusted by the modifying factor that accounts for the differences between the reference $f(D_1,\ldots,D_m)$ and reproduced marginal distribution $\Sigma_{s=1,\ldots,K}\, f(s,D_1,\ldots,D_m)$. The corrected distribution under one marginal condition is set as $f^{(1)}$ for the next step.

Step4. Scale the $f^{(1)}$ to ensure the marginal distribution shown in Equation (4-14). Similar to the step 3, the scaling equation below is for updating the $f^{(1)}$:

$$f^{(1)}(s,D_1,...,D_m)\times\frac{p(s)}{\int\cdots\int f^{(1)}(s,D_1,...,D_m)dD_1\cdots dD_m}\rightarrow f^{(2)}(s,D_1,...,D_m) \tag{4-17}$$

The ratio $p(s)/\int\cdots\int f^{(1)}(s,D_1,\ldots,D_m)dD_1\cdots dD_m$ is another modifying factor. If the marginal relation (4-14) is met then the factor becomes 1 leading to no change in $f^{(1)}$. Otherwise, $f^{(1)}$ is adjusted by the modifying factor accounting for the differences between the reference marginal distribution $p(s)$ and the reproduced marginal distribution $\int\cdots\int f^{(1)}(s,D_1,\ldots,D_m)dD_1\cdots dD_m$. The corrected distribution under marginal condition (4-14) is set as $f^{(2)}$.

Step5. Finish the procedure if the stopping rule is met, otherwise go to step 6.

Step6. Reset $f^{(2)}$ into $f^{(0)}$ and repeat steps 3 through 5.

Step 1 and 2 are initial steps to establish the marginal distributions $p(s)$ and $f(D_1,\ldots,D_m)$. $p(s)$ is a global distribution of the primary variable s constructed from well samples. $f(D_1,\ldots,D_m)$ is m-dimensional secondary data distribution. Steps 3 through 5 are employed to correct the initial

distribution with the considered marginal distributions. The correction is performed by directly accounting for the differences.

Step 5 terminates successive adjustments when the joint distribution becomes stable. One criterion for terminating iteration would be evaluating the differences between the joint distribution at iteration cycle k and $k-1$ and stopping if the averaged marginal error becomes less than a specific tolerance:

$$e_1 = | f^{repro}(D_1,...,D_m) - f^{ref}(D_1,...,D_m) |, e_2 = | p^{repro}(s) - p^{ref}(s) |$$

and

$$e = (e_1 + e_2)/2$$

The proposed algorithm is simple in concept. A small discrete variable example illustrates how the algorithm modifies the joint probabilities.

4.2.2 Examples

The proposed marginal fitting algorithm is tested with small synthetic examples to show how the method modifies the joint probabilities. Consider the following bivariate probability tables with respect to i and j variables:

j variable marginal

0.18						
0.20						
0.19						
0.23						
0.19						
	0.19	**0.16**	**0.26**	**0.20**	**0.19**	– *i* variable marginal

Initial bivariate probabilities

0.19	0.03	0.04	0.04	0.03	0.05
0.28	0.05	0.07	0.08	0.04	0.04
0.17	0.05	0.04	0.04	0.01	0.04
0.17	0.04	0.04	0.03	0.04	0.02
0.19	0.08	0.03	0.04	0.03	0.02
	0.25	0.21	0.23	0.15	0.16

The 5 × 5 cells have bivariate probabilities that should be constrained by the known marginal probabilities of i and j variables. The initial bivariate probabilities are required to impose marginal constraints. In practice, the joint probabilities are modeled from samples which may not match the known marginal probabilities. One example of initial bivariate probabilities is shown in the right and their reproduced marginals are different from the actual marginals. The first

attempt is to correct the probability table under the *i* variable marginal probabilities. Ratios of the known to the reproduced marginals are calculated, and these ratios are multiplied by probability values in each cell leading to an updated probability table. The figure below shows the process of fitting the first marginal:

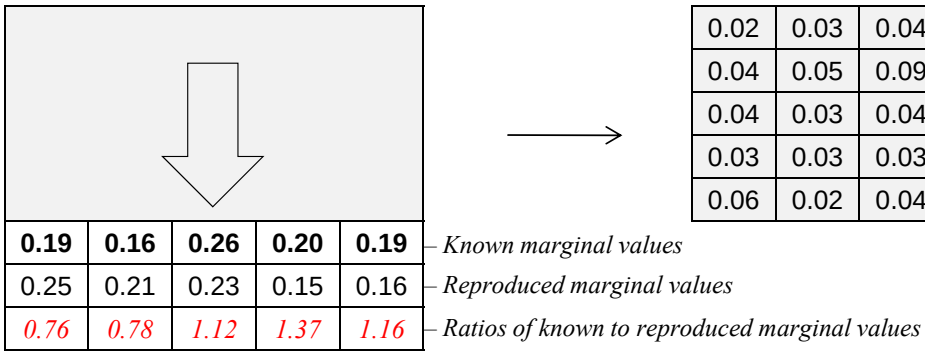

0.19	**0.16**	**0.26**	**0.20**	**0.19**
0.25	0.21	0.23	0.15	0.16
0.76	*0.78*	*1.12*	*1.37*	*1.16*

Known marginal values
Reproduced marginal values
Ratios of known to reproduced marginal values

0.02	0.03	0.04	0.03	0.06
0.04	0.05	0.09	0.05	0.05
0.04	0.03	0.04	0.01	0.05
0.03	0.03	0.03	0.05	0.02
0.06	0.02	0.04	0.05	0.02

The values of bivariate probability are summed up over *j* (in the big arrow direction) generating reproduced marginal values. The ratios of the known to the reproduced marginal probabilities are column basis and they are shown in the bottom row. These ratios are multiplied by each cell probabilities. Adjustments are made to each cell. The right table in the figure above is an updated bivariate probability. The second fitting step is to fit the first updated bivariate probabilities to the marginal probabilities of variable *j*. This second updating process is demonstrated in the figure below:

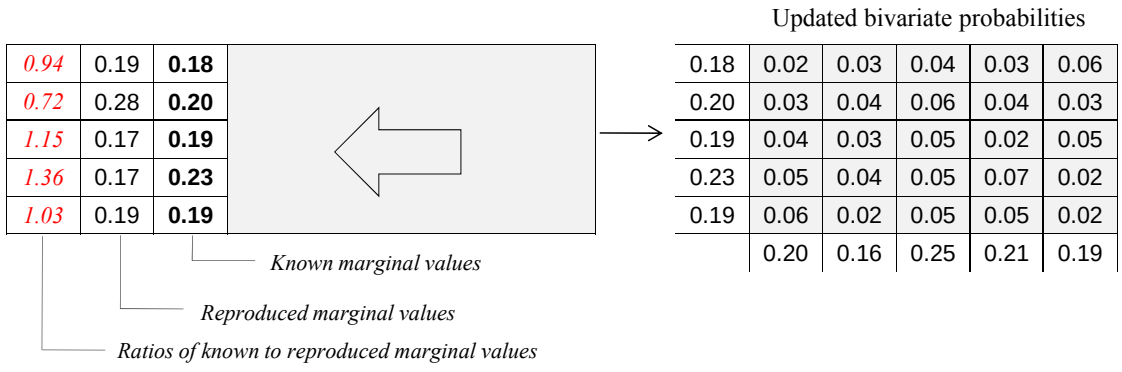

0.94	0.19	**0.18**
0.72	0.28	**0.20**
1.15	0.17	**0.19**
1.36	0.17	**0.23**
1.03	0.19	**0.19**

Known marginal values
Reproduced marginal values
Ratios of known to reproduced marginal values

Updated bivariate probabilities

0.18	0.02	0.03	0.04	0.03	0.06
0.20	0.03	0.04	0.06	0.04	0.03
0.19	0.04	0.03	0.05	0.02	0.05
0.23	0.05	0.04	0.05	0.07	0.02
0.19	0.06	0.02	0.05	0.05	0.02
	0.20	0.16	0.25	0.21	0.19

The modified cell probabilities are summed again over the *i* variable (in the direction of the big arrow). The reproduced marginal probabilities are shown along with the true marginal values in the above figure. Ratios of the known and the reproduced marginal probabilities are row basis. Probability values are multiplied by these ratios again. Adjustments are made to each cell. A set

of horizontal and vertical comparison constitute one cycle for fitting the bivariate probabilities to the known marginal probabilities. The updated bivariate probabilities shown in the right almost exactly reproduce the true marginal probabilities. Initial bivariate probabilities are changed by 28% on average after marginal correction. Another iteration could be performed with horizontal and vertical summing and comparing with marginal values again: correction under the *i* variable marginal probabilities and then correction under the *j* variable marginal probabilities. As iteration proceeds (2^{nd}, 3^{rd} cycle and so on), the marginal errors will monotonically decrease (convergence proof in section 4.3).

The 5×5 bivariate probability example demonstrates how the marginal fitting algorithm modifies the initial probabilities at each iteration step. Figure 4.3 shows another example of applying the algorithm to continuous variables. The initial bivariate pdf is modeled with samples. The extracted univariate marginal distributions from the bivariate pdf do not agree with the true marginal distributions. The extracted marginals and true marginals are shown as dashed and solid lines, respectively. The bivariate pdf is corrected under the marginal constraints and exactly reproduces the marginal distributions. The averaged marginal errors become 0.001% after 200 iterations.

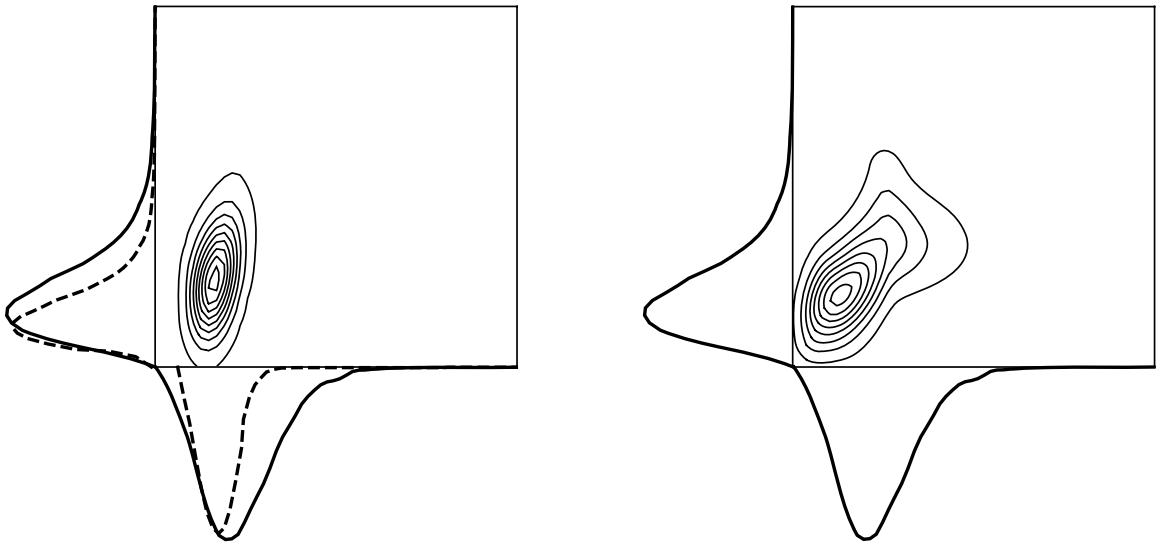

Figure 4.3: The example of the marginal fitting algorithm for the continuous variable. Initial bivariate pdf is shown in the left. The actual marginal and reproduced marginal distributions are shown as sold and dashed lines, respectively. The fitting algorithm updates the initial pdf as shown in the right. Each marginal pdf is exactly reproduced.

The Effect of Initial Distributions

The proposed marginal fitting algorithm modifies the initial distribution to reproduce the fixed marginal distributions that are projections of high dimensions on the lower dimensions. Multiple solutions for joint distributions, therefore, are possible as long as they meet the lower dimensional constraints. Figure 4.4 shows three different initial distributions and the resulting distributions obtained by the marginal fitting procedure for consistent, uncorrelated and inconsistent cases. The consistent case uses samples to model the initial distribution. The inconsistent case assumes negative correlation. The true bivariate distribution is modeled with exhaustive samples and shown in the right of Figure 4.4. The updated distributions generate the same accuracy of marginal errors (e.g. 0.0001%) for three different initial guess; however, the final distributions are different in shape. They preserve the overall relation of initial distribution: positive, uncorrelated and negative bivariate relation. The algorithm cannot correct the inconsistency of the resulting distribution despite satisfying marginal conditions. Fortunately, samples are available for the multivariate distribution modeling and most cases that we face will be consistent cases.

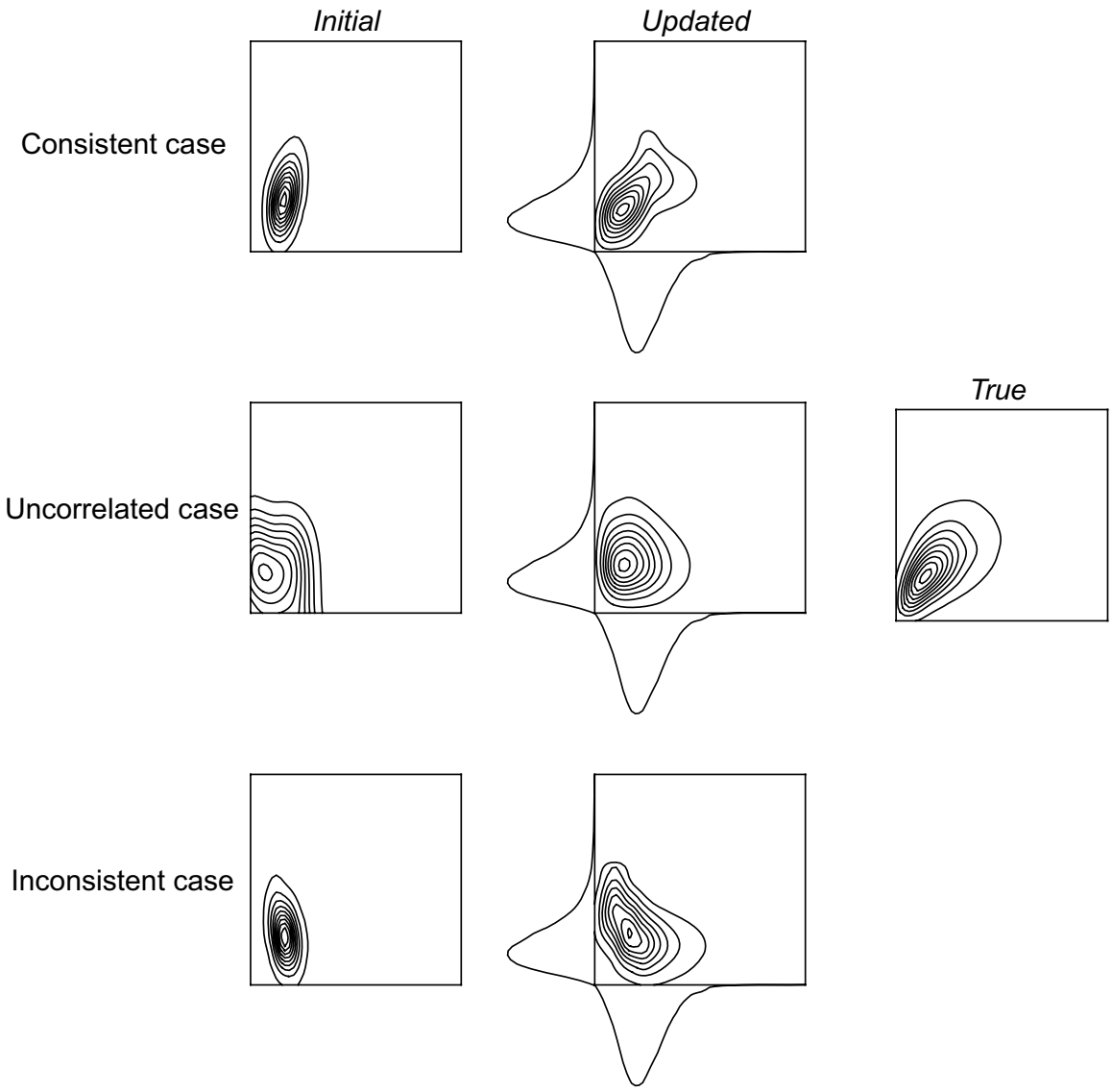

Figure 4.4: The effect of the initial distributions when applying the algorithm. Three different cases generate different final bivariate distributions with the same accuracy of marginal errors.

4.3 Convergence of Sequential Marginal Fitting Algorithm

The considered method is based on the iterative procedure for matching the calculated marginals to the fixed marginals. The final distribution should be stable and converge when iteration is terminated. The algorithm guarantees a monotonic decreasing of the marginal errors. A small discrete case is introduced to show convergence. The bivariate probabilities of RVs X and Y are denoted as $f^{(k)}(x_i,y_j)$, i=1,2 and j=1,2, at k^{th} iteration and they are assigned at four cell. The univariate marginal probability densities are denoted as $g(x_i)$ and $h(y_j)$, i=1,2 and j=1,2. The

$(k+1)^{th}$ iteration corrects the $f^{(k)}(x_i,y_j)$ distribution with respect to the marginal $g(x_i)$ leading to the modified $f^{(k+1)}(x_i,y_j)$ over i and j=1,2. $(k+2)^{th}$ iteration is corrects the $f^{(k+1)}(x_i,y_j)$ with respect to the marginal $h(y_j)$ leading to the modified $f^{(k+2)}(x_i,y_j)$. Similarly, $f^{(k)}(x_i,y_j)$ is a result of marginal correction by $g(x_i)$ and $h(y_j)$ at the previous $(k-2)$ and $(k-1)^{th}$ iterations. Figure 4.5 illustrates the example.

$h(y_2)$	$f^{(k)}(x_1, y_2)$	$f^{(k)}(x_2, y_2)$
$h(y_1)$	$f^{(k)}(x_1, y_1)$	$f^{(k)}(x_2, y_1)$
	$g(x_1)$	$g(x_2)$

Corrected f by marginal $g(x)$

$h(y_2)$	$f^{(k+1)}(x_1, y_2)$	$f^{(k+1)}(x_2, y_2)$
$h(y_1)$	$f^{(k+1)}(x_1, y_1)$	$f^{(k+1)}(x_2, y_1)$
	$g(x_1)$	$g(x_2)$

Corrected f by marginal $h(y)$

$h(y_2)$	$f^{(k+2)}(x_1, y_2)$	$f^{(k+2)}(x_2, y_2)$
$h(y_1)$	$f^{(k+2)}(x_1, y_1)$	$f^{(k+2)}(x_2, y_1)$
	$g(x_1)$	$g(x_2)$

Figure 4.5: Small discrete example showing the convergence.

At (x_1,y_1), $f^{(k+1)}(x_1,y_1)$ is the corrected probability by the marginal densities $g(x_1)$,

$$f^{(k+1)}(x_1, y_1) = \frac{g(x_1)}{f^{(k)}(x_1, y_1) + f^{(k)}(x_1, y_2)} f^{(k)}(x_1, y_1)$$

and $f^{(k+2)}(x_1,y_1)$ is the corrected probability by the marginal densities $h(y_1)$,

$$f^{(k+2)}(x_1, y_1) = \frac{h(y_1)}{f^{(k+1)}(x_1, y_1) + f^{(k+1)}(x_2, y_1)} f^{(k+1)}(x_1, y_1)$$

Inserting $f^{(k+1)}(x_1,y_1)$ into $f^{(k+2)}(x_1,y_1)$ leads to the following,

$$f^{(k+2)}(x_1, y_1) = \frac{h(y_1)}{\frac{g(x_1)}{f^{(k)}(x_1, y_1) + f^{(k)}(x_1, y_2)} f^{(k)}(x_1, y_1) + \frac{g(x_2)}{f^{(k)}(x_2, y_1) + f^{(k)}(x_2, y_2)} f^{(k)}(x_2, y_1)} \times \frac{g(x_1)}{f^{(k)}(x_1, y_1) + f^{(k)}(x_1, y_2)} f^{(k)}(x_1, y_1)$$

where $f^{(k+2)}(x_1,y_1)$ is composed of the fixed marginal $g(x)$ and $h(y)$, and the probability corrected at the previous k^{th} iteration. $f^{(k)}(x_i,y_j)$ is a result from the correction of the $f^{(k-2)}(x_i,y_j)$ with respect to the marginal $g(x)$ and $h(y)$, and thus the ratios $g(x_1)/\{f^{(k)}(x_1,y_1)+f^{(k)}(x_1,y_2)\}$ and $g(x_2)/\{f^{(k)}(x_2,y_1)+f^{(k)}(x_2,y_2)\}$ are equal to 1. The $f^{(k+2)}(x_1,y_1)$ then becomes,

$$f^{(k+2)}(x_1, y_1) = \frac{h(y_1)}{f^{(k)}(x_1, y_1) + f^{(k)}(x_2, y_1)} \times f^{(k)}(x_1, y_1)$$

whereas $f^{(k)}(x_1,y_1)$ is already corrected by the marginal densities $h(y_j)$ at $(k-1)^{\text{th}}$ iteration. Thus, the ratio $h(y_1)/\{f^{(k)}(x_1,y_1)+f^{(k)}(x_2,y_1)\}$ becomes unity and $f^{(k+2)}(x_1,y_1)$ is identical to the $f^{(k)}(x_1,y_1)$. The convergence of the $|f^{(k+2)}(x_1,y_1) - f^{(k)}(x_1,y_1)|=0$ will be reached if the marginal errors diminish. The same proof can be applied to other cells (x_1,y_2), (x_2,y_1) and (x_2,y_2).

Convergence to Correct Distribution

The sequential algorithm updates the given distribution by the marginal constraints. As the iteration proceeds, the marginal errors are decreased and the obtained distribution becomes stable with no changes in probabilities. The convergence of the obtained distribution to the correct distribution is proved. The modified joint distribution at k^{th} and $(k+1)^{\text{th}}$ iteration steps can be simply expressed by,

$$f_{P,S}^{(k)} = f_{P,S}^{(k-1)} \frac{f_S}{f_{\cdot,S}^{(k-1)}} \text{ and } f_{P,S}^{(k+1)} = f_{P,S}^{(k)} \frac{f_P}{f_{P,\cdot}^{(k)}}$$

where the subscript P indicates the primary variable and S indicates a set of secondary variables. f_P and f_S are marginal distributions of the primary and secondary variables deemed as a subset derived from the correct joint distribution $f_{P,S}^{(*)}$. $f_{\cdot,S}^{(k-1)}$ and $f_{P,\cdot}^{(k)}$ are the reproduced marginals from the obtained distribution at $(k\text{-}1)^{\text{th}}$ and k^{th} steps over the primary and secondary variables, respectively. To prove the convergence of $f_{P,S}^{(k)}$ and $f_{P,S}^{(k+1)}$ to $f_{P,S}^{(*)}$, Kullback-Leibler divergence measure is used (Kullback, S. and Leibler, R.A., 1951). KL divergence is a measure of similarity between two probability distributions. The measure is always non-negative and it is zero only if two distributions are identical. KL divergence between the correct distribution $f_{P,S}^{(*)}$ and the obtained distribution $f_{P,S}^{(k)}$ at k^{th} iteration step is,

$$D_{P,S}^{(k)} = \int_{P,S} f_{P,S}^{(*)} \log\left(\frac{f_{P,S}^{(*)}}{f_{P,S}^{(k)}}\right)$$

and it is expanded by,

$$\begin{aligned}
D_{P,S}^{(k)} &= \int_{P,S} f_{P,S}^{(*)} \log\left(\frac{f_{P,S}^{(*)}}{f_{P,S}^{(k)}}\right) \\
&= \int_{P,S} f_{P,S}^{(*)} \log\left(f_{P,S}^{(*)}\right) - f_{P,S}^{(*)} \log\left(f_{P,S}^{(k-1)} \cdot \frac{f_S}{f_{\cdot,S}^{(k-1)}}\right) \\
&= \int_{P,S} f_{P,S}^{(*)} \log\left(f_{P,S}^{(*)}\right) - f_{P,S}^{(*)} \log\left(f_{P,S}^{(k-1)}\right) - f_{P,S}^{(*)} \log\left(f_S\right) + f_{P,S}^{(*)} \log\left(f_{\cdot,S}^{(k-1)}\right) \\
&= \int_{P,S} f_{P,S}^{(*)} \log\left(\frac{f_{P,S}^{(*)}}{f_{P,S}^{(k-1)}}\right) - \left(\int_{P,S} f_{P,S}^{(*)} \log\left(f_S\right) - f_{P,S}^{(*)} \log\left(f_{\cdot,S}^{(k-1)}\right)\right)
\end{aligned}$$

The first integral term in the expansion above is KL divergence at $(k\text{-}1)^{\text{th}}$ step and thus,

$$
\begin{aligned}
D_{P,S}^{(k)} &= D_{P,S}^{(k-1)} - \left(\int_{P,S} f_{P,S}^{(*)} \log\left(f_S\right) - f_{P,S}^{(*)} \log\left(f_{\cdot,S}^{(k-1)}\right) \right) \\
&= D_{P,S}^{(k-1)} - \left(\int_{S} f_{\cdot,S}^{(*)} \log\left(f_{\cdot,S}^{(*)}\right) - f_{\cdot,S}^{(*)} \log\left(f_{\cdot,S}^{(k-1)}\right) \right) \text{ where } f_S = f_{\cdot,S}^{(*)} \\
&= D_{P,S}^{(k-1)} - D_S^{(k-1)}
\end{aligned}
$$

Finally, KL divergence at k^{th} step has the following relation with KL divergence at $(k\text{-}1)^{\text{th}}$ step,

$$
D_{P,S}^{(k)} = D_{P,S}^{(k-1)} - D_S^{(k-1)}
$$

Because the KL divergence is always non-negative, the following inequality holds,

$$
D_S^{(k-1)} = D_{P,S}^{(k-1)} - D_{P,S}^{(k)} \geq 0 \Leftrightarrow D_{P,S}^{(k-1)} \geq D_{P,S}^{(k)} \tag{4-18}
$$

Similarly, the relation below is derived for k^{th} and $(k+1)^{\text{th}}$ iteration,

$$
D_P^{(k)} = D_{P,S}^{(k)} - D_{P,S}^{(k+1)} \geq 0 \Leftrightarrow D_{P,S}^{(k)} \geq D_{P,S}^{(k+1)} \tag{4-19}
$$

Equations (4-18) and (4-19) show that KL divergence is monotonically decreasing and the sequential iteration makes the obtained joint distribution into the correct distribution.

The numerical experiments investigated in the next chapter show that the first few iterations drastically drop the marginal errors and generate stable joint distributions.

Chapter 5

Applications of Multivariate Distribution Modeling

This chapter implements modeling the joint probability distribution under the specified distribution constraints and demonstrates several applications of the methodology for reservoir facies modeling through incorporating diverse data. Synthetic and field data are tested and results are evaluated in terms of defined criteria.

Section 5.1 presents integration of secondary data for facies modeling. Mixtures of continuous secondary and discrete primary variables are jointly modeled. The constraints for the joint distributions are described. The marginal fitting algorithm discussed in Chapter 4 is applied to correct the joint distribution. Seismic data or inverted seismic attributes typically have larger scale than that of modeling cell or well data. The latter part of Section 5.1 illustrates how large scale seismic data can be integrated and can provide facies proportions for relatively large volumes.

Section 5.2 demonstrates the applicability of the joint modeling approach to debias global facies proportions. Obtaining representative statistics is crucial to geostatistical reservoir modeling, however, it is difficult to obtain unbiased statistics from the sparse well samples. This section demonstrates the usefulness of incorporating the secondary data to obtain the representative statistics through the modeling of joint relation.

Section 5.3 describes combining geologic analog information (or interpreted geologic map) with multiple soft secondary information through joint modeling. Mixed joint distribution of continuous and discrete variables is modeled in a nonparametric way and the marginal constraints are imposed to obtain a corrected joint distribution.

This application demonstrates the value of the joint distribution modeling technique for integrating different types of secondary and primary data. Nonparametric modeling enables us to model the data distribution without distribution assumption, which accounts for the joint relation among variables more realistically. The implemented marginal fitting algorithm makes the modeled joint distribution legitimate at less computational burden.

5.1 Integrating Multiple Soft Secondary Data

Consider facies modeling conditioned to multiple secondary data. The joint probability distribution of the primary facies and secondary variables is defined:

$$f(s, y_1..., y_m) \tag{5-1}$$

where s and $\mathbf{Y}=[y_1,\ldots,y_m]$ are random variables representing discrete facies codes taking $s=1,\ldots,K$ and continuous secondary data, respectively. If there are many secondary variables, for example $m \geq 5$, then aggregating those variables would be necessary by dimension reduction preprocessing. Aggregated variables are to be considered as secondary variables for integration.
The conventional approach to joint probability distribution modeling of categorical and continuous variables is to express it as a conditional distribution of continuous variables given the values of the categorical variables, times the marginal probability of the latter which is a probability of the categorical variable, for example $f(y_1,\ldots,y_m|s)p(s)$, $s=1,\ldots,K$ (Krzanowski, 1993). The joint expression shown in Equation (5-1), however, is a more general form and it can provide any lower order distributions by integrating any sub set of variables over the rest of variables, which allows us to compare the lower order distributions with reference distributions. These reference distributions are modeled from the exhaustive secondary data. K, the number of distinct facies, is typically limited between 2 and 6. The facies become difficult to distinguish if they are divided into more than 6 as the measured property distributions overlap. Once the joint probability distribution $f(s,y_1,\ldots,y_m)$ is modeled, a conditional probability of facies given the collocated secondary data at location $\mathbf{u}$ is immediately derived by the definition or a conditional probability (Bayes relation):

$$p(s \mid y_1,...,y_m) = \frac{f(s, y_1,...,y_m)}{f(y_1,...,y_m)}, \quad s = 1,...,K \tag{5-2}$$

5.1.1 Amoco Examples

The Amoco test data introduced in Chapter 3 are used again: the data set are extracted from a West Texas Permian Basin reservoir and contain reservoir properties such as porosity and facies types from 62 wells and exhaustively sampled seismic data over 10,400ft by 10,400ft area. Porosities sampled at 62 well locations are simulated over the area to be treated as secondary data in addition to the seismic data. Figure 5.1 shows cross plots of seismic and simulated porosity. This cross plot shows that the considered secondary data has an ability to separate the two facies: data points representing faces 1 (open circles) are located in the area of high porosity and seismic, and points representing facies 2 (black circles) are located in the area of low porosity and seismic values.

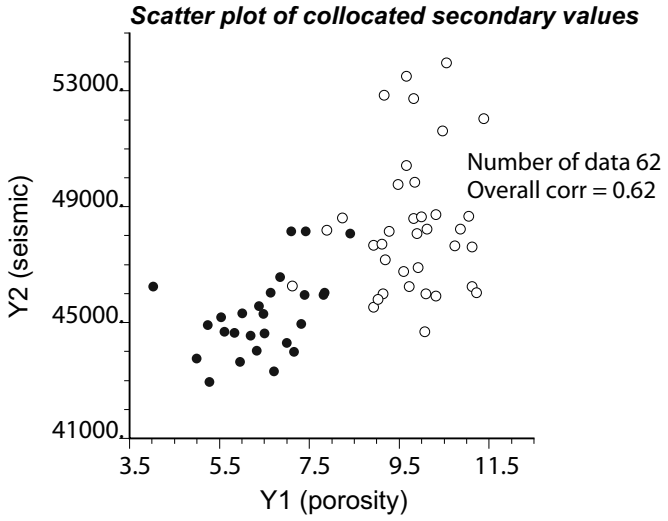

Figure 5.1: Cross plot of collocated secondary data.

The joint probability distribution of interest is $f(s,y_1,y_2)$ and the marginal distributions of $f(s,y_1,y_2)$ must amount to $p(s)$, s = 1,2 and $f(y_1,y_2)$ where y_1 and y_2 represent porosity and seismic data. The global probability (or proportion) p(s) are simply calculated by counting the corresponding number from 62 samples: $p(s=1)$ is 0.58=36/62 and $p(s=2)$ is 0.42=26/62. Because of the cluster of wells in the north-east corner, the representative proportions would be different from the naïve proportions. Cell declustering was performed to mitigate the geometric clustering effect, and the

declustered global proportions of facies are derived as $p(s=1) = 0.514$ and $p(s=2) = 0.486$ (Deutsch and Journel, 1998). The bivariate pdf of the secondary variables, $f(y_1,y_2)$, is another marginal distribution to constrain the joint distribution $f(s,y_1,y_2)$. There are 4335 samples available for $f(y_1,y_2)$ modeling. Figure 5.2 shows the modeled $f(y_1,y_2)$ by kernel density estimation. The bivariate distribution could be assembled by directly sampling the frequency from the 2-D histogram when the number of data is large (Doyen, 2007). The number of bins where the bivariate densities are estimated is chosen as 50 and so the bivariate probability densities are estimated at every 50 by 50 pixels in Figure 5.2.

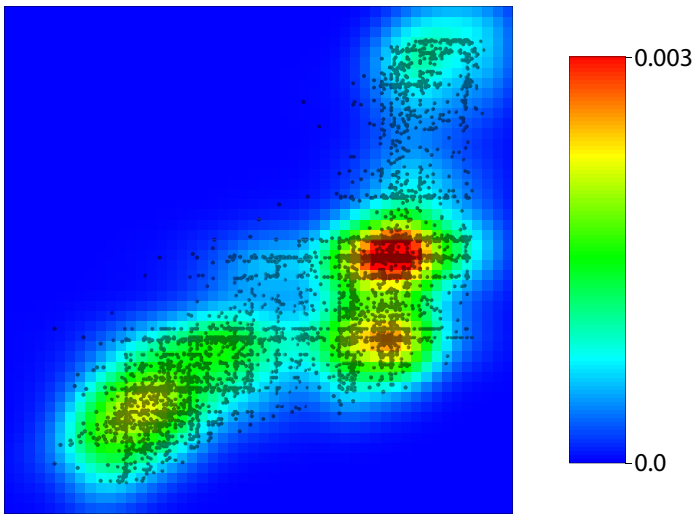

Figure 5.2: The modeled bivariate distribution of secondary data $f(y_1,y_2)$. The experimental 4225 data points are overlaid.

The 4225 data points are plotted with the smoothed bivariate distribution. The modeled probability distribution reasonably honors the means, variance and correlation coefficient from experimental data. The joint probability density function $f(s,y_1,y_2)$ is modeled based on the 62 data. The joint pdf by the product kernel estimator is modeled by:

$$f(s,y_1,y_2) = \frac{1}{nh_1 \times h_2} \sum_{i=1}^{n=62} \left(\prod_{j=1}^{m=2} \mathrm{w}\left(\frac{y_j - y_{j,i}}{h_j} \right) \right) \times \mathrm{I}(s_i) \qquad (5\text{-}3)$$

where w(·) is a 1-D normal kernel function. This equation is a slightly modified equation from the product kernel estimation shown in Equation (4-12). Since the primary variable is a discrete variable not a continuous variable indicator function $\mathrm{I}(s_i)$ is added. The indicator function $\mathrm{I}(s_i)$ takes 1 if facies from i^{th} data out of n(=62) data corresponds to the facies code being modeled,

otherwise taking 0. For example, $n_{s=1}$=36 samples out of 62 are used for modeling of $f(s=1,y_1,y_2)$, and $n_{s=2}$=26 samples out of 62 are used for modeling of $f(s=2,y_1,y_2)$. Equation (5-3) allows the kernel estimation with the mixed continuous and discrete variables. Kernel bandwidth h_j, j=1,2 is set differently for different secondary variable. Figure 5.3 shows the modeled joint pdf before being constrained by marginal conditions. Although the joint probability distributions are modeled in 3-dimensional space (1 primary + 2 secondary variables), the distributions are clipped and illustrated separately based on the facies variable for better visualizing and understanding. Kernel bandwidths are chosen based on the relation $h_j = \hat{\sigma}_j n^{-1(d+4)}, j = 1,2$ and $d = 2$ (Scott, 1992).

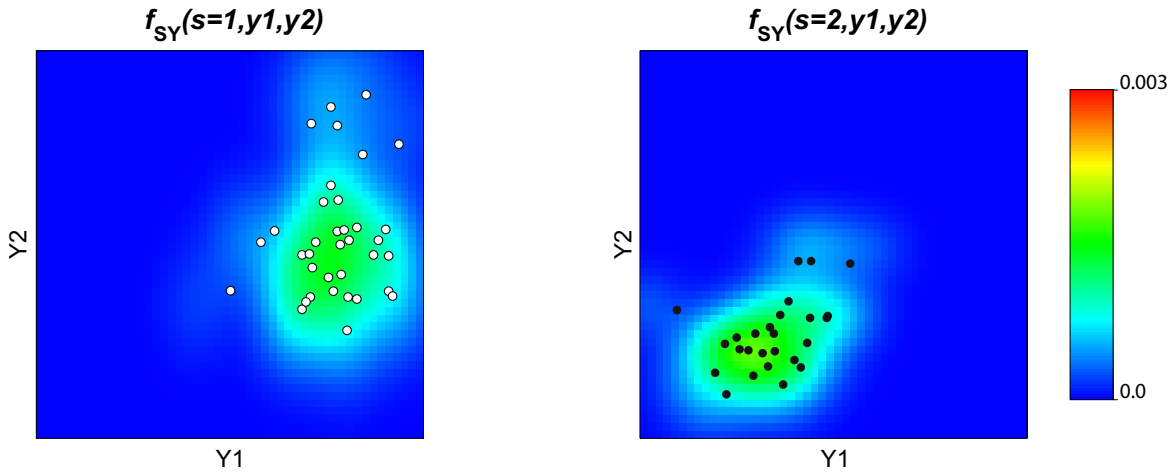

Figure 5.3: The estimated joint probability distributions. The 3-D distribution is displayed separately for each facies category.

The bivariate distributions (clipped by facies code) reasonably reflect the experimental data distributions. This reliance on data distribution is a strength of the nonparametric approach.

The modeled joint distributions should match the reference marginal distributions. The marginal relations are for this example:

$$\sum_{s=1}^{2} f(s, y_1, y_2) = f(y_1, y_2) \tag{5-4}$$

$$\int\int f(s, y_1, y_2) dy_1 dy_2 = p(s), \;\; s = 1,2 \tag{5-5}$$

The left sides of above relations are the lower order distributions from the joint distribution. The right sides are the reference distributions. The integration of $f(s=1,y_1,y_2)$ and $f(s=2,y_1,y_2)$ should

amount to $f(y_1,y_2)$, and totals of $f(s=1,y_1,y_2)$ and $f(s=2,y_1,y_2)$ over outcomes of (y_1,y_2) should amount to $p(s=1)$ and $p(s=2)$, respectively. The sequential marginal fitting algorithm detailed in Section 4.2 is applied to the initial joint distribution resulting in a corrected distribution that meets all required marginal conditions. Figure 5.4 shows the corrected distributions constrained by marginals using the algorithm. The unconstrained initial joint distributions are shown as well in the left of the figure. Accounting for Equations (5-4) and (5-5) can be interpreted as adding up the probability densities at every bins with the vertical direction and with horizontal direction in Figure 5.4. The reproduced marginals and the reference marginals are compared in those directions. The reproduced marginals from initial and corrected distributions are illustrated on (y_1,y_2) plane (bottom), and on axis of the primary variable, respectively.

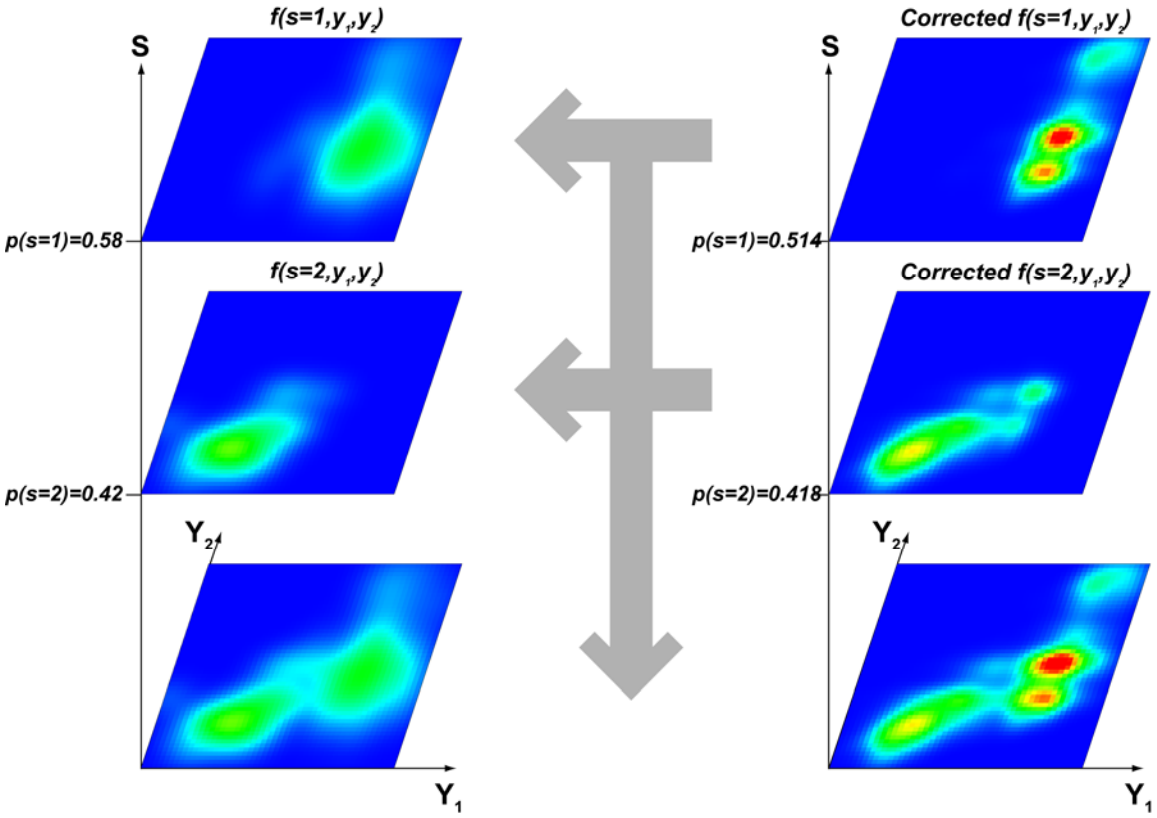

Figure 5.4: The joint probability distributions modeled by kernel estimator (left column) and modified distributions constrained by the imposed marginal conditions (right column). The arrow shown in the middle represents the direction of marginal fitting: two horizontal directions are to compare the probability of facies $p(s)$, and vertical direction is to compare the secondary data distribution $f(y_1,y_2)$.

Due to the richness of (y_1,y_2) samples and the reliability of $f(y_1,y_2)$, detailed variations on distributions are imparted to the corrected distributions. Areas of high porosity and high seismic values (upper right corner) get high probability of facies 1 after marginal correction. The probability of facies 2 increases around middle porosity and seismic value area (centre). These changes have an impact on the final estimates of facies probability.

The corrected joint distributions are obtained after 20 marginal fitting iterations. Figure 5.5 shows the averaged marginal errors between empirical distributions and reference distributions versus iteration numbers. The first few iterations drop the errors quickly and the averaged errors become less than 0.1% before 8 iterations. Each iteration involves $B^m+B^m\times K$ arithmetic operations and comparisons where B is number of bins, m is the number of secondary variables and K is the number of categories. The first loop B^m is for fitting with the distribution of secondary variables and the second loop $B^m\times K$ is for fitting with the probability of primary

variable. For the present example, a single iteration consists of $7500=50^2+50^2\times2$ arithmetic operations. 20 fitting iteration took a few seconds on a 3.2 GHz personal computer.

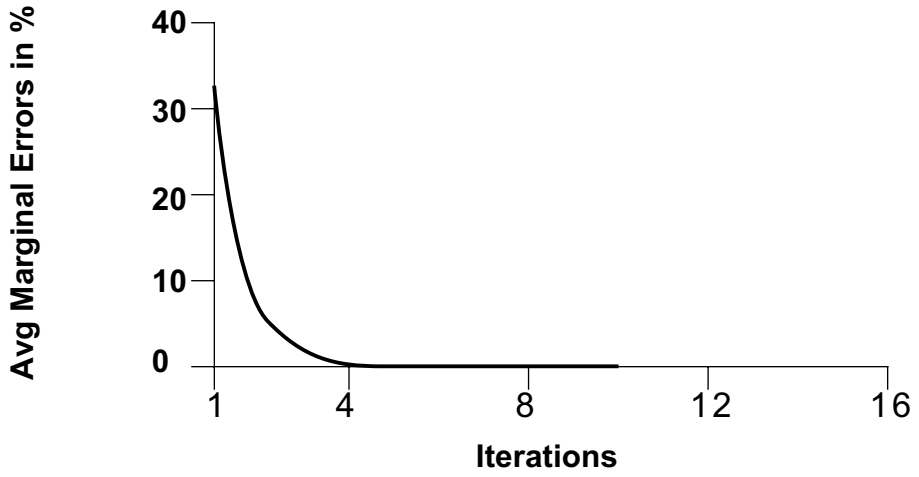

Figure 5.5: Averaged marginal errors versus iterations for Amoco test data.

Given the joint distributions between all of variables, the conditional probability of facies given secondary values, $p(s(\mathbf{u})|y_1(\mathbf{u}),y_2(\mathbf{u}))$, $\mathbf{u} \in A$, is immediately derived. In practice, the given secondary values $y_1(\mathbf{u})$ and $y_2(\mathbf{u})$ are actual data, but the closest values are looked up in the discretized y_1 and y_2 in probability modeling space. Discretization errors can be encountered when too few bins are considered. A large number of bins incurs a high cost of computation. Figure 5.6 shows secondary derived facies probabilities and their histograms. Visual inspection shows that local well data is reasonably honored by the estimated facies probability.

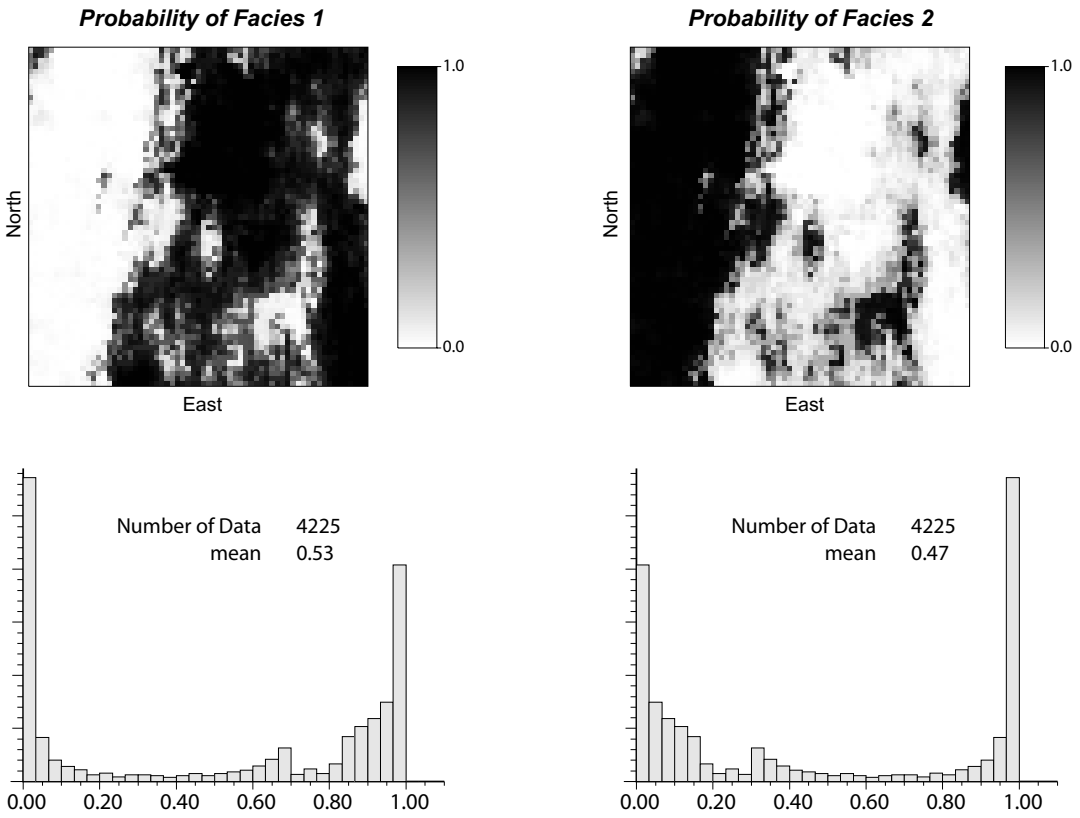

Figure 5.6: Estimated facies probability using the updated joint distribution and histograms of estimated soft values.

Accuracy Assessments

Close reproduction of facies proportions to the global proportion is a quick check. Averages of the estimated probabilities $p(s(\mathbf{u})|y_1(\mathbf{u}),y_2(\mathbf{u}))$ $\mathbf{u}\in A$ are close to the input representative proportions, $p(s=1)=0.514$ and $p(s=2)=0.486$.

The estimated local probability is evaluated based on the criterion introduced in Section 3.6: comparison of the predicted probability versus the proportions of samples actually occurring in the predicted probability. Figure 5.7 shows the accuracy plots of the results. The actual fractions of samples are calculated at the given predicted probability with 0.1 probability increment. The closeness to the 45° line indicates the goodness of the model. When few samples are counted as falling within a p predicted probability, the computed fractions are shown as open circles that might not be used for evaluating the model. The overall accuracy plot indicates the goodness of the probability model.

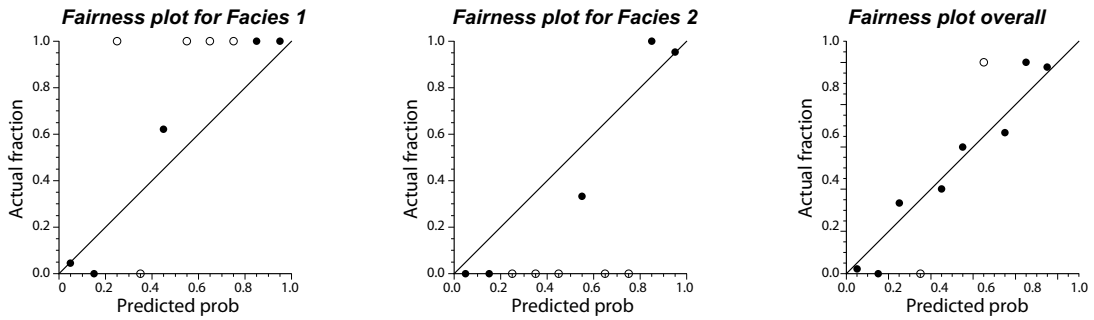

Figure 5.7: Fairness plots of the local probabilities for the Amoco case. Actual fractions with few samples are shown as open circles and they are not used to evaluate the estimated local probability.

Building Stochastic Models

The derived faces probability from the given secondary data is integrated with indicator well data. Sequential indicator simulation is performed using Bayesian updating equation to integrate the secondary derived probability. The reasonableness of the generated realizations is checked with the reproduction of variograms. Figure 5.8 shows the computed variograms from 21 realizations. The effectiveness of integrating secondary data is observed by the small fluctuations in the reproduced variograms.

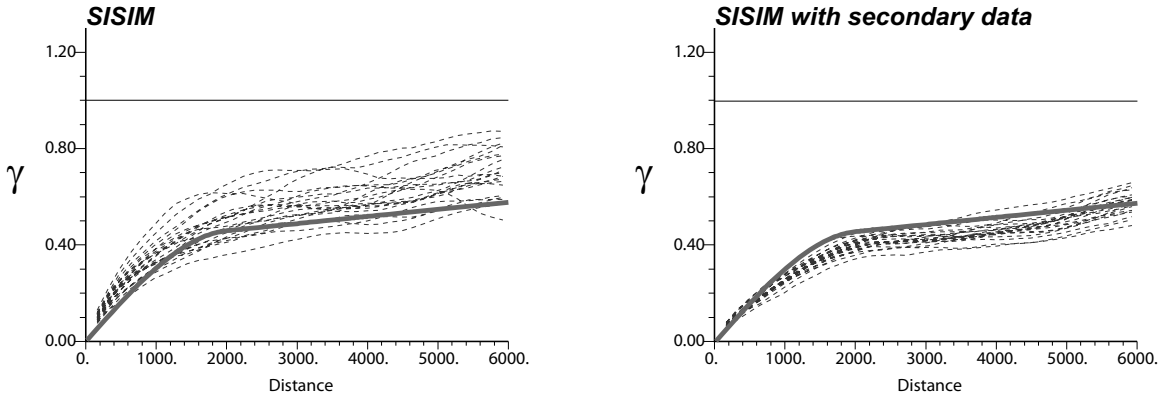

Figure 5.8: The reproduced variograms in NS direction from 21 realizations: SISIM without secondary data (left) and with secondary derived probability that are obtained from the multivariate pdf modeling technique.

5.1.2 West African Reservoir Example

Additional field data are tested with the proposed approach. A West African deepwater turbidite reservoir is modeled with several seismic attributes. The reservoir is located in an average water depth of 1,200ft and consists of stacked and amalgamated Micocene turbidite channel complex that fills the steep canyons (Hoffman et. al., 2005). Vertically, individual meandering channels exist within three stratigraphic units (Figure 5.9).

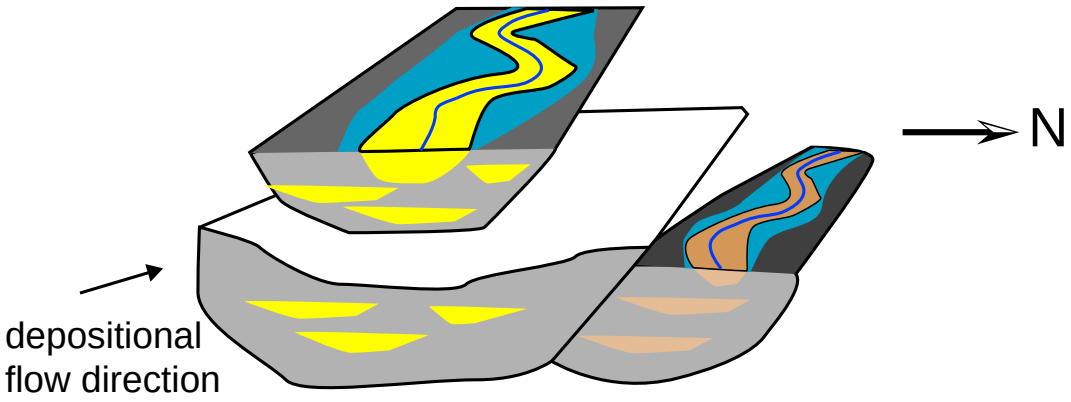

Figure 5.9: Interpreted stratigraphic units over the reservoir. Three massive bodies are interpreted with individual meandering channels. Four main facies are identified: high net-to-gross channel, sand, and low net-to-gross shale and shaly sand.

Four distinct facies are identified in core analysis: three sand facies with varying quality (coded 2 through 4) and a shale facies (coded 1). Sand facies represent a continuum of high, medium and low net-to-gross (NTG). The area extends 5850m × 4425m × 696ft and the following grid is defined over the area:

	X	Y	Z
Number of grids	78	59	116
Grid size	75m	75m	6ft

A total of 533,832 grid nodes are defined for the modeling, but only approximately 100,000 are active. Seismic inversion provided high resolution seismic attributes in 3-D: acoustic impedance, fraction of shale using three different inversion techniques and amplitude. All seismic attributes

were provided as normalized units within [0,1]. Figure 5.10 shows 3-D sections of the first seismic attribute with wells.

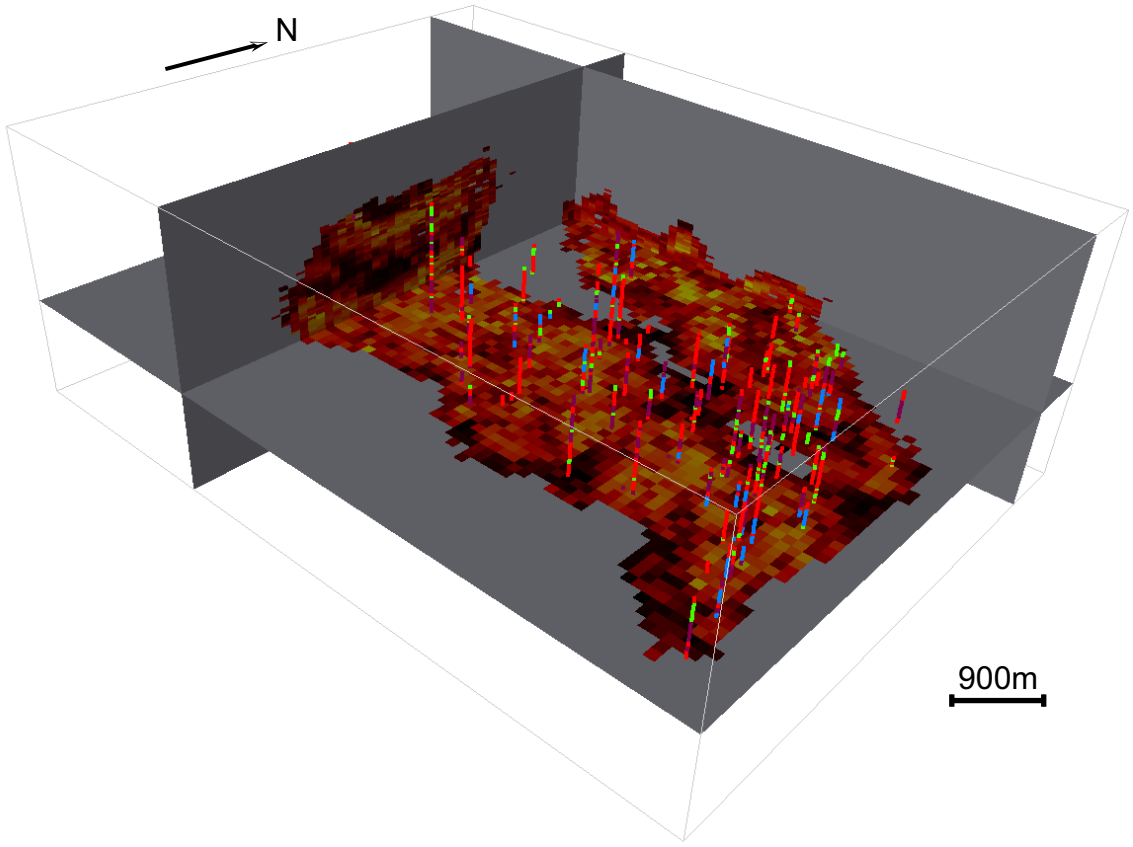

Figure 5.10: 3-D view of the first seismic attribute.

Figure 5.11 shows a histogram of the seismic attributes. The distribution of seismic variables 2 and 3 are almost the same distribution: very close mean, variance and quantiles each other. Seismic variables 1 and 4 are distributed over the full range of [0,1], but seismic variable 5 is limited by a maximum value of 0.34 with low variance.

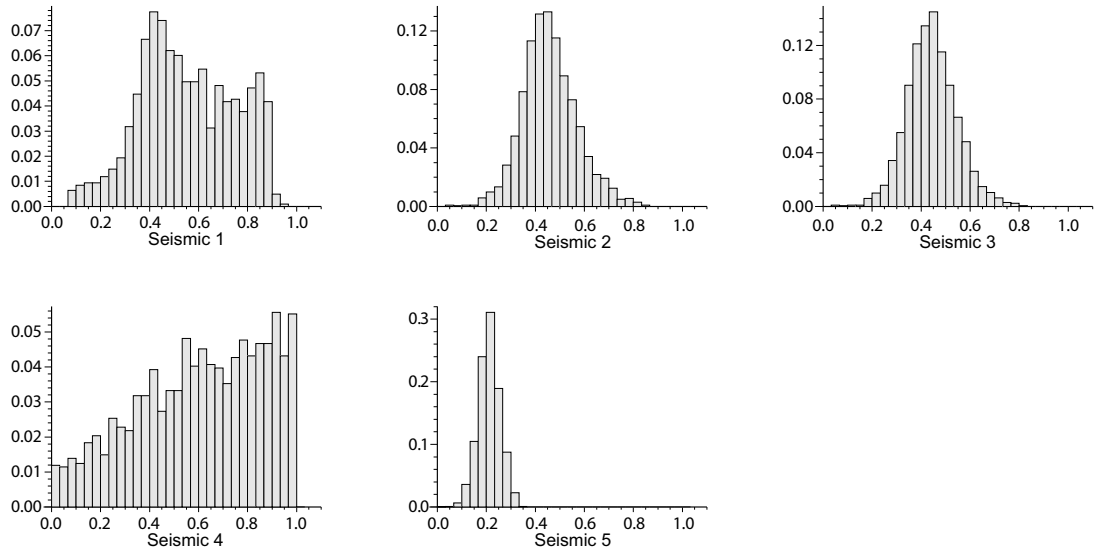

Figure 5.11: Distributions of seismic attributes sampled from well locations.

Table 5.1 summarizes the relations between seismic attributes (denoted as S1 ~ S5) and facies types (F1 ~ F4). This descriptive statistics can provide the overall interpretation about the redundancy and relevance among variables.

Table 5.1: Linear correlation among variables

	Seismic 1	Seismic 2	Seismic 3	Seismic 4	Seismic 5	F1	F2	F3	F4
Seismic 1	1.0	-0.25	-0.05	0.31	0.06	0.34	0.01	-0.08	-0.31
Seismic 2		1.0	0.91	-0.07	0.57	0.07	-0.06	-0.03	-0.02
Seismic 3			1.0	0.01	0.53	0.09	-0.03	-0.04	-0.05
Seismic 4				1.0	0.09	0.20	0.02	-0.03	-0.21
Seismic 5					1.0	0.25	-0.09	-0.02	-0.2

Seismic variables 2 and 3 have weak correlations with all facies types. Seismic variables 1, 4 and 5 are somewhat correlated to facies 1 and 4, but barely correlated to facies 2 and 3. Based on the summary of correlation and histograms, seismic variables 1, 4 and 5 can be candidates for secondary variables to be integrated. The key idea is to choose seismic attributes that maximize the correlation between the seismic and facies, and minimize the correlation between the seismic themselves. Seismic 1 and 5 (noted as RVs Y_1 and Y_2 hereafter) are chosen since they are more related to facies and less related to each other. One may assume that the magnitude of correlation between the considered seismic and facies does not seem to be high enough. Integrating diverse data, however, could make features unseen in the individual data emerge and thus secondary data with small correlations to the primary data are worth to be considered unless zero correlations are

observed (see the improvements in the correlation coefficient shown in Figure 5.19). It is possible to use all of seismic attributes data for facies modeling, for the proposed method implicitly accounts for data redundancy among all of variables; thus, information from data is maximally used and information from highly redundant data is used correctly. Despite this ability to account for data redundancy, variable selection (or variable merging by data aggregation) as a pre-processing step saves computational time.

Figure 5.12 shows a scatter plot of Y_1 and Y_2 and its modeled bivariate distribution. 50 bins are defined for each secondary variable. Too many bins lead to unreliable density estimates since few data fall into each bin interval or noise in the data is not sufficiently removed. Too few bins make imprecise blocky probability distributions. Discretization errors arise when too few bins are considered. Kernel estimation is used for modeling $f(y_1,y_2)$ and kernel bandwidths are based on the analytical suggestion.

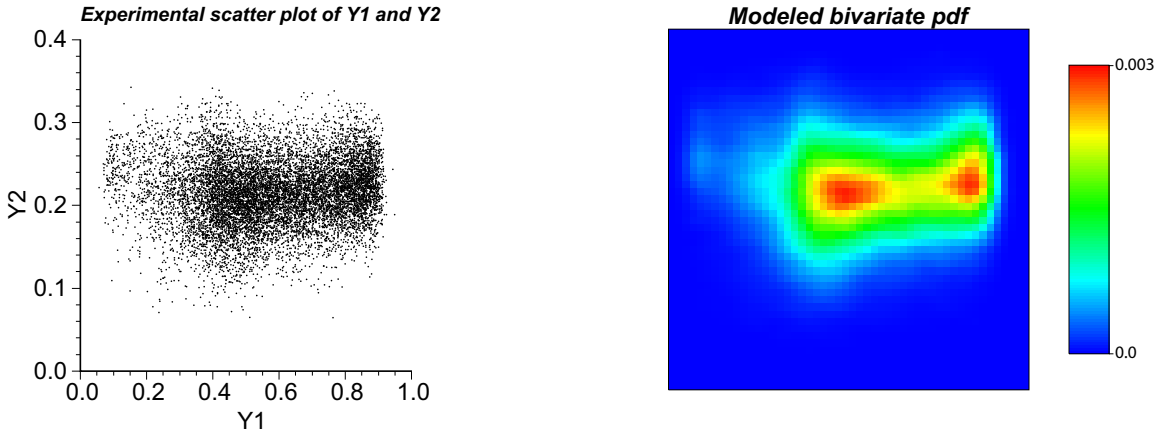

Figure 5.12: Scatter plots of exhaustive seismic values and its modeled probability distributions.

The proportions of the four facies are calculated using well samples. Cell declustering is applied to get unbiased proportions:

Code	Facies description	Proportions
1	Shale	$p(s=1)=0.447$
2	Shaly sand	$p(s=2)=0.103$
3	Clean sand	$p(s=3)=0.115$
4	Channel	$p(s=4)=0.308$

The prepared $f(y_1,y_2)$ and $p(s)$ are marginal constraints that $f(s,y_1,y_2)$ must consider. It is good practice to plot experimental data points before inferring the joint distribution. Figure 5.13 shows scatter plots of the selected seismic variables depending on different facies types. If the seismic data have good capability of identifying facies, then the data points will fall in distant groups. For this example, the scatter plots of mean values are shown in the bottom of Figure 5.13. Means of (Y_1,Y_2) for facies 2 and 3 closely overlap and means of (Y_1,Y_2) for facies 1 and 4 are somewhat separated. The chosen seismic data helps identify shale (F1) and channel facies (F4), and does not help recognize intermediate sand facies (F2 and F3). This results from the weak correlation of the selected seismic attribute 1 and 5 to the facies 2 and 3.

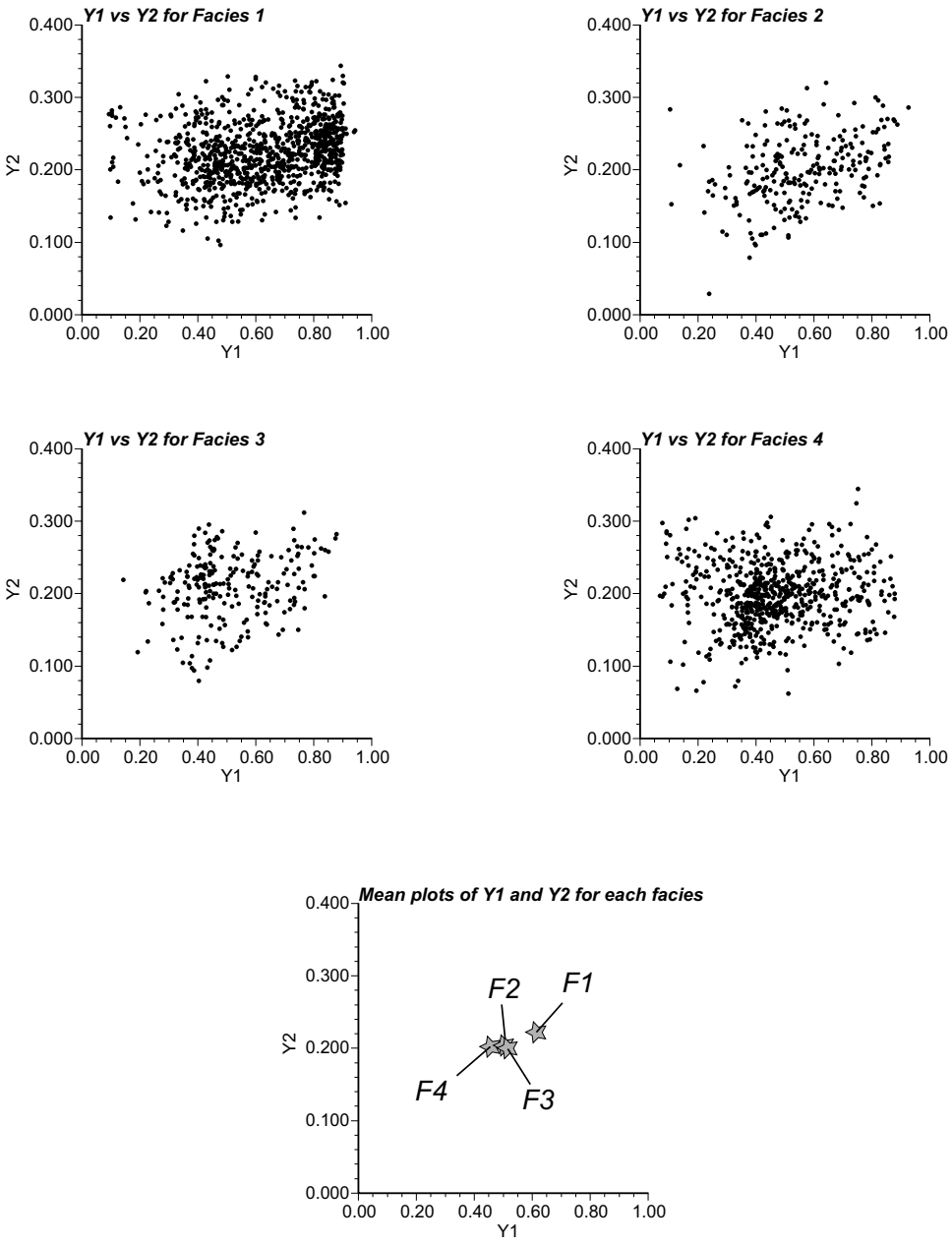

Figure 5.13: Scatter plots of the selected seismic variables (denoted as Y_1 and Y_2) with different facies types. The means of Y_1 and Y_2 for each facies are plotted in the bottom.

The joint distributions are modeled based on experimental data plots. The same number of bins (50) used for secondary data distribution modeling is applied. Kernel bandwidths are decided based on the analytical suggestion shown in Equation (4-12). The modeled joint distribution in 3-D are clipped and illustrated separately based on different facies types. Figure 5.14 represents the modeled initial joint distributions using the product kernel method.

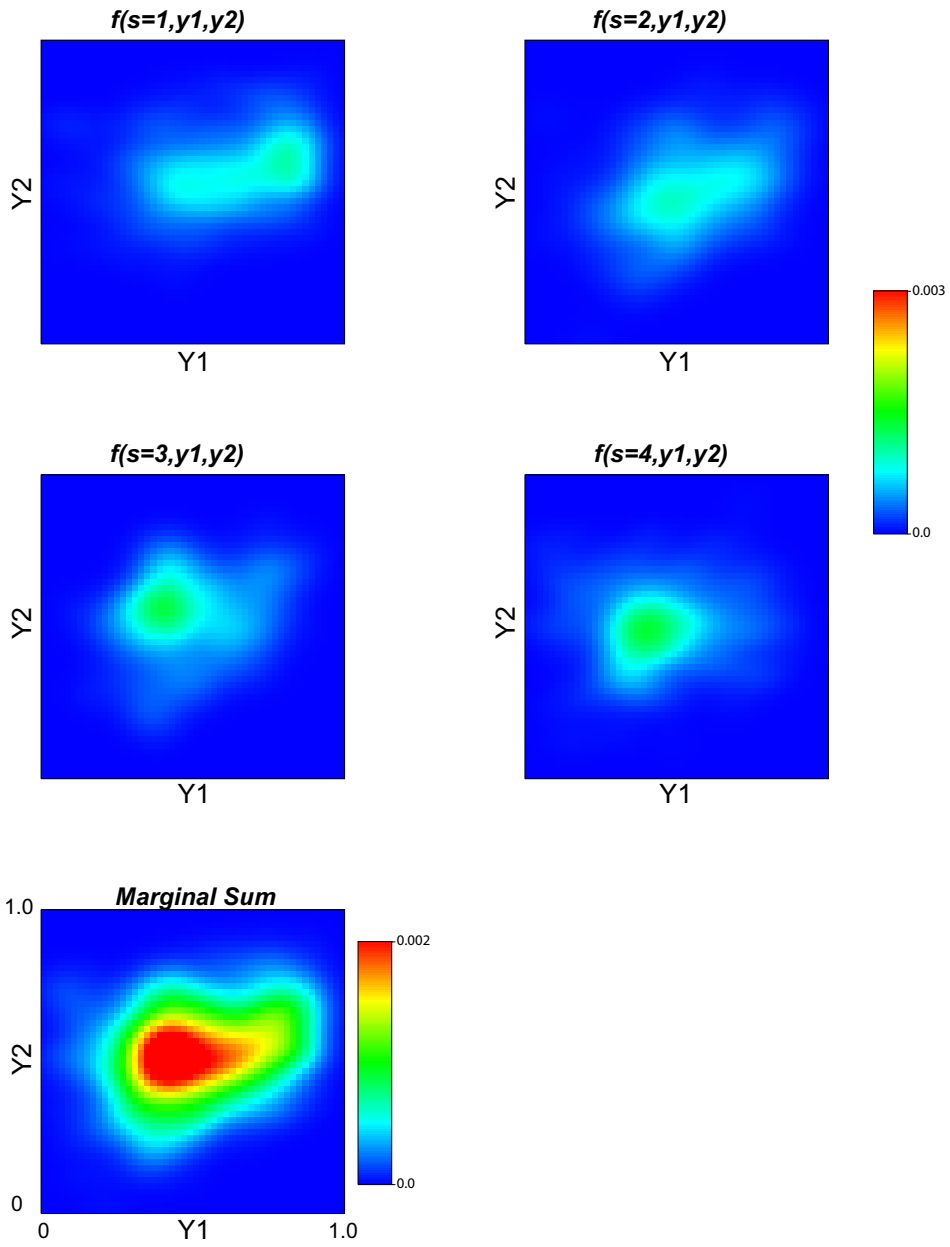

Figure 5.14: The modeled initial joint distributions (before constraining). Product kernel estimator is considered for multivariate nonparametric modeling. One reproduced marginal distribution is shown in the bottom.

Note the in the case of facies 1, the frequency of experimental data distribution is abruptly decreased at the high value area of seismic variable Y_1. The estimated distribution still shows smooth change of probability densities over that region. The summed bivariate distribution over the facies variable $\sum_{s=1}^{4} f(s, y_1, y_2)$ is shown in the bottom of Figure 5.14. There is a clear difference between the reproduced and the reference marginal distributions. Sequential marginal

fitting procedure was applied to correct the differences. The modified joint distributions become stable after 15 iterations in which averaged marginal errors reach less than 0.003%. Figure 5.15 shows the corrected distributions. For this example, each iteration involves $12{,}500=50^2+50^2\times4$ arithmetic calculations. The modified version show detailed variations in density distribution and reasonably reflect experimental data scatter plots. The corrected distribution $f(s=1,y_1,y_2)$ accounts for the abrupt decrease in experimental data frequency over high value area of Y_1.

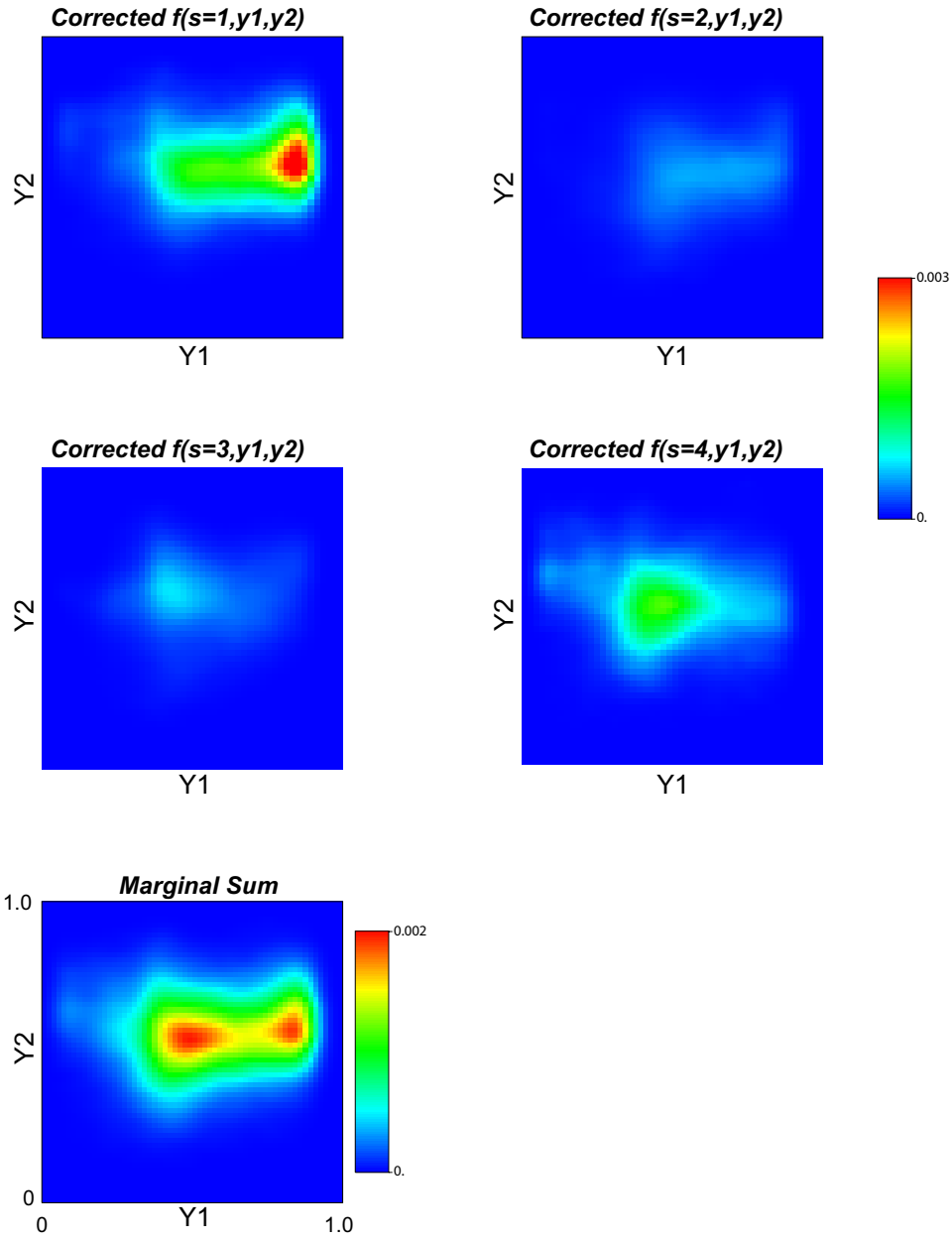

Figure 5.15: The corrected joint distribution $f(s,y_1,y_2)$ after applying marginal constraints.

The initial joint distributions have different shape with different choices of kernel bandwidths. A small exercise is performed to check the marginal relation without updating. Based on the optimal suggestion of kernel bandwidth $h_j = \hat{\sigma}_j n^{-1(d+4)}, j = 1,2$ and $d = 2$, up to ± 60% changes in h_j are tested. For each case of the initial joint distribution, the marginal distribution $f(y_1,y_2)$ is reproduced by the relation of $\sum_{s=1}^{4} f(s, y_1, y_2)$. Figure 5.16 illustrates the calculated marginal distributions from the initial distributions that are modeled by kernel method with different h_j. None of initial distributions reproduce the marginal distribution correctly.

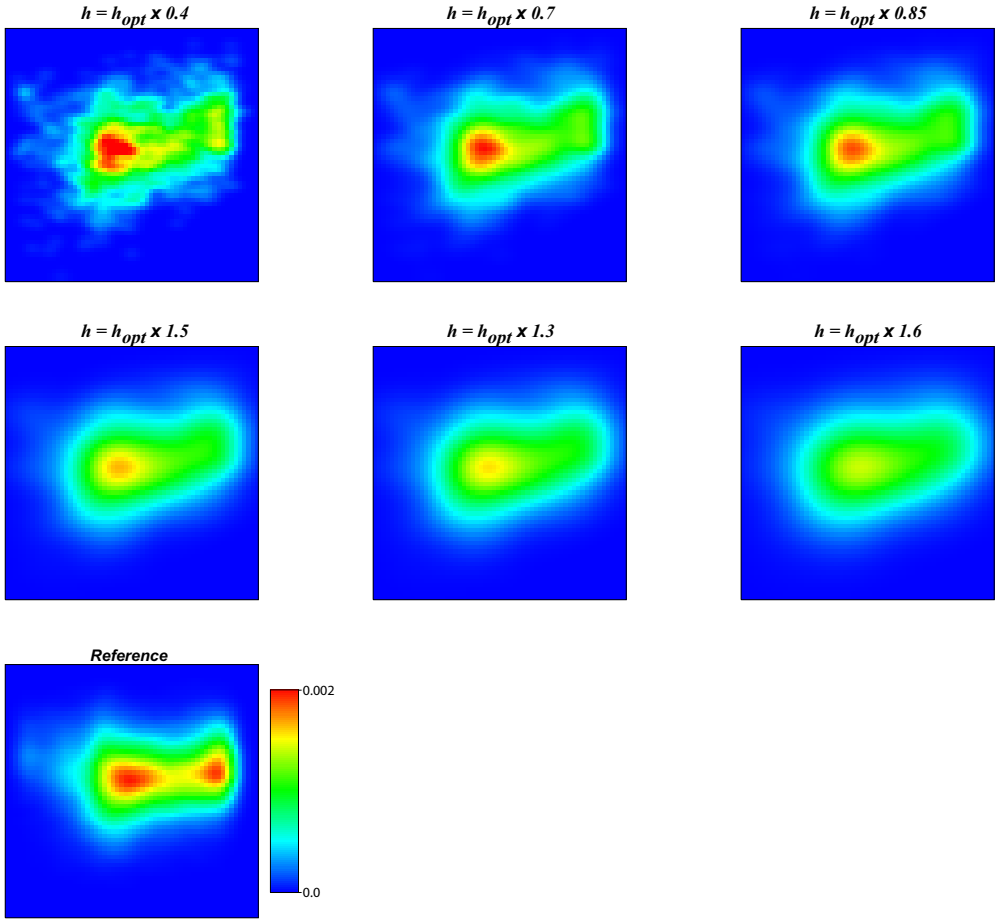

Figure 5.16: The joint distributions modeled with different conditions of kernel bandwidths. Based on theoretical kernel bandwidth h_{opt}, 60% changes are applied.

At every modeling locations $\mathbf{u} \in A$, the conditional probability of facies given the seismic values is derived from the corrected joint distribution:

$$p(s(\mathbf{u}) \mid y_1(\mathbf{u}), y_2(\mathbf{u})) = \frac{f(s(\mathbf{u}), y_1(\mathbf{u}), y_2(\mathbf{u}))}{f(y_1(\mathbf{u}), y_2(\mathbf{u}))}, \ \mathbf{u} \in A \tag{5-6}$$

The probability densities of the joint pdf $f(s,y_1,y_2)$ are numerically modeled with discretizated Y_1 and Y_2 values. The actual secondary values at location $\mathbf{u}$; thus, may not exactly match with the values at bins. The closest bin values are selected. Figure 5.17 plots the actual secondary values over $\mathbf{u} \in A$ and the looked up bin values. They are almost identical and so no explicit discretization error is observed.

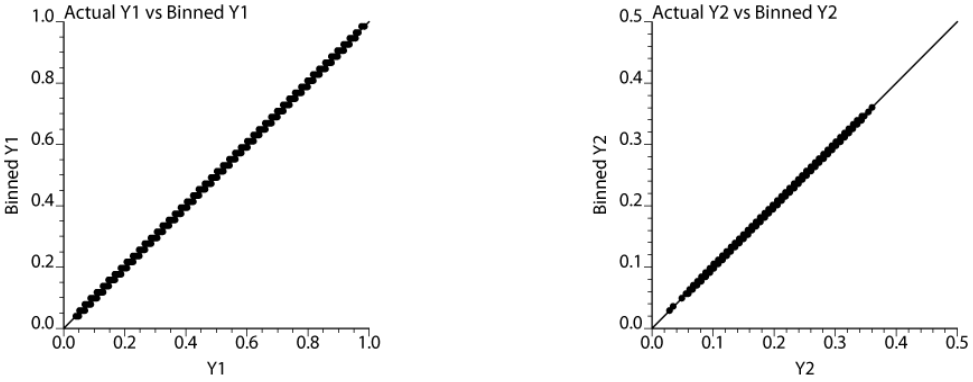

Figure 5.17: Cross plot of the actual secondary values and their corresponding bin values. 50 bins are defined for numerical joint density modeling and this level of binning does not invoke discretization errors.

The secondary derived probabilities are locally varying. The average of the locally estimated probabilities is close to the representative global means. Histograms of the local probabilities show means of $p(s|y_1,y_2)$, s=1,2,3,4, are very close to the declustered global proportions (see Figure 5.18).

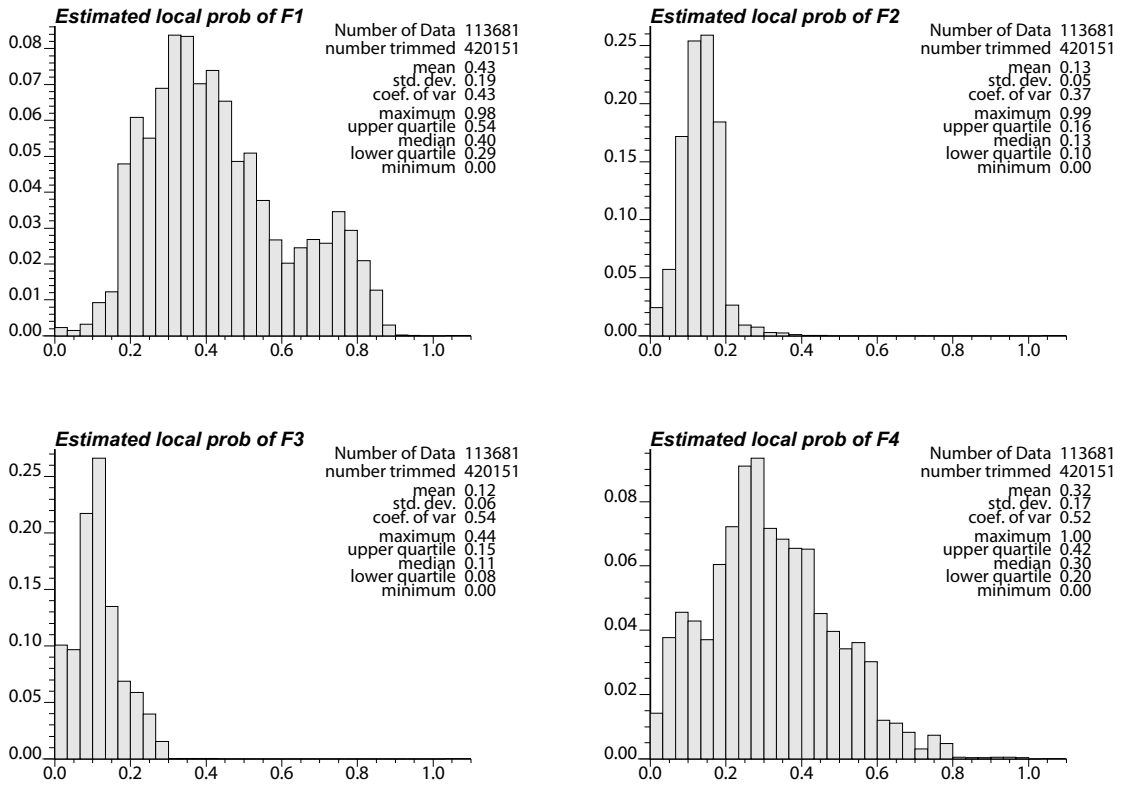

Figure 5.18: Histograms of the secondary derived facies probability. Averages of each histogram are close to the declustered global proportions.

As shown in Figure 5.19, the correlation between the probability from integrating Y_1(seismic 1) and Y_2(seismic 5) and the facies is increased for all facies. The correlation is increased Facies 2 and 3 particularly gain large improvements through integrating Y_1 and Y_2.

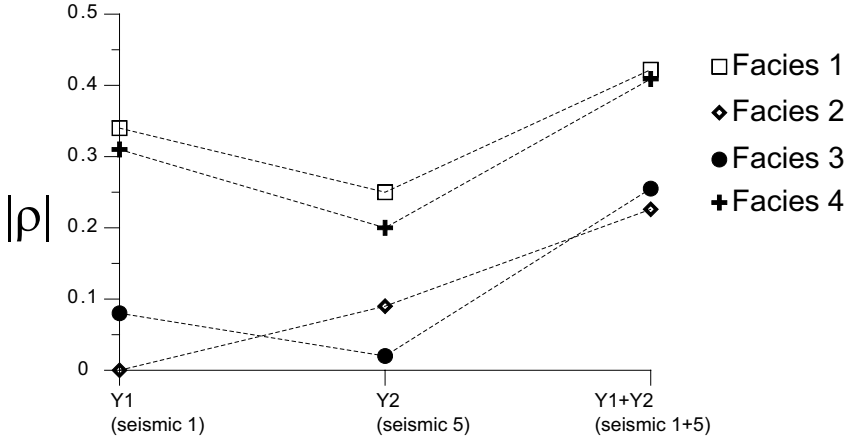

Figure 5.19: The improvements in the correlation between the used seismic and facies.

Accuracy Assessment

An accuracy evaluation of the estimated local probability is shown in Figure 5.20. The local probabilities are evaluated at every 0.1 predicted probability interval p=[0.05,0.15,0.25,…,0.95]. The closeness of the computed actual proportions to the predicted probability indicates the goodness of the estimated local probability. Unfilled circles in the plots are due to the null frequencies of the estimated probability at the corresponding predicted probability and these points may not be used to evaluate the model. The estimated probability is accurate and fair based on the overall accuracy plot.

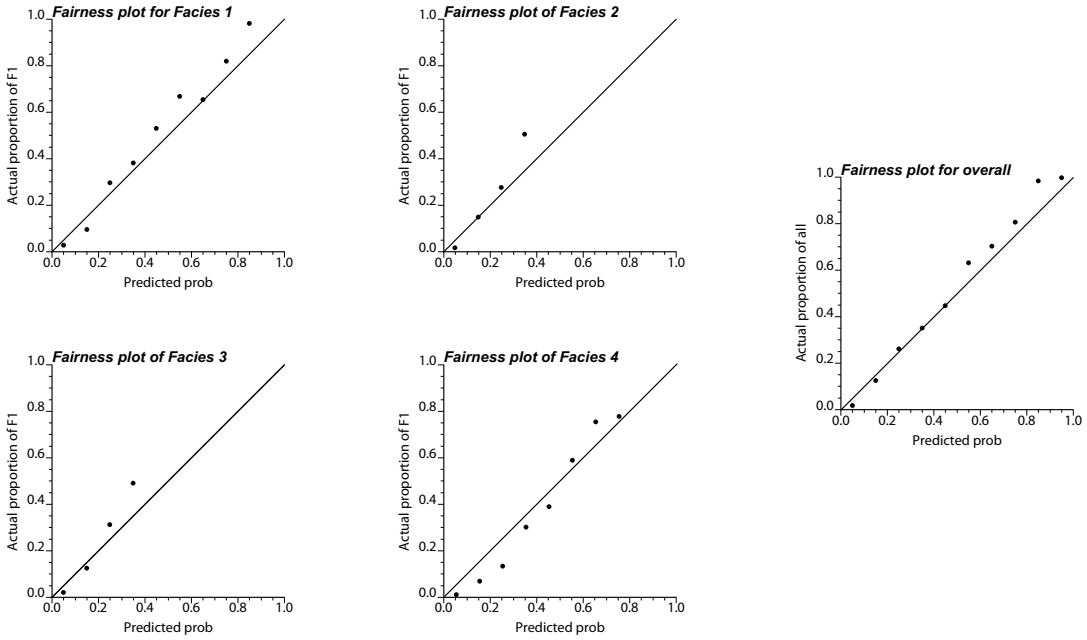

Figure 5.20: Fairness plots for the West African reservoir example. Actual fractions defined in section 3.6 are plotted against predicted probabilities. The actual fractions are reasonably all on the diagonal line for facies 1, 4 and overall.

Stochastic Modeling

A stochastic facies model is built using the facies probabilities derived from integrating seismic attributes. Indicator variograms are computed from the well data and they are fitted as shown in Figure 5.21. There is no horizontal anisotropy. The variograms of the four facies are largely fit by an exponential structure with a small range. The structure with a large range has a small contribution to the spatial continuity. 21 realizations of facies are generated by sequential indicator simulation. Figure 5.22 shows the E-type estimates of facies 4 (channel) calculated at

every modeling grids from 21 simulated facies. The sinuosity of channel is not well detected in the E-type estimate and the connectivity of channel is not reproduced properly.

The seismic derived facies probability is now integrated. The Bayesian updating equation is used to build the local conditional probability using the well data and the estimated facies probability from seismic data. The E-type estimate is also calculated from 21 realizations and it is shown in Figure 5.23. The meandering channel pattern is better identified and channel connectivity interpreted in the conceptual geology in Figure 5.9 is revealed more clearly. The validity of the stochastic models is based on the reasonable reproduction of the input statistics such as the input variogram: low fluctuation of the reproduced variogram being close to the input model is ideal. Figure 5.24 shows the reproduced variograms for the four facies at each principal direction.

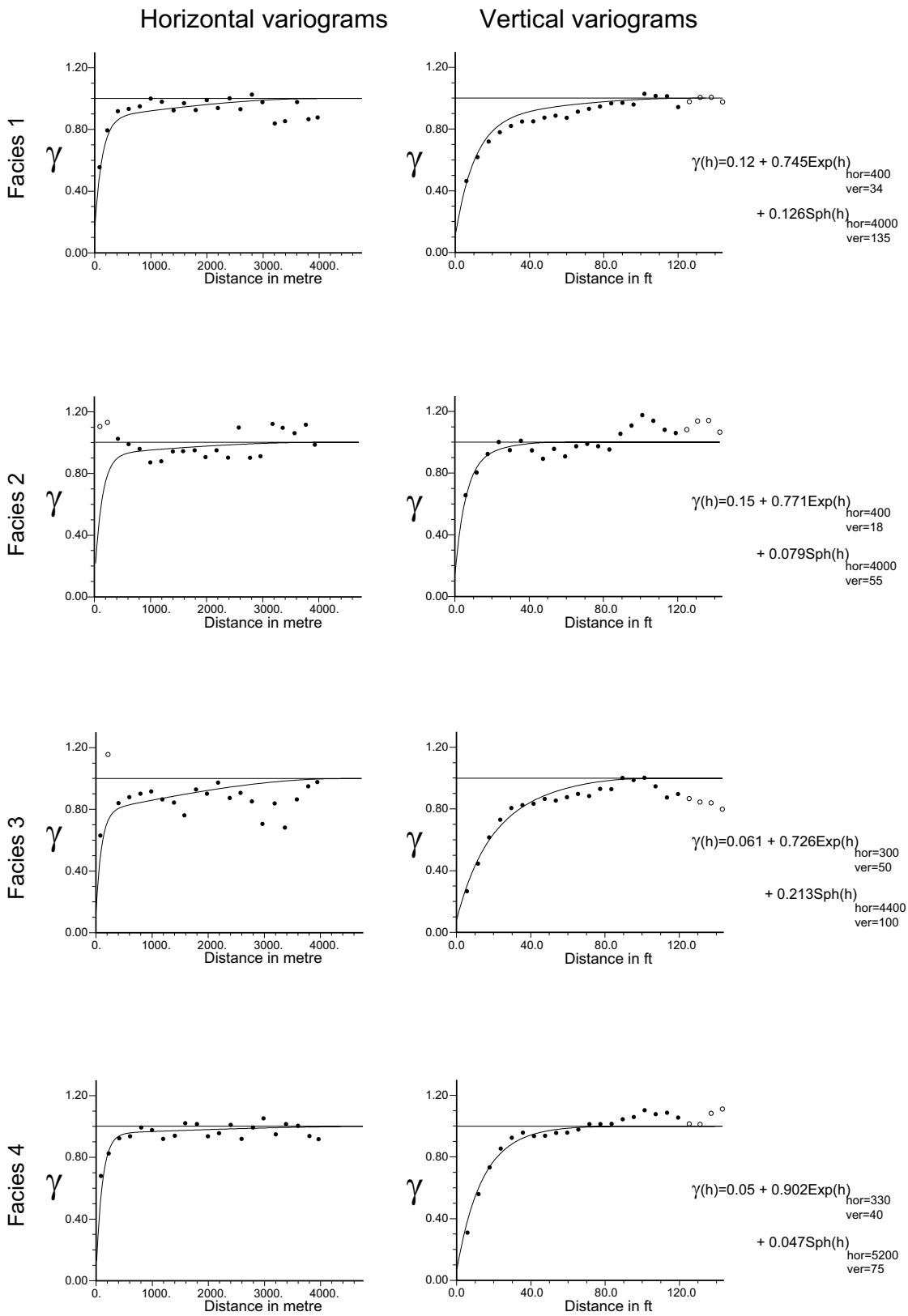

Figure 5.21: Experimental and modeled variograms for four facies.

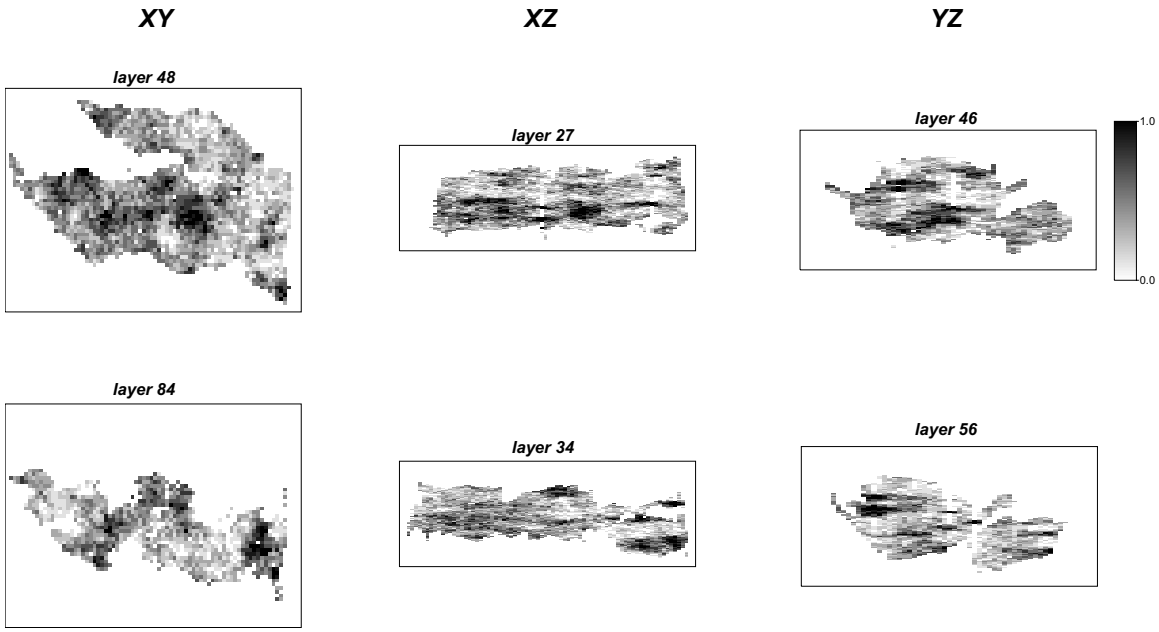

Figure 5.22: E-type estimate of channel facies from 21 realizations without secondary data.

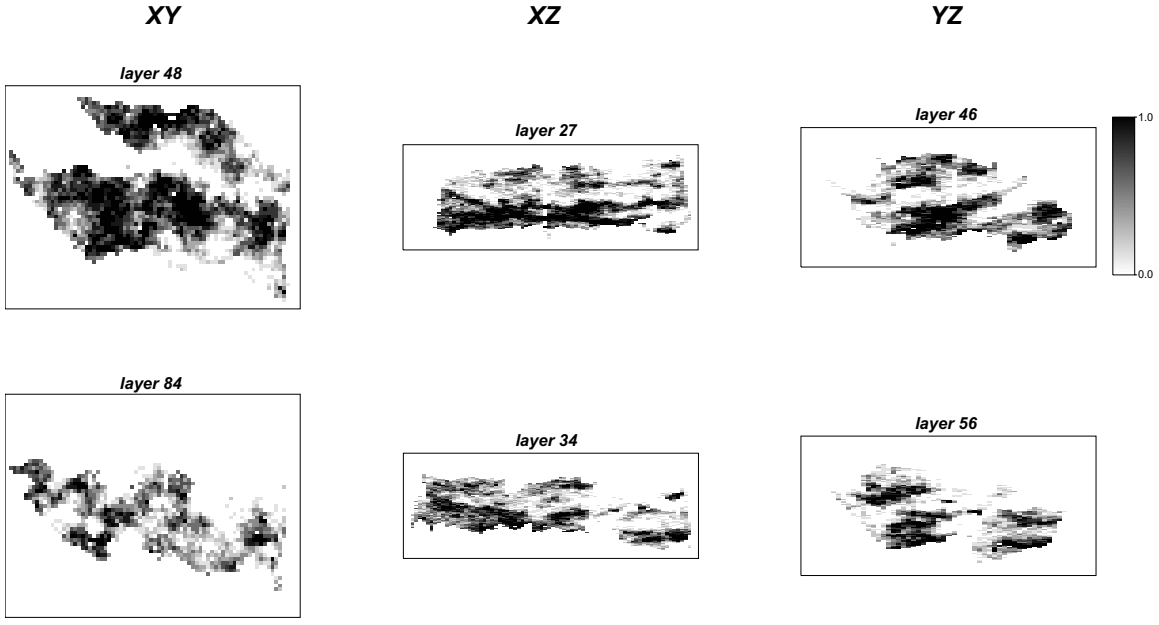

Figure 5.23: E-type estimate of channel facies from 21 realizations with secondary data.

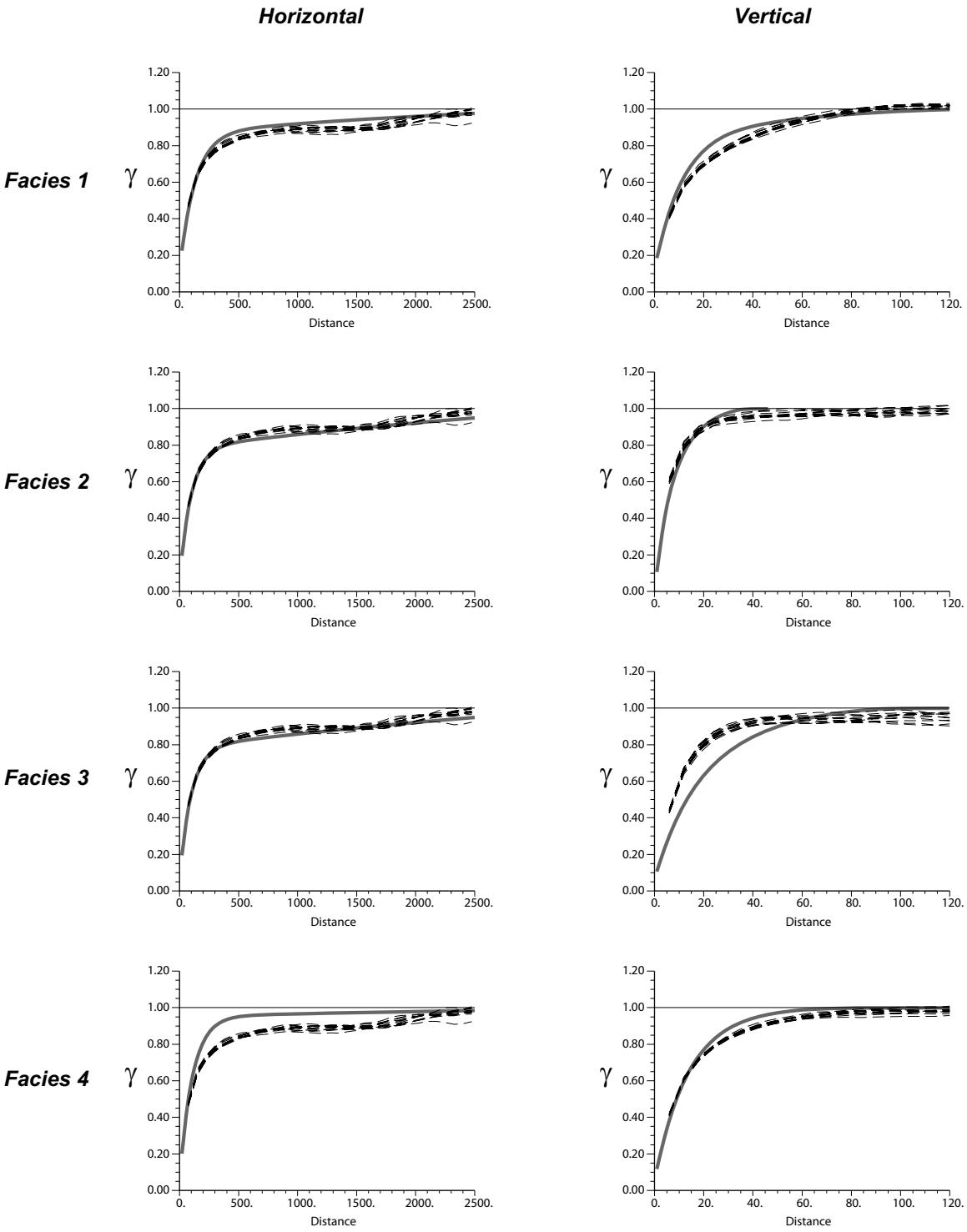

Figure 5.24: Variogram reproductions from the 21 realizations. Distances in horizontal and vertical directions are in meter and ft, respectively.

5.1.3 Accounting for Large Scale Secondary Data

It is important to integrate information from seismic data that delivers better areal coverage than the sparse sampling of well data. Seismic data, however, inexactly measures facies proportions because of geological complications and inherent limitations in seismic data acquisition (Deutsch, 1996). Poor vertical resolution of the seismic data warrants using a single 2D map representing vertically averaged facies proportions and the vertical volume is significantly larger than the typical geological modeling cell.

The developed method to integrate soft secondary data can be applied for integrating large scaled seismic data. The detailed process follows that described in Chapter 4: (1) model the secondary data distribution which is a distribution of block values in this case and get the representative global facies proportions, (2) model the joint distribution using kernel density estimation, (3) constrain the joint distribution to the joint distribution of the secondary data and the representative proportions, and (4) derive the conditional probabilities from the corrected joint distribution.

Figure 5.25 shows a synthetic reference image consisting of three facies types and selected wells from a reference image. The example is a vertical section of the reservoir with size of 100m in lateral and 50m in vertical direction. The modeling cell size is 1m-by-1m in horizontal and vertical direction.

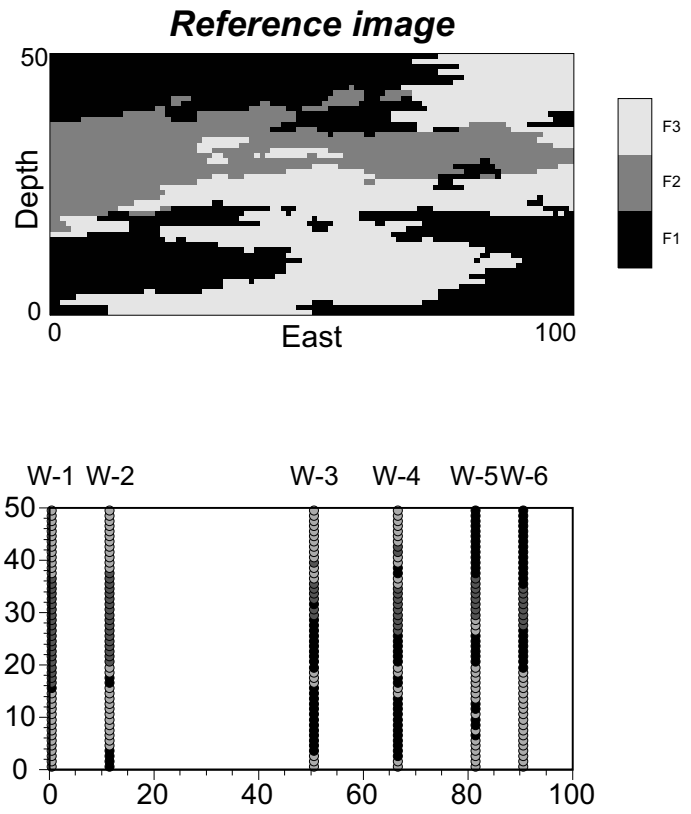

Figure 5.25: A synthetic reference images and well data extracted from the reference image. Coordinates are all in meter.

Two soft secondary variables are simulated. The vertical resolution of the secondary data is assumed to be 5 times larger than the modeling size and so secondary values are generated at every 1m in horizontal and 5m in vertical. Figure 5.26 shows the prepared secondary data. Sequential Gaussian simulation was used for generating secondary data and they are non-linearly correlated.

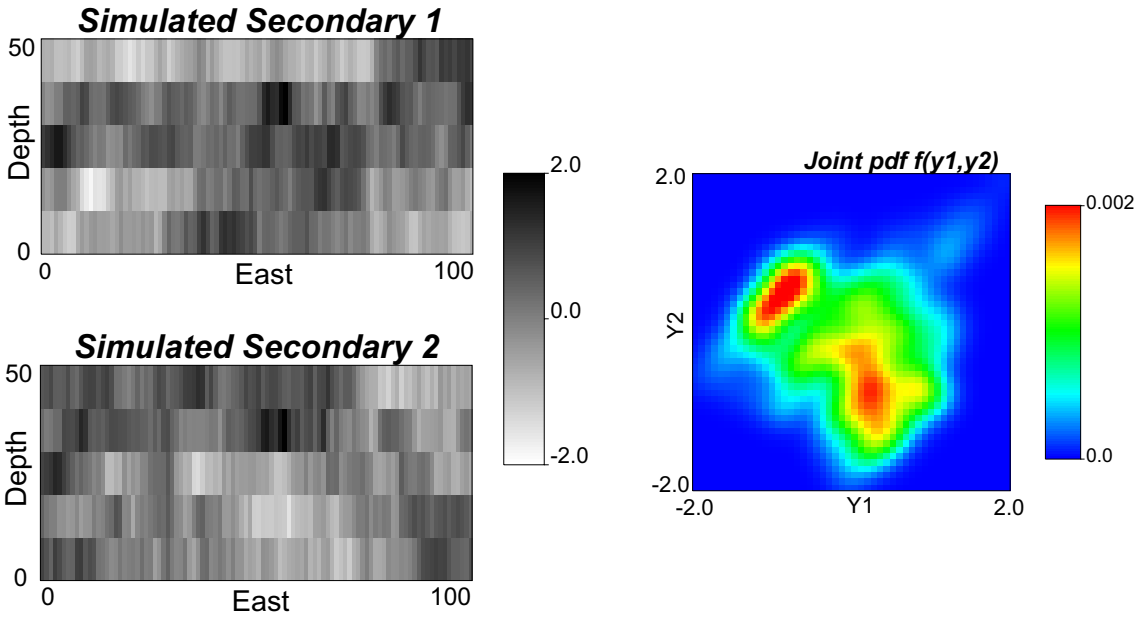

Figure 5.26: Two simulated secondary data. Vertical resolution is 5 times larger than the modeling cell size. Kernel method is used for the modeling of bivariate relation.

Figure 5.27 shows cross plots of block secondary values and facies proportions calculated from well data.

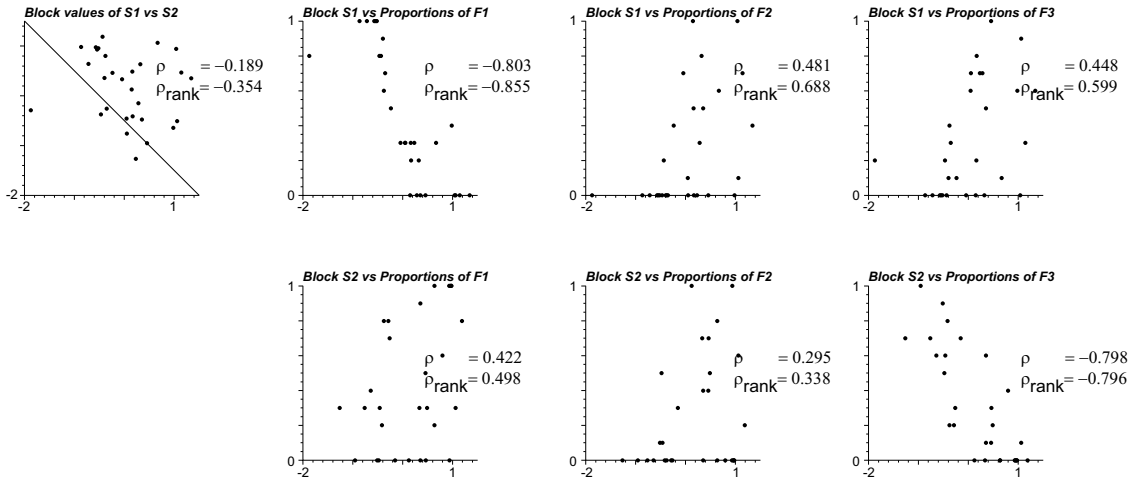

Figure 5.27: Cross plots of block secondary values and facies proportions from 6 vertical wells.

The magnitude of correlation between the secondary data and the proportions varies from 0.3 to 0.8. Simulated secondary $Y_1(\mathbf{u})$ has an intermediate positive correlation (approximately 0.5) to facies 2 and 3 but high negative correlation to the facies 1. Secondary $Y_2(\mathbf{u})$ has a low-to-

intermediate positive correlation to the facies 1 and 2 but high negative correlation to the facies 3, which represents secondary data $Y_2(\mathbf{u})$ would better identify facies 3 from facies 1 and 2.

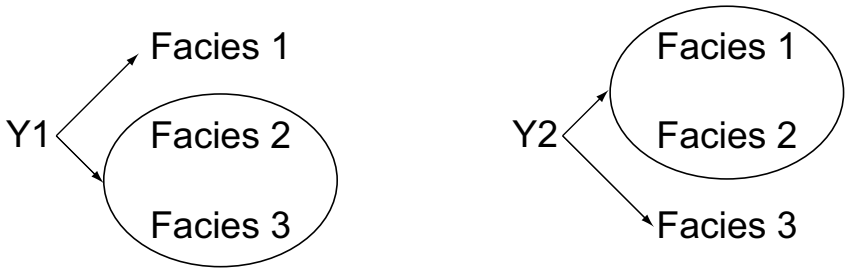

The two secondary data have a different capability of identifying different facies. This will show how the integration results benefit from the full use of complementary information.

Figure 5.28 shows the comparison of the facies proportions calculated from block average of the reference image and the secondary derived proportions. The scatter plot shows that the estimated proportions using the joint distribution modeling technique are in consistent with the true proportions.

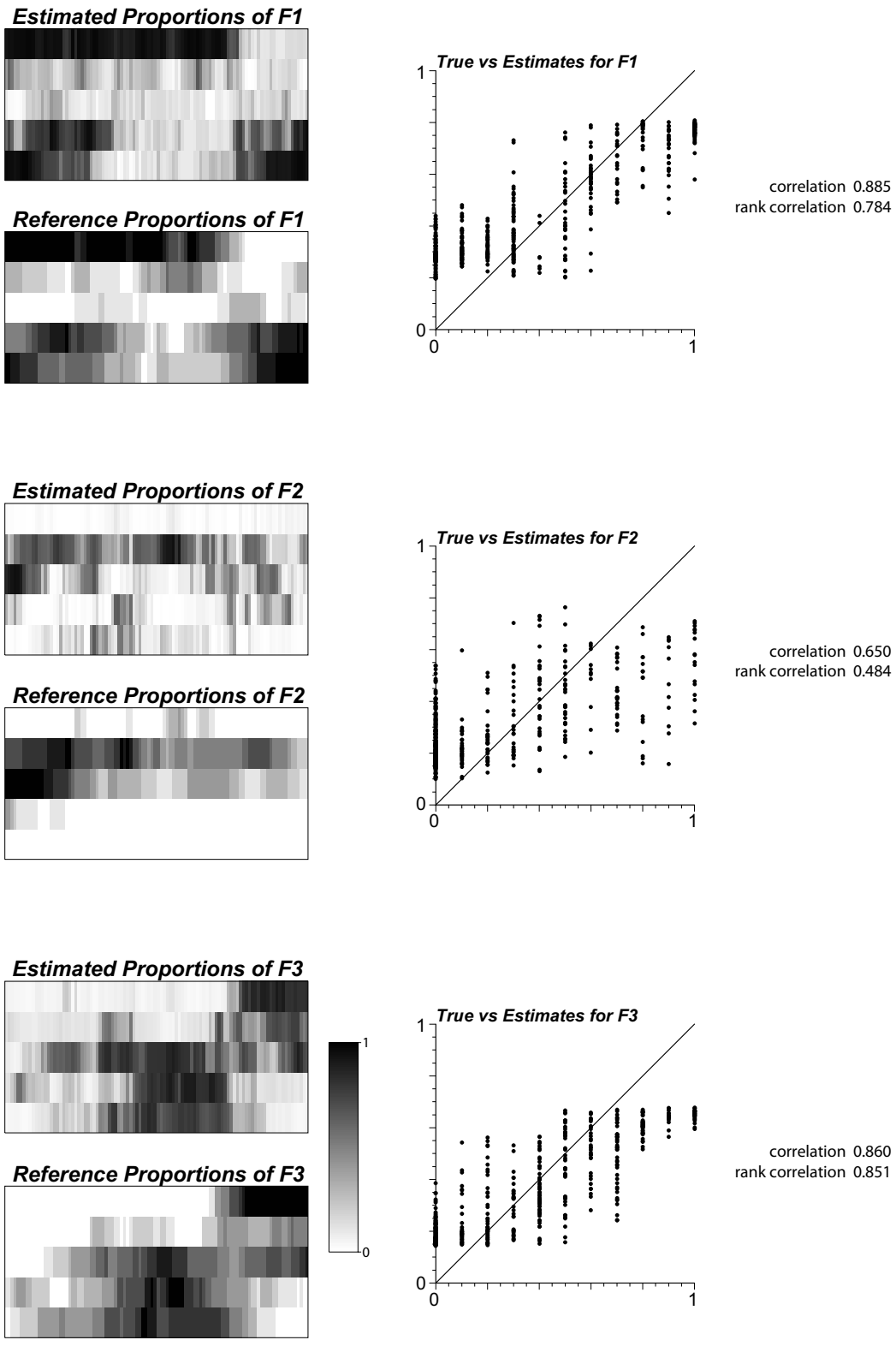

Figure 5.28: For visualizing purposes, the facies proportions from the true image and estimated proportions are shown in the left column. Right column shows the scatter plots between the true and estimated proportions.

Comparing to the experimental scatter plots, the strength of correlation increases after data integration. For example, each secondary data 1 and 2 has low correlation to the proportion of facies 2 (less than 0.5 for both secondary) but integrated proportions of facies 2 have a correlation of 0.65 that increases by 35%. Besides, even though two secondary data each has opposite correlation to facies 1 and 3 (for example, ρ_{Y1F1}= –0.803, ρ_{Y2F1}=–0.422 and ρ_{Y1F3}=0.448, ρ_{Y2F3} = –0.798), the integrated results have higher correlations to the facies 1 and 3 rather than individual correlations. This incremental improvement of information is the main advantage of data integration when the integration model is valid in terms of reasonable accounting for data redundancy and closeness.

Averages of the estimated proportions reasonably reproduce the global proportions. Figure 5.29 shows histograms of the estimated facies proportions. Note that the average of estimated proportions is highly close to the global proportions.

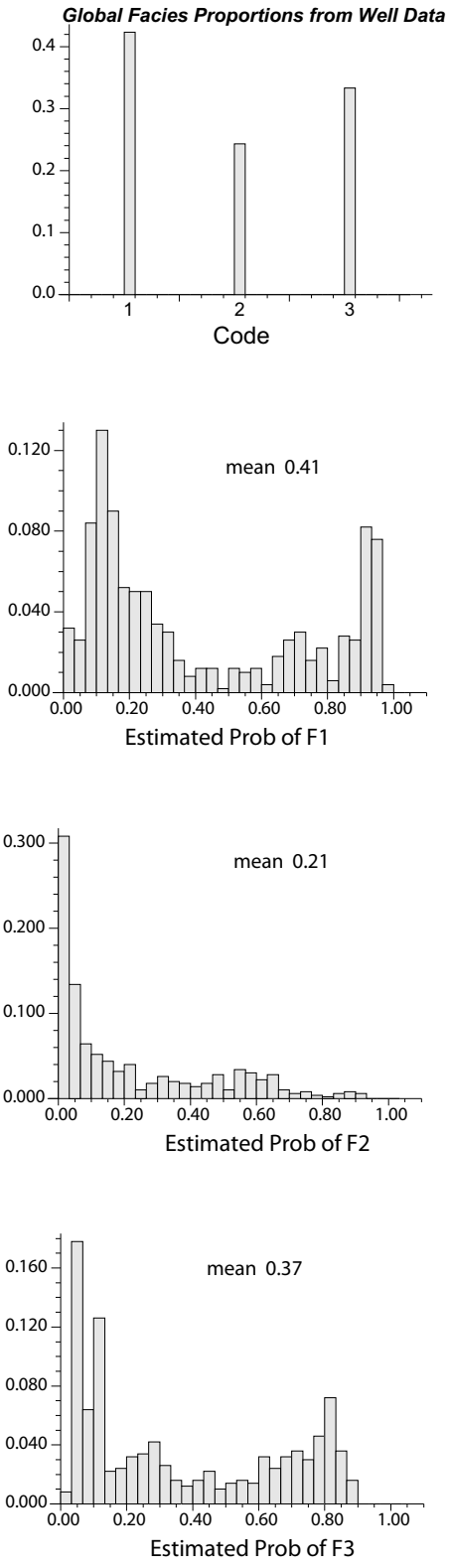

Figure 5.29: Histograms of secondary derived facies proportions. Averages of each facies proportions are very close to the global representative facies proportions.

5.2 Debiasing with Multiple Soft Secondary Data

Geostatistical models must reproduce the input statistics and spatial continuity; however, there is no intrinsic declustering or debiasing in geostatistical modeling methods. Sample clustering occurs when the domain of interest is sampled preferentially. It is natural that spatial data are collected in a non-representative way such as preferential drilling in high net-to-gross area.

As discussed in Section 2.2.5, declustering techniques are widely used techniques for correcting potentially biased sample statistics. Various types of declustering methods such as cell, polygonal and kriging weight declustering have been developed (Deutsch and Journel, 1998; Isaaks and Srivastava, 1989). Those techniques try to correct the bias inherent in sample statistics caused by geometric clustering.

A debiasing algorithm uses quantitative secondary data for correcting the bias inherent in samples. Soft secondary data may be representative of the entire area of interest, and the relation between the primary variable being predicted and secondary data is modeled. The joint probability distribution describes this relation. The central idea of debiasing is to extrapolate the primary distributions over the full range of the secondary values. For example, the global facies proportions can be debiased with respect to the secondary data distribution such as:

$$p^{debias}(s) = \int_{-\infty}^{\infty} f(s, \mathbf{y}) d\mathbf{y} \tag{5-7}$$

where the $f(s,\mathbf{y})$ is the modeled joint distribution that satisfies all the axioms of a joint pdf: positive densities, $\sum_{\forall s} \int f_{SY}(s, \mathbf{y}) d\mathbf{y} = 1$ and reproduction of lower order marginal distribution. The use of a linear assumption among secondary variables is straightforward. Challenges are to use secondary data accounting for non-Gaussian relations among them. The proposed debiasing approach with soft secondary data is based on three steps: (1) build the joint distribution of all secondary variables, build the initial joint distribution of the primary and all of secondary variables, (2) correct the initial distributions under the secondary marginal distributions, and (3) add up the corrected joint densities over the range of secondary values. These processes are nearly similar to the sequential marginal fitting algorithm introduced in Section 4.2 except that correcting the initial joint distribution by the marginal distribution of the primary variable is not done. The debiasing equation in (5-7) can be expressed again:

$$p^{debias}(s) = \int_{\mathbf{y}} \left(\frac{f(\mathbf{y})}{\sum_{s=1,\ldots,K} f^{(0)}(s,\mathbf{y})} \times f^{(0)}(s,\mathbf{y}) \right) d\mathbf{y} \tag{5-8}$$

$f^{(0)}$ is an initial distribution modeled by the kernel method. The arithmetic operation in the parenthesis corrects the $f^{(0)}$ by the secondary marginal distribution $f(\mathbf{y})$. Integrand operator outside the parenthesis adds up the corrected joint densities over possible outcomes of secondary values, leading to the debiased proportion $p(s)$.

Examples

A binary reference image is prepared to illustrate debiasing. The true global means are 0.453 and 0.547, respectively for code 0 and 1. A total of 16 well data are sampled from the reference image and samples are separated by 64 units. In an early stage of reservoir appraisal, few wells with little preferential drilling are often encountered. This synthetic example demonstrates that case.

The naïve global means of code 0 and 1 are 0.313(=5/16) and 0.688(=11/16) for each code. These naïve statistics are biased by more than 26% compared with true ones. Figure 5.30 shows reference image, sample data locations and simulated secondary data. Synthetic secondary data (Y) reflect the true facies distribution: low values tend to predict the code 0 and high values tend to predict code 1.

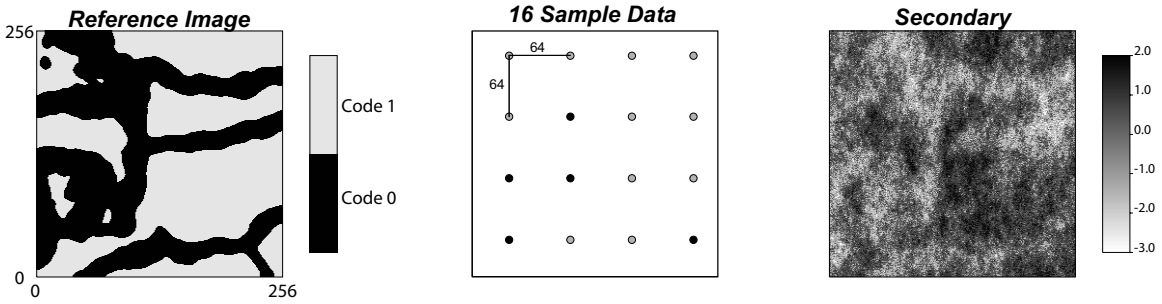

Figure 5.30: Prepared reference image, well sample locations extracted from reference image and a simulated secondary data. Sample means are biased by 26% or above based on the true statistics.

Declustering methods depend on the geometric configuration of the sample data locations and lead to equal weighting in this case. For example, declustered means are changed very little with

respect to the change of cell sizes generating 0.325 and 0.675 as a declustered proportions which are still biased by 23% based on the true values.

The initial bivariate distribution is modeled using kernel density estimation. Due to sample data paucity, the modeled distribution curves appear very smooth. Figure 5.31 illustrates the modeled $f(s=0,y)$ and $f(s=1,y)$ shown as a smooth solid line and the experimental data distribution of Y shown as a bar chart.

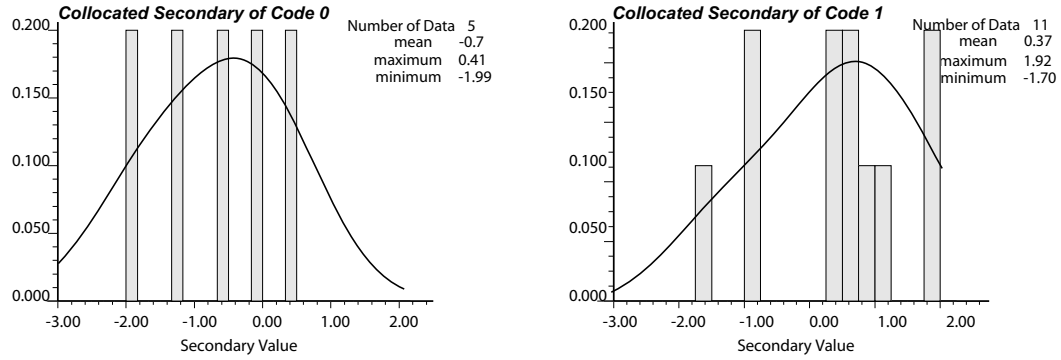

Figure 5.31: Experimental data distribution and the modeled distribution $f(s,y)$ based on sample data. The smooth line is a kernel estimator of bar chart.

The initial distributions are modified by a marginal constraint. The smooth curves shown in Figure 5.31 are summed and compared with the secondary data distribution $f(\mathbf{y})$. Figure 5.32 shows the modified distributions that have detailed variations in distribution. Those distributions exactly reproduce the secondary data distribution as shown in the bottom of the figure. Debiased global proportions of each code are obtained by (numerically) summing up the area below the updated curves.

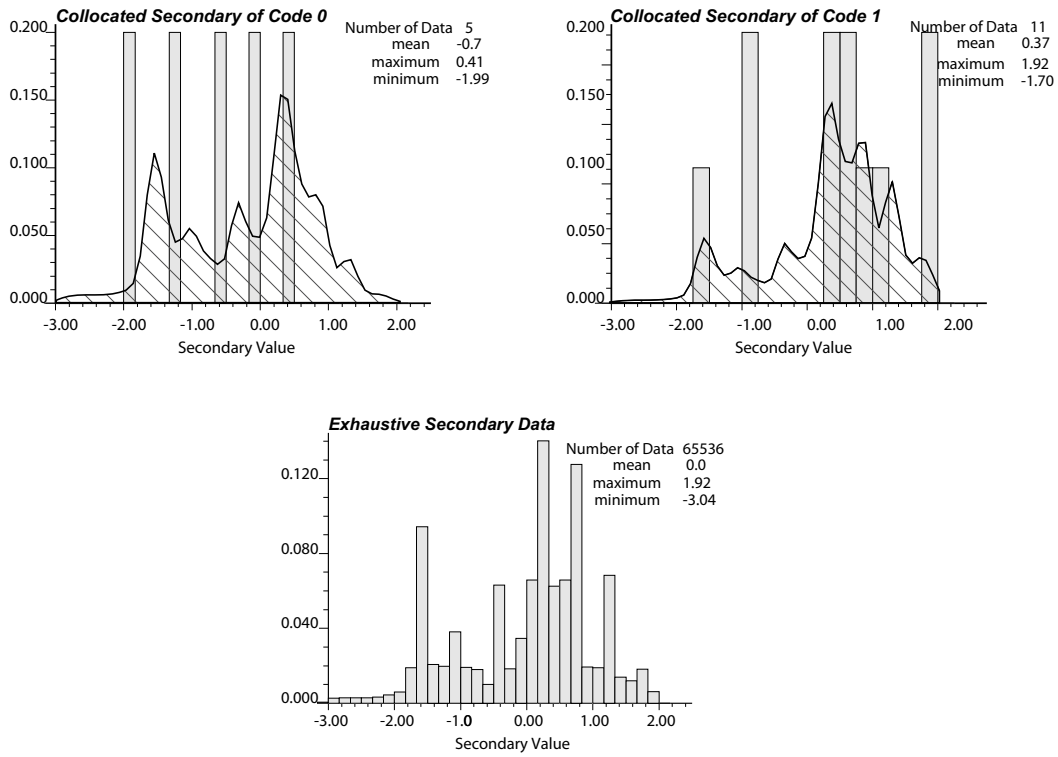

Figure 5.32: The modified bivariate distributions by imposed marginal condition. A marginal distribution of secondary data is shown in the bottom.

The global proportions are summarized in the table below for comparison:

	True	16 Samples with equal weights	Cell declustering	Debiasing
Code 0	0.453	0.313	0.325	0.415
Code 1	0.547	0.688	0.675	0.585

Cell declustering does not correct the bias because declustering techniques inherently assume the sample data cover the full range of the data values, that is, declustering methods assume bias arise only by spatial clustering, not by data value clustering. This example, however, shows that collocated secondary data values are limited to [-1.99,0.41] and [-1.7,1.92] for code 0 and 1, respectively (see summary statistics shown in Figure 5.31). The debiasing method is based on the use of secondary data that are distributed over the full range of secondary values, say [-3.04,1.92] for this example. The bias caused by clustering within the limited secondary values is mitigated by the coverage of the secondary data.

5.3 Integration of Soft Secondary and Geologic Map

Geologic map data are important to most reservoir studies. Geologic interpretation map is often treated deterministically. Geostatistical reservoir models are then validated in light of a conceptual geologic model. Geologic data is sometimes used for inferring the geostatistical modeling parameters such as horizontal range, ratio of horizontal to vertical range in 3-D variogram model and areal trend (Deutsch and Kupfersberger, 1999).

Whereas outcrop models can provide important information on reservoir architecture and heterogeneity, it is not entirely clear how such information can be integrated while constructing a probabilistic reservoir model (Caers and Zhang, 2004). Multipoint geostatistics is a newly developed field for integrating the geologic patterns drawn from the outcrop models. This new approach derives multiple point statistics from outcrop models, named as training images, and then anchored them into well data (Journel and Alabert, 1989; Guardiano and Srivastava, 1993; Strebelle, 2000). Soft secondary data are not directly integrated during the construction of local probability distribution. To combine multiple-point statistics and secondary data, previous works typically constructed local probability distribution conditioned to geologic data (or training images), and conditioned to the soft secondary data, and then combine the calibrated probabilities into the resulting probability. As described in Chapter 3, probability combination models have been developed for this unifying individual probability.

In this section, the joint pdf modeling technique under marginal constraints is extended for incorporating geologic data into soft secondary data. The main goal is to show that the proposed method can integrate both continuous and discrete secondary data in a rigorous way, and to show the improvements of integrating geologic map with soft secondary data. Soft secondary data often fails to capture the local complex variation of the geologic feature because the soft secondary data integration is pixel-based. A geology map that a prior geologic knowledge is transferred into can reflect local complex features.

The joint relation between geologic map or image and soft secondary values is modeled with a nonparametric method and the known marginal conditions are applied to modify the joint distribution. By direct modeling of the joint distribution, the geologic information is fused into the final probabilistic model without external data redundancy calibration that the probability combination requires.

Setting the Problem

Our interest is to model the joint probability distribution between a primary facies variable and all of secondary variables that include continuous data from seismic survey and discrete data from geologic map:

$$f(s, y_1, ..., y_m, g) \tag{5-9}$$

Although the geologic data is considered as secondary information, it is split into another variable represented by random variable g taking one of g=1,…,K where K is the number of distinct facies or geologic units. The marginal distributions that the joint pdf in (5-9) are the global proportions $p(s)$ and the (m+1) dimensional secondary data distribution:

$$\begin{matrix} p(s) \\ f(y_1, ..., y_m, g) \end{matrix} \tag{5-10}$$

The marginal relations are following:

$$\begin{aligned} &\sum_{g=1}^{K} \left(\int \cdots \int f(s, y_1, ..., y_m, g) dy_1 \cdots dy_m \right) = p(s), \;\; s = 1, ..., K \\ &\sum_{s=1}^{K} f(s, y_1, ..., y_m, g) = f(y_1, ..., y_m, g), \;\; g = 1, ..., K' \end{aligned} \tag{5-11}$$

where K' is the number of rock types from geology map. It does not have to be the same number of facies being modeled K. The joint pdf is numerically integrated over a sub set of variables to calculate the marginal distribution that are compared to the known distributions.

Example

Synthetic data are prepared for illustration. A 2D sinuous channel type reservoir is chosen as a reference image and 61 samples are randomly extracted from the reference image and treated as well data (Figure 5.33). Channel and non-channel are coded as 1 and 0, respectively.

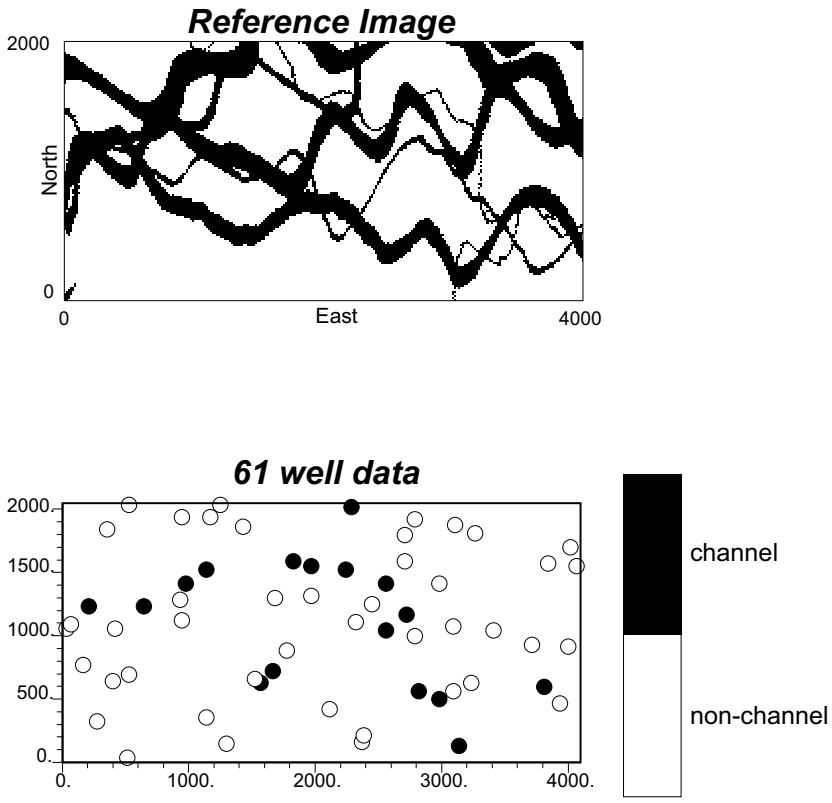

Figure 5.33: Reference image showing channel reservoir and 61 well data extracted from the reference image. X-Y coordinate is in meter.

Two seismic variables (Y_1 and Y_2) are generated using sequential Gaussian simulation and they are non-linearly correlated with the linear correlation of 0.572. The synthetic soft secondary variables are made to differentiate somehow the channel and non-channel facies. For instance, the linear correlation of Y_1 and reference image is 0.44, which simply states that higher value of Y_1 tend to higher possibility of code 1 (channel). Y_2 and reference data are positively correlated with ρ=0.47 as well. Improvements in channel identification are expected by integrating the two secondary data. Simulated Y_1 and Y_2 are shown in Figure 5.34 and a cross plot of two variables is located in the right of the figure.

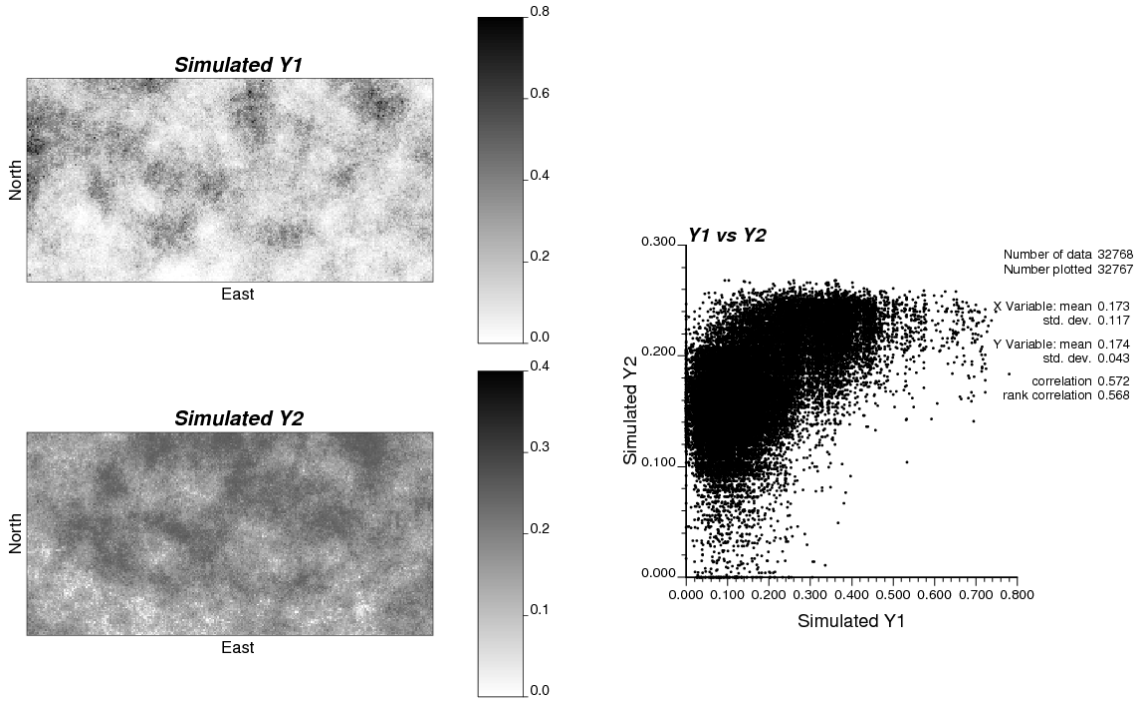

Figure 5.34: Two soft secondary variables are generated using the sequential Gaussian simulation and are correlated in a non-linear manner as shown in the cross plot of two variables. This non-linear pattern is to be accounted for by nonparametric technique.

One possible geologic map is prepared in Figure 5.35 showing a certain pattern of complex geologic features such as curvilinear channel. The image is not conditioned to well information; it is mapped to represent the complex geological/structural features in terms of expected orientation and curvature of channels. The geologic map data has same grid definition as the final modeling in X and Y direction.

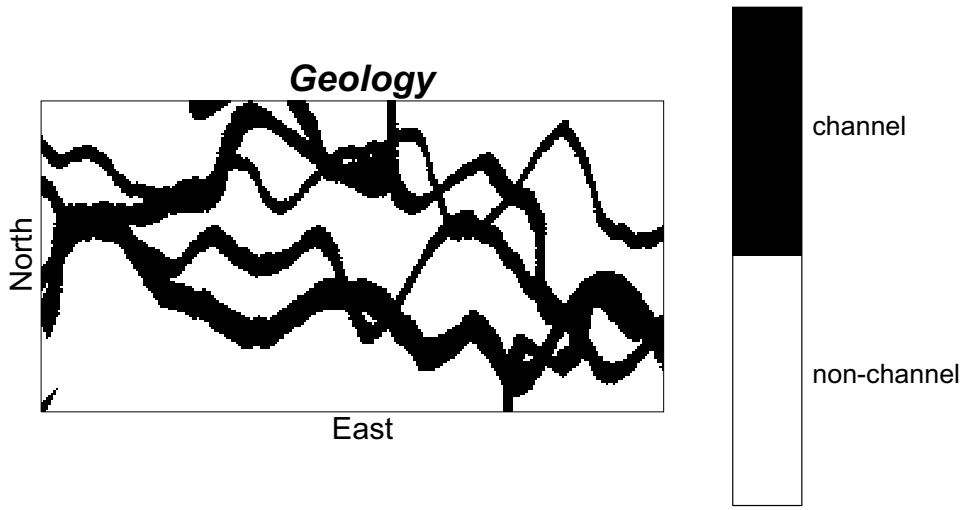

Figure 5.35: A geologic map used for integrating with soft secondary data.

Due to the spatial clustering of well data, cell declustering was used for obtaining representative global proportions which are to be used as one marginal constraint:

	s=0 (non-channel)	s=1(channel)
$p^{naive}(s)$	0.72	0.28
$p^{declus}(s)$	0.669	0.339

The joint distribution of all secondary variables (soft secondary and geologic map) $f(y_1,y_2,g)$ is first modeled. The kernel density estimator was used to generate a smooth density distribution. Since the geologic data is a type of discrete variable, the indicator function is added into the product kernel estimator:

$$f(y_1,y_2,g)=\frac{1}{Nh_1\times h_2}\sum_{i=1}^{N}\left(\prod_{j=1}^{n_{\text{soft sec}}=2}\mathrm{w}\left(\frac{y_j-y_{j,i}}{h_j}\right)\right)\times \mathrm{I}(g_i) \tag{5-12}$$

where N is the number of secondary values being equal to the number of modeling grids. $\mathrm{I}(g_i)$ is an indicator function of g_i taking 1 if facies code g_i of i^{th} datum out of N corresponds to the facies code g to be modeled, otherwise taking 0. The indicator function nullifies the kernel weights when the facies code of modeling and the actual codes from the data are different. Figure 5.36 illustrates the modeled secondary data distributions $f(y_1,y_2,g=0)$ and $f(y_1,y_2,g=1)$. The range of y_1 and y_2 is discretized into 50 bins for numerical approximation. This level of discretization does

not introduce significant approximation errors when plotting the actual values of $(y_1(\mathbf{u}),y_2(\mathbf{u}))$, $\mathbf{u}\in A$ against the looked-up discretized values.

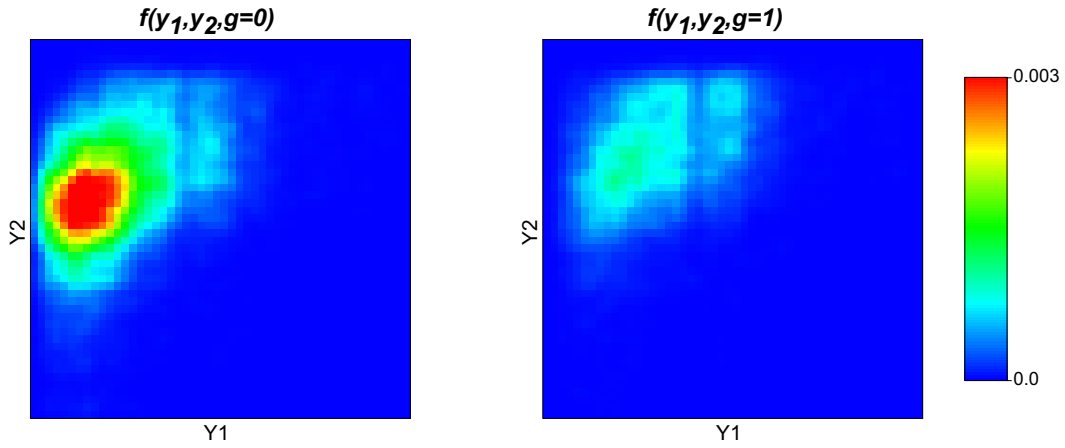

Figure 5.36: The modeled joint distribution of secondary data $f(y_1,y_2,g)$, g=0,1.

The joint distribution between all of variables is now modeled. To account for mixed continuous and discrete variables, the product kernel estimator is expanded such as:

$$f(s,y_1,y_2,g)=\frac{1}{nh_1\times h_2}\sum_{i=1}^{n=61}\left(\prod_{j=1}^{n_{\text{soft sec}}=2}\mathrm{w}\left(\frac{y_j-y_{j,i}}{h_j}\right)\right)\times \mathrm{I}(s_i)\times \mathrm{I}(g_i) \qquad (5\text{-}13)$$

Indicator functions $\mathrm{I}(s_i)$ and $\mathrm{I}(g_i)$ split entire sample data n=61 into smaller sub sets according to the outcomes of discrete random variable S and G. For examples, $\mathrm{I}(s_i)$ is a function of s_i taking 1 if facies from i^{th} data out of n=61 corresponds to the facies code being modeled, otherwise taking 0. Similarly, $\mathrm{I}(g_i)$ becomes 1 if geology code from $\underline{i}^{\text{th}}$ data out of n corresponds to the geology code being modeled, otherwise $\mathrm{I}(g_i)$ becomes 0. The table below shows the number of samples with different combination of facies and geology codes. The number in each cell is the number of samples used for modeling the joint pdf $f(s,y_1,y_2,g)$, s=0,1 and g=0,1.

		Geologic code at well locations	
		g=0 (non-channel)	g=1 (channel)
Actual facies at well locations	s=0 (non-channel)	30	5
	s=1 (channel)	14	12
		Total: 61	

Figure 5.37 shows the joint distribution modeled with the experimental data without introducing marginal constraints. Experimental data is superimposed with the smooth distribution maps.

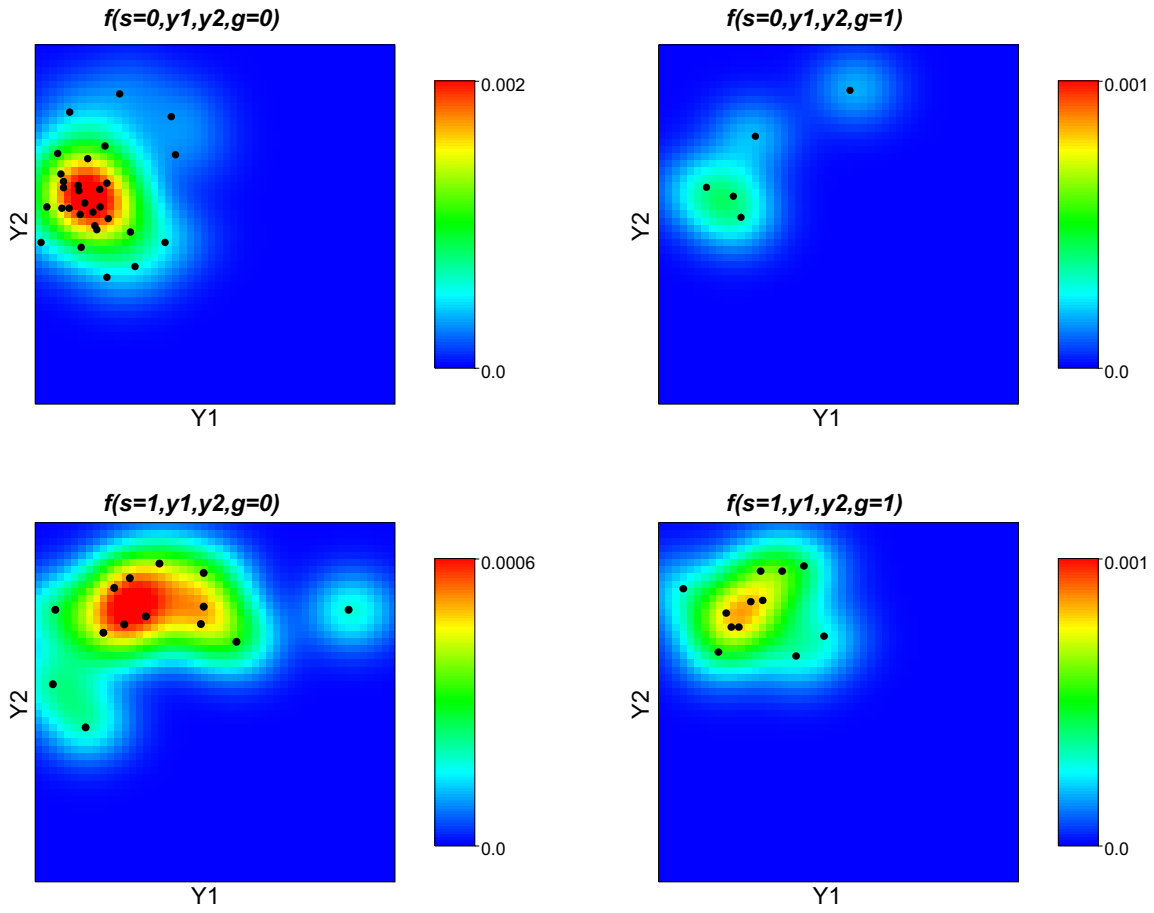

Figure 5.37: The modeled initial joint distributions using the kernel estimator.

The corrected joint distributions are shown in Figure 5.38. Overall patterns inherent in the experimental data plots are reflected and local variations in probability densities are enhanced by introducing marginal constraints. They fit exactly the imposed marginal distribution.

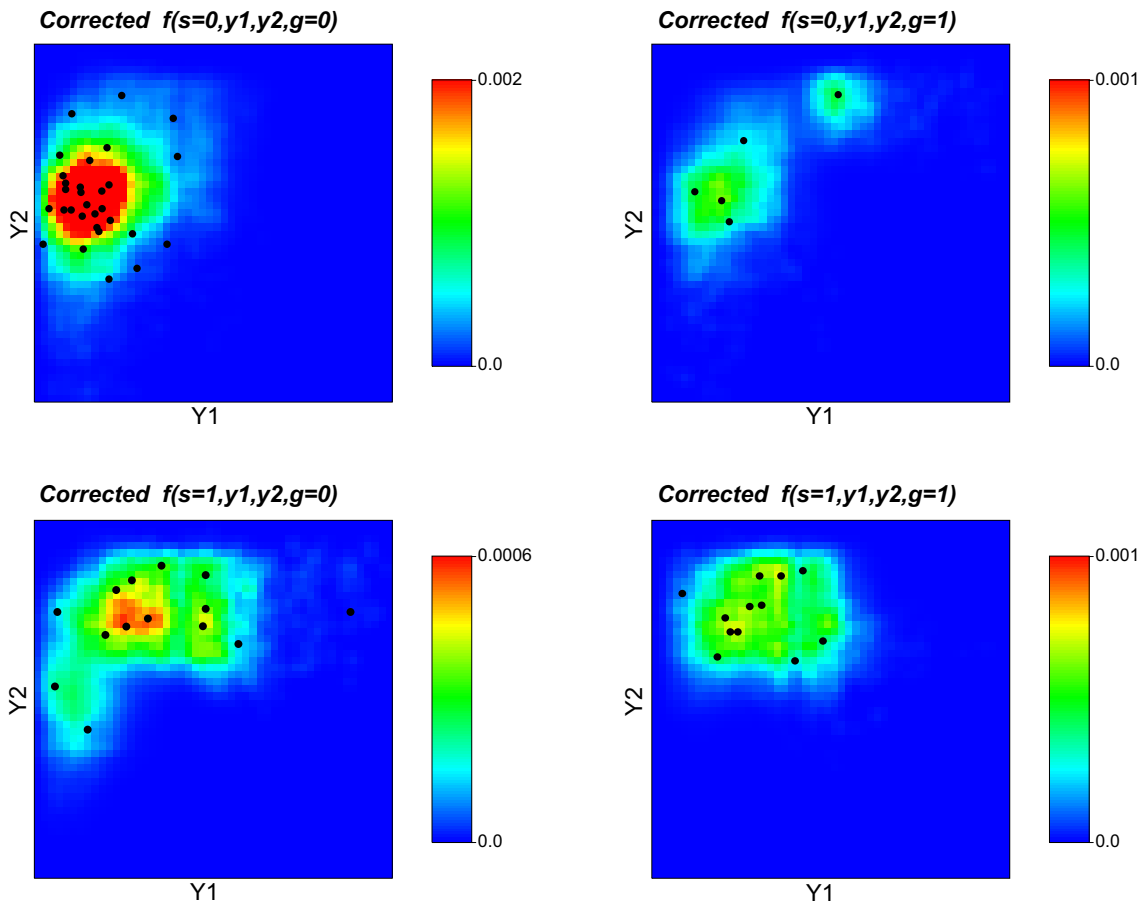

Figure 5.38: The corrected joint distributions under marginal constraints.

To enforce the marginal constraints, the sequential fitting algorithm was used. Figure 5.39 plots the calculated average marginal errors at each iteration step versus iteration number. The errors quickly drop during the first few iterations and the modified distributions become stable with averaged marginal error of 0.9×10^{-5}% after 20 iterations. The procedure took 6.2 sec on a 3.2 GHz personal computer.

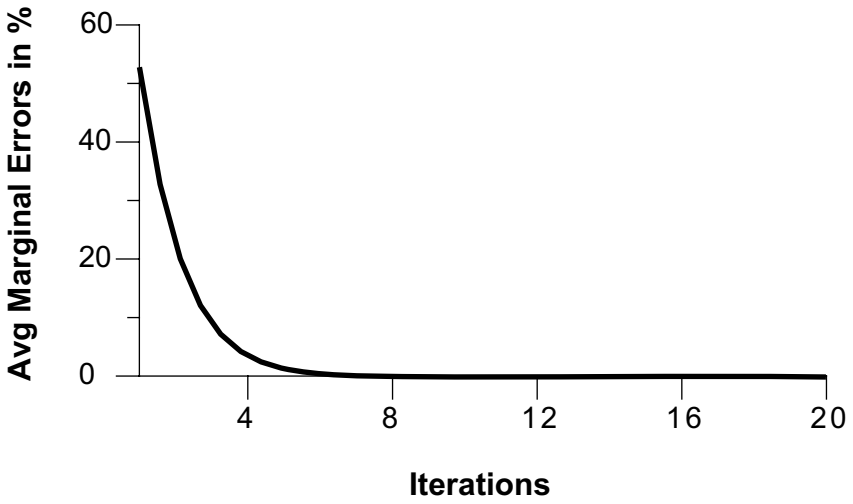

Figure 5.39: Averaged marginal errors in % against the marginal fitting iterations. Errors are calculated by comparing the reproduced marginals from the joint distributions and the reference marginals. Marginal errors converge into very small percentage with 20 iterations where the corrected distributions become stable.

The conditional probability of facies is derived from the modified joint distributions. Secondary values and the geologic code are input to the corrected joint distribution. The conditional probability is then immediately derived:

$$p(s(\mathbf{u}) \mid y_1(\mathbf{u}), y_2(\mathbf{u}), g(\mathbf{u})) = \frac{f^{Corr}(s(\mathbf{u}), y_1(\mathbf{u}), y_2(\mathbf{u}), g(\mathbf{u}))}{f(y_1(\mathbf{u}), y_2(\mathbf{u}), g(\mathbf{u}))}, \ \mathbf{u} \in A \qquad (5\text{-}14)$$

where f^{Corr} is the corrected joint distribution by the marginal fitting method with the imposed marginal conditions. In practice, there are differences between the actual secondary values $y_1(\mathbf{u})$ and $y_2(\mathbf{u})$ and the discretized values and these differences depend on the level of binning used for the soft secondary data. 50 bins seems to give reasonably small discretization errors (see Figure 5.40).

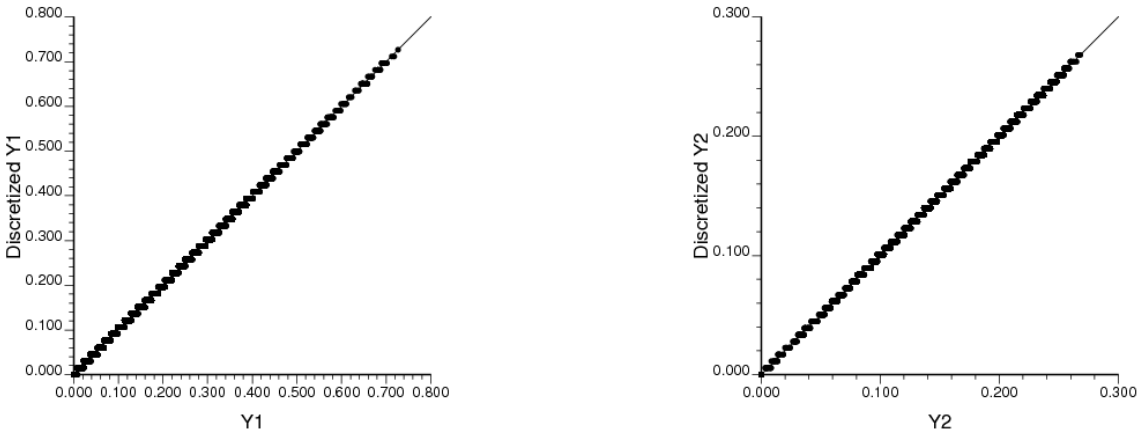

Figure 5.40: Cross plot of actual and the binned soft secondary values.

Figure 5.41 illustrates the map of channel probability (middle in the figure) that is obtained from integrating the soft secondary and geologic data. The resulting probability map is compared with the reference image (top in the figure) and it is consistent with the geology information and captures the expected meandering of the channel belts. One X-X' horizontal section is illustrated for comparing the estimated probability and true values (bottom in the figure).

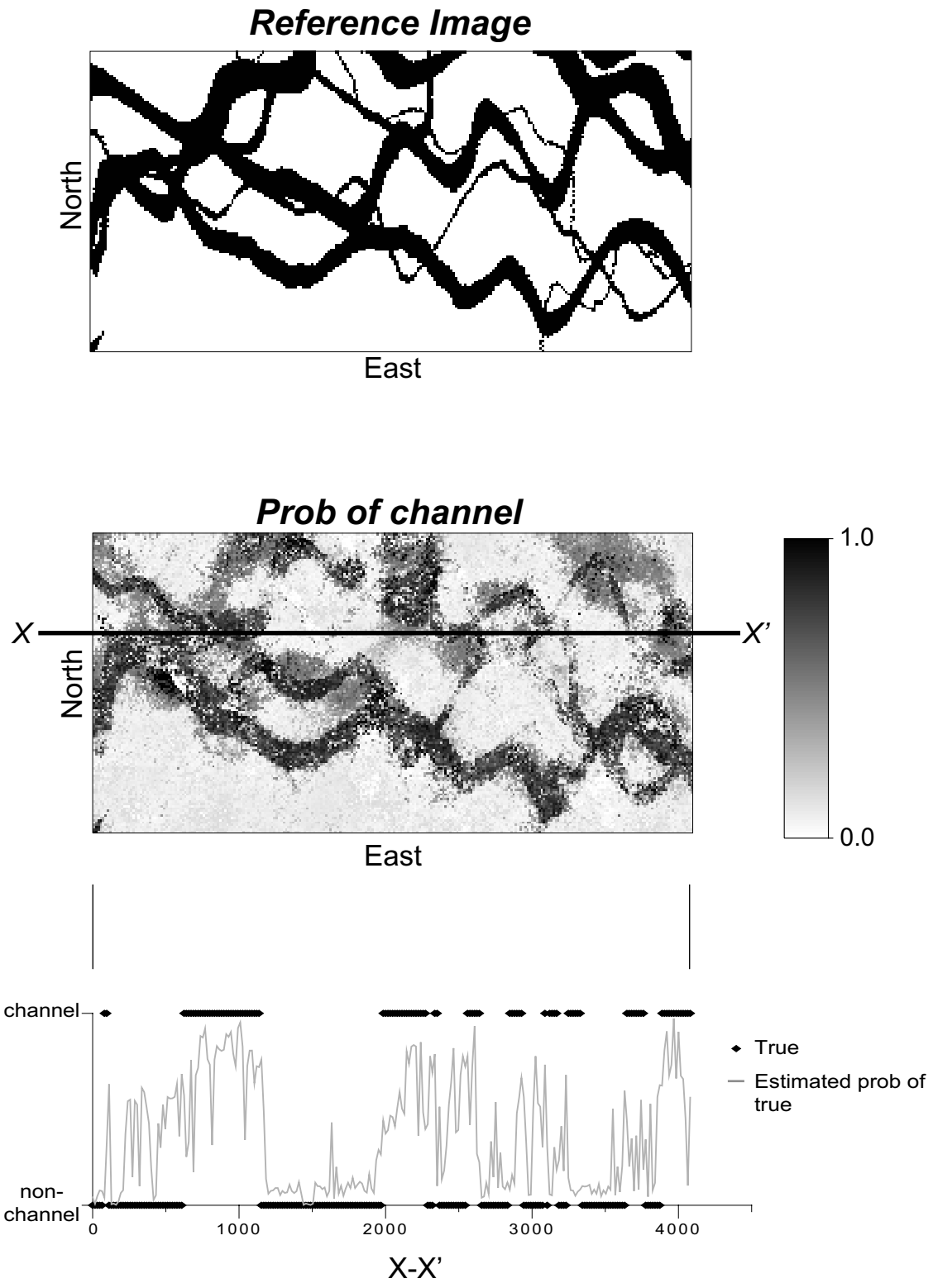

Figure 5.41: The estimated probability of channel is shown at the middle. A 1-D section through X-X' is plotted in the bottom showing the true values either 0 (non-channel) or 1 (channel) and the secondary guided channel probability (grey line).

Figure 5.42 shows the probability of channel estimated from integrating soft secondary and geology data (top), and from integrating soft secondary data only (bottom). Probabilities are shown if pixels have 0.65 or higher probability of channel which is two times larger than the global proportion of channel, p(channel) = 0.33. Channel connectivity is captured and complex heterogeneity is accounted for which is a result of the input geologic information. The result from considering soft secondary data shows a more patchy distribution of the channel probability.

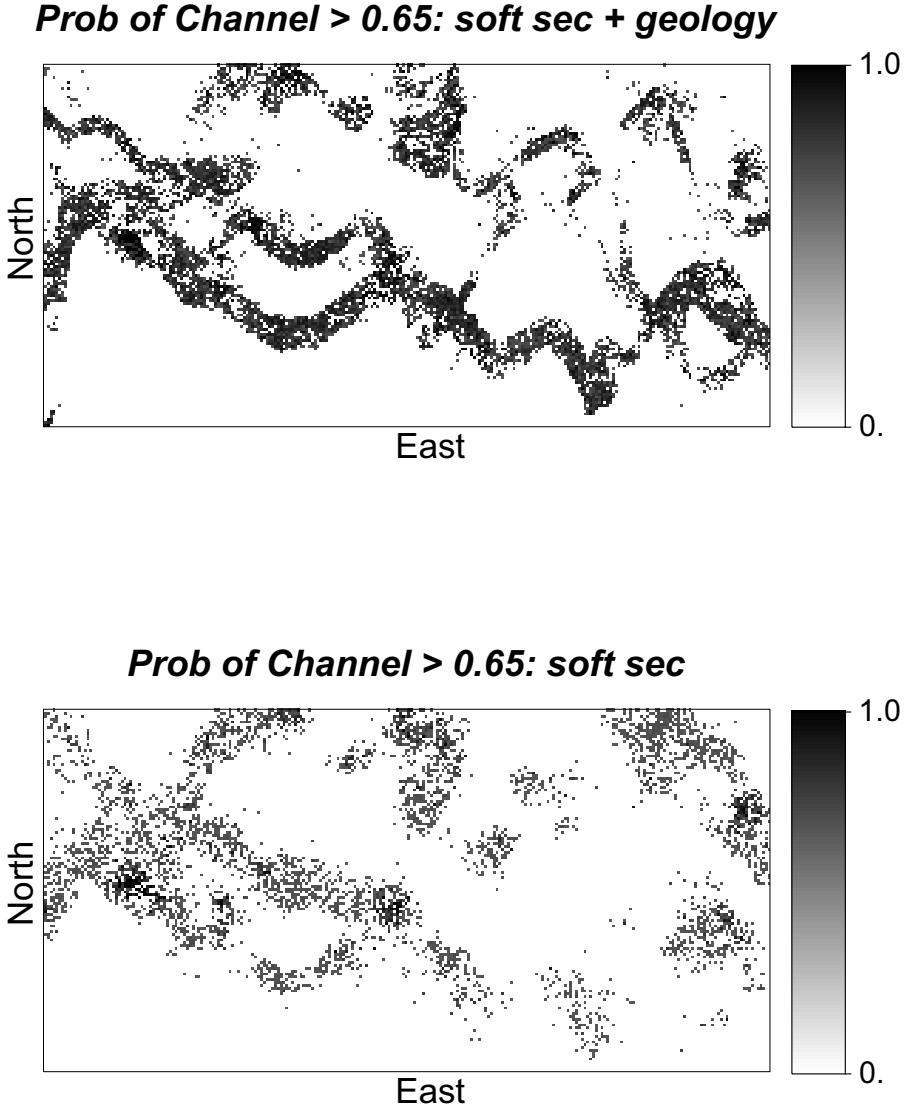

Figure 5.42: The estimated probability of channel from integrating soft secondary and geology data, and soft secondary data only. Maps show the probability higher than 0.65: there is no special meaning of cutoff 0.65. This figure points out geologic heterogeneity is better reproduced and isolated pixels are reduced when considering both soft secondary and prior geologic information.

5.4 Discussions

The main motivations for the method are that the joint distribution between the primary and the secondary data is possible and the joint distribution of the secondary data is quite well-known. The multivariate distribution modeling between the data is not enough. Marginal distribution conditions are evaluated and the proposed marginal fitting algorithm corrects the modeled initial joint distribution under the imposed conditions.

The multivariate distribution modeling under marginal constraints was applied to the various secondary data integration examples: integrating continuous secondary data for facies modeling, integrating large scaled soft secondary data for facies modeling and integrating soft secondary and discrete geologic map for facies modeling. For these applications, data redundancy between the secondary data is implicitly accounted for while the joint distribution modeling. The examples showed that the marginal fitting algorithm is stable and fast: the averaged marginal errors are quickly dropped and converged after a small number of iteration. The comparative study from different integration techniques such as PCS versus multivariate modeling approach is not done, but the reasonableness of the results are evaluated based on the fairness of the estimated local probabilities and the reproduction of input statistics.

By enforcing the marginal distributions, the secondary derived probability result always reproduced the declustered global proportion very well. The reproduced global proportions can be far different without imposing marginal conditions.

The proposed multivariate modeling technique has been applied to the categorical variable modeling. Application to the continuous variable modeling is described in Chapter 6. A new interpretation of the Bayesian updating (BU) is demonstrated. It is shown that how the primary data derived and the secondary data derived distributions can be integrated in a new form of BU equation.

Chapter 6

Advanced Application of the Multivariate Distribution Modeling

6.1 Bayesian Updating

Bayesian updating (BU) technique was first proposed in 1996 by Doyen and since then the technique has been widely adopted to integrate multiple soft secondary variables. BU is fundamentally equivalent to collocated cokriging using the Markov type screening assumption developed by Xu et al. but its formalism is different from the collocated cokriging (Doyen et al., 1996; Chiles and Delfiner, 1999; Xu et al., 1992). Collocated cokriging is an extended form of kriging expressed by a weighted linear combination of nearby primary and collocated secondary data, and the technique expresses the updated distribution by the combination of probability distributions conditioned to each primary and secondary variable. This section introduces the detailed derivation of Bayesian updating equation and proposes an alternative form to the conventional updating equation. The new expression gives an explicit interpretation of how probability distributions derived from disparate data sources can be combined leading to the final updated distribution, and where the global mean and variance intervene in the updating equation. Because the new updating equation decomposes the influence of the primary and secondary variable, separate calibration of secondary variable from primary variable is possible. An

approach to account for non-linear relations between the primary and secondary variables is proposed using the new form of updating equation. The joint probability density functions are modeled in a nonparametric way using the kernel density estimator. Because the (initial) joint distribution does not meet the marginality condition a fitting algorithm modifies the initial joint distribution into a corrected joint distribution that satisfies all lower order marginal conditions. The marginal fitting algorithm directly accounts for the differences between the empirical and reference marginal distributions. The conditional distribution at a given secondary value can be extracted from the corrected joint distribution and the mean and variance can be numerically estimated from the extracted conditional pdf. The secondary data derived estimates and variances are then combined with ones from the primary data to result in the updated distribution.

6.1.1 Resolution of Bayesian Updating

The primary and secondary variables are denoted as random variables Z and Y, and they are already transformed into normal score values with mean of 0 and variance of 1. A posterior distribution of interest is the conditional distribution of Z given the surrounding primary and collocated secondary data:

$$f(z(\mathbf{u}) \mid z(\mathbf{u}_1),...,z(\mathbf{u}_n), y(\mathbf{u})), \quad \mathbf{u} \in A \tag{6-1}$$

where $z(\mathbf{u}_1),\ldots, z(\mathbf{u}_n)$ are nearby primary data at different locations $\mathbf{u}_i$, i=1,…,n, and $y(\mathbf{u})$ is a collocated secondary data retained as conditioning data. A single secondary variable is considered as an example, but the equations derived in this work can be extended to multiple secondary variables using vector and matrix notation. Equation (6-1) is re-expressed as:

$$\begin{aligned} f\left(z(\mathbf{u}) \mid z(\mathbf{u}_1),...,z(\mathbf{u}_n), y(\mathbf{u})\right) &= \frac{f\left(z(\mathbf{u}), z(\mathbf{u}_1),...,z(\mathbf{u}_n), y(\mathbf{u})\right)}{f\left(z(\mathbf{u}_1),...,z(\mathbf{u}_n), y(\mathbf{u})\right)} \\ &= \frac{f\left(z(\mathbf{u}_1),...,z(\mathbf{u}_n), y(\mathbf{u}) \mid z(\mathbf{u})\right) f\left(z(\mathbf{u})\right)}{f\left(z(\mathbf{u}_1),...,z(\mathbf{u}_n), y(\mathbf{u})\right)} \end{aligned} \tag{6-2}$$

The conditional distribution $f(z(\mathbf{u}_1),\ldots, z(\mathbf{u}_n),y(\mathbf{u})|z(\mathbf{u}))$ in the numerator is approximated as $f(z(\mathbf{u}_1),\ldots,z(\mathbf{u}_n),y(\mathbf{u})|z(\mathbf{u})) \cong f(z(\mathbf{u}_1),\ldots,z(\mathbf{u}_n)|z(\mathbf{u}))\times f(y(\mathbf{u})|z(\mathbf{u}))$ under an independence assumption between collocated $y(\mathbf{u})$ and local surrounding primary data $[z(\mathbf{u}_1),\ldots,z(\mathbf{u}_n)]$ conditioned to estimate of primary variable Z at $\mathbf{u}$, $z(\mathbf{u})$. This independence assumption alleviates the

requirement of inferring the joint distribution $f(z(\mathbf{u}_1),\ldots,z(\mathbf{u}_n),y(\mathbf{u})|z(\mathbf{u}))$ which is difficult to model because it requires joint modeling of mixed variables from different locations. Equation (6-2) is approximated as:

$$f\left(z(\mathbf{u})\,|\,z(\mathbf{u}_1),...,z(\mathbf{u}_n),y(\mathbf{u})\right)=\frac{f\left(z(\mathbf{u}_1),...,z(\mathbf{u}_n)\,|\,z(\mathbf{u})\right)f\left(y(\mathbf{u})\,|\,z(\mathbf{u})\right)f\left(z(\mathbf{u})\right)}{f\left(z(\mathbf{u}_1),...,z(\mathbf{u}_n),y(\mathbf{u})\right)} \quad (6\text{-}3)$$

The conditional independence assumption decouples the posterior distribution into two terms: (1) distribution associated with the primary data at different locations, $f(z(\mathbf{u}_1),\ldots,z(\mathbf{u}_n)|z(\mathbf{u}))$, and (2) the distribution associated with the primary and secondary variable relation, $f(y(\mathbf{u})|z(\mathbf{u}))$. The probabilistic terms in the right hand side of Equation (6-3) constitute a *likelihood function* that treats the unknown estimate $z(\mathbf{u})$ as fixed. They are re-expressed as probability functions of the unknown estimate given the fixed data:

$$f\left(z(\mathbf{u})\,|\,z(\mathbf{u}_1),...,z(\mathbf{u}_n),y(\mathbf{u})\right)=\frac{f\left(z(\mathbf{u})\,|\,z(\mathbf{u}_1),...,z(\mathbf{u}_n)\right)}{f\left(z(\mathbf{u})\right)}\frac{f\left(z(\mathbf{u})\,|\,y(\mathbf{u})\right)}{f\left(z(\mathbf{u})\right)}f\left(z(\mathbf{u})\right)\cdot C \quad (6\text{-}4)$$

where normalizing C term is $f(z(\mathbf{u}_1),\ldots,z(\mathbf{u}_n))\times f(y(\mathbf{u}))/(f(z(\mathbf{u}_1),\ldots,z(\mathbf{u}_n),y(\mathbf{u}))$. Although Bayesian updating technique has been commonly used in many cases, there are few references explaining how the final updating equations are reached (Neufeld and Deutsch, 2004; Deutsch and Zanon, 2004). Equation (6-4) provides a posterior distribution through the multiplication of three probability distributions. $f(z(\mathbf{u})|z(\mathbf{u}_1),\ldots,z(\mathbf{u}_n))$ is a univariate conditional distribution of Z conditioned to local nearby data $z(\mathbf{u}_1),\ldots,z(\mathbf{u}_n)$. Under the multiGaussianity (MG) assumption, kriging parametrically constructs the $f(z(\mathbf{u})|z(\mathbf{u}_1),\ldots,z(\mathbf{u}_n))$ as a Gaussian distribution with mean equal to the kriging estimate and variance of kriging variance (Journel and Huijbregts, 1981; Verly, 1983):

$$f\left(z(\mathbf{u})\,|\,z(\mathbf{u}_1),...,z(\mathbf{u}_n)\right)=\frac{1}{\sqrt{2\pi\sigma_P^2(\mathbf{u})}}\exp\left\{-\frac{\left(z(\mathbf{u})-z_P(\mathbf{u})\right)^2}{2\sigma_P^2(\mathbf{u})}\right\} \quad (6\text{-}5)$$

where $z_P(\mathbf{u})$ and $\sigma^2_P(\mathbf{u})$ are the estimate and estimation variance obtained by simple kriging at $\mathbf{u}$. Subscript P means that those are estimates from the primary data.

Under the linear relation assumption between the primary and secondary data the $f(z(\mathbf{u})|y(\mathbf{u}))$ in Equation (6-5) becomes:

$$f(z(\mathbf{u}) \mid y(\mathbf{u})) = \frac{1}{\sqrt{2\pi\sigma_S^2}} \exp\left\{ -\frac{(z(\mathbf{u}) - z_S(\mathbf{u}))^2}{2\sigma_S^2} \right\} \tag{6-6}$$

$z_S(\mathbf{u})$ and $\sigma^2_S(\mathbf{u})$ are the estimate and variance obtained by the relation between the primary and secondary variables. Subscript S indicates they are secondary data derived moments. Due to the linear relation assumption between Z and Y, the conditional mean and variance $z_S(\mathbf{u})$ and $\sigma^2_S(\mathbf{u})$ are simply calculated as $z_S(\mathbf{u}) = \rho \times y(\mathbf{u})$ and $\sigma^2_S(\mathbf{u})=1-\rho^2$, where ρ is the linear correlation coefficient between Z and Y. $z_S(\mathbf{u})$ depends on the local secondary value $y(\mathbf{u})$ but the variance $\sigma^2_S(\mathbf{u})$ is constant over $\mathbf{u} \in A$. The last term $f(z(\mathbf{u}))$ in Equation (6-4) is a univariate Gaussian distribution:

$$f(z(\mathbf{u})) = \frac{1}{\sqrt{2\pi\sigma^2}} \exp\left\{ -\frac{(z(\mathbf{u}) - m)^2}{2\sigma^2} \right\} \tag{6-7}$$

Even though the primary variable Z has zero mean and unit variance (m=0, σ^2=1), m and σ^2 symbols are left in this equation. One can follow how the global mean and variance are used in the final updating equation by letting the symbols remain.

Elementary probability distributions consisting of a posterior distribution are all Gaussian (Equations (6-5), (6-6) and (6-7)). Multiplication of Gaussian distributions is another Gaussian; thus, the posterior distribution is Gaussian as well. Equations shown in (6-5), (6-6) and (6-7) are inserted into Equation (6-4) as follows:

$$\begin{aligned} & f\left(z(\mathbf{u}) \mid z(\mathbf{u}_1), \ldots, z(\mathbf{u}_n), y(\mathbf{u})\right) \\ & = \frac{f\left(z(\mathbf{u}) \mid z(\mathbf{u}_1), \ldots, z(\mathbf{u}_n)\right)}{f\left(z(\mathbf{u})\right)} \frac{f\left(z(\mathbf{u}) \mid y(\mathbf{u})\right)}{f\left(z(\mathbf{u})\right)} f\left(z(\mathbf{u})\right) \cdot C \\ & = \frac{\frac{1}{\sqrt{2\pi\sigma_P^2(\mathbf{u})}} \exp\left\{ -\frac{(z(\mathbf{u}) - z_P(\mathbf{u}))^2}{2\sigma_P^2(\mathbf{u})} \right\}}{\frac{1}{\sqrt{2\pi\sigma^2}} \exp\left\{ -\frac{(z(\mathbf{u}) - m)^2}{2\sigma^2} \right\}} \frac{1}{\sqrt{2\pi\sigma_S^2(\mathbf{u})}} \exp\left\{ -\frac{(z(\mathbf{u}) - z_S(\mathbf{u}))^2}{2\sigma_S^2(\mathbf{u})} \right\} \cdot C \end{aligned} \tag{6-8}$$

Terms inside the exponential functions are grouped and all terms independent of $z(\mathbf{u})$ are absorbed in the proportionality then:

$$f(z(\mathbf{u}) \mid z(\mathbf{u}_1),...,z(\mathbf{u}_n), y(\mathbf{u})) \propto \exp\left\{-\frac{\left(z(\mathbf{u})-z_P(\mathbf{u})\right)^2}{2\sigma_P^2(\mathbf{u})}+\frac{\left(z(\mathbf{u})-m\right)^2}{2\sigma^2}-\frac{\left(z(\mathbf{u})-z_S(\mathbf{u})\right)^2}{2\sigma_S^2(\mathbf{u})}\right\} \quad (6\text{-}9)$$

Equation (6-9) is arranged with respect to $z(\mathbf{u})$:

$$f(z(\mathbf{u}) \mid z(\mathbf{u}_1),...,z(\mathbf{u}_n), y(\mathbf{u})) \propto \exp\left\{-\underbrace{\left[\frac{1}{2\sigma_P^2(\mathbf{u})}-\frac{1}{2\sigma^2}+\frac{1}{2\sigma_S^2(\mathbf{u})}\right]}_{A} z^2(\mathbf{u})+\underbrace{\left[\frac{z_P(\mathbf{u})}{\sigma_P^2(\mathbf{u})}+\frac{z_S(\mathbf{u})}{\sigma_S^2(\mathbf{u})}-\frac{m}{\sigma^2}\right]}_{B} z(\mathbf{u})\right\} \quad (6\text{-}10)$$

Terms independent of $z(\mathbf{u})$ are absorbed in the proportionality again. Equation (6-10) follows a quadratic form of $\exp\{-Az^2 + Bz\}$ where A and B are parameterized coefficients. This can be easily converted into the basic form of Gaussian function:

$$f(z(\mathbf{u}) \mid z(\mathbf{u}_1),...,z(\mathbf{u}_n), y(\mathbf{u})) \propto \exp\left\{-Az^2(\mathbf{u})+Bz(\mathbf{u})\right\} \propto \exp\left\{-\frac{\left(z(\mathbf{u})-B/2A\right)^2}{2\left(1/2A\right)}\right\} \quad (6\text{-}11)$$

The posterior distribution $f(z(\mathbf{u})|z(\mathbf{u}_1),\ldots,z(\mathbf{u}_n),y(\mathbf{u}))$ becomes a Gaussian distribution with the mean of B/2A and variance of 1/2A while A and B are defined in Equation (6-10):

$$\sigma_{BU}^2(\mathbf{u}) = \frac{1}{2A} \text{ and } z_{BU}(\mathbf{u}) = \frac{B}{2A} \quad (6\text{-}12)$$

where $z_{BU}(\mathbf{u})$ and $\sigma_{BU}^2(\mathbf{u})$ are the mean and variance of the posterior distribution. The Bayesian updated variance and estimate at location $\mathbf{u}$ are finally:

$$\frac{1}{\sigma_{BU}^2(\mathbf{u})} = \frac{1}{\sigma_P^2(\mathbf{u})}+\frac{1}{\sigma_S^2(\mathbf{u})}-\frac{1}{\sigma^2}$$

$$\frac{z_{BU}(\mathbf{u})}{\sigma_{BU}^2(\mathbf{u})} = \frac{z_P(\mathbf{u})}{\sigma_P^2(\mathbf{u})}+\frac{z_S(\mathbf{u})}{\sigma_S^2(\mathbf{u})}-\frac{m}{\sigma^2} \quad (6\text{-}13)$$

A set of Equation (6-13) is a new form of Bayesian updating that can be compared with the conventional form below:

$$z_{BU}(\mathbf{u}) = \frac{z_P(\mathbf{u})\sigma_S^2 + z_S(\mathbf{u})\sigma_P^2(\mathbf{u})}{\sigma_P^2(\mathbf{u}) - \sigma_P^2(\mathbf{u})\sigma_S^2(\mathbf{u}) + \sigma_S^2(\mathbf{u})}$$
$$\sigma_{BU}^2(\mathbf{u}) = \frac{\sigma_P^2(\mathbf{u})\sigma_S^2(\mathbf{u})}{\sigma_P^2(\mathbf{u}) - \sigma_P^2(\mathbf{u})\sigma_S^2(\mathbf{u}) + \sigma_S^2(\mathbf{u})} \quad (6\text{-}14)$$

The equations in (6-13) and (6-14) are exactly same when $m = 0$ and $\sigma^2 = 1$ in Equation (6-13). The main advantage of the new expression is that the updated parameters z_{BU} and σ^2_{BU} are clearly decomposed into combination of local and global parameters derived from diverse sources. One possible applications of the new form would be accounting for the non-stationarity in the global statistics such as $m(\mathbf{u})$ and $\sigma(\mathbf{u})$ instead of $m(\mathbf{u})=m$ and $\sigma(\mathbf{u})=\sigma$ (Hong and Deutsch, 2008).

6.1.2 Accounting for Non-linear Relations between Primary and Secondary Variables

Several assumptions have been made to derive the Bayesian updating equation and the key assumptions are: (1) multiGaussianity of primary variables at different locations, which allows constructing the local conditional distribution $f(z(\mathbf{u})|z(\mathbf{u}_1),\ldots,z(\mathbf{u}_n))$ by simple kriging at $\mathbf{u}$, and (2) a linear relation between primary and secondary variables, which allows building the conditional distribution $f(z(\mathbf{u})|y(\mathbf{u}))$ by the linear correlation coefficient ρ. Only under this Gaussian assumption on the distributions (multivariate Gaussian in spatial context and multivariate Gaussian in variable context) is the analytical derivation of updating is possible.

Relaxing the linear relation assumption between primary and secondary variables is considered here. The multiGaussianity assumption is still adopted to build the local conditional distribution $f(z(\mathbf{u})|z(\mathbf{u}_1),\ldots,z(\mathbf{u}_n))$. Conventional Bayesian updating assumes the Gaussian relation after univariate normal score transformation of each variable. An illustration shown in Figure 6.1 represents a highly non-linear feature between two normal scored variables (normal scored values of porosity and permeability from the Amoco data set). Gaussianity of univariate marginal distribution is a necessary condition, but not a sufficient condition for joint Gaussianity.

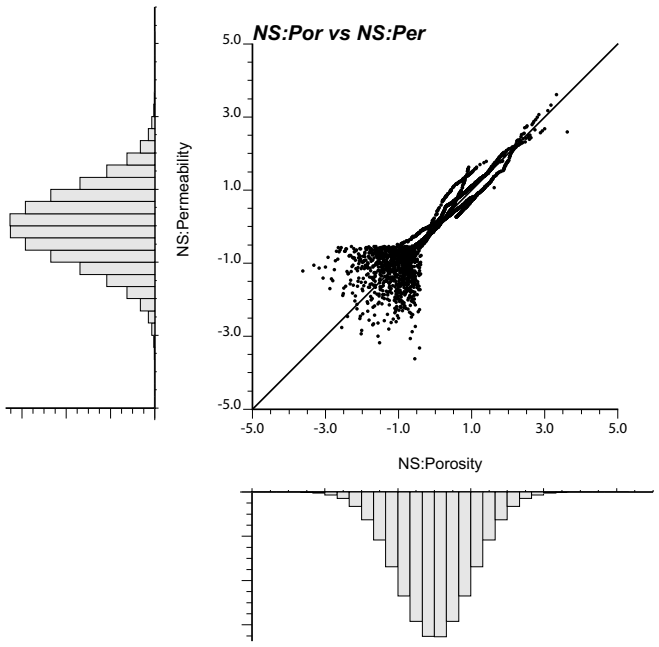

Figure 6.1: An illustration of non-linear relation after individual normal score transform of each variable.

Proposed Methodology

To capture the non-linear relation among primary and secondary variables, the joint relation is first modeled in a nonparametric way. Kernel density estimation is considered to model the joint pdf $f(z(\mathbf{u}),y(\mathbf{u}))$, $\mathbf{u}\in A$ without data distribution assumption; the method applies the specified kernel function to the pairs of collocated primary and secondary data and then approximates the underlying true distribution by summing the applied kernel function values. For a simple notation, the location vector ($\mathbf{u}$) is removed hereafter such as $f(z,y)$.

The product kernel estimator is widely used to model the joint distribution in practice. Bivariate pdf can be constructed by:

$$f(z,y)=\frac{1}{nh_1\times h_2}\sum_{i=1}^{n}\left(W\left(\frac{(z-Z_i)}{h_1}\right)\times W\left(\frac{(y-Y_i)}{h_2}\right)\right) \tag{6-15}$$

where $W(\cdot)$ is a univariate kernel applied to each variable Z and Y. h_1 and h_2 are kernel bandwidths for the variable Z and Y. The next step is aimed at checking axioms of the modeled joint pdf: non-negative density functions, closure condition and reproduction of lower order marginal distributions. The kernel density estimator meets the first two axioms if the used kernel function $W(\cdot)$ follows $W(x)\geq 0$ and $\int W(x)\mathrm{d}x=1$. The third condition is a marginality condition that

the p-variate joint pdf should reproduce p'-variate pdf where $p' < p$. The following are the marginal conditions that the modeled bivariate pdf must meet:

$$\int f(z,y)dz = f(y), \forall y \tag{6-16}$$

$$\int f(z,y)dy = f(z), \forall z \tag{6-17}$$

The marginal relation described in Equation (6-16) states that integration of the joint probability distribution over possible outcomes of the primary data should amount to the distribution of the secondary variable Y, $f(y)$. The second marginal relation (6-17) states that integration of the joint probability distribution over possible outcomes of the secondary variable should reproduce the distribution of the primary variable Z, $f(z)$. The global distribution of the primary variable f(z) is experimentally obtained from well samples. The secondary data pdf $f(y)$ is modeled with the densely sampled values over the area and the abundance of samples makes a very reliable $f(y)$. Given the marginal relations, the marginal fitting algorithm is used to impose them on the joint pdf $f(z,y)$. The marginals are derived from initial joint distribution and they are compared with the reference marginals. The differences are directly corrected in the correcting procedure. This correcting process consists of the following steps:

Step1. Model the distribution of secondary variable, $f(y)$ and global distribution of primary variable, $f(z)$. Declustering is considered for obtaining an unbiased $f(z)$ if required.

Step2. Model the joint distribution $f(z,y)$ and define it as $f^{(0)}$ to differentiate from the resulting joint distribution.

Step3. Scale the $f^{(0)}$ to ensure the marginal distribution shown in Equation (6-16). The scaling equation below is proposed for ensuring the imposed marginal condition:

$$f^{(0)}(z,y) \times \frac{f(y)}{\int f^{(0)}(z,y)dz} \rightarrow f^{(1)}(z,y) \tag{6-18}$$

The ratio $f(y)/\int f(z,y)dz$ is a modifying factor. If the marginal relation (6-16) is satisfied then this factor becomes 1 leading to no change in $f^{(0)}$. Otherwise, $f^{(0)}$ is adjusted by the modifying factor that accounts for the differences between the reference $f(y)$ and reproduced marginal distribution $\int f^{(0)}(z,y)dz$. The corrected distribution under the marginal condition is set as $f^{(1)}$ for the next step.

Step4. Scale the $f^{(1)}$ to ensure the marginal condition shown in Equation (6-17). Similar to the step 3, the scaling equation below is for updating the $f^{(1)}$:

$$f^{(1)}(z,y)\times\frac{f(z)}{\int f^{(1)}(z,y)dy}\rightarrow f^{(2)}(z,y) \tag{6-19}$$

The ratio $f(z)/\int\!\!\int f^{(1)}(z,y)dy$ is another modifying factor. If the marginal relation (6-17) is met then the factor becomes 1 leading to no change in $f^{(1)}$. Otherwise, $f^{(1)}$ is adjusted by the modifying factor accounting for the differences between the reference marginal distribution $f(z)$ and the reproduced marginal distribution $\int\!\!\int f^{(1)}(z,y)dy$. The corrected distribution under marginal condition (6-17) is set as $f^{(2)}$.

Step5. Terminate the procedures if stopping rule is met, otherwise go to step 6.

Step6. Reset $f^{(2)}$ into $f^{(0)}$ and repeat through steps 3 and 5.

Step 1 and 2 are initial steps to establish the marginal distributions $f(z)$ and $f(y)$. Steps 3 through 5 are employed to correct the initial distribution with the considered marginal distributions. Step 5 terminates successive adjustments when the joint distribution becomes stable.

The proposed marginal fitting algorithm corrects the initial joint pdf under marginal conditions. Once the joint pdf is achieved, conditional pdfs can be immediately derived. The conditional distribution given the secondary values, $f(z(\mathbf{u})|y(\mathbf{u}))$ at $\mathbf{u}$, is extracted from the corrected joint pdf $f(z,y)$. The conditional mean and variance are calculated using the extracted conditional distribution $z_S(\mathbf{u})$ and $\sigma^2_S(\mathbf{u})$. The obtained mean and variance are put into the Bayesian updating equation in Equation (6-13). Following charts (Figure 6.2) gives an overview of the proposed approach.

1. Model the f(z,y) by kernel density estimation

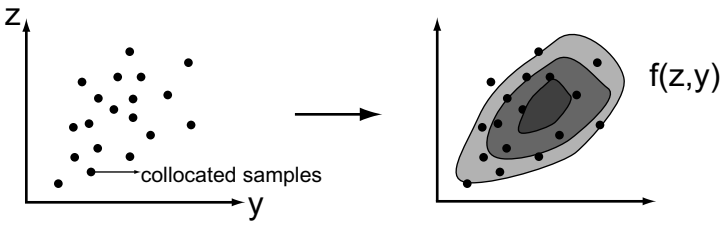

2. Correct the initial f(z,y) with marginal conditions
(Sequential marginal fitting algorithm) and set as $f^{corr}(z,y)$

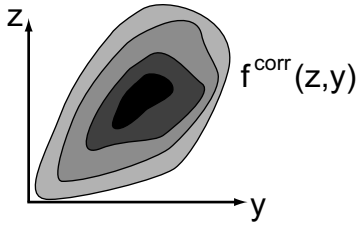

3. Extrac the conditional distribution f(z|y) from $f^{corr}(z,y)$
given secondary values

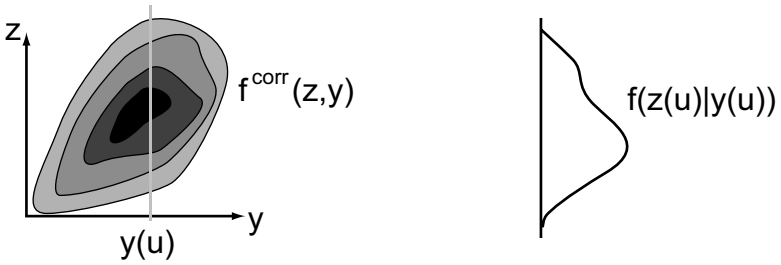

4. Calculate the mean and variance of the extracted f(z(u)|y(u))

5. Set the calculated mean and variance as $z_S(u)$ and $\sigma^2_S(u)$ and
inert them into the updating equation

Figure 6.2: Workflow for the proposed approach

The suggested algorithm accounts for non-linear features between primary and secondary variables and its modeled joint pdf exactly reproduces lower order marginal distributions. The conditional distribution given any value of secondary data can be drawn from the obtained joint distribution. The extracted conditional distribution may not be univariate Gaussian; it can be any shape (see the extracted univariate conditional pdf at step 3 in the above flow chart). Univariate Gaussian fitting is used for the extracted conditional distribution because the conditional pdf

$f(z(\mathbf{u})|y(\mathbf{u}))$ can be integrated with the primary-variable based conditional pdf $f(z(\mathbf{u})|z(\mathbf{u}_1),\ldots,z(\mathbf{u}_n))$ to an updated Gaussian distribution when the constituent distributions are both Gaussian.

6.1.3 Examples

The 2D Amoco data set is used for the application of the more flexible Bayesian updating method. Permeability is considered as the primary variable to be modeled and porosity is considered as the secondary variable. Sampled porosities at 62 wells are simulated to initialize the exhaustive secondary data. 65-by-65 grids nodes are defined in X and Y directions. Figure 6.3 illustrates the simulated porosity field and the permeability samples at well locations. Figure 6.4 shows a scatter plot of the normal scored permeability and porosity. The bivariate relation is not Gaussian despite both marginals being univariate normal. Evaluating the bivariate Gaussianity can be performed through plotting the squared generalized distances from data pairs against the chi-square distances (Johnson and Wichern, 2002). An illustration shown in the right of Figure 6.4 is a plot for the calculated distances from normal scored data pairs and analytical chi-square distances (Johnson and Wichern, 2002). The plot should resemble the straight line through the origin if bivariate normality is guaranteed. Systematic curved pattern shown on the chi-square distance plot suggests a lack of Gaussianity for the normal scored data pairs.

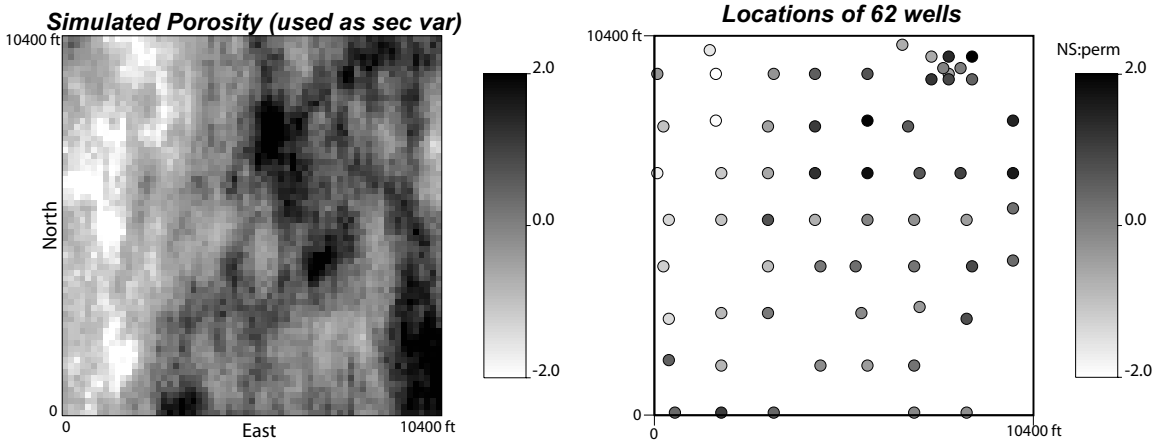

Figure 6.3: Simulated porosity used as secondary variable (left) for predicting permeability and sampled permeability at 62 well locations (right).

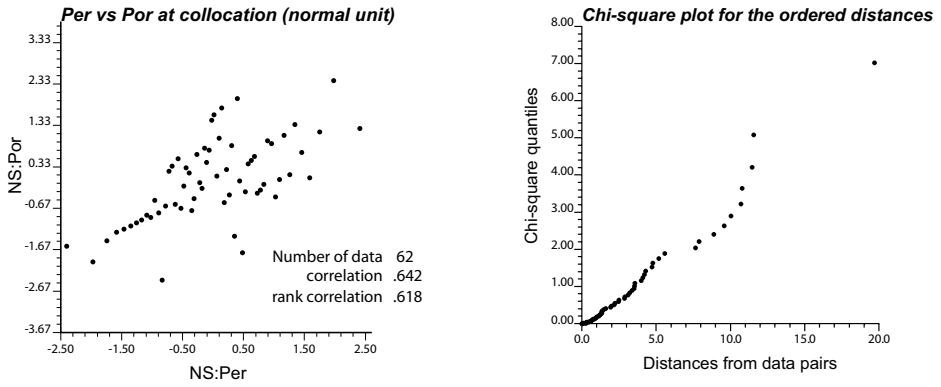

Figure 6.4: Cross plot of normal scored permeability (primary) and porosity (secondary) variables. To check the bivariate normality, the generalized square distances are calculated from data and plotted against the analytical chi-square distances. Systematic differences represent non-biGaussian relation.

The bivariate relation among the normal scored variables is modeled by the kernel density estimator and the described marginal fitting algorithm is applied to the modeled distribution. Kernel bandwidths are chosen using the analytical suggestion shown in Equation (4-12). The range of the primary and secondary variables are discretized into 50 bins and the joint densities are estimated at every 50×50 bins. Given the actual secondary value at location $\mathbf{u}$, $y(\mathbf{u})$, the closest binned y value is looked-up in order to extract the conditional distribution of Z at the conditioned $y(\mathbf{u})$. Too few bins may induce a discretization error. The bivariate pdf shown in Figure 6.7 is the refined pdf under the marginal constraints using the described marginal fitting method.

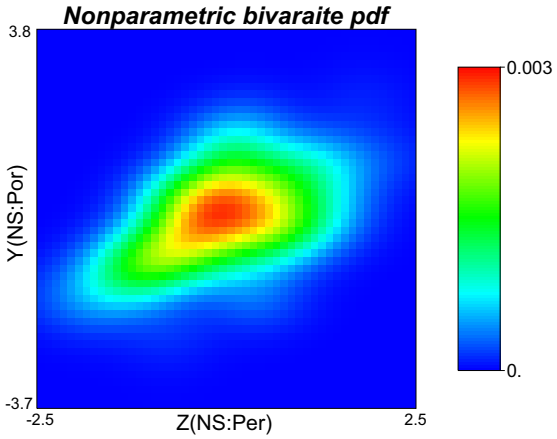

Figure 6.5: Modeled bivariate pdf. Horizontal and vertical axes represent the primary and secondary variables. The described marginal fitting algorithm was applied to obtain this joint pdf.

The averaged marginal errors quickly drop during first few iteration steps. 100 marginal fitting iterations make the bivariate pdf stable and it took a few seconds on a 3 GHz personal computer.

Based on the resulting bivariate distribution, the conditional means and variances are calculated. In this nonparametric modeling, the conditional mean and variance are not determined by the coefficient of correlation but are calculated based on the extracted conditional distribution $f(z(\mathbf{u})|y(\mathbf{u}))$, $\mathbf{u} \in A$. The conditional mean is numerically calculated through the binned values z_k, k=1,…,50:

$$m_L(\mathbf{u}) = E\{Z(\mathbf{u}) \mid Y = y(\mathbf{u})\} = \sum_{k=1}^{50} z_k f(z_k \mid y(\mathbf{u})) = \sum_{k=1}^{50} z_k \frac{f(z_k, y(\mathbf{u}))}{f(y(\mathbf{u}))} \tag{6-20}$$

The extracted 1-D pdf curve $f(z_k,y(\mathbf{u}))$ is a function of the binned primary variable z_k for a fixed $y(\mathbf{u})$. The conditional pdf $f(z_k|y(\mathbf{u}))$ is acquired by dividing $f(z_k,y(\mathbf{u}))$ by $f(y(\mathbf{u}))$. The conditional variances are calculated by:

$$\begin{aligned} \sigma_L^2(\mathbf{u}) &= Var\{Z(\mathbf{u}) \mid Y = y(\mathbf{u})\} \\ &= \sum_{k=1}^{50} \left[z_k - m_L(\mathbf{u})\right]^2 f(z_k \mid y(\mathbf{u})) = \sum_{k=1}^{50} \left[z_k - m_L(\mathbf{u})\right]^2 \frac{f(z_k, y(\mathbf{u}))}{f(y(\mathbf{u}))} \end{aligned} \tag{6-21}$$

Where $m_L(\mathbf{u})$ is a conditional mean of Z given the $y(\mathbf{u})$. Figure 6.6 demonstrates the conditional means and variances given the secondary data value (NS:por). Black dots superimposed with the bivariate pdf map represent the calculated conditional means. The conditional variances are plotted in the right. The conditional means are not linear and the conditional variances are not constant during the range of the secondary variable. Moreover, they are related to the variation of secondary values. For example, the change of conditional variance is rapid when the given secondary values (NS:por) are high or very low. In the intermediate range of secondary data, about from -2.1 to 1.8, the conditional variance tends to decrease with a moderate slope. Figure 6.7 shows the estimates and estimation variance derived from the secondary data.

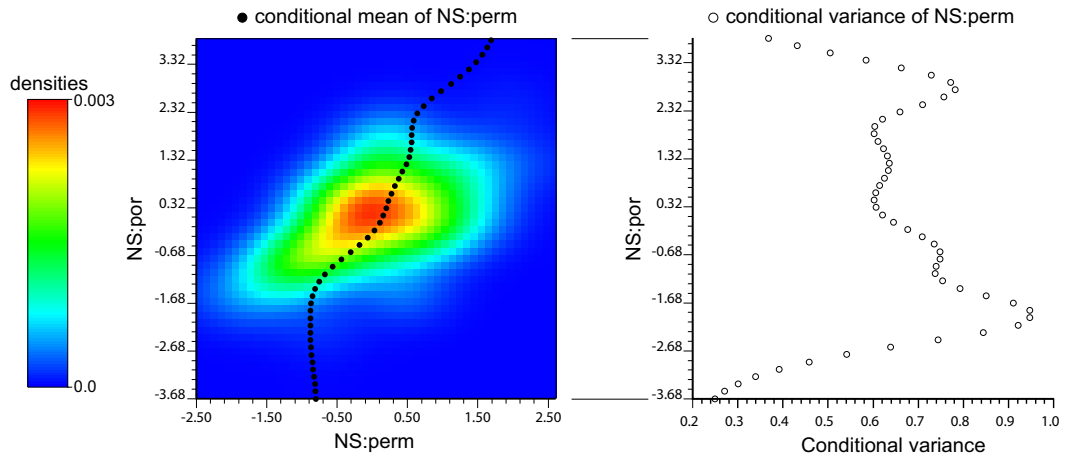

Figure 6.6: Conditional means and variances obtained from the joint pdf modeled in a nonparametric way. Black dots (left) are the calculated conditional means of NS:per with respect to the varying secondary values NS:por. Open circles (right) are the conditional variances with respect to the secondary values.

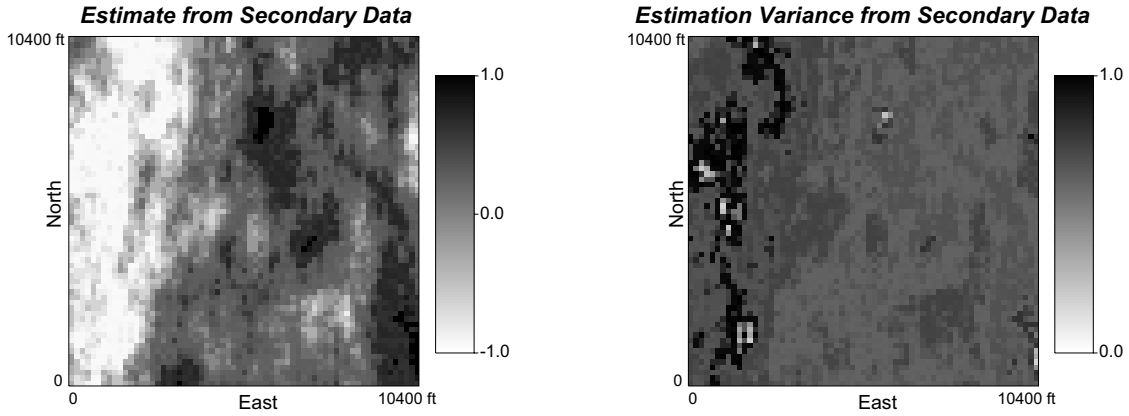

Figure 6.7: Secondary data derived estimates and variances

The conventional BU approach assumes a linear relation between the primary and secondary variable so that it provides a constant estimation variance over the domain. Figure 6.8 shows the comparison of the conditional estimates and estimation variance from the Gaussian assumption and the nonparametric approach. A correlation of 0.642 is calculated from the data pairs of normal scored porosity and permeability as plotted by open circles in the figure. The black solid line is an estimate given the secondary data with the linear regression, and grey dashed line is an estimate from the nonparametric approach. The regression line overestimates the permeability when the conditioned secondary value is high or low. The estimates from the two different approaches are similar when the intermediate range of secondary values is given. The right figure of Figure 6-8 represents the estimation variances given the secondary values. The variances

fluctuate from -59.9% to 70.1% compared with the constant variance 0.588 (solid vertical line) that are obtained from $1-\rho^2$.

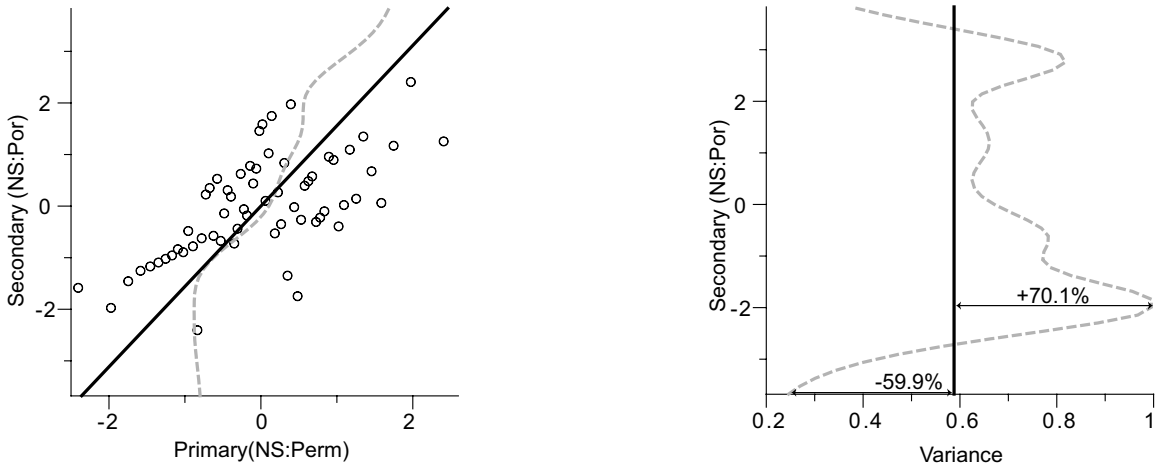

Figure 6.8: Comparison of estimates and estimation variance from two different approaches. Solid and dashed lines represent estimate and estimation variance using linear assumption among variables and nonparametric approach, respectively.

The fairness or accuracy concept reviewed in Chapter 3 is used to assess the estimated local probability distribution for the continuous variable. Deutsch (1997) proposed to compare the proportion of a data set falling into the symmetric *p*-probability intervals calculated from the local distribution, that is $[F^{-1}((1-p)/2),F^{-1}((1+p)/2)]$ with the expected proportion *p* where F is the conditional cumulative density function. This comparison is performed for every probability increments such as p=0.1,0.2,…,1 that can be seen in single plot, namely accuracy plot. Figure 6.9 shows accuracy plots of the local estimates from conventional linear assumption and nonparametric approach. The closeness of dots to the 45° line indicates the goodness of the probabilistic model. Quantitative measure of goodness is proposed by Deutsch (1997) and they are shown on the accuracy plot: G =1 in the best case and G = 0 in the worst case. The nonparametric method is marginally better than the conventional linear assumption.

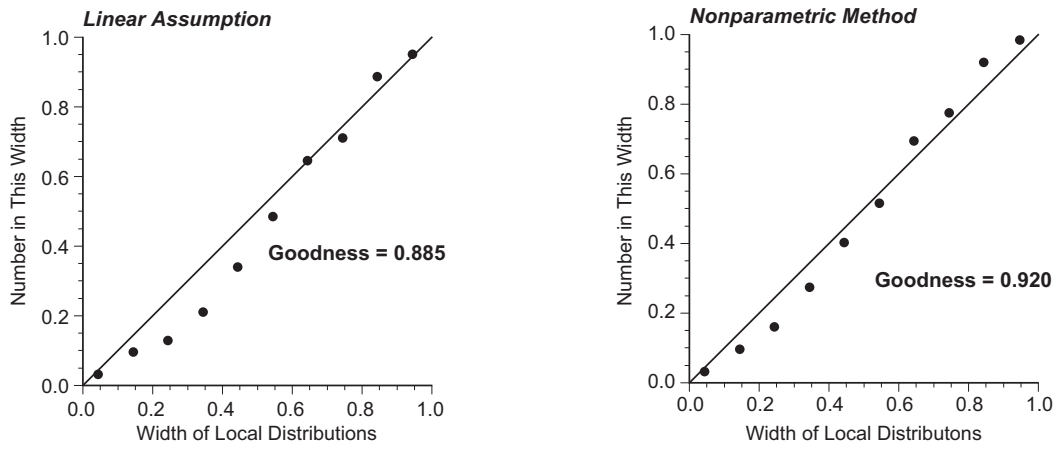

Figure 6.9: Accuracy plots for the estimates from the linear assumption and the nonparametric method.

Integrating more than two secondary variables is more challenging. Seismic amplitude data is added as another secondary variable. The modeling of the joint distribution is required in 3-D probability space. All three variables are transformed to normal units and denoted by Z, Y_1 and Y_2 for the primary permeability and secondary porosity and seismic amplitude. $f(z,y_1,y_2)$ are modeled based on the collocated samples and corrected by the marginal constraints. Figure 6.10 shows a 3-D visualization of trivariate pdf. Lower order marginal distributions are reproduced from the modeled $f(z,y_1,y_2)$. They all reasonably honor the experimental data scatter plots of Z versus Y_1 and Z versus Y_2. The secondary data pdf built from the exhaustive samples is almost exactly reproduced.

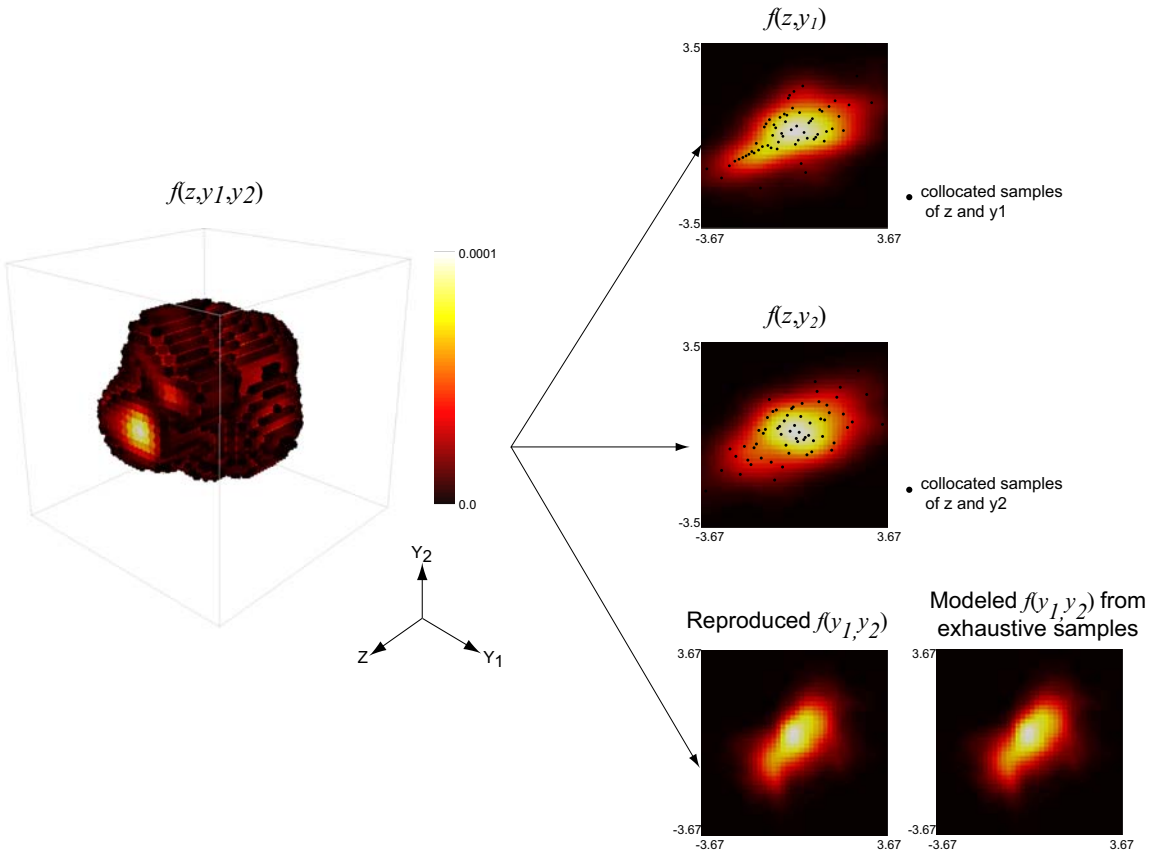

Figure 6.10: A trivariate pdf modeled by kernel density estimator with marginal correction process: the primary and two secondary variables are denoted as Z, Y_1 and Y_2, respectively. The lower order bivariate pdf reproduced from the trivariate pdf are checked with the input data scatter plots and distribution.

Figure 6.11 illustrates the estimates and estimation variances with respect to the conditioned secondary data Y_1 and Y_2. Upper row in the figure shows the estimates and the estimation variance from the linear assumption and the bottom row shows the estimates and estimation variance from the nonparametric approach. The estimates change in overall from low to high when the conditioned Y_1 and Y_2 change from low to high values because of positive correlation among variables. The effect of nonparametric approach is more obvious in the estimation variance as shown at the lower right in Figure 6.11. The linear assumption results in a constant estimation variance regardless of the conditioned secondary values Y_1 and Y_2. The nonparametric method generates the estimation variance that varies depending on the given secondary data values. The estimate and estimation variance over all locations $\mathbf{u} \in A$ are shown in Figure 6.12. The corresponding accuracy plot is shown in Figure 6.13 compared with the

accuracy plot from the linear assumption. The nonparametric method is once again marginally better than the conventional linear assumption method.

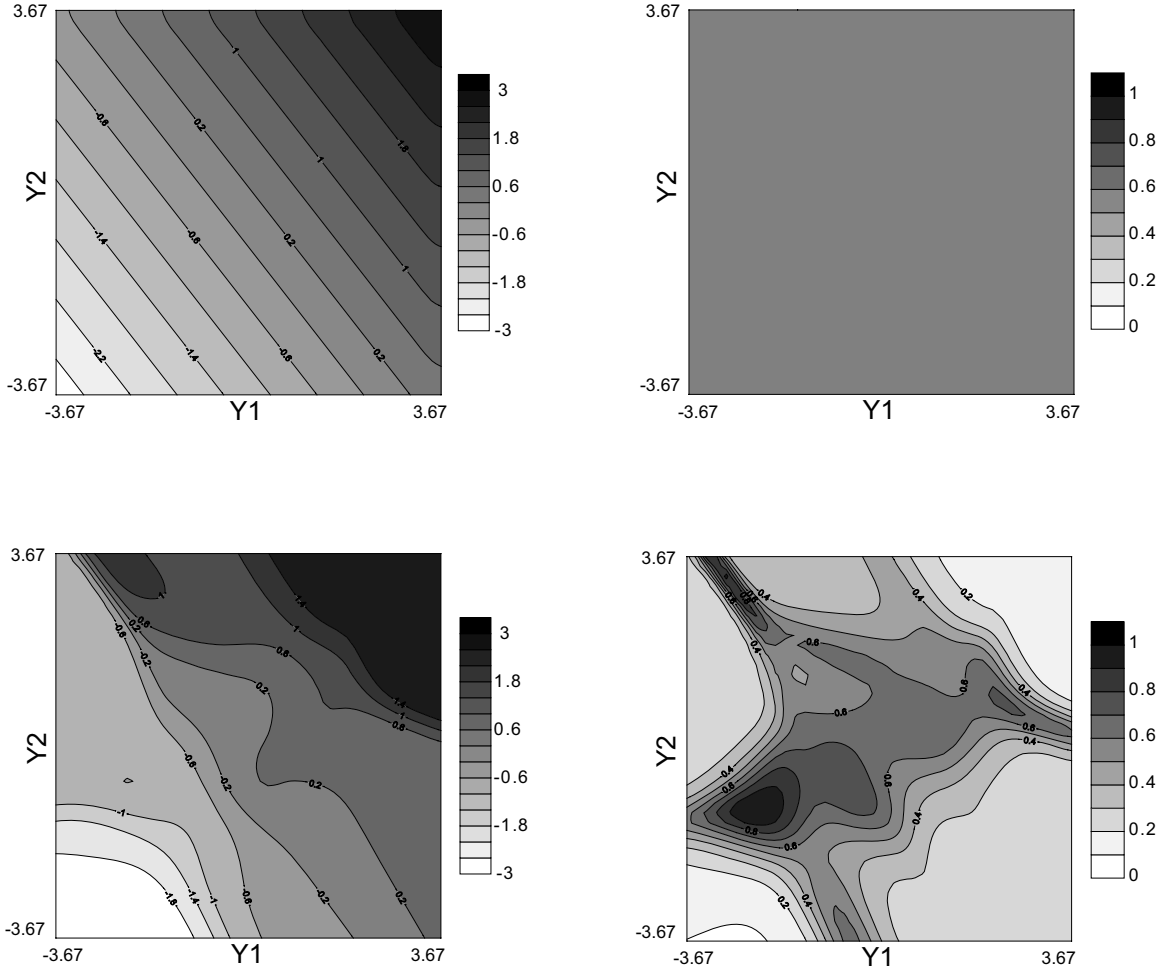

Figure 6.11: The estimates and estimation variances from two different methods. Upper low shows the estimates from the linear and nonparametric approach given the secondary data values Y_1 and Y_2. Bottom low shows the estimation variance. Nonlinearity in the estimates and estimation variances is obvious.

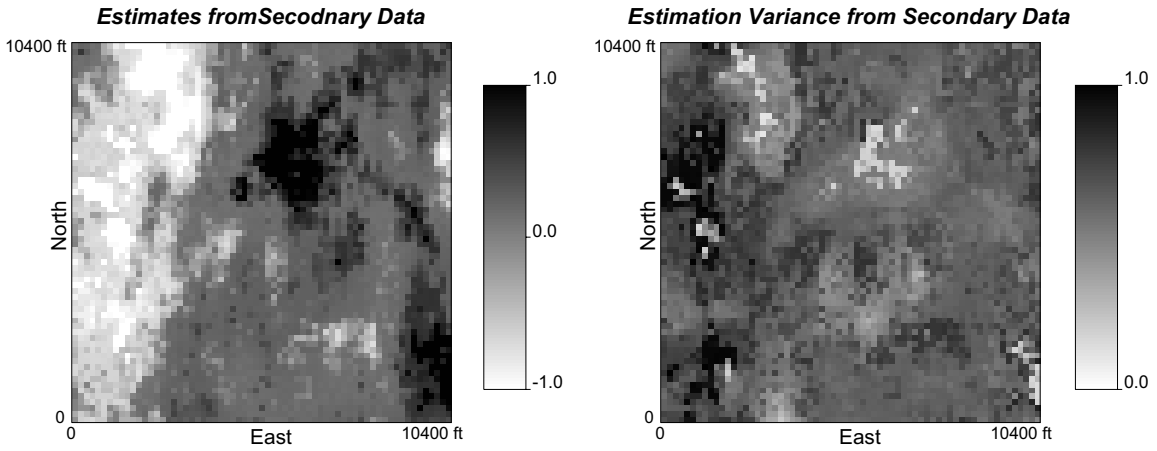

Figure 6.12: The estimates and estimation variances from integrating two secondary data using the nonparametric method for all locations $\mathbf{u} \in A$.

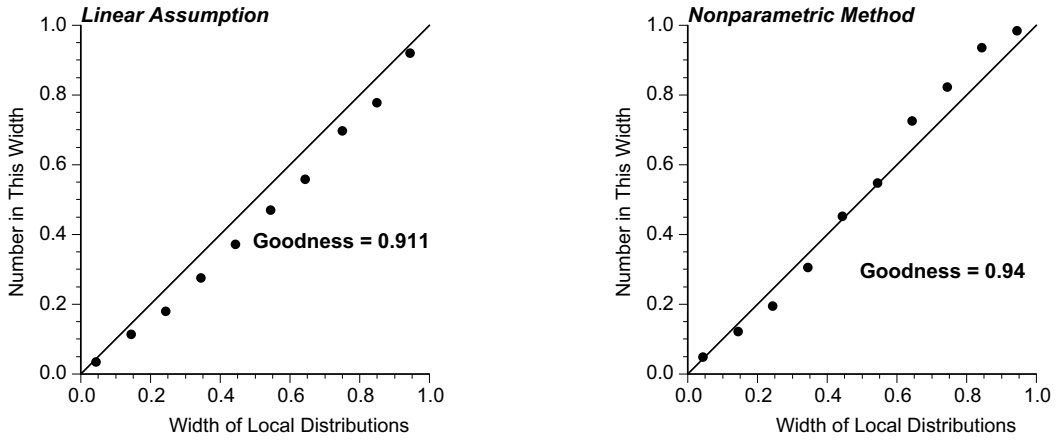

Figure 6.13: Accuracy plots for the results from the linear assumption (left) and nonparametric (right). Goodness statistics are shown on each plot.

Conditional Expectations and Variances

The conditional mean and variances of the primary variable are estimated using the extracted conditional distributions that are various in shapes and those estimates are different depending on the conditioning secondary values. If the variance of the random variable Z is finite then there is a theoretical relation between the conditional variance, conditional mean and global variance as following:

$$Var\{Z\} = Var\{E(Z \mid Y)\} + E\{Var(Z \mid Y)\}$$

which is known as the law of total variance stating that the total variability of the primary variable is sum of the variance of the conditional means and the average of the conditional variances (Billingsley, 1995). Another relation, known as the law of total expectation, is

$$E\{Z\} = E\{E(Z \mid Y)\}$$

These equations could be a way for evaluating the appropriateness of the modeled joint distribution because these theoretical relations are violated if the joint distribution is not a licit distribution.

6.2 Discussions

Bayesian updating has been widely adopted to integrate secondary data. The updating equation; however, is difficult to understand how information source is combined. New interpretation of Bayesian updating equation is introduced. Although the conventional and new expressions are mathematically equivalent, new forms have some advantages rather than old ones. New form of updating equation decomposes the posteriori pdf into the combination of elementary pdf related to the primary and secondary data and it can be clearly understood how different information source is combined.

The multivariate distribution modeling method is applied to account for the non-linear features among the primary and the secondary variables. Joint pdf is modeled in a nonparametric way and sequential marginal fitting algorithm refines the modeled joint pdf into the corrected joint pdf that meets all marginal constraints. The described marginal fitting algorithm directly accounts for the differences between empirical and reference marginal distributions. Given the joint pdf, the conditional pdf at a secondary value is extracted, and estimate and estimation variances are calculated using the extracted conditional pdf. The resulting estimation variance; thus, is not constant but locally varying which better reflects the relation of the primary and secondary variables.

The results are evaluated based on the described accuracy criteria and compared with the parametric method. In this particular example, the nonparametric method is marginally better than the parametric method.

Chapter 7

Summary and Conclusions

Inevitably, numerical reservoir models are uncertain because direct measurements are available at relatively few well locations relative to the size of the whole modeling area. With the limited amount of well data, large uncertainty exists in the spatial distribution of the primary variables being modeled. Supplementary information such as multiple seismic attributes and conceptual geologic data can aid in predicting the primary variables more accurately and realistically.

Incorporating all available data, however, is not an easy task because data are different measurements, exhibit nonlinear features, different precision and redundancy. For the problem of integrating diverse data, some previous studies adapted a Gaussian assumption so that the multivariate distribution of the given data is assumed multivariate Gaussian after univariate transformation. This type of parametric model is simple and easy to apply at the cost of not accounting for complex multivariate relations. Other previous studies are based on the combination of the univariate conditional probabilities that are calibrated individually. The essential part of such probability combination methods is to properly quantify the redundancy between the secondary data. Incorrectly quantified redundancy parameter makes the results biased leading to unfairly very high or low probabilities as demonstrated in Chapter 3. A new redundancy parameter calibration method is studied in Chapter 3 named as the Lamda model. The model calibrates the redundancy parameters from the differences between the known and the estimated values. Although the new model outperforms other combination models, the relation between data redundancy and the calibrated weights is not clearly understood.

The later part of the thesis, that is a key contribution of this work, is about the multivariate analysis framework to integrate available diverse data. The motivation for the developed

technique is that one can model the joint relation among the secondary data very reliably, and directly model the joint relation among the primary and the secondary data.

The methodology consists of two main parts. The first part is to model the multivariate distribution nonparametrically so that the complex multivariate features are reproduced. Nonparametric method allows the joint modeling of a mixture of continuous and discrete variables. By directly modeling the joint relations, data redundancy is directly accounted for. No explicit calibration is required. In reservoir modeling studies, the use of nonparametric density modeling is not new. Recent studies applied nonparametric techniques to integrate seismic data for the reservoir attribute modeling (Saggaf et al., 2000; Doyen, 2007). The work in this dissertation advanced the multivariate distribution modeling further. The second part of the developed multivariate analysis framework is to impose the known marginal distribution constraints. The modeled multivariate distribution is refined under the lower order distributions composed of the primary and the secondary data. The proposed iteration algorithm evaluates the marginal conditions and corrects the multivariate distribution. The correction procedure is done sequentially with respect to each of the primary and the secondary data distributions. The algorithm is proved to be converged to the correct distribution in Chapter 4 and is shown to be practically fast through particular examples in Chapter 5. The iteration is terminated when the stopping condition is met. Since the algorithm modifies the given joint distribution alternately using the marginals of the primary and the secondary, the averaged marginal error calculated at each iteration is used as a stopping rule. The first few iterations dropped the errors quickly. Finally, the obtained multivariate distribution accounts for the complex joint relations, data redundancy and meets all axioms of probability distribution functions.

As demonstrated in section 4.2, the marginal fitting procedure begins with the initial joint distribution that is modeled based on the collocated samples of primary and secondary data. Under few collocated samples which can happen to generate the wrong initial distribution, the resulting joint distribution after marginal fitting step will be far different from the underlying true distribution even it satisfies all of the necessary marginal conditions. This inconsistency case cannot be overcome by the proposed method.

Chapter 5 and 6 of this dissertation demonstrated several applications of the proposed methodology including integration of continuous secondary data for categorical variable modeling, integrating a mixture of continuous and categorical secondary data for categorical variable modeling, and integration of continuous secondary data for continuous variable modeling. The examples demonstrated that the proposed methodology is an effective method to integrate diverse data without distribution assumption and ad-hoc redundancy calibration.

Comparative study with other existing techniques was not performed. However, the results were evaluated based on the internal checking criteria and they all met the criteria satisfactorily.

Although the multivariate approach is robust and theoretically sound, the probability combination methods would be appealing in some applications. They are suitable for 3D trend modeling by combining lower order 1D vertical and 2D areal trends (Deutsch, 2002). Another application of the probability combining approach would be the case of non-isotopic sampling of the secondary data. An underlying assumption of the multivariate modeling approach is that all secondary variables are isotopically sampled over the entire domain of study. If different data have different spatial coverage, then the modeling of the joint relation and correcting of the multivariate distribution under marginal constraints may not be reliable. The probability combination approach may be more useful for that case.

Ideas for Future Work

Although the essential ideas of the new method are developed in this dissertation, several issues still remain. The following are some avenues for future research.

Nonparametric Modeling Methods

There are many nonparametric distribution modeling techniques available. Some techniques outperform the kernel method comprehensively implemented in this work. For example, the standard kernel density estimator is not an appropriate technique when applied to long-tailed or bounded distributions. The standard kernel estimator uses a fixed kernel bandwidth that may result in oversmoothing in areas of sparse samples and undersmoothing in the areas of abundant samples. An adaptive kernel method varies the kernel bandwidth locally based on the scarcity of samples used for the density modeling; kernel bandwidths increase with few samples and decrease with many samples.

Another nonparametric modeling technique is to use copular functions. Copula functions are joint distributions defined on the space of cumulative probabilities [0,1]. The copula approach transforms the samples of variables into the unit interval [0,1] and models the joint relation in [0,1] by analytically pre-defined copula functions. Because samples are uniquely mapped into the unit interval [0,1] and the joint relation is described in the unit space, binning of the variables is not required. Kernel density estimation requires binning the data. This procedure becomes computationally heavy if the number of bins is large with many variables. The copula method,

however, is a bin-free nonparametric modeling technique. Besides, some functions are parametrically defined to describe the joint relations. The possible drawback of the method would be a strong reliance of the joint distribution on the uniform marginal distribution. By keeping the marginal distribution uniform, the separability of possible outcomes of the primary variable is not possible in the joint distribution.

Variable Aggregation

The kernel density estimation is a heavy solution in terms of CPU and memory resources. The computational cost largely depends on the number of variables being integrated. For example, density estimation should be done at every B^m where B is the number of bins and m is the number of secondary data. In practice, the number of secondary data, m would be limited to 5 by ignoring irrelevant variables, merging highly relevant variables or both ignoring and merging. Data aggregation could be a pre-processing step before the multivariate analysis. In statistics, the principal component or factor analysis are widely used dimension reduction techniques. Super secondary variable concept based on the collocated cokriging merges the relevant variables by accounting for the redundancy among secondary variables and the closeness to the primary variable. No matter what aggregation methods are used, the purpose of variable aggregation is to reduce the number of secondary variables with the least loss of information in the original variables.

Bibliography

Almeida, A.S. and Journel, A.G. (1994) Joint simulation of multiple variables with a Markov-type coregionalization model. *Mathematical Geology*, 26:565-588.

Ballin, P.R., Journel, A.G. and Aziz, K.A. (1992) Prediction of uncertainty in reservoir performance forecasting. *Journal of Canadian Petroleum Technology*, 31:52-62.

Billingsley, P. (1995) *Probability and measure*: Wiley-Interscience.

Benediktsson, J.A. and Swain, P.H. (1992) Consensus theoretic classification methods. *IEEE Transactions on Systems, Man and Cybernetics*, 22:688-704.

Bishop, Y.M.M, Fienberg, S.E. and Holland, P.W. (1977) *Discrete multivariate analysis*. MIT Press

Bordley, R.F. (1982) A multiplicative formula for aggregating probability assessments. *Management Science*, 28:1137-1148.

Bourgault, G (1994) Robustness of Noise Filtering by Kriging Analysis. *Mathematical Geology*,26:733-752.

Bressan, M. and Vitria, J. (2003) Nonparametric discriminant analysis and nearest neighbor classification. *Pattern Recognition Letters*, 24:2743-2749.

Cacoullos, T. (1966) Estimation of a multivariate density. *Annals of the Institute of Statistical Mathematics*, 18:178-189.

Castro, S. (2005) *A probabilistic approach to jointly integrate 3D/4D seismic, production data and geological information for building reservoir models.* PhD thesis, Stanford University, Stanford, CA.

Castro, S., Caers, J., Otterlei, C., H∅ye, T., Andersen, T. and Gomel, P. (2005) A probabilistic integration of well log, geological information, 3D/4D seismic and production data: application to the Oseberg field, SPE 103152.

Carr, J.R. (1990) Application of Spatial Filter Theory to Kriging. *Mathematical Geology*, 22:1063-1079.

Caers, J. and Ma, X. (2002) Modeling conditional distributions of facies from seismic using neural nets. *Mathematical Geology*, 34:143-167.

Caers, J. and Zhang, T. (2004) Multiple-point geostatistics: A quantitative vehicle for integrating geologic analogues into multiple reservoir models. In *Integration of outcrop and modern analogues in reservoir modeling*: AAPG Memoir 80:383-394.

Chiles, J-P, Delfiner, P. (1999) *Geostatistics Modeling Spatial Uncertainty*, John Wiley & Sons.

Clemen, R.T. and Winkler, R.L. (1999) Combining probability distributions from experts in risk analysis. *Risk Analysis*, 19:187-203.

Coleou, T. (2002) Time-lapse filtering and improved repeatability with automatic factorial co-kriging (AFACK). Paper A-18, presented at the 64th EAGE Conference and Exhibition, Florence, 27–30 May.

Datta-Gupta, A., Lake, L.W. and Pope, G.A. (1995) Characterizing heterogeneous permeable media with spatial statistics and tracer data using sequential simulated annealing. *Mathematical Geology*, 27:763-787.

de Matos, M.C., Osorio, P.L.M. and Johann, P.R.S. (2007) Unsupervised seismic facies analysis using wavelet transform and self-organizing maps. *Geophysics*, 72:9-21.

Deming, W.E. and Stephan, F.F. (1940) On a least squares adjustment of a sampled frequency table when the expected marginal totals are known. *Annals of Mathematical Statistics*, 11:427-444.

Deutsch, C.V. (1996) Direct assessment of local accuracy and precisioin, *Geostatistics Wollongong 1996*, edited by Baafi, E., Kluwer Academic Publihsers.

Deutsch, C.V. and Journel, A.G. (1998) *GSLIB: Geostatistical Software Library and User's Guide*. Oxford University Press, New York.

Deutsch, C.V. (2002) *Geostatistical Reservoir Modeling*. Oxford University Press, New York.

Deutsch. C.V. (1999) A Short note on cross validation of facies simulation methods. In *Report 1, Centre for Computational Geostatistics*, Edmonton, AB, Canada.

Deutsch, C.V. (1992) *Annealing techniques applied to reservoir modeling and the integration of geological and engineering(well test) data*. PhD thesis, Stanford University, Stanford, CA.

Deutsch, C.V. and Hewett, T.A. (1996) Challenges in reservoir forecasting. *Mathematical Geology*, 28:829-842.

Deutsch, C.V., Srinivasan, S. and Mo, Y. (1996) Geostatistical reservoir modeling accounting for precision and scale of seismic data. SPE 36497.

Deutsch, C.V. (1996) Constrained smoothing of histograms and scatterplots with simulated annealing, *Technometrics*, 38:266-274.

Deutsch, C.V. and Zanon, S.D. (2004) Direct prediction of reservoir performance with Bayesian updating under a multivariate Gaussian model, Paper presented at the Petroleum Society's 5th Canadian International Petroleum Conference, Calgary, Alberta.

Doyen, P.M. (2007) *Seismic Reservoir Characterization An Earth Modeling Perspective*, EAGE Publications, Houten, Netherlands.

Doyen, P.M., den Boer, L.D. and Pillet, W.R. (1996) Seismic porosity mapping in the Ekofisk field using a new form of collocated cokriging. SPE 36498.

Dowd, P.A., Pardo-Iguzquiza, E. (2005) Estimating the boundary surface between geologic formations from 3D seismic data using neural networks and Geostatistics. *Geophysics*,70: P1-P11.

Dumay, J. and Fournier, F. (1988) Multivariate statistical analyses applied to seismic facies recognition. *Geophysics*, 53: 1151-1159.

Fournier, F. and Derain J-F (1995) A statistical methodology for deriving reservoir properties from seismic data. *Geophysics*, 60:1437-1450.

Friedman, N., Geiger, D. and Goldszmidt, M. (1997) Bayesian network classifiers. *Machine Learning*, 29:131-163.

Galli, A, Gerdil-Neuillet, F, Dadou, C (1983) Factorial kriging analysis: a substitute to spectral analysis of magnetic data. In *Geostatistics for Natural Resource Characterization*, edited by Verly, G., David, M., Journel, A.G. and Marechal, A., Riedel Publishers, Dordrecht.

Gomez-Hernandez, J. (1997) Issues on environmental risk assessment. *Geostatistics Wollongong 1996*, edited by Baafi, E.Y., Kluwer Academic Publishers.

Goovaerts, P. (1992) Factorial kriging analysis: a useful tool for exploring the structure of multivariate spatial soil information. *Journal of Soil Science*,43:597-619.

Goovaerts, P (1997) *Geostatistical for Natural Resources Evaluation*. Oxford University Press, New York.

Goovaerts, P. (1997) *Geostatistics for natural resources evaluation*. Oxford University press, New York.

Guardiano, F.B. and Srivastava, R.M. (1993) Multivariate geostatistics: beyond bivariate moments. *Geostatistics Troia 1992*, edited by Soares, A.

Hall, P., Sheather, S.J., Joines, M.C. and Marron, J.S. (1991) On optimal data-based bandwidth selection in kernel density estimation. *Biometrika*, 78:263-269.

Haldorsen, H.H. and Damsleth, E. (1990), Stochastic modeling. *Journal of Canadian Petroleum Technology*, 42:404-412.

Harris, J.M. and Langan, R.T. (1997) Crosswell seismic fills the gap in Geophysical Corner. *AAPG Explorer,* January.

Hong, S. and Deutsch, C.V. (2008) A short note: an alternative interpretation of Bayesian updating for non-stationary modeling, In *Report 10, Centre for Computational Geostatistics*, Edmonton, AB, Canada.

Hoffman, B. T., Wen, X-H, Strebelle, S., and Caers, J. (2005) Geologically consistent history matching of a deepwater turbidite reservoir, SPE 95557.

Isaaks, E.H. and Srivastava, R.M. (1989) *Introduction to Applied Geostatistics*. Oxford University Press, New York, USA.

Ireland, C.T. and Kullback, S. (1968) Contingency tables with given marginals, *Biometrika*, 55:179-188.

Izenman, A.J. (1991) Recent developments in nonparametric density estimation. *Journal of the American Statistical Association*, 86:205-224.

Jaquet, O (1989) Factorial Kriging Analysis Applied to Geological Data from Petroleum Exploration. *Mathematical Geology*,21: 683-691.

Journel, A.G. (1999) Markov models for cross-covariances. *Mathematical Geology*, 31:955-964.

Journel, A.G. and Alabert, F. (1989) Non-Gaussian data expansion in the earth sciences. *Terra Nova*, 1:123-134.

Journel, A.G. and Huijbregts, Ch.J. (1978) *Mining Geostatistics*. Academic Press, London.

Journel, A.G. (2002) Combining knowledge from diverse sources: an alternative to traditional data independence hypotheses. *Mathematical Geology*, 34:573-596.

John, A.K., Lake, L.W., Torres-Verdin, C. and Srinivasa, S. (2008) Seismic facies identification and classification using simple statistics. *SPE Reservoir Evaluation & Engineering*, 11:984-990.

Johnson, R.A. and Wichern, D.W. (2002) *Applied to Multivariate Statistical Analysis*. Prentice Hall, New Jersey.

Krzanowski, W.J. (1993) The location model for mixtures of categorical and continuous variables. *Journal of Classification*, 10:25-49.

Krishnan, S. (2008) The tau model for data redundancy and information combination in earth sciences: theory and application. *Mathematical Geosciences*, 40:705-727.

Krishnan, S. (2004) *Combining diverse and partially redundant information in the earth sciences.* PhD dissertation, Stanford University, Stanford, CA.

Krishnan, S., Boucher, A. and Journel, A.G. (2005) Evaluating information redundancy through the tau model. *Geostatistics Banff 2004*, edited by Leuangthong and Deutsch, Springer, Dordrecht, Netherlands, 1037-1046.

Kullback, S. and Leibler, R.A. (1951) On information and sufficiency, *Annals of Mathematical Statistics*, 22:79-86.

Kupfersberger, H, Deutsch, C.V. and Journel, A.G. (1998) Deriving constraints on small-scale variograms due to variograms of large-scale data. *Mathematical Geology*, 30:837-852.

Li, Q. and Racine, J. (2003) Nonparametric estimation of distributions with categorical and continuous data. *Journal of Multivariate Analysis*, 86:266-292.

Lee, T., Richards, J.A. and Swain, P.H. (1987) Probabilistic end evidential approaches for multisource data analysis. *IEEE Transactions on Geosciences and Remote Sensing*, GE-25:283-293

Liu, Y., Harding, A., Gilbert, R. and Journel, A.G. (2004) A work flow for multiple-point geostatistical simulation. *Geostatistics Banff 2004*. edited by Leuangthong, O. and Deutsch, C.V., Springer, Dordrecht, Netherlands, 245-254.

Lumley, D.E., Behrens, R.A., and Wang, Z. (1997) Assessing the technical risk of a 4-D seismic project. *The Leading Edge*, 16:1287-1291.

Marron, J.S. (1987) A comparison of cross –validation techniques in density estimation. *Annals of Statistics*, 15:152-162.

Mukerji, T., Jorstad, A., Avseth, P., Mavko, G. and Granli, J.R. (2001a) Mapping lithofacies and pore-fluid probabilities in a North Sea reservoir: seismic inversions and statistical rock physics. *Geophysics*, 66:988-1001.

Neufeld, C. and Deutsch, C.V. (2004) Incorporating secondary data in the prediction of reservoir properties using Bayesian updating. In *Report 6, Centre for Computational Geostatistics*, Edmonton, AB, Canada.

Nelson, R.B. (2006) *An introduction to copulas*. New York, Springer.

Parzen, E. (1962) On the estimation of a probability density function and the mode. *Annals of Mathematical Statistics*, 33:1065-1076.

Park, B.U. and Marron, J.S. (1990) Comparison of data-driven bandwidth selectors. *Journal of the American Statistical Association*, 85:66-72.

Pearl, J. (1988) *Probabilistic reasoning in intelligent systems: networks of plausible inference (representation and reasoning)*. Morgan Kaufmann Publisher, San Francisco.

Polyakova, E.I. and Journel, A.G. (2007) The nu expression for probabilistic data integration. *Mathematical Geology*, 39:715-733.

Pyrcz, M.J., Gringarten, E., Frykman, P. and Deutsch, C.V. (2006) Representative input parameters for geostatistical simulation. edited by Coburn, T.C., Yarus, R.J. and Chambers, R.L., *Stochastic Modeling and Geostatistics: Principles, Methods and Case Studies*, Vol. II: 123-137.

Rosenblatt, M. (1956) Remarks on some nonparametric estimates of a density function. *Annals of Mathematical Statistics*, 27:832-837.

Roberts, S.J. (1996) Parametric and non-parametric unsupervised cluster analysis, *Pattern Recognition*,30:261-272.

Saggaf, M.M. and Robinson, E.A. (2003) Estimation of reservoir properties from seismic data by smooth neural networks. *Geophysics*, 68:1969-1983.

Saggaf ,M.M., Toksoz, M.N. and Marhoon, M.I. (2003) Seismic facies classification and identification by competitive neural networks. *Geophysics*, 68:1984-1999.

Scott, D.W. (1992) *Multivariate Density Estimation: Theory, Practice, and Visualization*. John Wiley and Sons, Inc., New York.

Silverman, B.W. (1986) Density Estimation for Statistics and Data Analysis, Chapman and Hall, London.

Srivastava, R.M. (1987) Minimum variance or maximum profitability?, *CIM Bulletin*, 80:63-68.

Stain, S.R., Baggerly, K.A. and Scott, D.W. (1994) Cross-validation of multivariate densities. *Journal of the American Statistical Association*, 89:807-817.

Strebelle, S. (2002) Conditional simulation of complex geological structures using multi-point statistics. *Mathematical Geology*, 34:1-21.

Verly, G. (1983) The Multigaussian approach and its applications to the estimation of local reserves. *Mathematical Geology*, 15:259-286.

Wackernagel, H. (2003) *Multivariate Geostatistics*. Springer, Berlin.

Wand, M.P. and Jones, M.C. (1993) Comparison of smoothing parameterizations in bivariate kernel density estimation. *Journal of the American Statistical Association*, 88:520-528.

Wen, X.H., Deutsch, C.V., Cullick, A.S. (2002) Construction of Geostatistical aquifer models integrating dynamic flow and tracer data using inverse technique. *Journal of Hydrology*, 255:151-168.

Winkler, R.L. (1981) Combining probability distributions from dependent information sources. *Management Science*, 27:479-488.

Xu,W., Tran, T.T., Srivastava, R.M. and Journel, A.G. (1992) Integrating seismic data in reservoir modeling: the collocated cokriging alternative. SPE 24742, Washington, DC, October 4-7, 1992.

Yao, T, Mukerji, T, Journel, A.G., Mavko, G. (1999) Scale Matching with Factorial Kriging for Improved Porosity Estimation from Seismic Data. *Mathematical Geology*,31: 23-46.

A Symbols and Selected Terms

$\boldsymbol{A}$	The area of modeling
B	Number of bins for the nonparametric modeling
BU	Bayesian updating
CI	Conditional independence
$(D_1,...,D_m)$	Generic notation for m secondary data
E-type	The expected values calculated from the multiple realizations
FK	Factorial kriging
$f(s,\boldsymbol{y})$	Joint distribution of the primary variable s and soft secondary variable $\boldsymbol{y}$
$f^{(0)}$	The modeled joint distribution without marginal correction
$f^{(k)}$	The modeled joint distribution with marginal correction at k^{th} iteration step
γ(h)	Variogram of distance h
h_i	Kernel bandwidth for the variable i
$i^{**}(\mathbf{u};s)$	Indicator estimate using the primary and secondary data at **u**\
KDE	Kernel density estimation
K	The number of facies
MDE	Multivariate density estimation
MISE	Mean integrated square errors
n	Number of well samples
OFK	Ordinary factorial kriging
PCS	Probability combination schemes
$p(s)$	Global proportion of categorical variable s=1,…,K
p^{sec}	Secondary data derived probability
PR	Permanence of Ratios
p_{CI}	The conditional probability from the CI model
p_{PR}	The conditional probability from the PR model
$p_{Lamda\ 1}$	The conditional probability from the Lamda model with calibration method 1
$p_{Lamda\ 2}$	The conditional probability from the Lamda model with calibration method 2

p_{Tau}	The conditional probability from the Tau model
s	Random variable representing discrete facies
SFK	Simple factorial kriging
SISIM	Sequential Indicator Simulation
SGSIM	Sequential Gaussian Simulation
SMF	Sequential Marginal Fitting
NTG	Net-to-gross
$W(\cdot)$	Univariate kernel function
$(y_1,\ldots,y_m)$	Continuous secondary variable
$Z_s(\mathbf{u})$, $\sigma_s(\mathbf{u})$	Estimate and estimation variance of the primary variable derived from the secondary data at **u**
$Z_p(\mathbf{u})$, $\sigma_p(\mathbf{u})$	Estimate and estimation variance of the primary variable derived from the primary data at **u**

Appendix A

Factorial Kriging for Reservoir Feature Identification and Extraction

Kriging aims to estimate a regionalized variable at an unsampled location (Journel and Huijbregts, 1978; Deutsch and Journel, 1998). To apply the kriging algorithm the spatial structures should be modeled with the variogram or covariance. When dealing with nested variogram or covariance structures it may be of interest to extract specific structures such as isotropic short range feature, anisotropic long range feature or nugget effect. Such filtering that excludes undesired features and enhances interesting features can be achieved by factorial kriging (Carr, 1990; Goovaerts, 1997; Deutsch and Journel, 1998). The number of sub-features and the magnitude of that features are chosen from the modeled nested variogram. The effectiveness of factorial kriging in filtering undesired features and in enhancing target features has been discussed in previous works. Goovaerts (1992) applied factorial kriging into the analysis of multivariate spatial soil data. Noise filtering inherent in exploration geologic data and its robustness irrespective of additive or multiplicative noise type are discussed in Bourgault (1994). Application of factorial kriging to well data and seismic data is investigated in Jaquet (1989), Tao et al. (1999), and Dowd and Pardo-Iguzquiza (2005). Coleou (2002) presented the applicability of factorial cokriging to 4-D seismic data. Coleou (2002) showed that common spatial features between seismic surveys acquired at time t_0 and t_1 can be extracted by cross variogram modeling of those seismic data. Previous works discussed above demonstrated powerful capability of factorial kriging to decompose spatial features according to the scale and filter out the random noise.

A case study will show how factorial kriging is applied to identify and enhance target features. Conventional factorial kriging is considered first based on ordinary kriging that amounts to locally estimate the mean of $Z(\mathbf{u})$ within each search; the mean of each factor is assumed to be zero. Each factor is extracted using ordinary factorial kriging and the results are

discussed. Some drawbacks of the method are observed. Simple kriging concept is applied to the conventional factorial kriging, which is called simple factorial kriging in this appendix. We observed the significant difference from conventional ordinary factorial kriging. Factorial kriging has smoothing effect so as simple kriging. Simple factorial kriging was also applied to filter the noise inherent in many secondary datasets. The nugget effect due to measurement errors can be removed. Factorial kriging can filter out any unwanted structure that has been included in the variogram model.

Another application of factorial kriging is to integrate only relevant features extracted from original data. In some cases, the large scale features are more important than local variability. In this case, large scale features are extracted from secondary data using factorial kriging, then cokriging is used to estimate the primary variable with hard data and the large scale factor. The applicability of the method is tested using synthetic and real data and the results are discussed.

A.1 Linear Model of Regionalization

Factorial kriging analysis is a geostatistical method relying on the assumption that a regionalized phenomenon can be seen as a linear sum of varied independent sub-phenomena playing at different scales and each sub-phenomena presents its own spatial feature captured on variogram or covariance model. These linearly summed variogram or covariance comprise the variogram or covariance of the regionalized phenomenon.

The choice of a variogram model and its fitting must be validated by geologic and geophysical understanding of the phenomenon under study such as directions of anisotropy, measurement errors or artifacts, and the number of nested structure. From the experimental variogram of a regionalized variable, these key parameters are fitted to build a permissible variogram model that captures the spatial features of the attribute under study and adding geologic background knowledge may lead to a more robust model.

Factorial kriging analysis allows different components corresponding to these spatial features (also called factors hence the name factorial kriging) to be estimated. If factors act at different scales and they are apparent in the variogram model, then these factors can be decomposed by factorial kriging.

Figure A.1 shows the spatial components at different scales and their corresponding variograms: nugget, small scale isotropic and large scale anisotropic factors are simulated. By the linear model of regionalization, each factors are summed to make the primary attribute that is of interest by traditional kriging. The goal of factorial kriging is to decompose the primary attribute

to derive each factor, e.g., nugget, small and large scale factor in this example, that consists of the primary attribute, which can be interpreted as that factorial kriging performs from the parameterization to the spatial domain in Figure A.1. In theory, factorial kriging analysis is purely relying the input variogram regardless of the reasonableness of variogram, and the technique cannot incorporate any geological understanding under study. Thus, variogram modeling (this is noted as parameterization in Figure A.1) is very critical to the estimate of factors and one should revisit the variogram modeling if the estimated factor does not seem to be reasonable in terms of geologic interpretation.

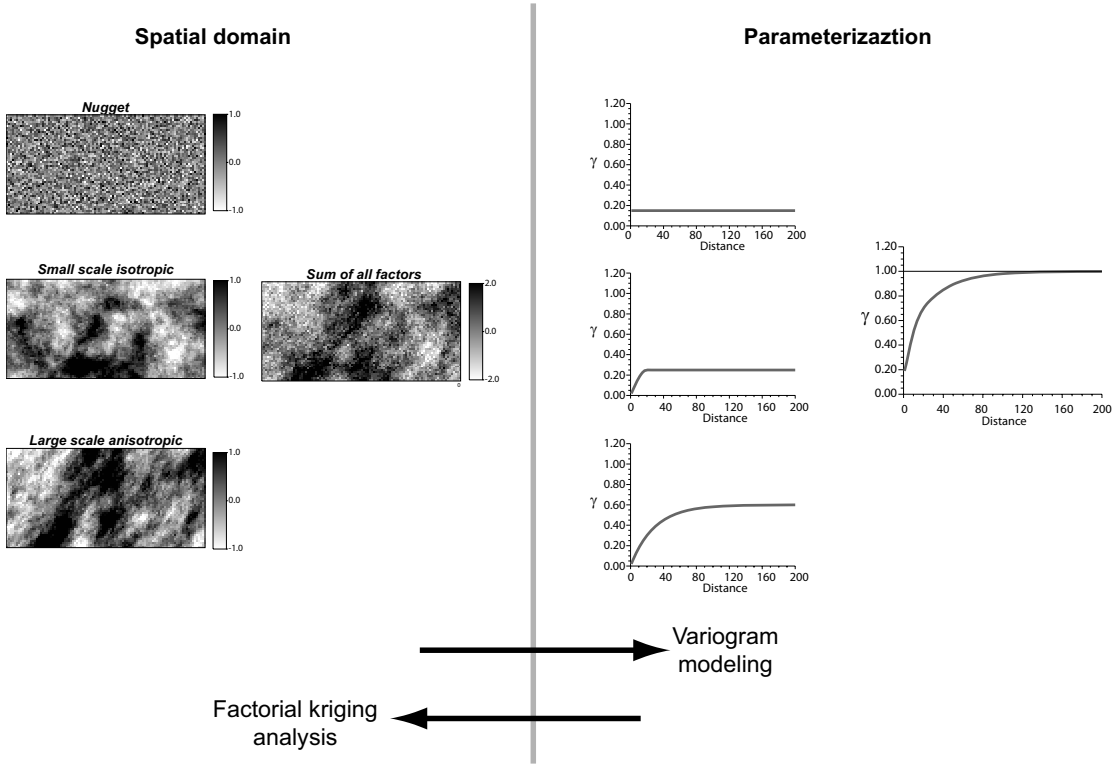

Figure A.1: This figure describes the spatial components at different scales and variograms corresponding to each component. Sub-phenomena depending on different scales are parameterized in the variogram with different contribution. The goal of factorial kriging is to estimate each sub-phenomena or factors from the modeled variogram of the primary attribute.

A.2 Factorial Kriging

A regionalized variable $Z(\mathbf{u})$ may be written as a sum of independent factors and a mean:

$$Z(\mathbf{u}) = \sum_{l=0}^{L} Z_l(\mathbf{u}) + m(\mathbf{u}) = \sum_{l=0}^{L} a_l Y_l(\mathbf{u}) + m(\mathbf{u}) \qquad \text{(A.1)}$$

The ($L+1$) standard factors $Z_l(\mathbf{u}) = a_l Y_l(\mathbf{u})$ all have a mean of 0 and a variance of 1. The a_l parameters are stationary, that is, they do not depend on location. The mean and variance of the $Z(\mathbf{u})$ variable are given by:

$$E\{Z(\mathbf{u})\} = E\left\{\sum_{l=0}^{L} a_l Y_l(\mathbf{u}) + m(\mathbf{u})\right\} = \sum_{l=0}^{L} a_l E\{Y_l(\mathbf{u})\} + m(\mathbf{u}) = m(\mathbf{u}) \tag{A.2}$$

$$Var\{Z(\mathbf{u})\} = \sum_{l=0}^{L} a_l^2 Var\{Y_l(\mathbf{u})\} + 0 = \sum_{l=0}^{L} a_l^2 \tag{A.3}$$

The variance of $Z(\mathbf{u})$ follows such a simple expression because $m(\mathbf{u})$ is a constant and the $Y(\mathbf{u})$ factors are standard and independent. These characteristics of m and Y also lead to a straightforward expression for the variogram of the $Z(\mathbf{u})$ variable:

$$\gamma(\mathbf{h}) = \sum_{l=0}^{L} a_l^2 \gamma_l(\mathbf{h}) \tag{A.4}$$

The $Z(\mathbf{u})$ regionalized variable is fully specified by $m(\mathbf{u})$, the ($L+1$) a_l values, and the $L+1$ variograms $\gamma_l(\mathbf{h})$. The a_l^2 parameters are the magnitude of each nested structure. One has access to the original data values $Z(\mathbf{u})$ at sample locations and the modeled variogram. One does not directly sample the a_l parameters that specify the importance of each factor. Moreover, the measurements of the $Y_l(\mathbf{u})$ factors are not available. The factors are distinguishable only when the constituent variograms $\gamma_l(\mathbf{h})$ are different from one another. The reasonableness of factorial kriging depends entirely on the fitted nested structures.

A.2.1 Ordinary Factorial Kriging (OFK)

Assume that the variable $Z(\mathbf{u})$ consists of factors $Z_l(\mathbf{u})$ and locally unknown mean values $m(\mathbf{u})$. Consider the problem of estimating the spatial component $Z_l(\mathbf{u})$ of the decomposition. The OK estimator of the spatial component is:

$$Z_l^*(\mathbf{u}) = \sum_{\alpha=1}^{n} \lambda_{\alpha,l} Z(\mathbf{u}_\alpha), \quad l = 0,...,L \tag{A.5}$$

$$m^*(\mathbf{u}) = \sum_{\alpha=1}^{n} \lambda_{\alpha,m} Z(\mathbf{u}_\alpha) \tag{A.6}$$

The weights are location dependent, but the ($\mathbf{u}$) has been dropped for clear notation. $\lambda_{\alpha,l}$ and $\lambda_{\alpha,m}$ are the weights for the estimation of l and mean factor. It is noted that $Z_l^*(\mathbf{u})$ is an l factor

estimate using original data $Z(\mathbf{u}_\alpha)$, which contains (L+1) factors, but unknown and only the weights are different being associated with l factor. The constraints on the weights are established to ensure the unbiasedness:

$$\sum_{\alpha=1}^{n}\lambda_{\alpha,m}=1 \text{ and } \sum_{\alpha=1}^{n}\lambda_{\alpha,l}=0 \tag{A.7}$$

$$\left(\text{since, } E\{Z_l^*(\mathbf{u})-Z_l(\mathbf{u})\}=\sum_{\alpha=1}^{n}\lambda_{\alpha,l}E\{Z(\mathbf{u}_\alpha)\}-0=\sum_{\alpha=1}^{n}\lambda_{\alpha,l}m(\mathbf{u})=0\right)$$

The error variance of the estimate of the l factor is expressed as double linear sum being similar to the derivation of kriging equation

$$\begin{aligned}\sigma^2_{error,l}(\mathbf{u}) &= Var\{Z_l^*(\mathbf{u})\}+Var\{Z_l(\mathbf{u})\}-2Cov\{Z_l^*(\mathbf{u}),Z_l(\mathbf{u})\}\\ &=\sum_{\alpha=1}^{n}\sum_{\beta=1}^{n}\lambda_{\alpha,l}\lambda_{\beta,l}C(\mathbf{u}_\alpha-\mathbf{u}_\beta)+C_l(0)-2\sum_{\alpha=1}^{n}\lambda_{\alpha,l}Cov\{Z(\mathbf{u}_\alpha),Z_l(\mathbf{u})\}\end{aligned} \tag{A.8}$$

The last term $Cov\{Z(\mathbf{u}_\alpha),Z_l(\mathbf{u})\}$ is reduced as,

$$Cov\{Z(\mathbf{u}_\alpha),Z_l(\mathbf{u})\}=C_l(\mathbf{u}-\mathbf{u}_\alpha) \tag{A.9}$$

Since the l factors, l = 0,…,L, are independent each other and since covariance can be shown as summing up of all factor covariance such as,

$$Cov\{Z(\mathbf{u}_\alpha),Z_l(\mathbf{u})\}=\sum_{l'=0}^{L}Cov\{Z_{l'}(\mathbf{u}_\alpha),Z_l(\mathbf{u})\} \tag{A.10}$$

$$\text{and } Cov\{Z_{l'}(\mathbf{u}_\alpha),Z_l(\mathbf{u})\}=\begin{cases}0, & \text{if } l'\neq l\\ C_l(\mathbf{u}-\mathbf{u}_\alpha), & \text{otherwise}\end{cases} \tag{A.11}$$

The weights associated with the factors (L+1 and mean factor) are obtained by minimizing the error variance under the unbiasedness constraint:

$$\begin{cases}\sum_{\beta=1}^{n}\lambda_{\beta,l}C(\mathbf{u}_\alpha-\mathbf{u}_\beta)+\mu_l=C_l(\mathbf{u}-\mathbf{u}_\alpha) \quad \sum_{\beta=1}^{n}\lambda_{\beta,l}=0, \quad l=0,...,L, \text{ and } \alpha=1,...,n\\ \sum_{\beta=1}^{n}\lambda_{\beta,m}C(\mathbf{u}_\alpha-\mathbf{u}_\beta)+\mu_m=0 \quad \sum_{\beta=1}^{n}\lambda_{\beta,m}=1, \quad \alpha=1,...,n\end{cases} \tag{A.12}$$

There are two interesting things to note. The ordinary factorial kriging system is very similar to the ordinary kriging system except the right hand side covariance terms. The left hand side (data-to-data covariance) does not change but the right hand side (data-to-estimation covariance) considers only the corresponding l^{th} covariance term. The resulting weights $\lambda_{\alpha,l}$, $\alpha = 1,\ldots,n$ and $l = 0,\ldots,L$ are interpreted as how the contribution of the l^{th} factor in the data value $Z(\mathbf{u}_\alpha)$. The other feature is that the estimated component $Z_l^*(\mathbf{u})$ with constraint $\sum_{\beta=1}^{n}\lambda_{\beta,l} = 0$ has too small variance that results in excessive smoothness, that is, $var\{Z_l^*(\mathbf{u})\} << var\{Z_l(\mathbf{u})\}$. Traditional factorial kriging constrains the sum of kriging weights associated with each factor to be zero, which removes the influence of the conditioning data. This will undermine the usefulness of the results for interpretation. For example, the large scale feature in the estimated large scale component using ordinary FK is less significant because the large scale feature is diluted in the estimated mean component (see examples in section A.3)

A.2.2 Simple Factorial Kriging (SFK)

Many previous works have used factorial kriging to extract specific features or to filter noise; however, most of the works were based on ordinary factorial kriging that addresses unknown mean. Factorial kriging with a stationary mean is proposed in this Appendix. This conforms to a simple kriging paradigm. Simple factorial kriging equations with no constraints minimize the error variance:

$$\begin{cases} \sum_{\beta=1}^{n}\lambda_{\beta,l}C(\mathbf{u}_\alpha - \mathbf{u}_\beta) = C_l(\mathbf{u} - \mathbf{u}_\alpha) \\ \alpha = 1,...,n \text{ and } l = 0,...L \end{cases} \tag{A.13}$$

There are no Lagrange parameters in the simple factorial kriging. The simple factorial kriging system of equations is similar to simple kriging equations except the right hand side. The simple kriging weights λ^{SK} are equivalent to the sum of the factorial simple kriging weights at the same location. Let us see the systems of simple kriging equations,

$$\sum_{\beta=1}^{n}\lambda_\beta^{SK}C(\mathbf{u}_\alpha - \mathbf{u}_\beta) = C(\mathbf{u} - \mathbf{u}_\alpha), \quad \alpha = 1,...,n \tag{A.14}$$

The right-hand-side can be decomposed into $l = 0,\ldots,L$, factors based on the linear model of regionalization,

$$C(\mathbf{u}-\mathbf{u}_\alpha)=\sum_{l=0}^{L} C_l(\mathbf{u}-\mathbf{u}_\alpha) \tag{A.15}$$

$$\sum_{\beta=1}^{n}\lambda_\beta^{SK}C(\mathbf{u}_\alpha-\mathbf{u}_\beta)=\sum_{l=0}^{L} C_l(\mathbf{u}-\mathbf{u}_\alpha)=\sum_{l=0}^{L}\sum_{\beta=1}^{n}\lambda_{\beta,l}C_l(\mathbf{u}_\alpha-\mathbf{u}_\beta) \tag{A.16}$$

since simple factorial kriging $\sum_{\beta=1}^{n}\lambda_{\beta,l}C(\mathbf{u}_\alpha-\mathbf{u}_\beta)=C_l(\mathbf{u}-\mathbf{u}_\alpha)$.

Thus, we have the following equality,

$$\sum_{l=0}^{L}\lambda_{\beta,l}=\lambda_\beta^{SK}, \qquad \beta=1,...,n \tag{A.17}$$

that shows simple kriging estimation $Z^{SK}(\mathbf{u})$ is equal to the sum of simple factorial estimate with the stationary mean m as follows:

$$Z^{SK}(\mathbf{u})=m+\sum_{l=0}^{L} Z_l^*(\mathbf{u}) \tag{A.18}$$

A.2.3 Local Search Area

One might point out that the long range feature can be detected if the local search area is extended enough to capture long range features. As discussed in Chiles and Delfiner (1999) it is reasonable that different size of neighborhood should be chosen for extracting different scales of spatial features. Galli et. al (1983) performed sensitivity analysis of the different number of conditioning data on the estimated factors and showed that even if short range factor is not sensitive to the conditioning data number, long range factor is affected by the increase in the number of nearby data. Most kriging and simulation algorithms; however, consider a limited number of nearby conditioning data because of the following reasons (Deutsch and Journel, 1998); CPU time required to solve a kriging system increases as the number of data cubed and the storage requirements for the main kriging matrix increases as the number of data squared. Even if computer can handle the large system of kriging equations, local search neighborhoods should be considered since adopting a global search would require knowledge of the covariance for the largest separation distance between the data which is typically poorly known. The covariance

values become more unstable beyond one half or one third of the field size. For these reasons, limited search neighborhoods are normally adopted for kriging, and consequently for factorial kriging.

A.2.4 Geostatistical Filtering Applied to Exhaustive Data

Random noise in exhaustive seismic data has no spatial correlation and obscures reservoir features. There are several kinds of noise depending on the source, but all can be placed in two categories; source-generated and ambient noise. Source-generated noise can take many forms, from surface waves to multiples to direct arrivals and head waves. A typical cyclic noise appears in the 2-D or 3-D seismic data in form of repeated stripes due to designing of repeated seismic survey. Ambient noise can be caused artificially or naturally such as man-made noise, animal, air currents, nearby power lines. This undesirable noise should be removed to enhance the original signal and identify intrinsic reservoir features.

As shown in the kriging system of equations, factorial kriging filters out the designated structures. Long scale structures are removed when short range covariances are used in the right hand side of the kriging equations and short scale structures are removed when long range covariances are used. The nugget effect is treated as a very short distance structure. The nugget effect is partly due to measurement errors; therefore, it might be better to filter out the nugget effect. Let us assume there are three factors noted as $l = 0, 1, 2$. 0^{th} factor is usually considered as nugget effect that is to be removed. The filtered seismic map is achieved by the following factorial kriging system of equations:

$$\sum_{\beta=1}^{n} \lambda_{\beta,l=1 \text{ and } 2} C(\mathbf{u}_\alpha - \mathbf{u}_\beta) = C_{l=1}(\mathbf{u} - \mathbf{u}_\alpha) + C_{l=2}(\mathbf{u} - \mathbf{u}_\alpha), \alpha = 1, ..., n \tag{A.19}$$

$$Z_{Filtered}(\mathbf{u}) = \sum_{\alpha=1}^{n} \lambda_{\alpha,l=1 \text{ and } 2} Z(\mathbf{u}_\alpha) \tag{A.20}$$

Geostatistical filtering applied to exhaustive data such as seismic data is represented in the following.

A.2.5 Integrating Spatial Components

One application of factorial kriging is data integration with more relevant features. The key idea is to filter out noise and artifacts in the secondary data and extract relevant features or factors. Factorial kriging of primary variables is then performed using relevant factors extracted from

secondary data. For example, large scale features are often more important than locally variable features. In this case, large scale features are extracted from the secondary data using simple factorial kriging. The extracted secondary features are then used as a secondary data in order to estimate primary variable, that is:

$$Z_l^*(\mathbf{u}) = \sum_{\alpha=1}^{n} \lambda_{\alpha,l} Z(\mathbf{u}_\alpha) + \nu_l Y_l(\mathbf{u}) \tag{A.21}$$

where $Z_l^*(\mathbf{u})$ is an estimated primary variable for the l factor. $\lambda_{\alpha,l}$ are the weights assigned for data samples to estimate l factor. $Y_l(\mathbf{u})$ is the extracted relevant secondary factor at collocation $\mathbf{u}$. ν_l is the weight assigned for secondary factor $Y_l(\mathbf{u})$ at estimation location $\mathbf{u}$.

This method may be called factorial collocated cokriging since the only collocated secondary factor is retained to estimate. The weights are obtained by solving collocated cokriging equations for l factor.

$$\begin{cases} \sum_{\beta=1}^{n_1} \lambda_{\beta,l}(\mathbf{u}) C_{ZZ}(\mathbf{u}_\alpha - \mathbf{u}_\beta) + \nu_l C_{ZY_l}(\mathbf{u}_\alpha - \mathbf{u}) = C_{ZZ}^l(\mathbf{u}_\alpha - \mathbf{u}), \ \alpha = 1,...,n \\ \sum_{\beta=1}^{n_1} \lambda_{\beta,l}(\mathbf{u}) C_{Y_l Z}(\mathbf{u} - \mathbf{u}_\beta) + \nu_l C_{Y_l Y_l}(0) = C_{Y_l Z}(0) \end{cases} \tag{A.22}$$

where Y_l is the extracted l^{th} component from the secondary data.

A.3 Experimental Results

To illustrate the usefulness of factorial kriging, synthetic data and real data are tested. The first example is a synthetic regular grid data. Synthetic 256×256 2-D Gaussian variables are simulated with a small nugget effect (10%) and two isotropic spherical structures equally explaining the remaining 90% of the variability. Simulated values have stationary zero mean and unit variance. The ranges of the spherical structures are 16 and 64 units. Data were sampled from the reference grid at a very close 5×5 spacing to produce sample data so that total 2601 data were stored. The modeled variogram for generating Gaussian variables is used as the fitted variogram using regular sample data. The reference grid, sample data and used variogram are shown on Figure A.2. No obvious anisotropic spatial features are observed in the reference map.

Ordinary factorial kriging estimates the mean and each factor independently. In this first example the mean and three factors are to be estimated with ordinary factorial kriging. Maps of

the estimated factors are shown on Figure A.2. The nugget factor is non-zero at the data locations and constant at all other locations. The nugget factor has no spatial structure. Note that the color scale is changed to visualize the variability of the long range factor. Note that the estimate of the mean reflects the most variability because of the unbiasedness constraints which forces the sum of the weights to be 0 for each factor. Although the kriging equations and unbiasedness condition achieve unbiasedness, it is unrealistic that the estimated mean factor has the majority of the variability. Furthermore, the estimated long range structure has unreasonably low variability, as shown in Figure A.2. Recall that the modeled variogram showed that the long range structure contributes 45% of the total variability. The long scale features are mainly captured by the mean factor. The short range estimated factor appears to vary within short distances. The sum of the estimate of each factor adds up to the ordinary kriging estimate.

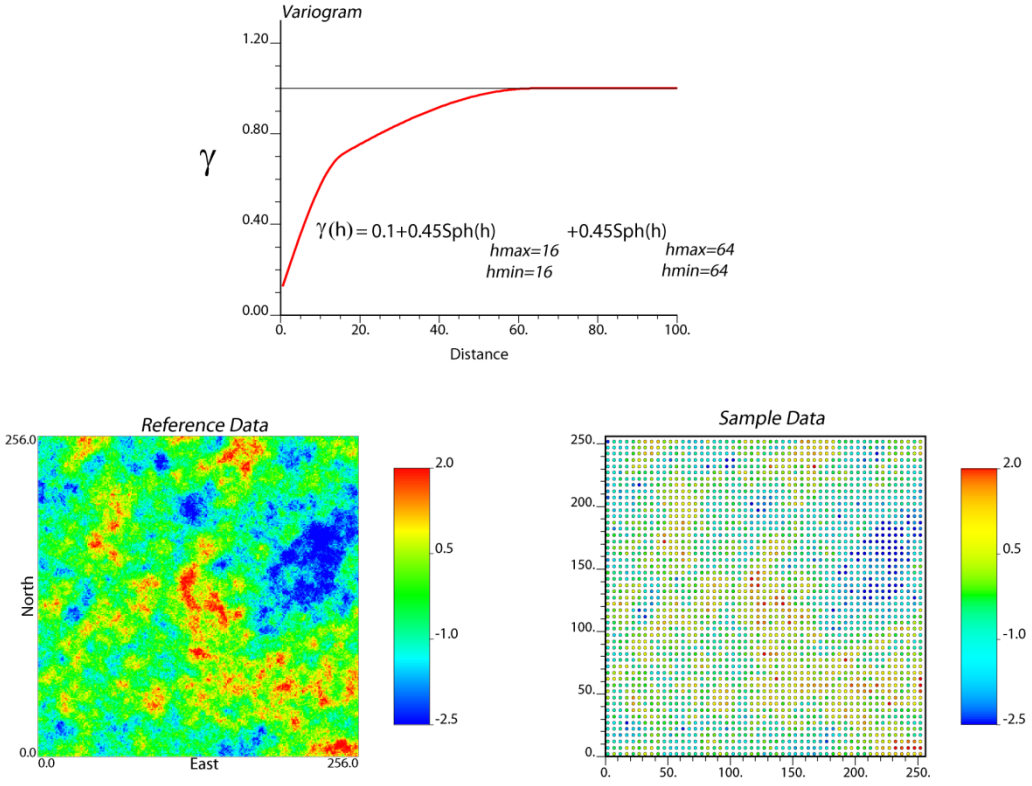

Figure A.2: The used variogram for generating simulation values (zero mean and unit variance Gaussian value), simulated values (bottom left) and sampled data (bottom right) are shown.

The ordinary kriging estimates are shown in the right bottom of Figure A.3 and it is ensured that sum of all factor estimates reproduced data exactly.

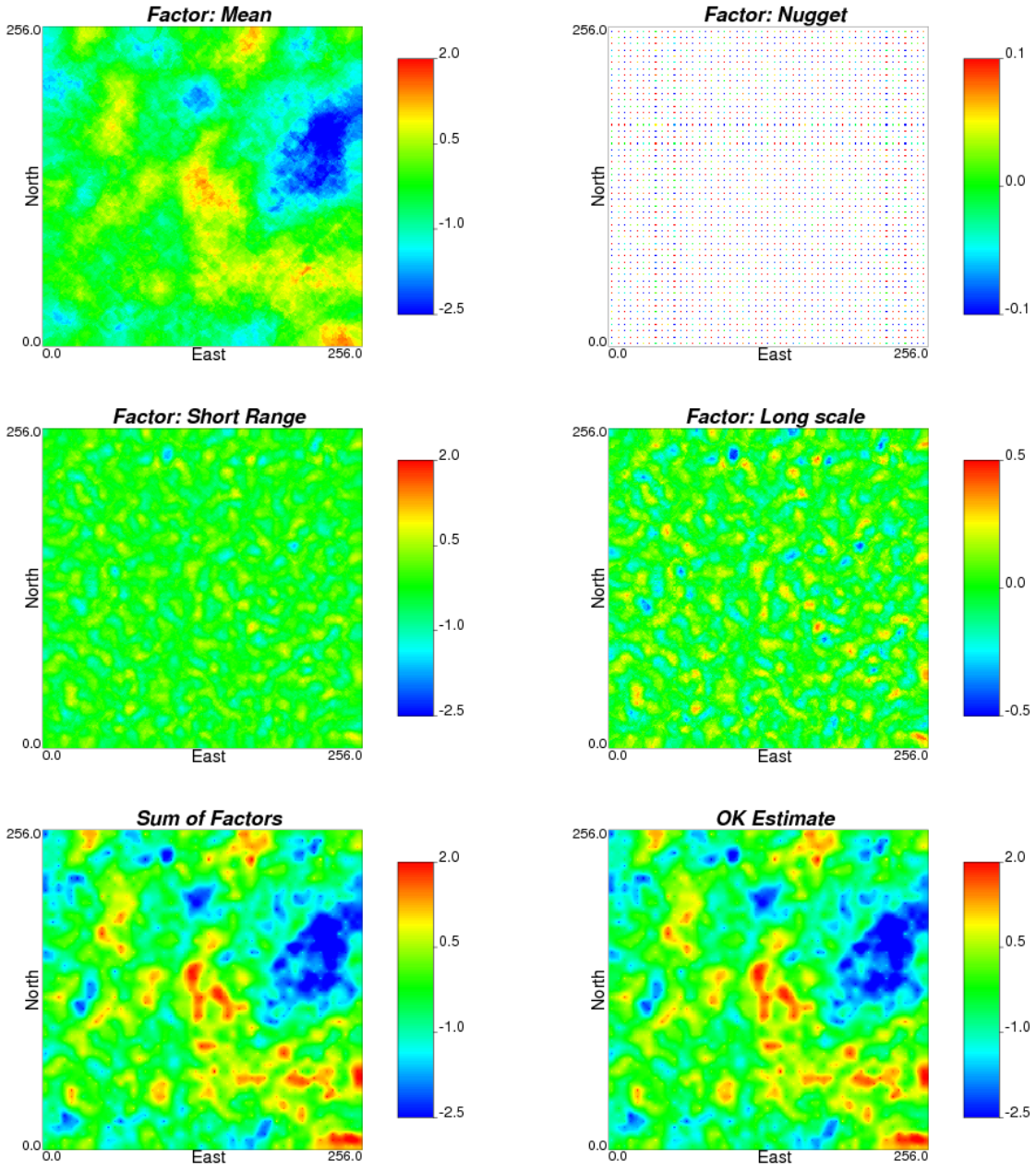

Figure A.3: Estimated factors using ordinary factorial kriging. Mean, nugget, short scale and long scale factors are estimated. Sum of the estimated factors exactly reproduce ordinary kriging estimate over every grids.

The simple factorial kriging estimates of each factor are shown in Figure A.4. The same kriging parameters such as search radius, minimum (8) and maximum number (18) of conditioning data, are used except unconstrained kriging weights. The mean value is assumed to

be constant. The nugget, isotropic short range and long range factors are estimated and shown in Figure A.4. The short range factor estimates appear to have variability within short distance and long range factor estimates appear to have variability over large distances. The simple factorial estimates reflect realistic features contrary to the ordinary factorial kriging estimates. A clear improvement in feature identification of short scale and large scale spatial components through simple factorial kriging is observed. The sum of all estimated factors reproduces the simple kriged estimate as derived in Equations (A.14) and (A.18). Table 1 shows the variance of each estimated factor by ordinary and simple factorial kriging, respectively. The variance table shows the significant difference between ordinary and simple factorial estimates. The numeric values show the calculated variance for each factor. The first column is the contribution of each factor obtained by nested variogram modeling (shown in Figure A.1). The second and third columns show the variance of each estimated factor with OFK and SFK. The last column in Table 1 shows how much OFK smoothes the estimated factors compared to SFK. The estimated mean factor using OFK has 70% variability which is the majority of variability. SFK has more variability than OFK and SFK produces more reasonable results in terms of feature identification. Smoothing still exists in the SFK estimates, but not to the extent of OFK.

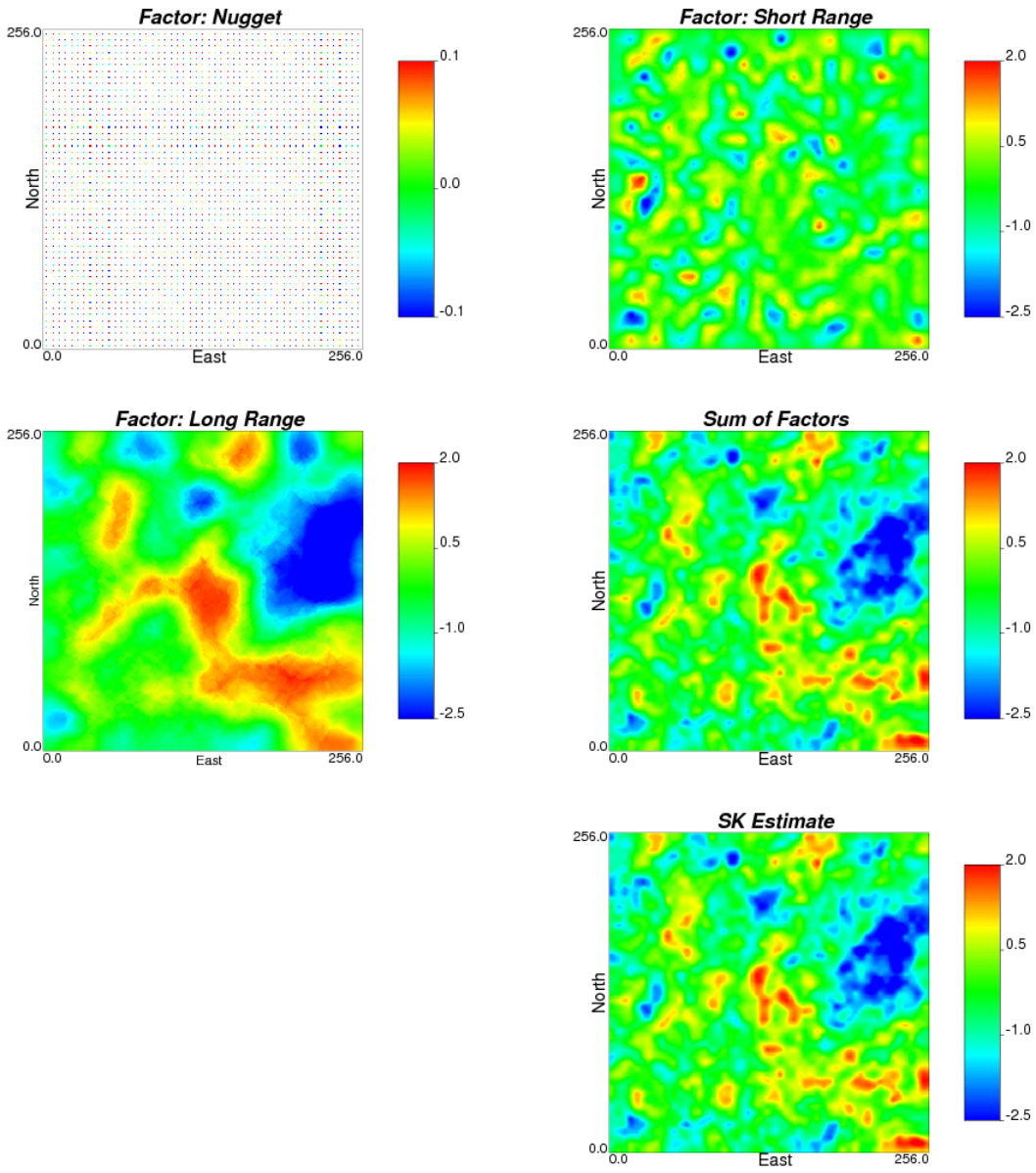

Figure A.4: Estimated factors using simple factorial kriging. Sum of the estimated factors and simple kriging estimate are shown as well.

Table A.1: Variance table for each estimated factor by OFK and SFK using the first synthetic example.

Factors	$b_l = (a_l^2)$	OFK	SFK	diff in %
mean	–	0.7	0 (constant)	–
$l = 0$ (nugget)	0.1	0.0	0.0	0
$l = 1$ (short range)	0.45	0.25	0.55	25
$l = 2$ (long range)	0.45	0.05	0.45	98

The second example (cluster.dat) is from Deutsch and Journel (1998). The example contains irregularly spaced well data over an area of 50×50 distance units. 140 clustered samples were used for the analysis. The data values are first transformed to be Gaussian unit using normal score transformation before applying factorial kriging. The locations of the normal score values are shown in the left of Figure A.5. The omnidirectional variogram was modeled since there is no obvious anisotropy. Three nested variogram structures were used; 20% nugget structure (very short distance), 40% short range and 40% long range structure (Figure A.5). In some areas, high values and low values are clustered with short distance, which contributes to the 40% short range structure in the variogram. Factorial kriging results should recognize this short scale as well as long scale. Ordinary factorial kriging was performed first. Figure A.6 illustrates four estimated factors in normal score units: mean, nugget, short range and long range factors. Just like in the first synthetic example, the mean factor has the majority of the variability. The nugget factor estimates only exist at the data locations. The short range factors have variability within short distances; however, the long range features are not clearly identified. The simple factorial kriging estimated factors are shown in Figure A.7. The simple factorial kriging estimates appear more reasonable.

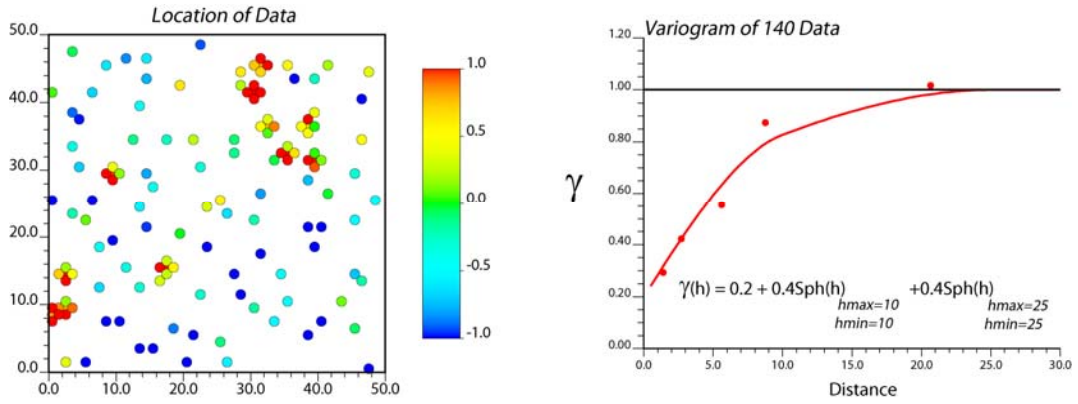

Figure A.5: 140 normal score data location and its modeled variogram (shown as solid line).

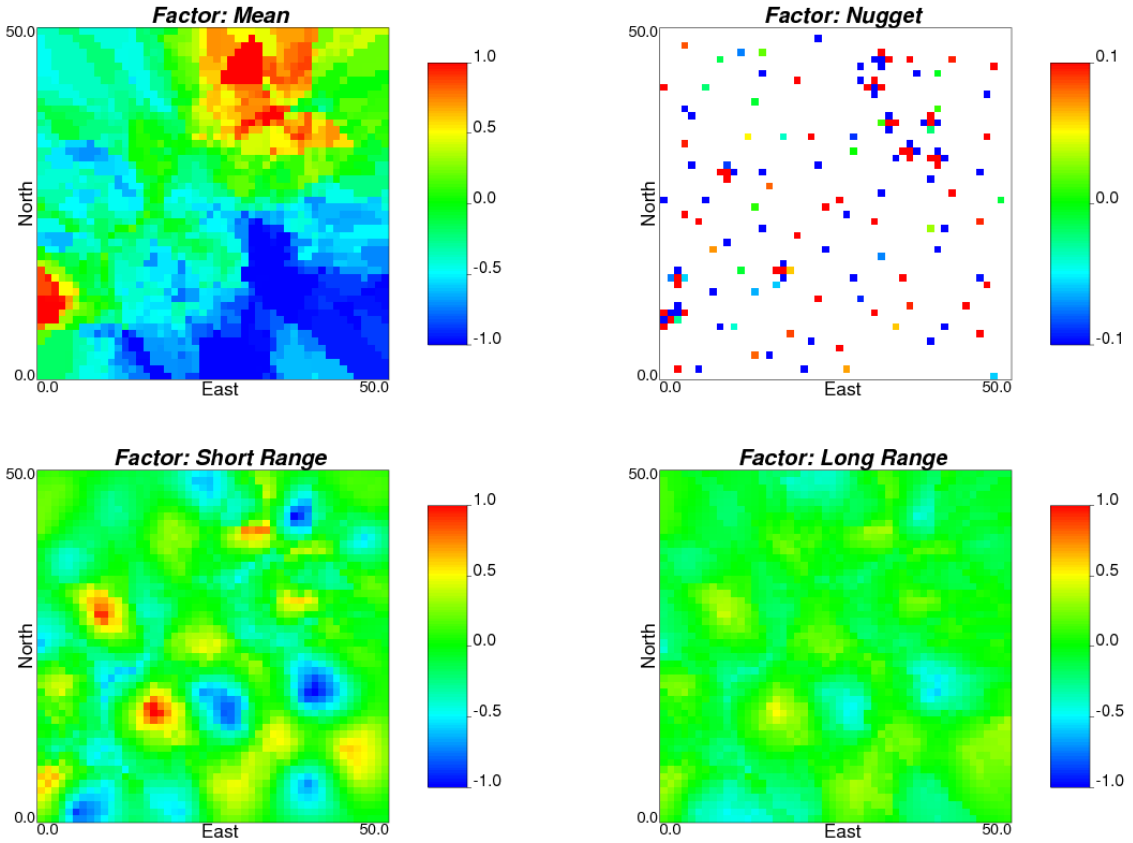

Figure A.6: Ordinary factorial kriging result of the second example.

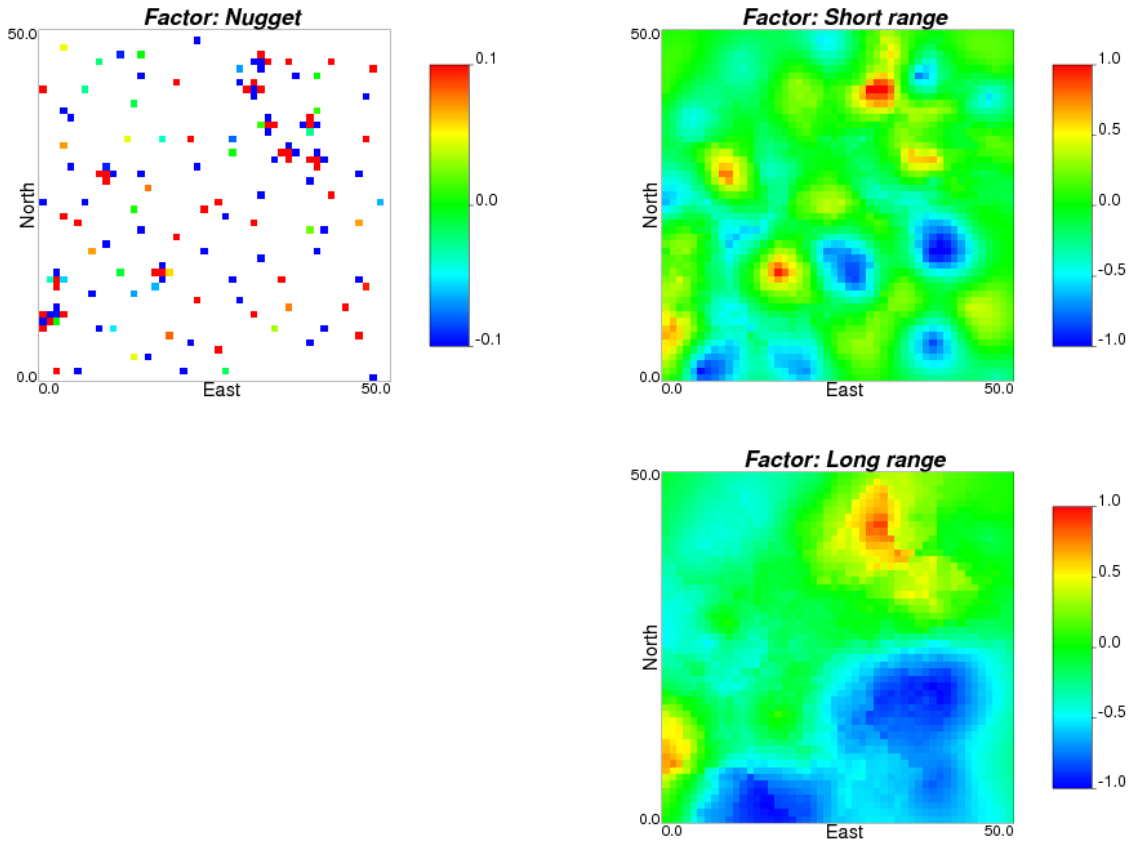

Figure A.7: Simple factorial kriging result of the second example.

A.3.1 Filtering of Exhaustive Data

The first two sparse-data examples show one application of factorial kriging. In many cases, such as with seismic data, factorial kriging can decompose the data map into several factors depending on the spatial scale. Identification of scale dependent feature is often quite useful in reservoir modeling.

The considered exhaustive data was originally published in Deutsch (1992). The data consist of a 164×85 grid of gray scale values that have been transformed to a standard normal distribution (represented as RGB color in Figure A.8). All distances are relative to the discretization units of the image with the image being 164 pixels by 85 pixels (top of Figure A.8). The variogram model consists of four nested structures with (h_1, h_2) being the coordinates in the two directions corresponding to the sides of the image. The spherical and exponential structures are classical in geostatistics. The dampened hole effect cosine model is not as commonly used; it is defined as:

$$DH_{d,a}(h) = 1.0 - \exp\left(\frac{-ha}{d}\right)\cos(ha) \tag{A.23}$$

There are four components in the variogram model that correspond to factors in the interpretation of factorial kriging:

1. A short scale anisotropic spherical structure that explains 45% of the total variability (the longer range is in the horizontal h_2 direction and the shorter range is in the vertical h_1 direction).
2. A second short scale anisotropic spherical structure (with a more pronounced anisotropy along the same horizontal and vertical directions) that explains an additional 22% of the variability,
3. A third anisotropic long range exponential structure (the range parameter is 40.0, thus, the effective range is 120.0 in the horizontal direction and 0.0 in the vertical direction) that explains 45% of the variability, and
4. Finally, a dampened hole effect model in the vertical direction to account for the periodicity.

The modeled variogram is shown at the bottom of Figure A.8.

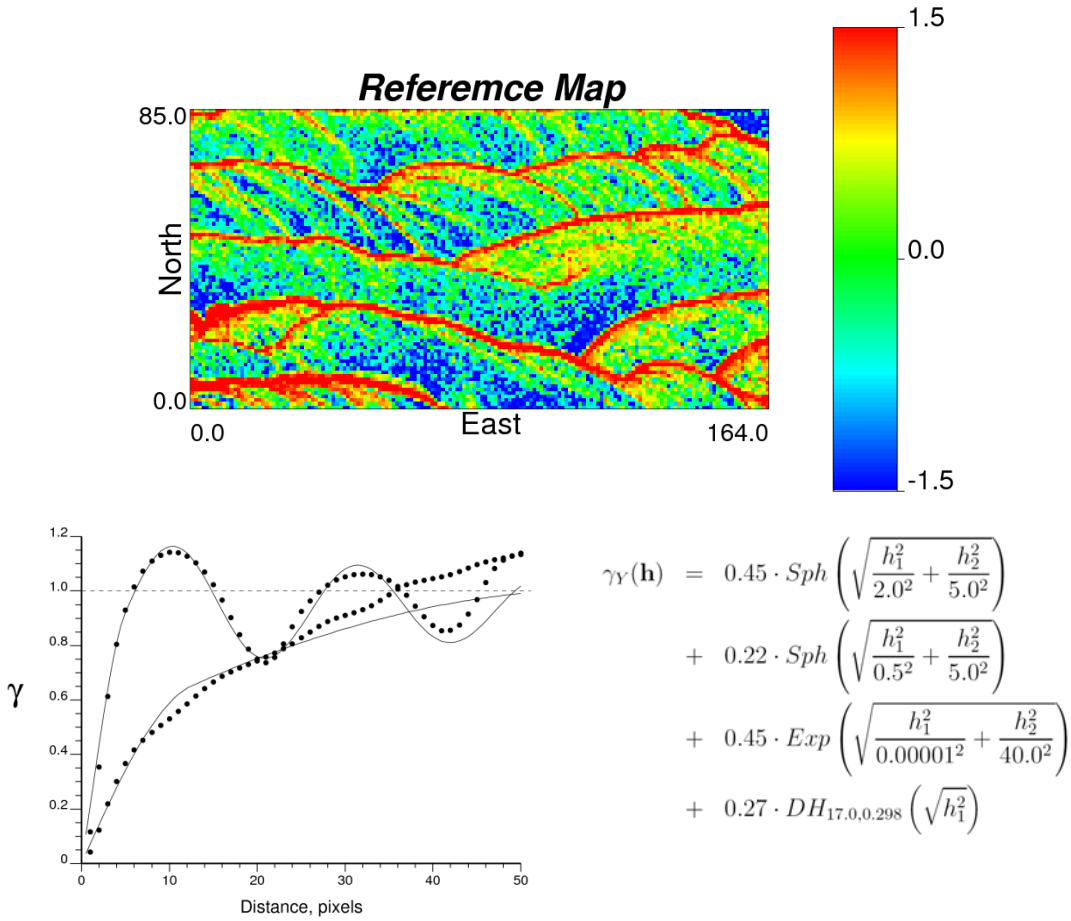

Figure A.8: Reference data for geostatistical filtering application and its modeled variogram.

Ordinary factorial kriging leads to five factors: the mean and the four specified spatial structures above. Figure A.9 shows the estimated factors based on the modeled variogram using OFK. The mean factor explains most of the variability (same as the previous two examples). The amount of variance used in each nested structure affects the variability of the factor. The anisotropic short range structure modeled with 22% variability seems fairly constant overall due to large amount of smoothness in OFK. The anisotropic long range structure does reveal more continuity in the horizontal direction. There are quite a few large negative values in the factor representing the dampened hole effect that results in noisy estimation map. OFK does not reveal the cyclic pattern. Instead, that pattern was captured by the mean factor. Summing up of all estimated factors should amount to the original reference data, however, it does not in OFK. Sum of estimated factors looks noisy due to the noisy dampened hole estimate factor (large negative values). Simple factorial kriging applied to the same exhaustive data having complex spatial features and

factor estimation results are shown in Figure A.10. Cyclic pattern of data is significant in the estimated dampened hole factor. Sum of estimated factors amounts to the reference image. One of possible extension of factorial kriging to exhaustive data set is to filter out the undesired spatial features. For example, repetitive seismic survey may invoke periodic systematic noise which is better to be removed to enhance the clarity of the data. The considered data has contains cyclic spatial features that is mainly characterized as dampened hole effect in the variogram. We treated the data as seismic data interrupted with cyclic noise. Thus, that feature is to be removed for enhancing signal-to-noise ratio of seismic data. Cyclicity filtered image is simply derived from summing of the other estimated factors. In OFK, sum of mean, two anisotropic short range, anisotropic long range factors is equivalent to the cyclicity filtered image. In SFK, sum of two anisotropic short range, anisotropic long range factor is equivalent to the filtered image. Two filtered image are compared in Figure A.11 and it should be noted that SFK shows better performance in terms of removing periodic structure. Geostatistical filtering is basically depending on the number and types of fitted variogram. This is one advantage of geostatistical filtering technique since geologic knowledge can be added when fitting the experimental variogram hence more realistic structure may be extracted.

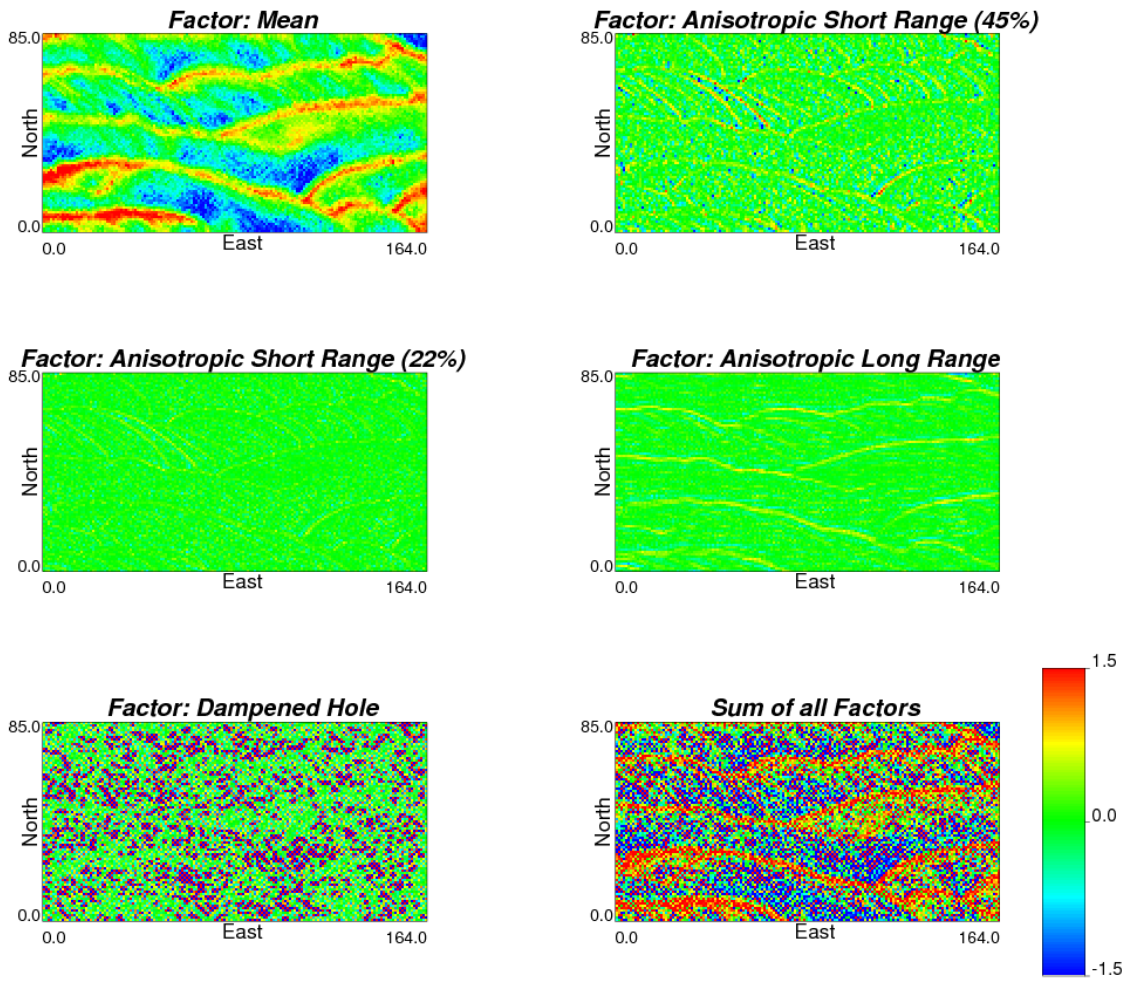

Figure A.9: Factor estimate of the exhaustive data using ordinary factorial kriging.

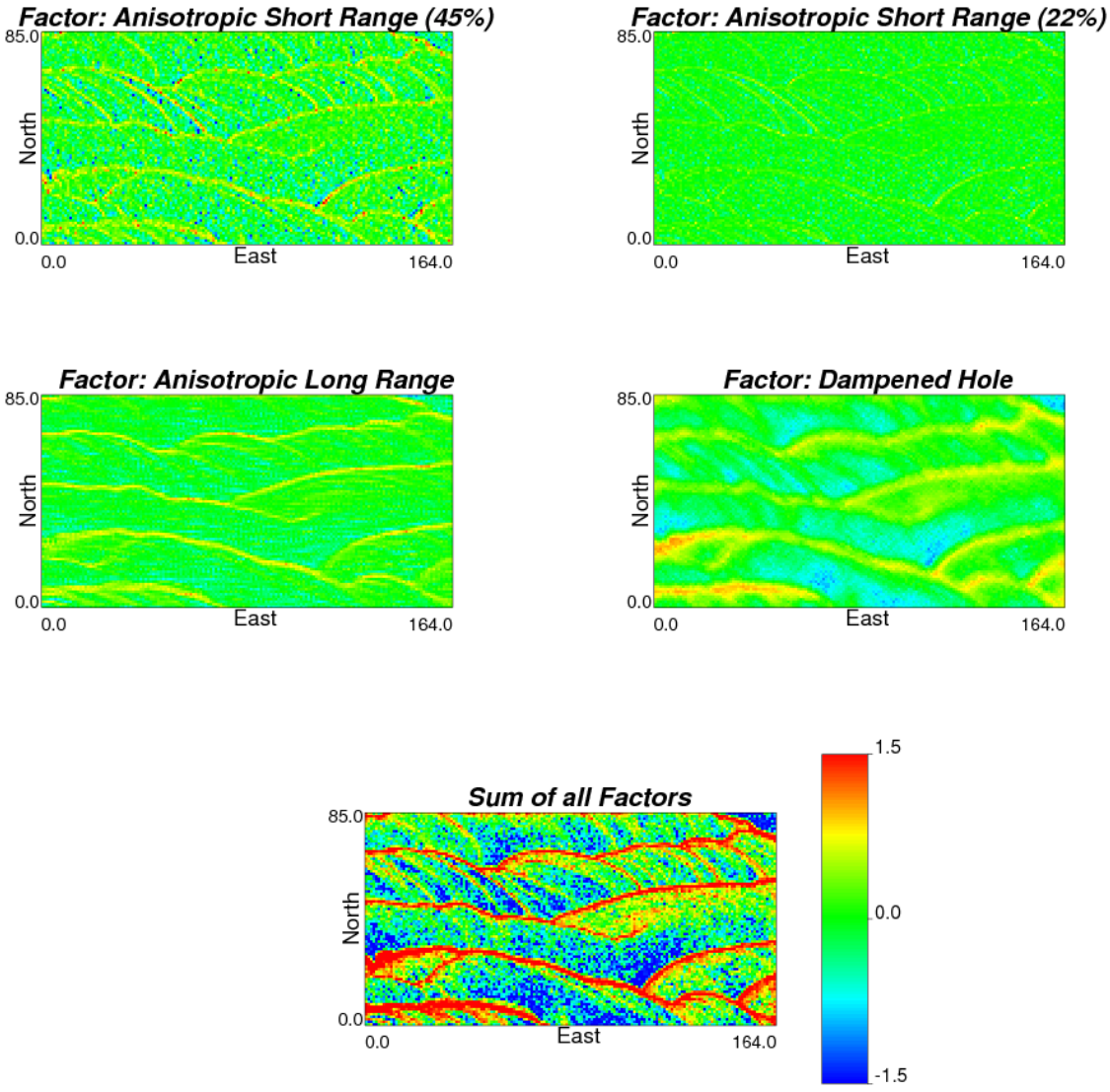

Figure A.10: Factor estimate of the exhaustive data using simple factorial kriging. Note that summing up of all estimated factors amounts to the reference map shown Figure A.7.

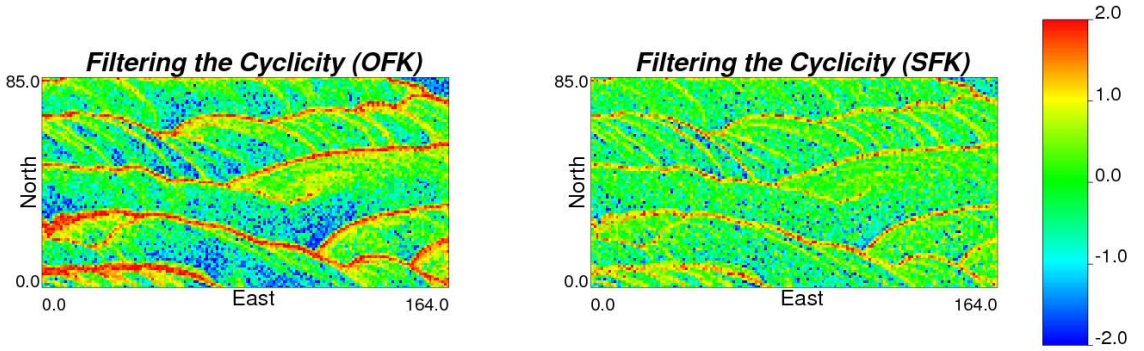

Figure A.11: Cyclic spatial feature is filtered out by OFK and SFK. SFK alleviates the pattern which we assumed noise inherent in data.

A.3.2 Combining Spatial Components

Another application of factorial kriging is to integrate relevant features with primary data. Factorial kriging can filter out unwanted spatial features depending on the purpose of study. Filtered secondary data then can be used as a new secondary data to be combined with primary. Another petroleum field data (Amoco.dat) is tested for factorial data integration (Deutsch and Journel, 1998). We have one primary porosity variable to be estimated and one exhaustively sampled seismic-derived acoustic impedance. Secondary data is sampled by 65 × 65 with 160 unit distance. Variables were first transformed into normal space. Modeled variogram of porosity provide two identified spatial features, i.e. 20% isotropic small scale and 70% anisotropic large scale features (major direction in N-S and minor direction in E-W).

$$\gamma(\mathbf{h}) = 0.2Sph(\mathbf{h})_{\substack{\text{hmin=hmax=1000}}} + 0.8Sph(\mathbf{h})_{\substack{\text{hmin=5000}\\ \text{hmax=17000}}} \tag{A.24}$$

Secondary variable appears to vary smoothly over the domain. The variogram of the secondary data is fitted with two features: 25% isotropic small scale and 75% isotropic large scale features. Anisotropic direction of secondary variable is same as primary variable: major in N-S and minor in E-W.

$$\gamma(\mathbf{h}) = 0.25Sph(\mathbf{h})_{\substack{\text{hmin=hmax=1000}}} + 0.75Sph(\mathbf{h})_{\substack{\text{hmin=4000}\\ \text{hmax=10000}}} \tag{A.25}$$

Maps of the primary and secondary data are shown in Figure A.12 with the variograms. No nugget filtering is required since the variogram has no nugget contribution. Simple factorial

kriging with exhaustive secondary data was performed and two factors are extracted separately: isotropic small scaled feature and isotropic large scaled feature. To check the relationships between primary porosity and extracted factors, correlation coefficient is calculated. Let us clarify the notation: Z is primary variable (normal score value), Y_{total} is original secondary variable (normal score value), $Y_{l=1}$ and $Y_{l=2}$ are factor 1 and factor 2 extracted from secondary variable. Correlation (ρ_{ZY}) of primary Z and total secondary variable Y_{total} is 0.615. It is noted that correlation coefficient is slightly changed when plotting extracted factor 1 and 2 with primary variable,

$$\rho_{ZY_{l=1}} = 0.34 < \rho_{ZY_{total}} = 0.615$$
$$\rho_{ZY_{l=2}} = 0.65 > \rho_{ZY_{total}} = 0.615$$

The large scale factor is highly correlated to the primary variable. This is a reasonable result since the variogram of primary porosity has greater contribution of large scale feature (80% variability) than small scale feature (20% variability). Besides, the variogram of seismic data shows 75% variability contribution of large scale feature. There are two evident options for data integration. One option is to use extracted relevant factor as a new secondary variable. Simple cokriging is applied to the primary variable using the new secondary data (extracted relevant factor). The second factor is used as secondary data. This factor is transformed into normal scores. In this integration option, the long range structure is enhanced and short range structure is weakened because large scale feature is imposed both by primary (80%) and secondary data (75%), but small scale feature is imposed only by primary data (20%). The other option is to apply simple factorial cokriging to the primary variable using the extracted relevant secondary variable. Equation (A.22) explains the latter option.

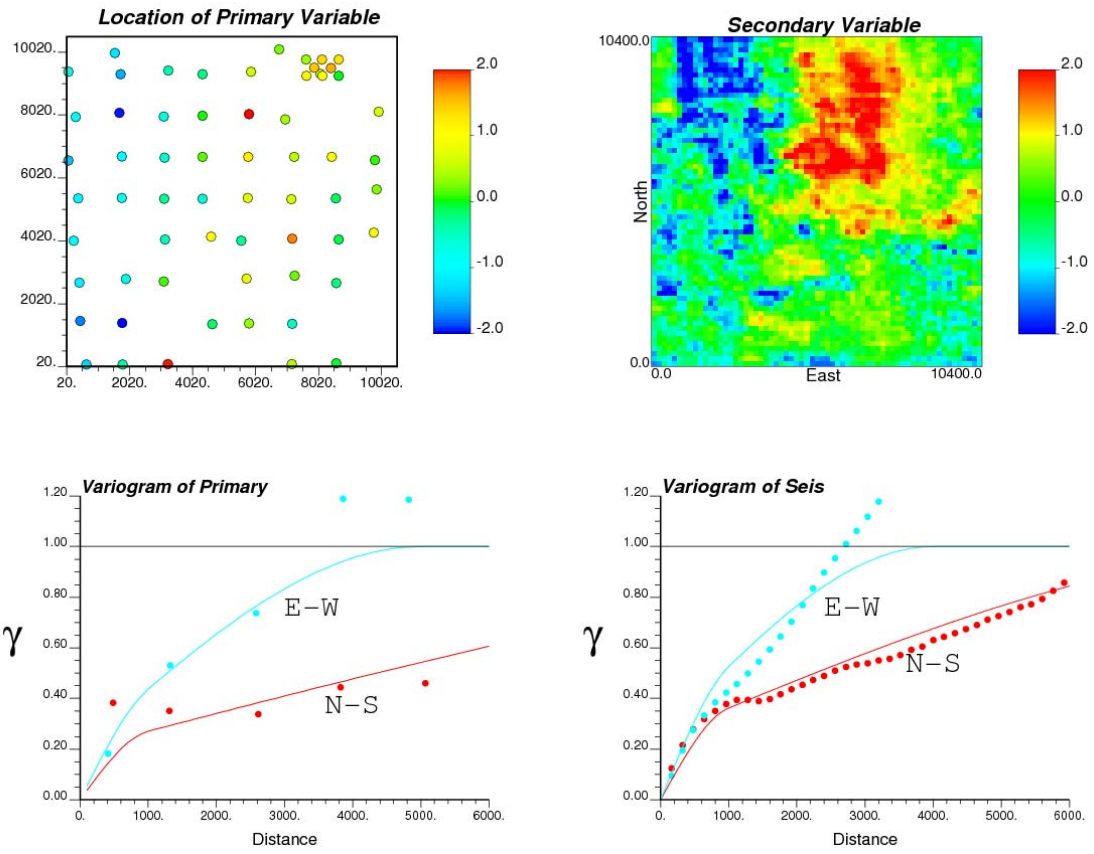

Figure A.12: Location of primary variable and exhaustively measured secondary variable are shown in the upper (already transformed into Gaussian space). Both primary and secondary variable have the common anisotropy direction; horizontal major direction is in N-S and horizontal minor continuity direction is in E-W. Dots and solid lines represent calculated variograms and their modeled variograms, respectively.

Figure A.13 represents the cokriging result with the second data integration option. Two spatial features are extracted from secondary data: short range and long range features. The results of simple factorial cokriging with short range factor is shown at the bottom left of Figure A.13. The results of simple factorial cokriging with long range factor are shown at the bottom right of Figure A.13. To compare the effectiveness of incorporating secondary data, simple factorial estimate only using primary data are illustrated in the top of Figure A.13. The anisotropic long range structure is significant along with N-S direction. The variance of small scale factor is very low due to smoothness effect. Cokriged short and long range feature have more variability rather than the factor estimation with primary data only.

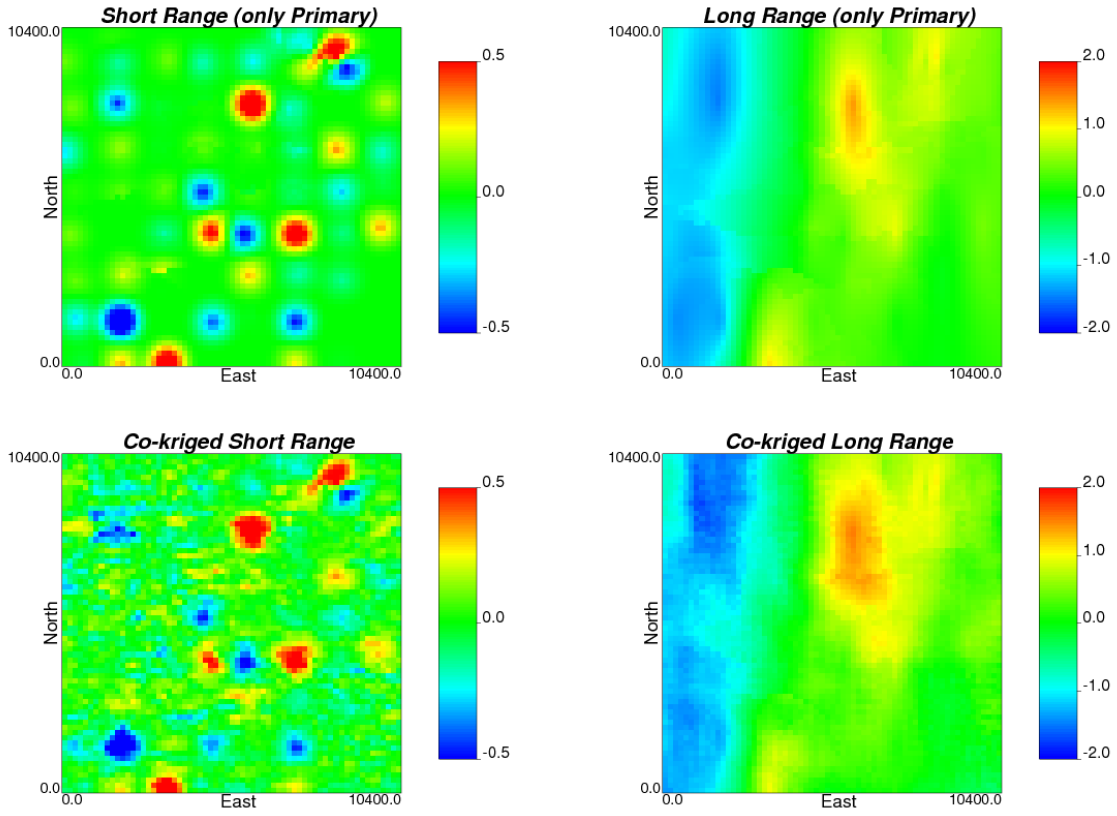

Figure A.13: Simple factorial co-kriging result for short range and long range factor identification (bottom). Simple factorial estimate only using primary data are shown in the upper for the comparison.

A.4 Discussions

Factorial kriging is a popular variant of kriging based on the variogram and there has been significant interest for the application of factorial kriging as a spatial filtering in seismic data or as enhancing the spatial components of consideration. A simple factorial kriging concept has been introduced in addition to the conventional ordinary factorial kriging. Those methods were tested on synthetic example; the results show most of the variability in the mean because of the ordinary kriging constraints. In the simple factorial kriging, the mean is assumed to be constant overall and simple factorial kriging extracts features with different scale.

Another application of factorial kriging is to mask noise in exhaustive seismic data and to amplify the specific spatial features. Exhaustive data having complex spatial features was tested. Simple factorial kriging successfully filtered out the undesignated features and enhanced the specific spatial features. Factorial kriging approach makes it possible to integrate more relevant

feature with primary variable. We tested factorial collocated cokriging using sparely sampled porosity and extracted relevant factor from seismic data. After factorial collocated cokriging, we could clearly identify scale dependent structures compared with the factorial kriging with primary only.